AD-A179 501 WORKSHOP SYMPOSIUM ON NEURAL MODELS OF SENSORY-MOTOR CONTROL HELD IN CAMB..(U) BOSTON UNIV MA CENTER FOR ADAPTIVE SYSTEMS D BULLOCK ET AL. 06 MAR 87 1/3

UNCLASSIFIED AFOSR-TR-87-0457 AFOSR-86-0220 F/G 5/10 NL

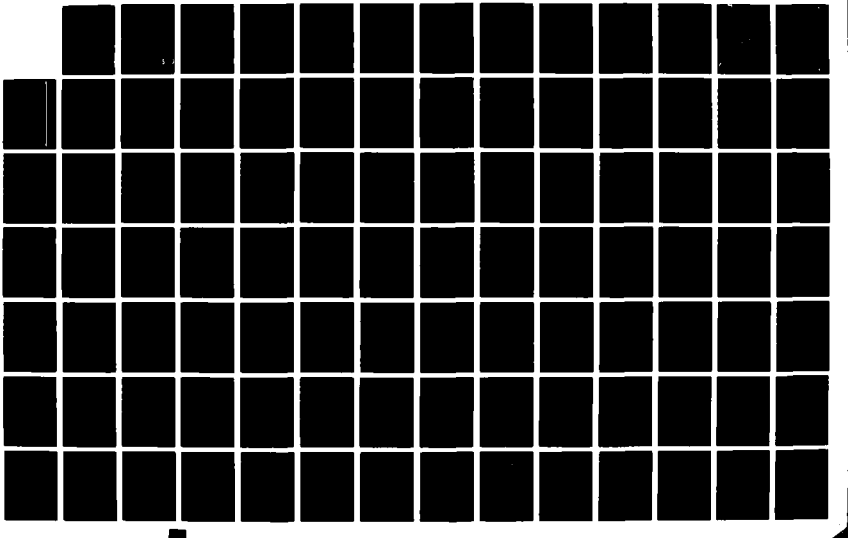

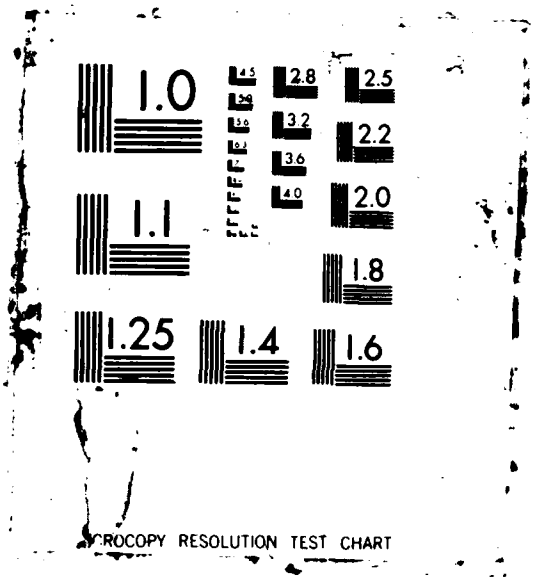
1.0
1.1
1.25
1.4
1.6
1.8
2.0
2.2
2.5
2.8
3.2
3.6
4.0
ROCOPY RESOLUTION TEST CHART

DTIC FILE COPY (2)

AD-A179 501

REPORT DOCUMENTATION PAGE

1a. REPORT SECURITY CLASSIFICATION: unclassified	1b. RESTRICTIVE MARKINGS
2a. SECURITY CLASSIFICATION AUTHORITY	3. DISTRIBUTION / AVAILABILITY OF REPORT: Approved for public release; distribution unlimited.
2b. DECLASSIFICATION / DOWNGRADING SCHEDULE	
4. PERFORMING ORGANIZATION REPORT NUMBER(S)	5. MONITORING ORGANIZATION REPORT NUMBER(S): AFOSR-TR- 87-0457
6a. NAME OF PERFORMING ORGANIZATION: Center for Adaptive Systems; 6b. OFFICE SYMBOL (If applicable)	7a. NAME OF MONITORING ORGANIZATION: Air Force Office of Scientific Research/NL
6c. ADDRESS (City, State, and ZIP Code): Boston University, 111 Cummington Street, Boston, MA 02215	7b. ADDRESS (City, State, and ZIP Code): Building 410, Bolling AFB DC 20332-6448
8a. NAME OF FUNDING / SPONSORING ORGANIZATION: AFOSR/NL; 8b. OFFICE SYMBOL (If applicable): NL	9. PROCUREMENT INSTRUMENT IDENTIFICATION NUMBER: AFOSR 86-0228
8c. ADDRESS (City, State, and ZIP Code): AFOSR/NL, Building 410, Bolling AFB DC 20332-6448	10. SOURCE OF FUNDING NUMBERS: PROGRAM ELEMENT NO. 61102F; PROJECT NO. 2313; TASK NO. A5; WORK UNIT ACCESSION NO.

11. TITLE (Include Security Classification): Workshop Symposium on Neural Models of Sensory-Motor Control

12. PERSONAL AUTHOR(S): Daniel Bullock and Stephen Grossberg

13a. TYPE OF REPORT	13b. TIME COVERED	14. DATE OF REPORT (Year, Month, Day)	15. PAGE COUNT
final	FROM 7/1/86 TO 6/30/7	March 6, 1987	10 pages

16. SUPPLEMENTARY NOTATION

17. COSATI CODES			18. SUBJECT TERMS (Continue on reverse if necessary and identify by block number)
FIELD	GROUP	SUB-GROUP	

19. ABSTRACT (Continue on reverse if necessary and identify by block number)

The Symposium on Neural Models of Sensory-Motor Control was held on Aufust 19 and 20, 1986, at Harvard University as part of the annual meeting of the Society for Mathematical Psychology. The Symposium was divided into two sessions, each with four 50-minute presentations. The first session focused on neural models of the human oculo-motor system. The second session began with two papers on arm movement planning. Speakers were not asked to prepare papers for a formal publication. Papers supplied by Bullock and Grossberg, by Grossbers, by Hollerbach and Atkeson, by Kelso, and Scholz, and by Optician and Miles are enclosed.

20. DISTRIBUTION / AVAILABILITY OF ABSTRACT	21. ABSTRACT SECURITY CLASSIFICATION
☒ UNCLASSIFIED/UNLIMITED ☐ SAME AS RPT ☐ DTIC USERS	UNCLASSIFIED
22a. NAME OF RESPONSIBLE INDIVIDUAL: JOHN F TANGNEY	22b. TELEPHONE (Include Area Code): (202) 767-5021 — 22c. OFFICE SYMBOL: NL

DD FORM 1473, 84 MAR — 83 APR edition may be used until exhausted. All other editions are obsolete. — SECURITY CLASSIFICATION OF THIS PAGE

16 MAR 1987

FINAL REPORT

A WORKSHOP SYMPOSIUM ON NEURAL MODELS OF SENSORY-MOTOR CONTROL

AFOSR 86-0228

Stephen Grossberg, Principal Investigator
Center for Adaptive Systems
Boston University
111 Cummington Street
Boston, MA 02215
(617) 353-7857

February, 1987

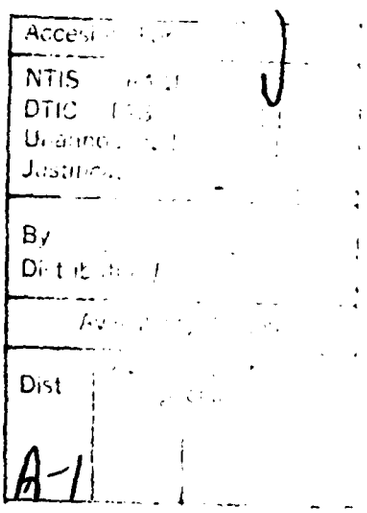

The Symposium on Neural Models of Sensory-Motor Control made possible by this grant was held on August 19 and 20, 1986, at Harvard University as part of the annual meeting of the Society for Mathematical Psychology. The Symposium was advertised by the Society (see attached program) as well as by direct mailings from the Center for Adaptive Systems at Boston University (announcement attached). In addition, announcements of travel scholarships for qualified junior scientists (graduate students and postdoctoral fellows) were placed in several journals. The invited speakers included:

Professor Michael Arbib, University of Massachusetts at Amherst
Professor Daniel Bullock, Boston University
Professor Stephen Grossberg, Boston University
Professor John Hollerbach, Massachusetts Institute of Technology
Professor Scott Kelso, Florida Atlantic University
Dr. Lance Optican, National Institutes of Health
Professor Barry Peterson, Northwestern University
Professor David Robinson, Johns Hopkins University
Professor Gregor Schöner, Florida Atlantic University

I. SUMMARY OF THE SYMPOSIUM

The Symposium was divided into two sessions, each with four 50-minute presentations. The first session focused on neural models of the human oculo-motor system, a system for which several advanced mathematical models are now available. Robinson detailed a new model of the neural system for smooth pursuit (tracking-type) eye movements. Optican presented new data and a model for adaptive control of ocular drift following saccadic (ballistic-type) eye movements. Grossberg outlined a new model for several adaptive components of the neural system for learning and maintaining accurate saccadic eye movements. Finally, Peterson detailed experiments performed to constrain modeling of the neural and computational linkage between the oculo-motor and the neck-motor systems.

The second session began with two papers on arm movement planning. Hollerbach presented experimental and computational studies indicating that human arm-movement

planning probably occurs in joint-coordinates. Bullock then presented a neural model for automatic trajectory formation in joint coordinates and related the model to a wide range of experimental studies of arm-movement kinematics. To close the second session, Kelso and Schöner presented studies of frequency-dependent phase transitions during rhythmical finger movements of the two hands, and Arbib presented a wide-ranging discussion of issues in physiological and computational studies of visually controlled locomotion in the presence of barriers.

II. TRAVEL SCHOLARSHIPS

Besides reaching members of the Society for Mathematical Psychology, which has recently begun to build a significant constituency with interests in network models (see attached program), the Symposium offered a rare opportunity for ten junior scientists who received travel scholarships funded by the grant. These junior scientists were:

Thomas Anastasio, Johns Hopkins Hospital
Rick Canfield, University of Denver
Barry Hughes, University of Wisconsin
Richard Ivry, University of Oregon
Dieter Jaeger, University of Michigan
Bruce Kay, Haskins Laboratories
Anne Luebke, Johns Hopkins School of Medicine
Lloyd Minor, University of Chicago
Kevin Munhall, Haskins Laboratories
Mark Nelson, California Institute of Technology

III. INTERACTIONS

Reactions from the junior scientists were very favorable. Several remarked that the Symposium was among the most technically competent and informative that they had experienced in any setting. Most salient to them were the scope and precision of the models and the seriousness of the treatment of adaptive brain properties by some of the speakers. A number expressed intentions to pursue a more quantitative tack in their

future brain studies, and several asked about further avenues for advanced training in neural modeling. Finally, a number of the experimentalists volunteered to share new data bearing on the predictions of some of the presented models.

Reactions among the speakers were also quite favorable. Several were quite excited by unanticipated convergence towards common conclusions despite divergent research methods. Of course, speakers had been selected because of their shared dedication to computational models that are responsive to psychophysical and physiological data. However, the speakers still represented a broad spectrum of backgrounds and predilections. Nevertheless, several speakers were able to outline network solutions to problems posed by prior speakers without any advance notice of the specifics of other speakers' presentations. These spontaneous remarks increased the coherence of the Symposium and illustrated how the same underlying neural circuitry is often manifested in diverse behavioral properties.

IV. PAPERS

Speakers were not asked to prepare papers for a formal publication because many speakers were already overburdened with paper-preparation commitments. Several of the speakers have nevertheless supplied preprints or reprints that treat the topics of their Symposium presentations. Typically, the paper's treatment is more ambitious than that of the 50-minute presentation during the Symposium. The five papers supplied by Bullock and Grossberg, by Grossberg, by Hollerbach and Atkeson, by Kelso, Schöner, and Scholz, and by Optican and Miles are enclosed.

V. BUDGET

Most expenses associated with the Symposium were equal to or less than what had been anticipated. Harvard University provided inexpensive dormitory accomodations for the junior scientists, three junior scientists who had planned to come were forced by unforseen circumstances to change their plans, airfares were strongly discounted because participants

made early reservations, and several participants unexpectedly came to the Symposium from nearby locations in New England. As a result, $2941.15 remains in the Symposium budget. A list of expenditures-to-date is attached.

SYMPOSIUM EXPENDITURES

Travel Stipends for Speakers

Michael Arbib	$460.80
Daniel Bullock	$ 46.00
Stephen Grossberg	$ 49.00
John Hollerbach	$ 50.00
Scott Kelso	$583.20
Lance Optican	$343.94
Barry Peterson	$382.38
David Robinson	$347.08
Gregor Schöner	$338.00

Total travel stipends for speakers: $2600.40

Travel Stipends for Junior Scientists

Thomas Anastasio	$341.00
Rick Canfield	$373.00
Barry Hughes	$225.50
Richard Ivry	$393.85
Dieter Jaeger	$121.00
Bruce Kay	$103.80
Anne Luebke	$283.00
Lloyd Minor	$293.00
Kevin Munhall	$163.80
Mark Nelson	$460.50

Total travel stipends for junior scientists: $2758.45

Other Expenses

Dinner for Speakers	$ 200.00
Advertising and Mailing	$1250.00
Photocopying	$1250.00

Total other expenses: $2700.00

TOTAL EXPENSES: $8058.85

A Symposium at the Annual Meeting of the Society for Mathematical Psychology

NEURAL MODELS OF SENSORY-MOTOR CONTROL

Co-sponsored by the
AFOSR Life Sciences Program
and the
Center for Adaptive Systems, Boston University

August 19–20, 1986
Harvard University
William James Hall, Room 1, 33 Kirkland Street
Cambridge, Massachusetts

AUGUST 19, P.M.:

1:30–2:20: David Robinson, Johns Hopkins University
"A model of the human smooth pursuit system"

2:20–3:10: Lance Optican, National Institutes of Health
"Adaptive suppression of post-saccadic ocular drift"

3:10–3:25: Coffee break

3:25–4:15: Stephen Grossberg, Boston University
"Neural dynamics of adaptive sensory-motor control: Ballistic eye movements"

4:15–5:05: Barry Peterson, Northwestern University
"Sensory-motor transformation in ocular-motor and neck-motor systems"

AUGUST 20, A.M.:

8:40–9:30: John Hollerbach, Massachusetts Institute of Technology
"Deducing planning variables from experimental arm trajectories: Pitfalls and possibilities"

9:30–10:20: Daniel Bullock, Boston University and University of Denver
"Neural dynamics of planned arm movements: Invariants, synergies, and trajectory formation"

10:20–10:35: Coffee break

10:35–11:25: Scott Kelso and Gregor Schöner, Florida Atlantic University
"A synergetic (and stochastic) treatment of nonequilibrium phase transitions in movement"

11:25–12:15: Michael Arbib, University of Massachusetts at Amherst
"Visual control of approach and avoidance behavior"

A few travel scholarships for graduate and postdoctoral students of motor-control are still available. If interested, call Daniel Bullock (617-353-9482) as soon as possible. For further information about the symposium, call 617-353-7857. Further information about the SMP annual meeting is attached.

HARVARD UNIVERSITY
DEPARTMENT OF PSYCHOLOGY AND SOCIAL RELATIONS

William James Hall
33 Kirkland Street
Cambridge, Massachusetts 02138

SOCIETY FOR MATHEMATICAL PSYCHOLOGY
Nineteenth Annual Meeting
August 19 to 21, 1986

To Members and Friends:

Herewith is information regarding the arrangements for the 19th Annual Meeting of the Society for Mathematical Psychology:

(1) the meeting program
(2) meeting registration form
(3) reservation form for accommodations on the Harvard Campus
(4) information on hotels and motels in the neighborhood
(5) a map of the Harvard Campus.

Meetings

Sessions will be held in William James Hall at 33 Kirkland St. (see map), approximately 5 min. walking time from Hastings Hall. Slide projectors and overhead projectors will be available, courtesy of the Psychology Department.

Messages: Telephone messages for registered attendees will be received on Tuesday, Wednesday, and Thursday mornings, 10-12 am, (617) 495-3836.

Receptions: An open house will be held on Monday evening, August 18, from 7:30 to 10:00 pm in the Common Room of Hastings Hall. Registration will be open at that time (and place).

All attendees are invited to a reception/cocktail party from 6:00 to 7:30 pm on Tuesday, August 19 at the Estes house, 95 Irving St., Cambridge (see map).

Registration

Enclosed is a form for pre-registration. The work of the committee will be simplified considerably if you pre-register. We will also provide opportunities for registration in William James Hall on the morning of Tuesday, August 19.

Registration fees are $40 for members, $50 for guests, and $15 for students.

The registration fee covers programs, costs of the sessions, the preconference reception on August 18 and refreshments at coffee breaks.

Local Travel

Public transportation from Boston's Logan Airport to Harvard Square is available at 60¢ via subway. Take the free Massport bus from your terminal to the Mass Transit Station, the Blue Line train to Government Center Station, then the Green Line to Park Street Station, and finally the Red Line to Harvard Square. Time normally runs 40-60 min. There is a taxi stand at Harvard Sq. From Harvard Square it is only a 10-15 min. walk to the Dormitory or William James Hall. Taxis from the airport to the Campus are normally available at about $12.00.

Parking

Parking on the Campus is by permit only. Temporary permits will be issued at $3.00 per day. Space will be assigned to the Group, so it is necessary to estimate the number of cars that will be involved so we request that you indicate on the registration form if you will have a car. Permits will be issued on arrival at the registration desk.

Housing

Arrangements have been made for members of the Society for Mathematical Psychology to stay in Hastings Hall during the period beginning Monday, August 18, and extending through noon on Thursday, August 21. Hastings Hall is a dormitory operated by the Harvard Law School; it is not a hotel and services are appropriate to college dormitories - no room service, no room telephones, no private TV, no airconditioning, etc. Bathrooms are on landings between floors and are shared by no more than six persons. Linen is provided, but there is no daily maid service. The cost will be $25.00 per night. The rooms are in groups with separate entrances and stairways. It will be necessary for the committee to make the room assignments prior to the guests' arrival so if you wish to be with specific other persons, please specify on your reservation form and every effort will be made to assign rooms accordingly.

A dormitory reservation form is enclosed with this memo; all reservations must be made prior to July 15, 1986, and must be accompanied by a non-refundable deposit of $25.00. The balance is due on arrival.

There are many hotels and motels within reasonable distance of the Campus. These are listed below with rates for single and double occupancy; these rates are current and assurance was given that they would not change before August; however, the committee cannot be responsible if the hotels change their minds. Those of you who prefer hotels will need to make your own arrangements with the hotel of your choice.

Housing (continued)

The Embassy Suites Hotel has offered special rates to the Society. The Hotel provides two room suites with pullman kitchens. Included in the rate is free shuttle service to and from Harvard Square, free parking, and complementary breakfasts. The Hotel is located on the Allston-Cambridge off-ramp from the Massachusetts Turnpike and at the River Bridge off-ramp from Storrow Drive, so it is easy to reach. It is probably not within walking distance of the Campus for any of the less hardy souls.

	Single	Double
Embassy Suites Hotel 400 Soldiers' Field Rd., Brighton, MA 02134 (617) 783-0090	$95	$115

Other hotel and motels, with rates, as quoted over the phone on April 1, are listed below, grouped by distance from the campus. Addresses and phone numbers are included for your convenience in making reservations.

Within walking distance of the Campus:	Single	Double
Sheraton Commander Hotel (5 min.) 16 Garden St., Cambridge, MA 02138 (617) 547-4800	$108	$119
Harvard Motor House (10 min.) 110 Mt. Auburn St., Cambridge, MA 02138 (617) 864-5200	73	83
Quality Court (15 min.) 1651 Massachusetts Ave., Cambridge, MA 02138 (617) 491-1000	68	75-85
Charles Hotel (15 min.) 1 Bennett St., Cambridge, MA 02138 (617) 864-1200	130-165	150-185
Probably not within walking distance:		
Best Western Homestead 220 Alewife Brook Pkwy., Cambridge, MA 02138 (617) 491-1890	68	76
Charles River Motel 1800 Soldiers' Field Rd., Brighton, MA 02135 (617) 254-0200	55	65
Holiday Inn 30 Washington St., Somerville, MA 02143 (617) 628-1000	80-88	87-95
Howard Johnson's Motel 777 Memorial Dr., Cambridge, MA 02138 (617) 492-7777	79	89
Hyatt Regency Hotel 575 Memorial Dr., Cambridge, MA 02139 (617) 492-1234	125-165	145-185
Royal Sonesta Hotel 5 Cambridge Pkwy., Cambridge, MA 02142 (617) 491-3600	79-89	79-89

Pre-Registration and Housing Request

NAME _____ Date _____

Address _____

_____

Phone _____

Expected time of arrival _____

Departure date _____

Housing in Hastings Hall is desired for the nights of August 18 ___ , 19 ___, 20 ___ . Housing may be fully prepaid, but a deposit for a minimum of one night ($25.00) is required to secure a room.

On-Campus parking is requested for _____ (1, 2, or 3) days. Enclosed is (3, 6, or 9 dollars) to prepay parking. (Prepayment is optional).

The registration fee of $ _____ is enclosed.

Checks should be made payable to Harvard University.

Pre-registration, housing requests and deposits, parking requests, and registration fees should be sent to:

Society for Mathematical Psychology
Attn: Ray Estes
William James Hall
33 Kirkland St.
Cambridge, MA 02138

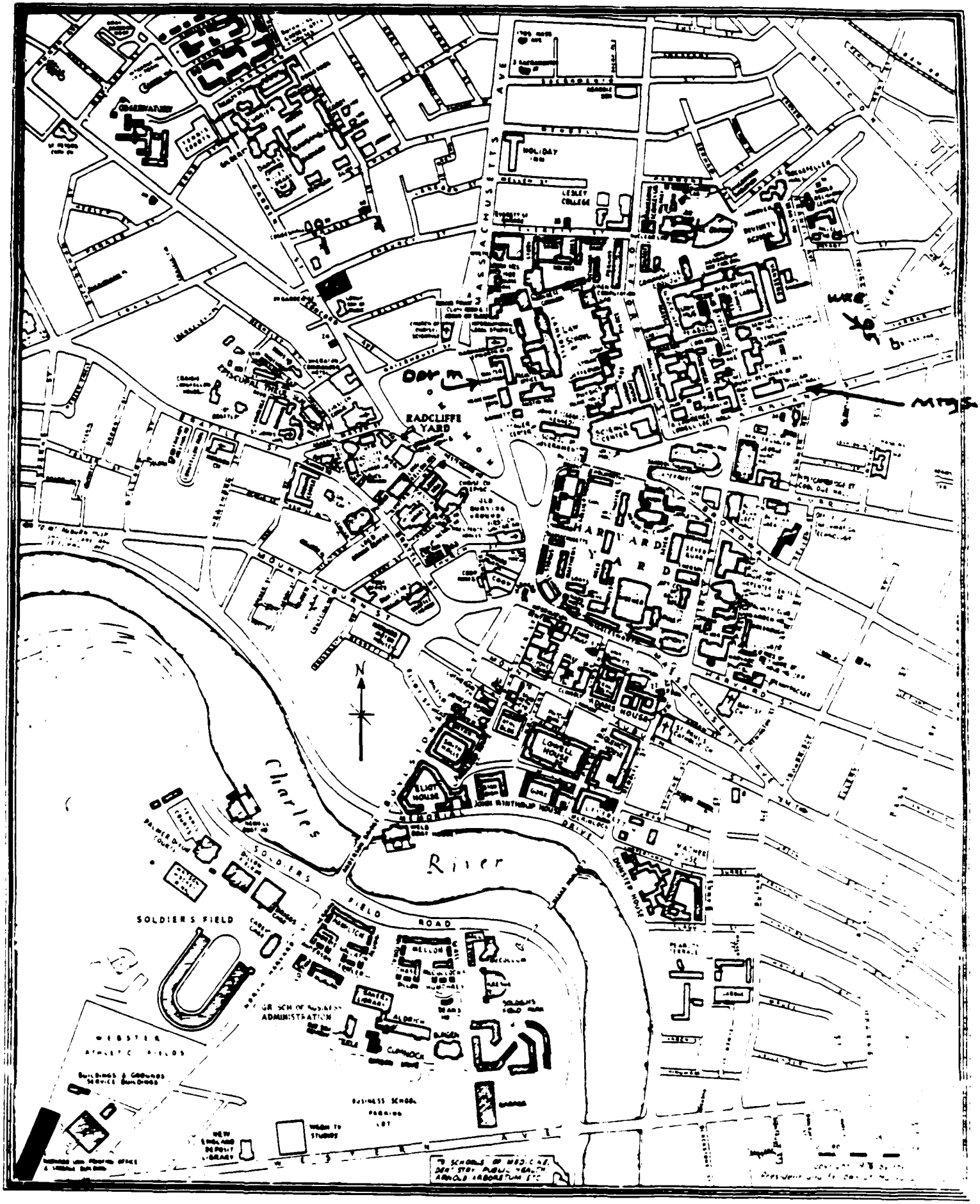
RADCLIFFE YARD
HARVARD YARD
Charles River
SOLDIERS FIELD
SOLDIERS FIELD ROAD
WEBSTER ATHLETIC FIELDS
ELIOT HOUSE
LOWELL HOUSE
WINTHROP HOUSE
DUNSTER HOUSE
HOLYOKE HOUSE
MEMORIAL DRIVE
MASSACHUSETTS AVE
HOLMES FIELD
BUSINESS SCHOOL PARKING LOT
N

NINETEENTH ANNUAL MATHEMATICAL PSYCHOLOGY MEETING

THE SOCIETY FOR MATHEMATICAL PSYCHOLOGY

August 19, 20, 21, 1986

William James Hall
Harvard University
33 Kirkland St.
Cambridge, MA

Program Committee:
W. K. Estes
R. Duncan Luce
Richard G. Swensson

MONDAY EVENING
AUGUST 18

7:30 to 10:00 p.m. RECEPTION Hastings Hall, Harvard Law School. (Common Room)

TUESDAY MORNING
AUGUST 19

8:30 a.m. REGISTRATION
William James Hall, Lobby

COGNITION I
William James I

Chair: **Richard A. Chechile**, Tufts University

9:00 a.m. J. W. Whitlow, Jr., Rutgers University
Evolution of associative memory

9:25 a.m. Nestor A. Schmajuk, Boston University
A Real time model for classical conditioning

9:50 a.m. Gail Carpenter and Stephen Grossberg, Boston University. *Neural dynamics of adaptive pattern recognition and category learning*

10:15 a.m. Robert M. Nosofsky, Indiana University
Rules and exemplars in identification categorization and recognition

PSYCHOPHYSICS
William James 105

Chair: **Jean Claude Falmagne**, New York University

9:00 a.m. William F. Dawson and Carole Havens, University of Notre Dame. *Regression reduction and individual differences in power functions*

9:25 a.m. Stephen Link, McMaster University
Differences between comparing numerals and comparing distances

9:50 a.m. D. E. Robinson and B. G. Berg, Indiana University. *A partitioned variance model for multiple observations*

10:15 a.m. Richard G. Swensson and Philip E. Judy, Harvard Medical School and Brigham and Women's Hospital. *Sex discrimination and ring detection on noisy images: the same task?*

10:40 to 11:00 a.m. Coffee Break

11:00 a.m. **INVITED ADDRESS**
William James I

Chair: **W. K. Estes**, *Harvard University*

Speaker: Scott Weinstein, University of Pennsylvania. *Theory of machine inductive inference*

12:00 to 1:30 p.m. LUNCH BREAK

TUESDAY AFTERNOON

SYMPOSIUM
NEURAL MODELS OF SENSORY-MOTOR CONTROL I
William James I

Chair: **Daniel Bullock**, Boston University

1:30 p.m. **David Robinson**, Johns Hopkins University. *Limit cycle oscillations in the human smooth pursuit system*

2:10 p.m. **Lance Optican**, National Institutes of Health. *Adaptive suppression of post saccadic ocular drift*

2:50 to 3:10 p.m. Coffee Break

3:10 p.m. **Stephen Grossberg**, Boston University. *Neural dynamics of adaptive sensory motor control: Ballistic eye movements*

3:50 p.m. **Barry Peterson**, Northwestern University. *Sensory motor transformations in cerebellar motor and neck motor systems*

4:40 p.m. DISCUSSION

DECISION AND CHOICE I
William James 105

Chair: **Elke Weber**, University of Illinois

1:30 p.m. **Barbara Mellers** and **Elizabeth Hartka**, University of California, Berkeley. *Models of four selection decisions*

1:55 p.m. **Mary Kay Stevenson**, Purdue University. *Discounting models of decisions with delayed consequences*

2:20 p.m. **Soonmook Lee**, Ohio State University. *Beyond individual: Beyond axioms or decision analysis*

2:45 p.m. **Michael H. Birnbaum**, California State University, Fullerton and **Carolyn Anderson** and **Linda Hynan**, University of Illinois Champaign-Urbana. *Theories of intuitive probability*

3:10 to 3:30 p.m. Coffee Break

MEASUREMENT AND STATISTICS I
William James 105

Chair: **Louis Narens,** University of California, Irvine

3:30 p.m. **Geoffrey J. Iverson,** Northwestern University — *An ordinal generalization of analysis of variance*

3:55 p.m. **R. Duncan Luce,** Harvard University — *General structures that map into the system of physical measurement*

4:20 p.m. **James T. Townsend,** Purdue University — *Comparison of distributions and use in experiment theory inference*

4:45 p.m. **Hubert Thomas,** The Pennsylvania State University — *On the "file drawer" problem*

TUESDAY EVENING
AUGUST 19

6:00 to 7:30 p.m. RECEPTION/COCKTAIL PARTY
Wick Estes Home, 95 Irving St.

WEDNESDAY MORNING
AUGUST 20

SYMPOSIUM
NEURAL MODELS OF SENSORY-MOTOR CONTROL II
William James I

Chair: **Stephen Grossberg,** Boston University

9:00 a.m. **John Hollerbach,** Massachusetts Institute of Technology — *Dedicating planning variables from experimental arm trajectories: Pitfalls and possibilities*

9:30 a.m. **Daniel Bullock,** Boston University and University of Denver — *Neural dynamics of planned arm movements: Invariants, synergies, and trajectory formation*

10:20 a.m. **Scott Kelso** and **Gregor Schöner,** Florida Atlantic University — *Exergetic and stochastic treatment of nonequilibrium phase transitions in movement*

11:00 a.m. **Michael Arbib,** University of Massachusetts at Amherst — *Visual control of approach and avoidance behavior*

11:30 a.m. DISCUSSION

COGNITION II
William James 105

Chair: **Alice F. Healy,** University of Colorado

9:00 a.m. **David M. Rieder,** California State University at San Bernardino — *Lexical retrieval analysis of retroactive inhibition*

9:25 a.m. **Stephen C. Hittle,** State University of New York at Albany — *The topology of free recall*

9:50 a.m. **Scott D. Gronlund** and **Richard M. Shiffrin,** Indiana University — *A model of sentence memory*

10:15 a.m. **Steven Clark** and **Richard M. Shiffrin,** Indiana University — *Familiarity and recall supplemented models of recognition*

10:40 to 11:00 a.m. Coffee Break

11:00 a.m. **Elke U. Weber,** University of Illinois, Champaign-Urbana — *Matrix vs convolution correlation models of distributed memory*

11:25 a.m. **Bennet B. Murdock, Jr.,** University of Toronto — *Probabilistic encoding and learning in a distributed memory model*

11:50 a.m. **John Hogden** and **Earl Hunt,** University of Washington — *Theorems on parallel learning systems*

12:15 to 1:30 p.m. LUNCH BREAK

WEDNESDAY AFTERNOON

DECISION AND CHOICE II
William James I

Chair: **Gail Carpenter,** Boston University

1:30 p.m. **John Rotondo,** AT&T Bell Laboratories — *A generalization of Luce's choice axiom and a new class of choice models*

1:55 p.m. **Jerome R. Busemeyer,** Purdue University — *Restle and Tversky choice processes are empirically distinguishable*

2:20 p.m. **Stephen Grossberg,** Boston University and **William E. Gutowski,** Merrimack College — *The neural dynamics of decision making under risk*

2:45 p.m. **Shawn P. Curley,** University of Michigan — *Testing descriptive polynomial models of choice under ambiguity*

3:10 p.m. **Robert L. Stout,** Butler Hospital — *A decision theoretic approach to longitudinal behavior monitoring*

PERCEPTION
William James 105

Chair: **Richard G. Swensson,** Harvard Medical School

1:30 p.m. **Laurence T. Maloney,** University of Michigan and **Ewart A.C. Thomas,** Stanford University — *Distributional assumptions and conservatism in signal detection*

1:55 p.m. **Michael A. Zagorski,** Memorial University of Newfoundland — *A representation and machine model of mini foveal form perception*

2:20 p.m. **Tarow Indow,** University of California, Irvine — *Problems in spatial representation of colors*

2:45 p.m. **Thaddeus M. Cowan,** Kansas State University — *Inferences about geometric designs*

3:10 p.m. **Jonathan Doner,** University of Virginia — *An organizational approach to perceptual modelling*

3:35 to 4:00 p.m. Coffee Break

4:00 p.m. **INVITED ADDRESS**
William James I

Chair: **R. Duncan Luce,** Harvard University

Speaker: William J. McGill, University of California, San Diego — *Gnats gnawing at the foundations of signal detection theory, or retreat from gnosis*

5:30 p.m. **BUSINESS MEETING**
William James I

Chair: **James T. Townsend,** Purdue University

THURSDAY MORNING
AUGUST 21

MEASUREMENT AND STATISTICS II
William James 105

Chair: **Geoffrey Iverson,** Northwestern University

9:00 a.m. **William H. Batchelder,** University of California, Irvine — *New results on test theory without an answer key*

9:25 a.m. **William Stout,** University of Illinois, Urbana/Champaign — *A nonparametric approach for assessing latent trait unidimensionality*

9:50 a.m. **David J. Weiss,** California State University, Los Angeles — *Coping with nonrandom dropout*

10:15 a.m. **Hei-Ki-Dong,** Ball Foundation — *Ridge constants and maximum likelihood estimation in common factor analysis*

10:40 to 11:00 a.m. Coffee Break

11:00 a.m. **Louis Narens,** University of California, Irvine — *Approaches to meaningfulness*

11:25 a.m. **J.-M. Bernard** and **H. Rouanet,** Groupe Mathématiques et Psychologie, Sorbonne — *Bayesian analysis of sequential categorical data*

11:50 a.m. **M.-P. Lecoutre** and **H. Rouanet,** Groupe Mathématiques et Psychologie, Sorbonne — *Probabilistic judgements in situations of statistical prediction*

COGNITION III
William James I

Chair: **Robert L. Stout,** Butler Hospital

9:00 a.m. **Raul Zwick** and **Thomas Wallsten,** University of North Carolina at Chapel Hill — *Breaking the language barrier: Talking about linguistically expressed probabilities*

9:25 a.m. **Timothy P. McNamara,** Vanderbilt University and **Alice F. Healy,** University of Colorado — *Mediated priming in reading and lexical decisions*

9:50 a.m. **Carol Krumhansl** and **Mark A. Schmuckler,** Cornell University — *Key finding in music: An algorithm based on pattern matching to tonal hierarchies*

10:15 a.m. **Richard A. Chechile,** Tufts University — *The syntactic recognition hypothesis*

10:40 to 11:00 a.m. Coffee Break

11:00 a.m. **Richard Schweickert,** Purdue University — *The rectangle condition: A test of simple partial output models*

11:25 a.m. **Donald L. Fisher,** University of Massachusetts at Amherst — *Programmable perceptions: Serial and parallel visual search*

11:50 a.m. **John M. Miyamoto** and **Emily Dibble,** University of Washington — *Conjunction and disjunction errors in counterfactual reasoning*

12:15 to 1:30 p.m. LUNCH BREAK

THURSDAY AFTERNOON

SYMPOSIUM
PARALLEL MECHANISMS IN COGNITIVE PROCESSES
William James I

Chair: **James L. McClelland,** Carnegie Mellon University

1:30 p.m. **James L. McClelland** – *Introductory remarks*

1:40 p.m. **Alan Kawamoto,** Carnegie Mellon University — *Interactive processes in lexical ambiguity resolution*

2:10 p.m. **Gary Cottrell,** University of California, San Diego — *A connectionist model of case role assignment*

2:40 p.m. **Gregory Stone,** Arizona State University — *A distributed model of priming effects*

3:10 p.m. **Michael Jordan,** University of Massachusetts — *Parallel models of production processes*

NEURAL DYNAMICS OF PLANNED ARM MOVEMENTS: EMERGENT INVARIANTS AND SPEED-ACCURACY PROPERTIES DURING TRAJECTORY FORMATION

by

Daniel Bullock†
Center for Adaptive Systems
Department of Mathematics
Boston University
Boston, Massachusetts 02215

and

Stephen Grossberg‡
Center for Adaptive Systems
Department of Mathematics
Boston University
Boston, Massachusetts 02215

September, 1986

† Supported in part by the National Science Foundation (NSF IST-84-17756).

‡ Supported in part by the Air Force Office of Scientific Research (AFOSR 85-0149 and AFOSR F49620-86-C-0037) and the National Science Foundation (NSF IST-84-17756).

Acknowledgements: We wish to thank Carol Yanakakis and Cynthia Suchta for their valuable assistance in the preparation of the manuscript and illustrations.

TABLE OF CONTENTS

ABSTRACT

A real-time neural network model, called the Vector Integration to Endpoint, or VITE, Model, is developed and used to quantitatively simulate behavioral and neural data about planned and passive arm movements. Invariants of arm movements emerge through network interactions rather than through an explicitly precomputed trajectory. Motor planning occurs in the form of a Target Position Command, or TPC, which specifies where the arm intends to move, and an independently controlled GO command, which specifies the movement's overall speed. Automatic processes convert this information into an arm trajectory with invariant properties. These automatic processes include computation of a Present Position Command, or PPC, and a Difference Vector, or DV. The DV is the difference of the PPC and the TPC at any time. The PPC is gradually updated by integrating the DV through time. The GO signal multiplies the DV before it is integrated by the PPC. The PPC generates an outflow movement command to its target muscle groups. Opponent interactions regulate the PPC's to agonist and antagonist muscle groups. This system generates synchronous movements across synergetic muscles by automatically compensating for the different total contractions that each muscle group must undergo. Quantitative simulations are provided of the speed-accuracy trade-off known as Woodworth's Law, of Fitts' Law, of isotonic arm movement properties before and after deafferentation, of synchronous and "central error correction" compensatory properties of isometric contractions, of velocity amplification during target switching, of velocity profile invariance and asymmetry, of the symmetrization of velocity profiles at higher movement speeds, of the automatic compensation for staggered onset times of synergetic muscles, of vector cell properties in precentral motor cortex, of the inverse relationship between movement duration and peak velocity, and of peak acceleration as a function of movement amplitude and duration. It is shown that TPC, PPC, and DV computations are needed to actively modulate, or gate, the learning of associative maps between TPC's of different

modalities, such as between the eye-hand system and the hand-arm system. By using such an associative map, looking at an object can activate a TPC of the hand-arm system, as Piaget noted. Then a VITE circuit can translate this TPC into an invariant movement trajectory. An auxiliary circuit, called the Passive Update of Position, or PUP, Model, is described for using inflow signals to update the PPC during passive arm movements due to external forces. Other uses of outflow and inflow signals are also noted, such as for adaptive linearization of a nonlinear muscle plant, and sequential read-out of TPC's during a serial plan, as in reaching and grasping. Comparisons are made with other models of motor control, such as the mass-spring and minimum-jerk models.

1. Introduction: Are Movement Invariants Explicitly Planned?

The subjective ease with which we carry out simple action plans—rotating a wrist-watch into view, lifting a coffee cup, or making a downstroke while writing—masks the enormously complex integrative apparatus needed to achieve and maintain coordination among the thousands of sensors, neurons, and skeleto-motor units that contribute to any act's planning and execution. Moreover, recent studies of the kinematics of planned arm movements (Abend, *et al.*, 1982; Atkeson and Hollerbach, 1985; Howarth and Beggs, 1981) have shown that the integrative action of all these separate contributors produces velocity profiles whose global shape is remarkably invariant over a wide range of movement sizes and speeds. This raises a fundamental question for the theory of sensory-motor control, and for the neurosciences in general: How can the integrated activity of thousands of separate elements produce globally invariant properties?

Two broad species of answers to this question can be contemplated. The first includes theories that posit the existence of a high level stage involving explicit computation and internal representation of the invariant, in this case the velocity profile, as a whole. This representation is then used as a basis for performing the desired action. Such theories have been favored recently by many workers in the field of robotics, and at least one theory of this type has already been partially formulated to accommodate kinematic data on human movements: the "minimized Cartesian jerk theory" (Hogan, 1984; Flash and Hogan, 1985), which is a special case of global optimization analysis. The second species of answers includes theories in which no need arises for explicit computation and representation of the invariant trajectory as a whole. In models associated with such theories, a trajectory with globally invariant properties emerges in real-time as the result of events distributed across many interacting sensory, neural, and muscular loci.

This article describes a theory of arm trajectory invariants that conforms to the latter ideal (Bullock and Grossberg, 1986a). Our analysis suggests that trajectory invariants are best understood not by focusing on velocity profiles as such, but by pursuing more

fundamental questions: What principles of adaptive behavioral organization constrain the system design that governs planned arm movements? What mechanisms are needed to realize these principles as a real-time neural network? Our development of this topic proceeds via analyses of learned eye-hand coordination, synchronization among synergists, intermediate position control during movement, and variable velocity control. These analyses disclose a neural network design whose qualitative and quantitative operating characteristics match those observed in a wide range of experiments on human movement. Because velocity profile invariance, including the observed velocity asymmetry ignored by prior models, is among the neural network's emergent operating characteristics, our work shows that neither an explicit trajectory nor a kinematic invariant need be explicitly represented within a motor control system at any time. Thus our work supports a critical insight of workers in the mass-spring modeling tradition that movement kinematics need not be explicitly pre-programmed. By the same token, our results reject a mass-spring model in its customary form and argue against models based upon optimization theory. Instead we show how a movement control system may be adaptive without necessarily optimizing an explicit cost function.

To further support these conclusions, we use the neural model to quantitatively simulate Woodworth's Law and Fitts' Law, the empirically derived speed-accuracy tradeoff function relating error magnitudes, movement distances and movement durations; isotonic arm movement properties before and after deafferentation (Bizzi, Accornero, Chapple, and Hogan, 1982, 1984; Evarts and Fromm, 1978; Polit and Bizzi, 1978); synchronous and compensatory "central error correction" properties of isometric contractions (Freund and Büdingen, 1978; Ghez and Vicario, 1978; Gordon and Ghez, 1984, 1986a, 1986b.); velocity amplification during target switching (Georgopoulos, Kalaska, and Massey, 1981); velocity profile invariance and asymmetry (Abend, Bizzi, and Morasso, 1982; Atkeson and Hollerbach, 1985; Georgopoulos, Kalaska, and Massey, 1981; Beggs and Howarth, 1972; Morasso, 1981; Soechting and Lacquaniti, 1981); the symmetrization of velocity profiles

at higher movement speeds (Beggs and Howarth, 1972); vector cell properties in precentral motor cortex (Evarts and Tanji, 1974; Georgopoulos, Kalaska, Caminiti, and Massey, 1982; Georgopoulos, Kalaska, Crutcher, Caminiti, and Massey, 1984; Kalaska, Caminiti, and Georgopoulos, 1983; Tanji and Evarts, 1976); the inverse relationship between movement duration and peak velocity (Lestienne, 1979); and peak acceleration as a function of movement amplitude and time (Bizzi, Accornero, Chapple, and Hogan, 1984). In addition, the work reported here extends a broader program of research on adaptive sensory-motor control (Grossberg, 1978, 1986a, 1986b; Grossberg and Kuperstein, 1986), which enables functional and mechanistic comparisons to be made between the neural systems governing arm and eye movements, suggests how eye-hand coordination is accomplished, and provides a foundation for work on mechanisms of trajectory realization which compensate for the kinematical properties generated by variable loads and movement velocities (Bullock and Grossberg, 1986b).

2. Flexible Organization of Muscle Groups into Synergies

In order to move a part of the body, whether an eye, head, arm, or leg, many muscles must work together. For example, muscles controlling several different joints—shoulder, elbow, wrist, and fingers—may contract or relax cooperatively in order to perform a reaching movement. When groups of muscles cooperate in this way, they are said to form a synergy (Bernstein, 1967; Kelso, 1982).

Muscle groups may be incorporated into synergies in a flexible and dynamic fashion. Whereas muscles controlling shoulder, elbow, wrist, and fingers may all contract or relax synergetically to produce a reaching movement, muscles of the fingers and wrist may form a synergy to perform a grasping movement. Thus, one synergy may activate shoulder, elbow, wrist, and finger muscles to reach towards an object, and another synergy may then activate only finger and wrist muscles to grasp the object while maintaining postural control over the shoulder and elbow muscles. Groups of fingers may move together synergetically to

play a chord on the piano, or separate fingers may be successively activated in order to play arpeggios.

One of the basic problems of motor control is to understand how neural control structures quickly and flexibly reorganize the set of muscle groups that are needed to synergetically cooperate in the next movement sequence. Once one squarely faces the problem that many behaviorally important synergies are not hard-wired, but are rather dynamically coupled and decoupled through time in ways that depend upon the actor's experience and training, the prospect that the trajectories of all synergists are explicitly preplanned seems remote at best.

3. Synchronous Movement of Synergies

When neural commands organize a group of muscles into a synergy, the action of these muscles often occurs synchronously through time. It is partly for this reason that the complexity of the neural commands controlling many movements often goes unnoticed. These movements seem to occur in a single gesture, rather than as the sum of many asynchronous components.

Figure 1

In order to understand the type of control problem that must be solved to generate synchronous movement, consider a typical arm movement of reaching forward and across the body midline with the right hand in a plane parallel to the ground. Suppose for simplicity that the synergist acting at the shoulder is responsible for across-midline motion, that the synergist acting at the elbow is responsible for forward motion, and that the hand is to be moved from points B1, B2, or B3 to point E. Figure 1 illustrates the effects of two distinct control schemes that might be used to produce these three movements. In the first scheme, the two synergists begin their contractions synchronously, contract at the same rate, and cease contracting when their respective motion component is complete. This typically results in asynchronous contraction terminations, and in bent-line movements.

because the synergist responsible for the longer motion component takes longer to complete its contribution. With this scheme, approximately straight-line motions and synchronous contraction terminations occur only in cases like the B2-E movement, for which the component motions happen to be of equal length. In the second scheme, the two synergists contract, not at equal rates, but at rates that have been adjusted to compensate for any differences in length of the component motions. This results in synchronous contraction terminations. Normal arm movement paths are similar to those implied by the second control scheme (e.g., Morasso, 1981) and experimental studies (Freund and Büdingen, 1978) have shown that contraction rates are made unequal in a way that compensates for inequalities of distance.

What types of adaptive problems are solved by synchronization of synergists? Figure 1 provides some insight into this issue. Without synchronization, the direction of the first part of the movement path may change abruptly several times before the direction of the last part of the movement path is generated (Figure 1). This creates a problem because transporting an object from one place to another with the arm may destabilize the body unless one can predict, and anticipatorily compensate for, the arm movement's destabilizing effects, which are always directional. In the same way, many actions require that forces be applied to surfaces in particular directions. The first control scheme makes the direction in which force is applied difficult to predict and control. Both of these problems are eliminated by the approximately straight-line movement paths which become possible when synergists contract synchronously. Finally, if the various motions composing a movement failed to end synchronously, it would become difficult to ensure smooth transitions between sequentially ordered movements.

In summary, the untoward effects of asynchrony place strong constraints on the mechanisms of movement control: Across the set of muscles whose synergistic action produces a multi-joint movement, contraction durations must be roughly equal, and, because contraction distances are typically unequal, contraction rates must be made unequal in a way

that compensates for inequalities of distance.

4. Factoring Target Position and Velocity Control

Inequalities of distance are translated into neural commands as differences in the total amounts of contraction by the muscles forming the synergy, and thereby into mechanical terms as the total amounts of change in the angles between joints (Hollerbach, Moore, and Atkeson, 1986). In order to compensate for differences in contraction, information must be available that is sufficient to compute the total amounts of contraction that are required. Thus a representation of the initial contraction level of each muscle must be compared with a representation of the target, expected, or final contraction level of the muscle. A primary goal of this article is to specify how this comparison is made. Although information about target position and initial position are both needed to control the total contraction of a muscle group, these two types of information are computed and updated in different ways, a fact that we believe has caused much confusion about whether only target position needs to be coded (Section 7).

Another source of confusion has arisen because target position information is needed to form a trajectory. This is the type of information which invites concepts of motor planning and expectation. However tempting it may be to so infer, concepts of motor planning and expectation do *not* imply that the *whole trajectory* is *explicitly* planned.

A second aspect of planning enters into trajectory formation which also does not imply the existence of explicit trajectory planning. This aspect is noticed by considering that the hand-arm system can be moved between fixed intital and target positions at many different velocities. When, as a result of a changed velocity, the overall movement duration changes, the component motions occurring around the various joints must nonetheless remain synchronous. Since fixed differences in initial and target positions can be converted into synchronous motions at a wide range of velocities, there must exist an independently controlled velocity, or GO signal (Section 11). The independent control of target position

commands and velocity commands is a special case of a general neural design which has been called the *factorization of pattern and energy* (Grossberg, 1978, 1982).

5. Synchrony versus Fitts' Law: The Need for a Neural Analysis of Synergy Formation

Our discussion of synchronous performance of synergies has thus far emphasized that different muscles of the hand-arm system may need to contract by different amounts in equal time in order to move a hand through a fixed distance. When movement of a hand over different distances is considered, a striking contrast between behavioral and neural properties of movement becomes evident. This difference emphasizes that synergies are assembled and disassembled through time in a flexible and dynamic way.

Fitts' Law (Fitts, 1954; Fitts and Peterson, 1964) states that movement time (MT) of the arm is related to distance moved (D) and to width of target (W) by the equation

$$MT = a + b\log_2(\frac{2D}{W}), \tag{1}$$

where a and b are empirically derived constants. Keele (1981) has reviewed a variety of experiments showing that Fitts' Law is remarkably well obeyed despite its simplicity. For example, the law describes movement time for linear arm movements (Fitts, 1954), rotary movements of the wrist (Knight and Dagnall, (1967), back-and-forth movements like dart throwing (Kerr and Langolf, 1977), head movements (Jagacinski and Monk, 1985), movements of young and old people (Welford, Norris, and Schock, 1969), and movements of monkeys as well as humans (Brooks, 1979).

Equation (1) asserts that movement time (MT) increases as the logarithm of distance (D) moved, other things being equal. The width parameter W in (1) is interpreted as a measure of movement accuracy (Section 27). Although movement distance and time may covary on the behavioral level that describes the aggregate effect of many muscle contractions, such a relationship does not necessarily hold on the neural level, where individual

muscles may contract by variable amounts, or "distances", in order to achieve synchronous contraction within a constant movement time.

A fundamental issue is raised by this comparison of behavioral and neural constraints. This issue can be better understood through consideration of the following gedanken example. When each of two fingers is moved separately through different distances, each finger may separately obey Fitts' Law. Then the finger which moves a larger distance should take more time to move, other things being equal. In contrast, when the two fingers move the above distances as part of a single synergy, then each finger should complete its movement in the same time in order to guarantee synergetic synchrony. Thus either one of the fingers must violate Fitts' Law, or it must reach its target with a different level of accuracy. Kelso, Southard, and Goodman (1979) and Marteniuk and MacKenzie (1980) have experimentally studied this type of synchronous behavior, and have documented within-synergy violations of Fitts' Law.

Such examples suggest that Fitts' Law holds for the aggregate behavior of the largest collection of motor units which form a synergy during a given time interval. Fitts' Law need not hold for all subsets of the motor units which comprise a synergy. These subsets may, in principle, violate Fitts' Law by travelling variable distances in equal time in order to achieve synchrony of the aggregate movement. To understand how Fitts' Law can be reconciled with movement synchrony thus requires an analysis of the neural control mechanisms which flexibly bind muscle groups, such as those controlling different fingers, into a single motor synergy. If such a binding action does not involve explicit planning of a complete trajectory, yet does require activation of a target position command and a GO command, then neural machinery must exist which is capable of *automatically* coverting such commands into complete trajectories with synchronous and invariant properties. One of the primary tasks of this article is to describe the circuit design of this neural machinery and to explain how it works.

6. Some General Issues in Sensory-Motor Planning: Multiple Uses of Outflow versus Inflow Signals

Before beginning a mechanistic analysis of these circuits, we summarize several general issues about motor planning to place the model developed in this article within a broader conceptual framework. In Sections 8–13 and 27–29, a number of key experiments are reviewed to more sharply constrain the theoretical analysis. In Sections 21–28 computer simulations of these data properties are reported.

Figure 2

Neural circuitry automates the production of skilled movements in several mechanistically distinct ways. Perhaps the most general observation is that animals and humans perform marvelously dexterous acts in a world governed by Newton's Laws, yet can go through life without ever learning Newton's Laws, and indeed may have a great deal of difficulty learning them when they try. The phenomenal world of movements is a world governed by motor plans and intentions, rather than by kinematic and inertial laws. A major challenge to theories of biological movement control is to explain how we move so well within a world whose laws we may so poorly understand.

The computation of a hand or arm's present position illustrates the complexity of this problem. Two general types of present position signals have been identified in discussions of motor control: *outflow* signals and *inflow* signals. Figure 2 schematizes the difference between these signal sources. An outflow signal carries a movement command from the brain to a muscle (Figure 2a). Signals that branch off from the efferent brain-to-muscle pathway in order to register present position signals are called *corollary discharges* (Helmholtz, 1866; von Holst and Mittelstaedt, 1950). An *inflow* signal carries present position information from a muscle to the brain (Figure 2b). A primary difference between outflow and inflow is that a change in outflow signals is triggered only when an observer's brain generates a new movement command. A new inflow signal can, in contrast, be generated

by passive movements of the limb. Evidence for influences of both outflow (Helmholtz, 1866) and inflow (Ruffini, 1898; Sherrington, 1894) has accumulated over the past century. Disentangling the different roles played by outflow and inflow signals has remained one of the major problems in motor control. This is a confusing issue because both outflow and inflow signals are used in multiple ways to provide different types of information about present position. The following summary itemizes some of the ways in which these signals are used in our theory.

Although one role of an outflow signal is to move a limb by contracting its target muscles, the laws which govern the muscle plant are not known *a priori* to the outflow source. It is therefore not known *a priori* how much the muscle will actually contract in response to an outflow signal of prescribed size. It is also not known how much the limb will move in response to a prescribed muscle contraction. In addition, even if the outflow system somehow possessed this information at one time, it might turn out to be the wrong information at a later time, because muscle plant characteristics can change through time due to development, aging, exercise, changes in blood supply, or minor tears. Thus the relationship between the size of an outflow movement command and the amount of muscle contraction is, in principle, undeterminable without additional information which characterizes the muscle plant's actual response to outflow signals.

To establish a satisfactory correspondence between outflow movement signals and actual muscle contractions, the motor system needs to compute reliable present position signals which represent where the outflow command tells the muscle to move, as well as reliable present position signals which represent the state of contraction of the muscle. Corollary discharges and inflow signals can provide these different types of information. Grossberg and Kuperstein (1986) have shown how a comparison, or match, between corollary discharges and inflow signals can be used to modify, through an automatic learning process, the total outflow signal to the muscle in a way that effectively compensates for changes in the muscle plant. Such automatic gain control produces a linear correspon-

dence between an outflow movement command and the amount of muscle contraction even if the muscle plant is nonlinear. The process which matches outflow and inflow signals to linearize the muscle plant response through learning is called *adaptive linearization* of the muscle plant. The cerebellum is implicated by both the theoretically derived circuit and experimental evidence as the site of learning.

Given that corollary discharges are matched with inflow signals to linearize the relationship between muscle plant contraction and outflow signal size, outflow signals can also be used in yet other ways to provide information about present position. In Sections 17–23, it is shown how outflow signals are matched with target position signals to generate a trajectory with synchronous and invariant properties. Thus outflow signals are used in at least three ways, and all of these ways are automatically registered: They send movement signals to target muscles; they generate corollary discharges which are matched with inflow signals to guarantee linear muscle contractions even if the muscle plant is nonlinear; and they generate corollary discharges which are matched with target position signals to generate synchronous trajectories with invariant properties.

Inflow signals are also used in several ways. One way has already been itemized. A second use of inflow signals is suggested by the following gedanken example. When you are sitting in an armchair, let your hands drop passively towards your sides. Depending upon a multitude of accidental factors, your hands and arms can end up in any of infinitely many final positions. If you are then called upon to make a precise movement with your arm-hand system, this can be done with the usual exquisite accuracy. Thus the fact that your hands and arms start out this movement from an initial position which was not reached under active control by an outflow signal does not impair the accuracy of the movement.

A wealth of evidence suggests, however, that comparison between target position and present position information is used to move the arms. Moreover, as will be shown below, this present position information is computed from outflow signals. In contrast, during the passive fall of an arm under the influence of gravity, changes in outflow signal commands

are not responsible for the changes in position of the limb. This observation identifies the key issue: How is the outflow signal updated due to passive movement of a limb so that the next active movement can accurately be made? Since the final position of a passively falling limb cannot be predicted in advance, it is clear that inflow signals must be used to update present position when an arm is moved passively by an external force.

This conclusion calls attention to a closely related issue that must be dealt with to understand the neural bases of skilled movement: How does the motor system know that the arm is being moved passively due to an external force, and not actively due to a changing outflow command? Such a distinction is needed to prevent inflow information from contaminating outflow commands when the arm is being actively moved. The motor system must use internally generated signals to make the distinction between active movement and passive movement, or postural, conditions. Computational gates must be open and shut based upon whether these internally generated signals are on or off (Grossberg and Kuperstein, 1986).

A third role for inflow signals is needed due to the fact that arms can move at variable velocities while carrying variable loads. Because an arm is a mechanical system embedded in a Newtonian world, an arm can generate unexpected amounts of inertia and acceleration when it tries to move novel loads at novel velocities. During such a novel motion, the commanded outflow position of the arm and its actual position may significantly diverge. Inflow signals are needed to compute mismatches leading to partial compensation for this uncontrolled component of the movement.

Such novel movements are quite different from our movements when we pick up a familiar fountain pen or briefcase. When the object is familiar, we can predictively adjust the gain of the movement to compensate for the expected mass of the object. This type of automatic gain control can, moreover, be flexibly switched on and off using signal pathways that can be activated by visual recognition of a familiar object. Inflow signals are used in the learning process which enables such automatic gain control signals to be activated in

an anticipatory fashion in response to familiar objects (Bullock and Grossberg, 1986b).

This listing of multiple uses for outflow and inflow signals invites comparison between how the arm movement system and other movement systems use outflow and inflow signals. Grossberg and Kuperstein (1986) have identified and suggested neural circuit solutions to analogous problems of sensory-motor control within the specialized domain of the saccadic eye movement system. Several of the problems to which we will suggest circuit solutions in our articles on arm movements have analogs with the saccadic circuits developed by Grossberg and Kuperstein (1986). Together these investigations suggest that several movement systems contain neural circuits that solve similar general problems. Differences between these circuits can be traced to functional specializations in the way these movement systems solve their shared problems of movement.

For example, whereas saccades are ballistic movements, arm movements can be made under both continuous and ballistic control. Whereas the eyes normally come to rest in a head-centered position, the arms can come to rest in any of infinitely many positions. Whereas the eyes are typically not subjected to unexpected or variable external loads, the arms are routinely subjected to such loads. Whereas the eyes typically generate a stereotyped velocity profile between a fixed pair of initial and target positions, the arms can move with a continuum of velocity profiles between a fixed pair of initial and target positions. Our analyses show how the arm system is specialized to cope with all of these differences between its behaviors and those of the saccadic eye movement system.

7. Neural Control of Arm Position Changes: Beyond the STE Model

A number of further specialized constraints on the mechanisms controlling planned arm movements are clarified by summarizing shortcomings of one of the simplest models of movement generation, namely the Spring-to-Endpoint (STE) Model recommended by many theorists to formalize "mass-spring" properties of movement control (Cooke, 1980; Feldman, 1974; Kelso and Holt, 1980; Sakitt, 1980). As Nichols (1985) has recently ob-

served, many possible models address mass-spring properties of movement. Our criticisms pertain only to the STE Model which is explicitly specified in this section. In particular, no part of our critique denies that the peripheral motor system has mass-spring properties that may be critical to overall motor function. Indeed, in Bullock and Grossberg (1986b), we analyse neural command circuits which exploit mass-spring muscle properties to generate well-controlled movements.

The components of the STE Model for movement control can be summarized as follows. Imagine that the eye fixates some object that lies within reach. To touch the object, it is necessary to move the tip of the index finger from its current position to the target position on the object's nearest surface. The STE Model suggests that this is accomplished by simply replacing the arm position command that specifies the arm's present posture with a new arm position command that specifies the posture the arm would have to assume in order for the index finger to touch the chosen object surface.

Instatement of the new arm position command is suggested to generate the desired movement as follows. The arm is held in any position by balancing the muscular and other forces (e.g., gravity) that are currently acting on the limb. Instatement of a new command changes the pattern of outflow signals that contract the arm muscles. A step change in the pattern of contraction creates a force imbalance that causes the limb to spring in the direction of the larger force at a rate proportional to the force difference. The limb comes to rest when all the forces acting on it are once again balanced. Despite its elegance, the STE Model exhibits several deficiencies which highlight properties that an adequate control system needs to have. We briefly summarize two fundamental problems: (1) confounding of speed and distance control, and (2) inability to quickly terminate movement at an intermediate position.

The first problem, the speed-distance confound, follows from the dependence of movement rate on the force difference, which in turn depends on the distance between the starting and final positions. This might at first seem to be a desirable property, because

it appears to compensate for different distances in the manner needed to ensure synchronization of synergists (Section 3). However, consider also the need to vary the speed of a fixed movement. An actor seeking to perform the same movement at a faster speed would have to follow a two-part movement plan: Early in the movement, instate a virtual target position that is well beyond the desired end point and along a line drawn from the initial through the true target position. This command will create a very large initial force imbalance and launch the limb at a high speed. Then, at some point during the movement, instate the true target position command, and let the arm coast to the final position. This example illustrates that the STE Model requires a complex and neurally implausible scheme for achieving variable speed control for movements of fixed length.

A second problem with the STE Model concerns the critical need to quickly abort an evolving movement and stabilize current arm position. Such a need arises, for example, when an animal wishes to freeze upon detection of a predator who uses motion cues to locate prey. It also arises when an action, such as transporting a large mass, begins to destabilize an animal's overall state of balance. At such times, it is often adaptive to quickly freeze and maintain the current arm position. This is an easy task if the movement command is never much different from the arm's present position. Freezing could then be quickly achieved by preventing further changes in the currently commanded position. In an STE Model, this simple freeze strategy is unavailable, because a large discrepancy exists between present arm position and the target position command throughout much of the trajectory. To implement a freezing response using the STE Model, the system would somehow have to quickly determine and instate a new target position command capable of maintaining the arm's present position. But this is precisely the type of information whose relevance is denied by the STE Model.

8. Gradual Updating of PPC's during Trajectory Formation

Several lines of experimental evidence point to deficiencies of the STE Model. One line

of evidence, due to Bizzi and his colleagues, demonstrates that a type of gradual updating of the movement command occurs which is inconsistent with the STE model. Earlier studies from the Bizzi lab partially supported the STE model.

The experiments of Polit and Bizzi (1978) studied monkeys who were trained to move their forearms, without visual feedback of hand position, from a canonical starting position to the position of one of several lights. The monkeys' arm movements were studied both before and after a dorsal rhizotomy was performed to remove all sensory feedback from the arm. Before deafferentation, the monkey could move its hand to the target's position without visual feedback, even if its accustomed position with respect to the arm apparatus was changed. After deafferentation, so long as the spatial conditions of training were maintained—in particular the canonical starting orientation and position with respect to the known target array—the animal remained able to move its hand to the target position. However, if the initial position of the elbow of the deafferented arm was passively shifted from the position used throughout training, then the animal's forearm movements terminated at a position shifted by an equal amount away from the target position. Thus the movement of the forearm did not compensate for the change in initial position. Instead the same final synergy of forearm-controlling muscles was generated in both cases.

The fact that deafferented monkeys moved to shifted positions emphasized the critical role of the target position command in setting up the movement trajectory. The fact that normal monkeys could compensate for rotation in a way that deafferented monkeys could not indicated an additional role for inflow signals when the arm is moved passively by an external force (Section 29).

The later experiments of Bizzi, Accornero, Chapple, and Hogan (1982, 1984) carried out an additional manipulation. The results of these experiments are inconsistent with the STE assumption that the arm's motion is governed exclusively by the spring-like contraction of its muscles towards the position specified by a new target position command. In these experiments, the monkey was again deprived of visual and inflow feedback, and

placed in its canonical starting position. In addition, its deafferented arm was surreptitiously held at the target position, then released at variable intervals after activation of the target light. Under these circumstances, the arm travelled back towards the canonical starting position, before reversing direction and proceeding to the target. The arm travelled further backward toward the starting position the sooner it was released after target activation. Moreover, when the arm was moved to the target position and then released in the absence of any target presentation, it sprang back to its canonical starting position. Bizzi *et al.* (1984, p.2742) concluded that "the CNS had programmed a slow, gradual shift of the equilibrium point, a fact which is not consistent with the 'final position control' [read STE] hypothesis."

The Bizzi *et al.* (1984) description of their results as a "gradual shift of the equilibrium point" carries the language of the STE Model into a context where it may cause confusion. From a mathematical perspective, the intermediate positions of a movement trajectory are not, by definition, equilibrium points. In order to explicate the Bizzi *et al.* (1984) data, we show how three quantities are computed and updated through time: a target position command (TPC) which is switched on once and for all before the movement; an outflow movement command, called the Present Position Command (PPC), which is continously updated until it matches the TPC; and the arm position which closely corresponds to the PPC.

We call a movement for which a single TPC is switched on before the movement begins an *elementary* movement. Once it is seen how a single TPC can cause gradual updating of the PPC, movements can also be analysed during which a sequence of TPC's is switched on, either under the control of visual feedback or from a movement planning network which can store and release sequences of TPC's from memory with the proper order and timing (Grossberg and Kuperstein, 1986).

Our analysis of how the PPC is gradually updated during an elementary movement partially supports the Bizzi *et al.* (1984) description of a "gradual shift in equilibrium

point" by showing that the arm remains in approximate equilibrium with respect to the PPC, even though none of these intermediate arm positions is an equilibrium point of the system. The only equilibrium point of the system is reached when both the neural control circuit and the arm itself both reach equilibrium. That happens when the PPC matches the TPC, thereby preventing further changes in the present position command and allowing the arm to come to rest.

These conclusions refine, rather than totally contradict, the main insight of the STE Model. Instead of concluding that the arm springs to the position coded by the TPC, we suggest that the spring-like arm tracks the series of positions specified by the PPC as it approaches the TPC. This conception of trajectory formation contrasts sharply with that suggested by Brooks (1986, p.138) in response to the Bizzi data. Brooks inferred that "animals learn not only the end points and their stiffness, but also a series of intermediate equilibrium positions. In other words, they learn an internal 'reference' trajectory that determines the path to be followed and generates torques appropriately to reduce mismatch between the intended and actual events." In a similar fashion, Hollerbach (1982, p.192) suggested that we practice movements to "learn the basic torque profiles." In contrast, we suggest that the read-out of the TPC is learned, but that the gradual updating of the PPC is automatic. A number of auxiliary learning processes are also needed to update the PPC after passive movements due to an external force (Section 30), to adaptively linearize the response of a nonlinear muscle plant (Grossberg and Kuperstein, 1986), and to adaptively compensate for the inertial effects of variable loads and velocities (Bullock and Grossberg, 1986b). These additional learning processes enable the automatic updating of the PPC to generate controllable movements without requiring that the entire trajectory be learned.

9. Duration Invariance during Isotonic Movements and Isometric Contractions

Further information concerning the gradual updating process whereby PPC's match

a TPC can be inferred from the detailed spatiotemporal properties of arm trajectory formation. Freund and Büdingen (1978) have studied "the relationship between the speed of the fastest possible voluntary contractions and their amplitudes for several hand and forearm muscles under both isotonic and isometric conditions. These experiments showed the larger the amplitude, the faster the contraction. The increase of the rate of rise of isometric tension or of the velocity of isotonic movements with rising amplitude was linear. The slope of this relationship was the same for three different hand and forearm muscles examined ... the skeleto-motor speed control system operates by adjusting the velocity of a contraction to its amplitude in such a way that the contraction time remains approximately constant ... this type of speed control is a necessary requirement for the synchrony of synergistic muscle contractions" (p.1).

Figure 3

Two main issues are raised by this study. First, it must be explained why, "comparing isotonic movements and isometric contractions, the time from onset to peak was similar in the two conditions" (p.7). Figure 3 shows the fastest voluntary isometric contractions of the extensor indicis muscle. Second, it must be explained why the force develops gradually in time with the shapes depicted in Figure 3. Concerning this property, Georgopoulos (1986, p.150) has written: "We do not know why this strategy is adopted." Below it is shown that both duration invariance and the force development through time are emergent properties of the PPC-updating process (see Section 22).

10. Compensatory Properties of the PPC Updating Process

Ghez and his colleagues (Ghez and Vicario, 1978; Gordon and Ghez, 1984, 1986a, 1986b) have confirmed the duration invariance reported by Freund and Büdingen (1978) in an isometric paradigm which also disclosed finer properties of the PPC updating process. These authors suggest that "compensatory adjustments add to preprogrammed specification of rapid force impulses to achieve more accurately targeted responses" (Gordon and

Ghez, 1986b).

In their isometric task, subjects were instructed to maintain superposition of two lines on a CRT screen. The experimenter could cause one of the lines to jump to any of three positions. Subjects could exert force on an immobile lever to move the other line towards the target line. Equal increments of force produced equal displacements of the line. Thus more isometric force was needed to move the line over a larger distance to the target line.

Figure 4

Figure 4 defines the major variables of their analysis. The force target is represented by the solid black horizontal line. If the subject performs errorlessly—that is, reaches target without overshoot—the value of the peak force will equal the value of the force target, as in the black curve. Overshoots and undershoots in force are represented by the gray and dashed curves, respectively. Figure 5 plots the data of Gordon and Ghez (1986b) in a way that illustrates duration invariance. The horizontal line through the data points shows that force rise time is essentially independent of peak acceleration ($\frac{d^2F}{dt^2}$) for all the target distances.

Figure 5

Gordon and Ghez (1986b) separately analysed the data for each of the three target distances, and thereby derived the three oblique lines in Figure 5. They interpreted these lines as evidence for an "error correction" process because a negative correlation exists between peak acceleration and the force rise time, or duration. Thus, if the acceleration for a small target distance was too high early in a movement, the trajectory was "corrected" by shortening the rise time. Had this compensation not occurred, the high acceleration could have produced a peak force appropriate for a larger target distance.

Gordon and Ghez (1986b) assumed that trajectories are preplanned and that their peak accelerations are a signature indicating which trajectory has been preplanned. It is from this perspective that they interpreted the compensatory effect shown in Figure

5 as an "error correction" process. In contrast, we suggest in Sections 13 and 21 that this compensatory effect is one of the automatic properties whereby PPC's are gradually updated. We hereby provide an explanation of the compensatory effect that avoids invoking a special mechanism of "error correction" for a movement which does not generate an error in achieving its target. In addition, this explanation provides a unified analysis of the Bizzi *et al.* (1984) data on isotonic movements and the Gordon and Ghez (1986b) data on isometric contractions.

11. Target Switching Experiments: Velocity Amplification, GO Signal, and Fitts' Law

Our explanation of the Freund and Büdingen (1978) and Gordon and Ghez (1986a) data considers how a single GO signal applied to all components of the synergy defined by a TPC can cause duration invariance. Georgopoulos, Kalaska, and Massey (1981) have collected data which provide further evidence for the interaction of a GO signal with the process which instates a TPC and thereby updates the PPC. In their experiments, monkeys were trained to move a lever from a start position to one of eight target positions radially situated on a planar surface. Then the original target position was switched to a new target position at variable delays after initiation of movement towards the first target.

Part of the data confirm the fact that "the aimed motor command is emitted in a continuous, ongoing fashion as a real-time process that can be interrupted at any time by the substitution of the original target by the new one. The effects of this change on the ensuing movement appear promptly, without delays beyond the usual reaction time" (p.725). Figure 6 depicts movement paths found during the target switching condition. We explain these data in terms of how instatement of a second TPC can rapidly modify the future updating of the PPC.

Figure 6

In addition, Georgopoulous *et al.* (1981) found a remarkable amplification of peak

velocity during the switched component of the movement: "the peak velocity attained on the way to the second target was generally much higher (up to threefold) than that of the control ... these high velocities cannot be accounted for exclusively by a mechanism that adjusts peak velocity to the amplitude of movement ... The cause of this phenomenon is unclear" (pp.732-733). In Section 25, we explain this phenomenon in terms of the independent control, or factorization, of the GO mechanism and the TPC-switching mechanism that was described in Section 4. In particular, the GO signal builds up continuously in time. When the TPC is switched to a new target, the PPC can be updated much more quickly because the GO signal which drives it is already large. The more rapid updating of the PPC translates into higher velocities.

These target switching data call attention to a more subtle property of how a GO signal energizes PPC updating, indeed a property which has tended to mask the very existence of the GO signal: How can a GO signal which was activated with a previous TPC interact with a later TPC without causing errors in the ability of the PPC to track the later TPC? How does the energizing effect of a GO signal transfer to any TPC? A solution of this problem is suggested in Section 18.

The fact that peak velocity is amplified without affecting movement accuracy during target switching implies a violation of Fitt's Law, as Massey, Schwartz, and Georgopoulous (1985) have noted. Our mechanistic analysis of synergetic binding via instatement of a TPC and of subsequent PPC updating energized by a previously activated GO signal provides an explanation of this Fitts' Law violation as well as of Fitts' Law itself (Section 28).

12. Velocity Profile Invariance and Asymmetry

Many investigators have noted that the velocity profiles of simple arm movements are approximately bell-shaped (Abend, Bizzi, and Morasso, 1982; Atkeson and Hollerbach, 1985; Beggs and Howarth, 1972; Georgopoulous, Kalaska, and Massey, 1981; Howarth

and Beggs, 1971; Morasso, 1981; Soechting and Lacquaniti, 1981). Moreover the shape of the bell, if rescaled appropriately, is approximately preserved for movements that vary in duration, distance, or peak velocity. Figure 7 shows rescaled velocity profiles from the experiment of Atkeson and Hollerbach (1985). These velocity profiles were generated over a fixed distance at several different velocities. Thus both the duration scale and the velocity scale were modified to superimpose the curves shown in Figure 7.

Figure 7

On the other hand, Beggs and Howarth (1972) showed that "at high speeds the approach curves of the practised subjects are more symmetrical than at low speeds" (p.451). Since velocity profiles associated with slow movements are more asymmetric than those associated with fast movements, they cannot be exactly superimposed. All the velocity profiles shown in Figure 7 are taken from slow (1–1.6 sec) movements, and exhibit the sort of more gradual deceleration than acceleration that Beggs and Howarth (1972) reported for such movements. Asymmetry and its degree are of theoretical importance because the Minimum Jerk Model of Hogan (1984) predicts symmetric velocity profiles, whereas our model shows how the gradual updating of the PPC can generate velocity profiles which exhibit the type of speed-dependent asymmetry that is found in the data (Section 23).

Both the fact that asymmetry exists in velocity profiles and that the degree of asymmetry depends upon movement speed indicate the need for an analysis of the neural dynamics whereby a trajectory unfolds in real-time. In contrast, the Hogan (1984) model's global optimization criterion forces a strictly symmetric velocity profile because it does not represent a process of temporal unfolding. Beggs and Howarth (1972) suggested that the asymmetry reflects a learned strategy of approaching the target as quickly as possible before making corrective movements near the target. For example, these corrective movements could be made under visual guidance by instating a corrected TPC as the arm approached the target. The approach to such a new TPC would take more time, on the average, than

the final approach to the previously tracked TPC, thereby causing greater velocity profile asymmetry. Our simulation results show that velocity profiles become more symmetric as movement speed increases even in the absence of newly instated TPC's. Thus the greater symmetry of velocity profiles at higher speeds may be due to the combined effects of PPC updating properties as the GO signal is parametrically increased, and the consequent elimination of corrective TPC's as the target is rapidly approached. In support of this analysis, Jeannerod (1984, p.252) noted that "the low velocity phase is still observed in the absence of visual feedback, and even in the no-vision situation. This finding, however, does not preclude that visual feedback, when present, will be incorporated ... In the present study, movement duration and low-velocity phase duration were found to be increased in the visual feedback situation."

In summary, our explanation of these data shows how a circuit capable of flexibly binding muscle groups into synchronous synergies automatically implies the observed velocity profile asymmetry. Thus we suggest an explanation of movement invariants, such as duration invariance and synchrony, using a control circuit which never computes an explicit trajectory and whose outputs exhibit a type of asymmetry which other models have not been able to explain.

13. Vector Cells in Motor Cortex

Before quantitatively developing our model, it remains to indicate how the Present Position Command (PPC) is gradually updated until it matches a fixed Target Position Command (TPC). Sections 15–18 motivate this mechanism through an analysis of the types of information that can be used by a developing system to learn TPC's. The summary here is merely descriptive and is made to link these introductory remarks to supportive neural data.

When a new TPC is switched on, its relationship to the current PPC can be arbitrary. Any realizable pair of positions can be coded by the TPC and the PPC. In order to track

the TPC, the PPC needs to change in a *direction* determined by the difference between the TPC and the PPC. In addition, the *amount* of required change is also determined by this difference. An array which measures both the direction and the distance between a pair of arrays TPC and PPC is called a *difference vector*, or DV. At any given time, the DV between the TPC and the PPC—namely, $DV = TPC - PPC$—is computed at a match interface (Figure 8).

Figure 8

How does such a DV update the present PPC? Clearly the PPC must be updated in the direction specified by the DV. Hence we assume that the PPC cumulatively adds, or *integrates*, through time all the DV's which arise at the match interface. Due to this arrangement, the PPC gradually approaches the TPC. At a time when the PPC equals the TPC, the DV equals zero; hence, although the PPC may continue to integrate DV's, it will not further change until either the switching on of a new TPC creates a non-zero DV, or the PPC is updated by inflow information during a passive movement (Section 30).

Figure 9

Georgopoulos and his colleagues (Georgopoulos, Kalaska, Caminiti, and Massey, 1982; Georgopoulos, Kalaska, Crutcher, Caminiti, and Massey, 1984; Kalaska, Caminiti, and Georgopoulous, 1983) have found cell populations in the motor cortex whose collective properties mirror those of the vector-computing nodes at the match interface of our model (Figure 8). Figure 9 shows a histogram of the average number of spikes per unit time recorded from a single such neuron. This temporal behavior closely matches that of DV cells in our model (Figure 17). The vector cells in motor cortex, just like the DV cells in the model, are very broadly tuned to direction (Figure 10). The DV cells in the model are inhibited only if the inhibitory signal from the PPC exceeds the excitatory signal from the TPC. Thus there exists a broad range of directions in which a given component of the model DV is positive.

Figure 10

Figure 11 plots data from a vector cell population *in vivo* alongside the velocity profile of the corresponding movement. Note that the asymmetry in the velocity profile is in the same direction as the asymmetry in the vector cell population profile. This correspondence suggests that the velocity asymmetry is at least partially due to the neural control circuit, as our model also suggests.

Figure 11

Georgopoulos *et al.* (1984, p.510) also noted that: "No obvious invariance in cell discharge was observed when the final position was the same ... these results show that, at the level of motor cortex, it is the direction of movement and not its endpoint that is the principle determinant of cell discharge during the initiation and execution of movement. Therefore, if the hypothesis be true that the endpoint of the movement is the controlled spatial variable (Polit and Bizzi, 1979) then the motor cortex seems to be distal to that end-point specifying process." In other words, if one accepts the STE Model, these data suggest that the TPC cells occur closer to the periphery than the DV cells. On the other hand, if one accepts our model, these data imply that the PPC cells occur closer to the periphery than the DV cells, but that the TPC cells occur more central than the DV cells. A combination of anatonomical and physiological experiments can be used to test this prediction. It should also be noted, however, that the STE Model on which the conclusion of Georgopoulos *et al.* (1984) is based is inconsistent with the very existence of vector cells, because the spring-like properties of the muscles themselves, rather than a neural computation of vectors, determines the direction and length of movement in the STE Model.

Several further properties of cells in precentral motor cortex, documented by Evarts and Tanji (1974; Tanji and Evarts, 1976), lend support to identifying them with the vector cells in our model. In their experiments, monkeys were trained to either push or pull a

lever. During each trial (schematized in Figure 12a) animals first held the lever in a medial position for 2-4 sec. Then either a green or a red *priming* signal was illuminated. If green, the forthcoming movement required for reward was a push: if red, a pull. Finally, .6-1.2 seconds after the priming signal, the *release* signal occurred. This release signal took the form of an externally imposed push or pull on the lever held by the monkey. It both cued movement onset and perturbed the position of the lever so as to increase or decrease its initial distance from target.

Figure 12

Figure 12b summarizes operating characteristics of two cells. The first cell increased its activity after a "push" priming signal, but was inhibited by a "pull" priming signal; the second cell showed the opposite response. From these data alone, it would not be clear whether these cells' activities code DV's or TPC's. However, their further characteristics confirm their status as DV cells. The second bracket for each cell in Figure 12b indicates that their activities decline as movement proceeds in their preferred direction. This decline rules out the TPC interpretation. In the model, it occurs because the movement progressively cancels the difference with which DV cell activity is correlated.

The third bracket for each cell indicates that the initial position perturbations also have the effect they must have if the DV interpretation is correct: perturbations that make the starting point closer to target subtract from activity levels, whereas contrary perturbations add to activity levels. This occurs automatically in the model because PPC's, and thus the corresponding DV's, are updated by sensory feedback during passive movements (Section 30).

Though the foregoing considerations argue strongly for the existence of DV cells in precentral motor cortex, it might be argued that the DV's could be measuring force rather than positional values. Indeed, Evarts interpreted his early experimental data (Evarts, 1968) as suggestive of force coding. However, the data of Schmidt, Jost and Davis (1975)

appear to rule out this alternative interpretation. After varying position and force independently, they concluded that "motor cortex cell firing patterns appear to be unrelated to the large values of rate of change of force seen in this experiment" (p.213).

The data summarized in Sections 7-13 weigh heavily against the STE Model and models based upon optimization principles. So too do the formal shortcomings of these models noted in Sections 7 and 12. We now show that a new model, called the VITE, or "vector integration to endpoint," Model overcomes these formal shortcomings and provides a parsimonious quantitative explanation of all the behavioral and neural data summarized above and in the subsequent sections.

14. Learning Constraints Mold Arm Control Circuits

Rejecting the STE Model does not entail rejecting all dependence upon endpoint commands. An analysis of sensory-motor learning during eye-hand coordination enables us to identify processes which supplement endpoint, or target position, commands to overcome the shortcomings of the STE Model (Grossberg, 1978). The central role of learning constraints in the design of sensory-motor systems has elsewhere been developed for the case of the saccadic eye movement system (Grossberg and Kuperstein, 1986).

We focus our discussion of learning within the arm movement system upon the basic problem of how, when an observer looks at an object, the observer's hand knows where to move in order to touch the object? We discuss this issue from the perspective of eye-hand coordination in a mammal, but the issues that are raised, as well as the conclusions that are drawn, generalize to many other species and sensory-motor systems. Why learning processes are needed to solve this problem is illustrated by the following example.

The movement command which guides the hand to a visual target at a fixed position relative to the body is not invariant under growth. If a young arm, with relatively short limb segments, and an old arm with relatively long limb segments, react to the same command—that is, assume equal angles at analogous joints—then the tips of the two arm's

fingers will be at different loci with respect to the body frame. In short, any animal that grows over an extended period will need to learn new movement commands even if its only ambition is to perform the same act earlier and later in its life cycle. Put the other way, that animals do remain able to reach desired targets throughout periods of limb growth implies plasticity in their sensory-motor commands. Because such growth is slow relative to the rate of learning, failures of sensory-motor coordination are rarely noticeable. In humans, exceptions occur during the first few months of life, prior to experiential tuning of the infant's initially coarse sensory-motor mapping (Fetters and Todd, 1986; von Hofsten, 1979, 1982).

15. Comparing Target Position with Present Position to Gate Intermodality Learning

Thus, as the arm grows, the motor commands which move it to a fixed position in space with respect to the body must also change through learning. Many arm movements are activated in response to visually seen objects which the individual wishes to grasp. We therefore formulate this learning process as follows: How is a transformation learned and adaptively modified between the parameters of the eye-head system and the hand-arm system so that an observer can touch a visually fixated object?

Following Piaget's (1963) analysis of *circular reactions*, let us imagine that an infant's hand makes a series of unconditional movements, which the infant's eyes unconditionally follow. As the hand occupies a variety of positions that the eye fixates, a transformation is learned from the parameters of the hand-arm system to the parameters of the eye-head system. A reverse transformation is also learned from parameters of the eye-head system to parameters of the hand-arm system. This reverse transformation enables an observer to intentionally move its hand to a visually fixated position.

How do these two sensory-motor systems know what parameters are the correct ones to map upon each other? This question raises the fundamental problem that many neural

signals, although large, are unsuitable for being incorporated into behavioral maps and commands. They are "functional noise" to the motor learning process. The learning process needs to be actively modulated, or gated, against learning during inappropriate circumstances.

In the present instance, not all positions which the eye-head system or the hand-arm system assume are the correct positions to associate through learning. For example, suppose that the hand briefly remains at a given position and that the eye moves to foveate the hand. An infinite number of positions are assumed by the eye as it moves to foveate the hand. Only the final, intended, or expected position of the eye-head system is a correct position to associate with the position of the hand-arm system.

Learning of an intermodal motor map must thus be prevented except when the eye-head system and the hand-arm system are near their intended positions. Otherwise, all possible positions of the two systems could be associated with each other, which would lead to behaviorally chaotic consequences. Several important conclusions follow from this observation (Grossberg, 1978; Grossberg and Kuperstein, 1986).

(1) All such adaptive sensory-motor systems compute a representation of target position (also called expected position, or intended position). Thus the importance of endpoint computations is confirmed. This representation is the TPC. In addition:

(2) All such adaptive sensory-motor systems also compute a representation of present position. This representation is the PPC.

(3) During movement, target position is matched against present position. Intermodal map learning is prevented except when target position approximately matches present position (Figure 13). A *gating*, or modulator, signal is thus controlled by the network at which target position is matched with present position. This gating signal enables learning to occur when a good match occurs and prevents learning from occurring when a bad match occurs. This matching process takes place at the match interface that was

described in Section 13. The DV controls the gating signal.

(4) In order to compare target positions with present positions, both types of data must be computed in the same coordinate system. Present eye position is computed with respect to head coordinates. Thus there is an evolutionary pressure to encode target position in head coordinates.

Figure 13

16. Trajectory Formation using DV's: Automatic Compensation for Present Position

The above discussion of how *intermodality* sensory-motor transformations are learned also sheds light upon how *intramodality* movement trajectories are formed. Intermodality transformations associate TPC's because only such transformations can avoid the multiple confusions that could arise through associating arbitrary positions along a movement trajectory. TPC's are not, however, sufficient to generate intramodality movement trajectories. In response to the same TPC, an eye, arm, or leg must move different distances and directions depending upon its present position when the target position is registered.

PPC's can be used to convert a single TPC into many different movement trajectories. Computation of the difference between target position and present position at the match interface in Figure 8 generates a difference vector, or DV, that can be used to automatically compensate for present position. Such automatic compensation accomplishes a tremendous reduction in the memory load that is placed upon an adaptive sensory-motor system. Instead of having to learn whole movement trajectories, the system only has to learn intermodality maps between TPC's. As shall be shown below, the DV's which are computed from target positions and present positions at the match interface can be used to automatically and continuously update the PPC movement commands from which the trajectory is formed. In summary, consideration of the types of information that can be used to learn intermodality commands during motor development leads to general con-

clusions about the quantities from which intramodality movement trajectories are formed, and thus about the way in which other neural systems, such as sensory, cognitive, and motivational systems, can influence the planning of such trajectories.

Computation of TPC's, PPC's, and DV's is a qualitatively different approach to generating a trajectory than are traditional computations based upon a Newtonian analysis of movement kinematics. In a Newtonian analysis, every position within the trajectory is assumed to be explicitly controlled (Atkeson and Hollerbach, 1985; Brody and Paul, 1984; Hogan, 1984; Hollerbach, 1984). Such computations lead to a combinatorial explosion which is hard to reconcile with the rapidity of biological movement generation in real-time. In a vector computation, the entire trajectory is never explicitly planned. Instead, a TPC is computed which determines where the movement expects, or intends, to terminate. The subtraction of the PPC is an automatic process which compensates for the variability of the starting position. The DV which is hereby computed can be used to generate an accurate movement without ever explicitly computing a planned sequence of trajectory positions for the whole movement. In arm movements, a continuous comparison is made between a fixed TPC and all the PPC's that are computed during the movement. All of these compensations for changes in present position are automatically registered, and therefore place no further burden upon the computation of planned movement parameters. In addition, such automatic compensations for present position spontaneously generate the major invariants of arm movements that have been discovered to date (Sections 22-29). Thus the general problem of how DV's are computed is a central one for the understanding of trajectory formation in several movement systems.

17. Matching and Vector Integration during Trajectory Formation

We now specify in greater detail a model of how TPC's, PPC's, and DV's interact with each other through time to synthesize a movement trajectory. Each PPC generates a pattern of outflow movement signals to arm system muscles (Figure 8). Each such outflow

pattern acts to move the arm system towards the present position which it encodes. Thus, were only a single PPC to be activated, the arm system would come to rest at a single physical position. A complete movement trajectory can be generated in the form of a temporal succession of PPC's. Such a movement trajectory can be generated in response to a single TPC that remains active throughout the movement. Although a TPC explicitly encodes only the endpoint of the movement, the process whereby present positions are automatically and continuously updated possesses properties that are much more powerful than those of an STE Model.

This process of continuous updating proceeds as follows. At every moment, a DV is computed from the fixed TPC and the PPC (Figure 8). This DV encodes the difference between the TPC and the PPC. In particular, the DV is computed by subtracting the PPC from the TPC at the match interface.

Because a DV computes the difference between the TPC and the PPC, the PPC equals the TPC only when all components of the DV equal zero. Thus, if the arm system's commands are calibrated so that the arm attains the physical position in space that is coded by its PPC, then the arm system will approach the desired target position in space as the DV's computed during its trajectory approach zero. This is accomplished as follows.

At each time, the DV computes the direction and amplitude which must still be moved to match the PPC with the TPC. Thus the DV computes an error signal of a very special kind. These error signals are used to continuously update the PPC in such a way that the changing PPC approaches the fixed TPC by progressively reducing the vector error to zero. In particular, the match interface at which DV's are computed sends excitatory signals to the stage where PPC's are computed. This stage integrates, or adds up, these vector signals through time. The PPC is thus a cumulative record of all past DV's, and each DV brings the PPC a little closer to the target position command.

In so doing, the DV is itself updated due to negative feedback from the new PPC to

the match interface (Figure 8). This process of updating present positions through vector integration and negative feedback continues continuously until the PPC equals the TPC. Several important conclusions follow from this analysis of the TPC formation process.

Two processes within the arm control system do double duty: A PPC generates feedforward, or outflow, movement signals *and* negative feedback signals which are used to compute a DV. A DV is used to update intramodality trajectory information *and* to gate intermodality learning of associative transformations between TPC's. Thus the match interface continuously updates the PPC when the arm is moving *and* disinhibits the intermodality map learning process when the arm comes to rest.

Within the circuit depicted in Figure 8, "position" and "direction" information are separately coded. Positional information is coded within the PPC and directional information is coded by the DV at the match interface. On the other hand, the computations which give rise to positional and directional information are not independent, since DV's are integrated to compute PPC's, and PPC's are subtracted from TPC's to compute DV's.

18. Intentionality and the GO Signal: Motor Priming without Movement

The circuit depicted in Figure 8 embodies the concept of intention, or expectation, through its computation of a TPC. The complete movement circuit embodies intentionality in yet another sense, which leads to a circuit capable of variable speed control. The need for such an additional process can also be motivated through a consideration of eye-hand coordination (Grossberg, 1978, 1982).

When a human looks at a nearby object, several movement options for touching the object are available. The object could be grasped with the left hand or the right hand. The object could even be touched with one's nose or one's toes! We assume that the eye-head system can simultaneously activate TPC's in several motor systems via the intermodality associative transformations that are learned to these systems. An additional "act of will," or GO signal, is required to convert one or more of these TPC's into overt movement

trajectories within only the selected motor systems.

Figure 14

There is only one way to implement such a GO signal within the circuit depicted in Figure 8. This implementation is described in Figure 14. The GO signal must act at a stage intermediate between the stages which compute DV's and PPC's: The GO signal must act after the match interface so that is does not disrupt the process whereby DV's become zero as PPC's approach the TPC. The GO signal must act before the stage which computes PPC's so that changes in the GO signal cannot cause further movement after the PPC matches the TPC. Thus, although the GO signal changes the outputs from the match interface before they reach the present position stage, the very existence of such processing stages for continuous formation of a trajectory enables the GO signal to act without destroying the accuracy of the trajectory.

The detailed computational properties of the GO signal are derived from two further constraints. First, the absence of a GO signal must prevent the movement from occurring. This constraint suggests that the GO signal multiplies, or *shunts*, each output pathway from the match interface. A zero GO signal multiplies every output to zero, and hence prevents the PPC from being updated. Second, the GO signal must not change the direction of movement that is encoded by a DV. The direction of movement is encoded by the *relative* sizes of all the output signals generated by the vector. This constraint reaffirms that the GO signal *multiplies* vector outputs. It also implies that the GO signal is *nonspecific*: The *same* GO signal multiplies each output signal from the matching interface so as not to change the direction encoded by the vector.

In summary, the GO signal takes a particularly simple form. When it equals zero, the present position signal is not updated. Hence no overt movement is generated. On the other hand, a zero GO signal does not prevent a TPC from being activated, or a DV from being computed. Thus a motor system can become ready, or primed, for movement before

its GO signal turns on. When the GO signal does turn on, the movement can be rapidly initiated. The size of the GO signal regulates overall movement speed. Larger GO signals cause faster movements, other things being equal, by speeding up the process whereby directional information from the match interface is integrated into new PPC's. In models of cognitive processing, the functional analog of the GO signal is an attentional gain control signal (Carpenter and Grossberg, 1986a, 1986b; Grossberg, 1986c, 1986d; Grossberg and Stone, 1986).

Georgopoulos, Schwartz, and Kettner (1986) have reported data consistent with this scheme. In their experiment, a monkey is trained to withhold movement for 0.5 to 3 seconds until a lighted target dims. They reported that cells with properties akin to DV cells computed a direction congruent with that of the upcoming movement during the waiting period. These data support the prediction that the neural stage where the GO signal is registered lies between the DV stage and the PPC stage.

19. Synchrony, Variable Speed Control, and Fast Freeze

The circuit in Figure 14 is now easily seen to possess qualitative properties of synchronous synergetic movement, variable speed control, and fast freeze-and-abort. We apply the circuit properties that each muscle synergist's motor command is updated at a rate that is proportional both to the synergist's distance from its target position and to a variable-magnitude GO signal, which is broadcast to all members of the synergy to initiate and sustain the parallel updating process.

To fix ideas, consider a simple numerical example. Suppose that, prior to movement initiation, muscle synergist A is 4 distance units from its target position and muscle synergist B is 2 distance units from its target position. In that case, if the mean rates at which PPC's are updated for the two synergists are in the same proportion as the distance (i.e., 2:1), then the updating of synergist A will take $4/2$ time units while the updating of synergist B will take $2/1$ time units. Thus both processes will consume approximately 2

time units. Although the PPC updating process occurs at different rates for different synergists, it consumes equal times for all synergists. The result is a synchronous movement despite large rate variations among the component motions.

Changing the magnitude of the GO signal governs variable speed control. Because both of the updating rates in the example (2 and 1) are multiplied by the same GO signal, the component motions will remain synchronous, though of shorter or longer duration, depending on whether the GO signal multiplier is made larger or smaller, respectively. In general, the GO signal's magnitude varies inversely with duration and directly with speed. Finally, if the value of the GO signal remains at zero, no updating and no motion will occur. Thus very rapid freezing can be achieved by completely inhibiting the GO signal at any point in the trajectory. The fact that target position may be very different from present position when the GO signal is withdrawn does not interfere with freezing, as it would using a STE Model, because the arm position closely tracks the PPC, which stops changing as soon as the signal shuts off.

20. Opponent Processing of Movement Commands

Mammalian motor systems are organized into pairs of agonist and antagonist muscles. We now note a new functional role for such an opponent organization: An opponent organization is needed to convert DV's into PPC's which can eventually match an arbitrary TPC. Figure 15 depicts how opponent organization is joined to the system's other processing constraints.

Figure 15

The need for opponent signals can be seen from the following examples. If a target position signal is larger than the corresponding present position signal, then a positive output signal is generated by the corresponding component of the DV. Such positive output signals increase the present position signal until it matches the target position signal. Increasing the present position signal causes the target muscle group to contract. The

opponent muscle group must also simultaneously relax. Inhibitory signals to the present position node of the opponent muscle instate this latter property. When these inhibitory signals are integrated by the present position node of the opponent muscle, the output signal to the opponent muscle decreases, thereby relaxing the muscle.

The need for opponent processing can also be seen by considering the case in which the target position signal is smaller than the present position signal. Then the corresponding component of the DV is negative. Since only nonnegative activities can generate output signals, no output signal is generated by this component of the DV to its corresponding present position node. How, then, is this present position signal decreased until it matches the target position signal? The answer is now obvious, since we have just considered the same problem from a slightly different perspective: If a negative vector component corresponds to an antagonist muscle group, a positive vector component corresponds to its opponent agonist muscle group. This positive vector component generates inhibitory signals to the present position command of the antagonist muscle, thereby relaxing the antagonist muscle until its PPC equals its TPC.

21. System Equations

A quantitative analysis of movement invariants requires the development of a rigorous real-time mathematical model of the constraints summarized in the preceding sections. Qualitative algebraic analysis is insufficient because the trajectory is an emergent property of a nonlinear integration and feedback process under variable gain control. Our model defines the simplest system that is consistent with these constraints. To fix ideas, we explicitly study how the TPC to an agonist muscle group generates a trajectory of PPC signals to that muscle group. Generalizations to synergetic movement of multiple agonist-antagonist muscle groups follow directly from this analysis. Figure 16 locates the mathematical variables that are defined below. The network depicted in Figure 16 obeys

the following system of differential equations:

$$\frac{dV}{dt} = \alpha(-V + T - P) \tag{2}$$

and

$$\frac{dP}{dt} = G[V]^+. \tag{3}$$

In (2) and (3), $T(t)$ is a target position input, $V(t)$ is the activity of the agonist's DV population, $P(t)$ is the activity of the agonist's PPC population, $G(t)$ is the GO signal, $\frac{dV}{dt}$ is the rate of change of V, and $\frac{dP}{dt}$ is the rate of change of P.

Figure 16

Equation (2) says that the activity $V(t)$ averages the difference of the input signals $T(t)$ and $P(t)$ at a rate α through time. The TPC input $T(t)$ excites $V(t)$, whereas the PPC input $P(t)$ inhibits $V(t)$ as part of the negative feedback loop between $V(t)$ and $P(t)$.

Equation (3) says that $P(t)$ cumulatively adds, or *integrates*, the product $G[V]^+$, where

$$[V]^+ = \begin{cases} V & \text{if } V > 0 \\ 0 & \text{if } V \leq 0. \end{cases} \tag{4}$$

In other words, the DV population elicits an output signal $[V]^+$ to the PPC population only if the activity V exceeds the output threshold 0. The output signal is a linear function of V at suprathreshold values. The output signal $[V]^+$ is multiplied, or gated, by the GO signal $G(t)$ on its way to the PPC stage. The activity $P(t)$ at the PPC stage integrates the gated signal through time.

In particular, $G(t) = 0$ implies $\frac{dP}{dt}(t) = 0$. In other words, if the GO signal is shut off within a given time interval, the $P(t)$ is constant throughout that time interval. Fast-freeze can hereby be rapidly obtained by simply switching $G(t)$ quickly to zero no matter how far $P(t)$ may be from $T(t)$ at that time. In addition, this circuit generates compensatory, or "error correcting," trajectories, as described in Section 10. For example, suppose that the GO signal starts out larger than usual or that there is a slight delay in instatement of the

TPC relative to onset of the GO signal. In either case, $P(t)$ can initially increase faster than usual. As a result, $T - P(t)$ can rapidly become smaller than usual. Consequently, updating of $P(t)$ terminates earlier than usual.

This compensatory process illustrates two critical features of the VITE Model: (1) Trajectories are not pre-formed. (2) Because the GO signal feeds in between the DV stage and the PPC stage and because the DV is continuously inhibited by feedback from the PPC stage, accuracy is largely insulated from random variations in the size or onset time of the GO signal, variations in the onset time of the TPC, or momentary perturbations of the PPC due to internal noise or inflow signals.

The system of equations (2)–(4) is explicitly solved for a particular choice of GO signal in Appendix 1. In Sections 22–29, we display the results of computer simulations which demonstrate that this simple model provides a quantitative explanation of all the data thus far summarized. In most of these simulations, we write the GO signal in the form

$$G(t) = G_0 g(t). \tag{5}$$

Constant G_0 is called the GO *amplitude* and function $g(t)$ is called the GO *onset function*. The GO amplitude parameterizes how large the GO signal can become. The GO onset function describes the transient build-up of the GO signal after it is switched on. In our simulations, we systematically studied the influence of choosing different GO amplitudes G_0 and onset functions from the family

$$g(t) = \begin{cases} \frac{t^n}{\beta^n + \gamma t^n} & \text{if } t \geq 0 \\ 0 & \text{if } t < 0. \end{cases} \tag{6}$$

In (6), we chose β and γ equal to 1 or 0. If $\beta = 0$ and $\gamma = 1$, then $g(t)$ is a step function which switches from 0 to 1 at time $t = 0$. If $\beta = 1$ and $\gamma = 1$, then $g(t)$ is a slower-than-linear function of time if $n = 1$ and a sigmoid, or S-shaped, function of time if $n > 1$. In both of these cases, function $g(t)$ increases from $g(0) = 0$ to a maximum of 1, and attains the value $\frac{1}{2}$ at time $t = \beta$. If $\beta = 1$ and $\gamma = 0$, then $g(t)$ is a linear function of time if $n = 1$

and a faster-than-linear function of time if $n > 1$. We will demonstrate below that an onset function which is a faster-than-linear or sigmoid function of time generates a PPC profile through time that is in quantitative accord with data about the arm's velocity profile through time. On the other hand, if muscle and arm properties attenuate the increase in velocity at the beginning of a movement, then linear or even slower-than-linear onset functions could also quantitatively fit the data. Direct physiological measurements of the GO signal and PPC updating processes would enable a more definitive selection of the onset function to be made.

22. Computer Simulation of Movement Synchrony and Duration Invariance

In simulations of synchronous contraction, the same GO signal $G(t)$ is switched on at time $t = 0$ across all VITE circuit channels. We consider only agonist channels whose muscles contract to perform the synergy. Antagonist channels are controlled by opponent signals as described in Section 20. We assume that all agonist channels start out at equilibrium before their TPC's are switched to new, sustained target values at time $t = 0$. In all agonist muscles, $T(0) > P(0)$. Consequently, $V(t)$ in (2) increases, thereby increasing $P(t)$ in (3) and causing the target muscle to contract. Different muscles may be commanded to contract by different amounts. Then the size of $T(0) - P(0)$ will differ across the VITE channels inputting to different muscles. Thus our task is to show how a VITE circuit behaves given a single GO function $G(t)$ if the initial value $T(0) - P(0)$ is varied.

Figure 17 depicts a typical response to a faster-than-linear $G(t)$ when $T(0) > P(0)$. Although $T(t)$ is switched on suddenly to a new value T, $V(t)$ gradually increases-then-decreases, while $P(t)$ gradually approaches its new equilibrium value, which equals T. The rate of change $\frac{dP}{dt}$ of P provides a measure of the velocity with which the muscle group that quickly tracks $P(t)$ will contract. Note that $\frac{dP}{dt}$ also gradually increases-then-decreases with a bell-shaped curve whose decelerative portion ($\frac{d^2P}{dt^2} < 0$) is slightly longer than its accelerative portion ($\frac{d^2P}{dt^2} > 0$), as in the data described in Sections 8, 9, 12, and 13.

Figure 17

Figure 18 demonstrates movement synchrony and duration invariance. This figure shows that the V curves and the $\frac{dP}{dt}$ curves generated by widely different $T(0) - P(0)$ values and the same GO signal $G(t)$ are perfectly synchronous through time. This property is proved mathematically in Appendix 2. These simulated curves mirror the data summarized in Sections 12 and 13.

Figure 18

23. Computer Simulation of Decreasing Velocity Profile Asymmetry at Higher Velocities

The next simulations reproduce the data reviewed in Section 12 concerning the greater symmetry of velocity profiles at higher movement velocities. In these simulations, the initial difference $T(0) - P(0)$ between TPC and PPC was held fixed and the GO amplitude G_0 was increased. Figure 19a,b,c shows that the profile of $\frac{dP}{dt}$ becomes more symmetric as G_0 is increased. Figure 19d shows that if both the time axis t and the velocity axis $\frac{dP}{dt}$ are rescaled, then curves corresponding to movements of the same size at different speeds can approximately be superimposed, except for the mismatch of their decelerative portions, as in the data summarized in Section 12.

Figure 19

24. Why Faster-than-Linear or Sigmoid Onset Functions?

The parametric analysis of velocity profiles in response to different values of $T(0) - P(0)$ and G_0 led to the choice of a faster-than-linear or sigmoid onset function $g(t)$. In fact, the faster-than-linear onset function should be interpreted as the portion of a sigmoid onset function whose slower-than-linear part occurs at times after $P(t)$ has already come very close to T.

Figure 20 shows what happens when a slower-than-linear $g(t) = t(3 + t)^{-1}$ or a linear $g(t) = t$ is used. At slow velocities (small G_0), the velocity profile $\frac{dP}{dt}$ becomes increasingly asymmetric when a slower-than-linear $g(t)$ is used. At a fixed slow velocity, the degree of asymmetry increases as the slower-than-linear $g(t)$ is chosen to more closely approximate a step function. A linear $g(t)$ leads to an intermediate degree of asymmetry. A faster-than-linear, or sigmoid, $g(t)$ leads to slight asymmetry at small values of G_0 as well as greater symmetry at large values of G_0. A sigmoid $g(t)$ can be generated from a sudden onset of GO signal if at least two cell stages average the GO signal before it gates $[V]^+$ in (3). A sigmoid $g(t)$ contains a faster-than-linear part at small values of t, and an approximately linear part at intermediate values of t. Thus a sigmoid $g(t)$ can generate different degrees of asymmetry depending upon how much of the total movement time occurs within each of these ranges.

Figure 20

We have also simulated a VITE circuit using sigmoid GO signals whose rate of growth increases with the size of the GO amplitude. Such covariation of growth rate with amplitude is a basic property of neurons which obey membrane, or shunting, equations (Grossberg, 1970, 1973; Sperling and Sondhi, 1968). Such a sigmoid GO signal $G(t)$ can be simply defined as the output of the second neuron population in a chain of shunting equations perturbed by a step function input with amplitude G_0. Thus, let

$$G_0(t) = \begin{cases} G_0 & \text{if } t \geq 0 \\ 0 & \text{if } t < 0 \end{cases} \tag{7}$$

$$\frac{d}{dt}G_1 = -AG_1 + (B - G_1)G_0 \tag{8}$$

and

$$\frac{d}{dt}G_2 = -AG_2 + (B - G_2)G_1. \tag{9}$$

Then $G_2(t)$ is a sigmoid function of the desired shape. The GO signal $G(t)$ can be set equal to $G_2(t)$, as we did, or even to a sigmoid signal $f(G_2(t))$ of $G_2(t)$. A typical result

is shown in Figure 21. In this series of simulations, exemplified by Figure 21, the range of symmetry ratios, namely .44–.5, was similar to that found in Figure 19 using a faster-than-linear signal function. Final choice of a best-fitting $G(t)$ awaits a more direct experimental determination of the PPC profile through time.

Figure 21

25. Computer Simulation of Velocity Amplification during Target Switching

Velocity amplification by up to a factor of three can be obtained by switching to a new value of T while a previously activated GO signal is still on. Figure 22 demonstrates this effect by comparing two computer simulations. In the first simulation, onset of $T(t)$ and $g(t)$ were both synchronous at time $t = 0$ (Figure 22a). In the second simulation, onset of $g(t)$ preceded onset of $T(t)$ by a time equivalent to about 300 msec (Figure 22b). Note the much higher peak velocity (235 versus 102) attained in Figure 22b. This effect, which matches the "anomalous" velocity multiplication observed in the target-switching experiments of Georgopoulos *et al.* (1981), is due to the prior build-up of the GO signal during response execution.

Figure 22

In the ensuing sections, computer simulations will be compared with a variety of data which were not reviewed in the preceding sections.

26. Reconciling Staggered Onset Times with Synchronous Termination Times

Within the context of a target-switching experiment, velocity amplification may appear to be a paradoxical property. On the other hand, such a property has an adaptive function in the many situations where a hand will fail to reach a moving target unless it both changes direction and speeds up. In addition, we now show that the same mechanism can generate

synchronous termination times of synergetic muscle components which may individually start to move at staggered onset times.

The need for this latter property has recently been emphasized by a study of Hollerbach, Moore, and Atkeson (1986), who showed that nearly straight movement paths can result from muscle coordinate planning if the onset times of muscles acting at different joints are appropriately staggered *and* if all the muscles reach their final positions synchronously. Their study did not, however, explain how a neural mechanism could generate synchronous muscle offsets despite staggered muscle onsets.

We now show that the posited interaction of a growing GO signal with components of a DV that may be switched on at different times automatically generates synchronous offsets as an emergent property of the VITE circuit. Thus the interaction of a GO signal with a DV both helps to linearize the paths generated by individual TPC's and, as in the target-switching experiments, enables the hand to efficiently track a moving target by quickly reacting to read-out of an updated TPC.

Figure 23

Figure 23 depicts the results of four blocks, labelled I, II, III, and IV, of computer simulations. Each block represents the onset time, offset time, and duration of three simulations. In the leftmost simulations of each block, onset of a DV component and a GO signal were synchronous. In the other two simulations of each block, a different DV component was read-out at successively longer delays with respect to the onset time of the GO signal. Due to duration invariance (Appendix 2), the results are independent of the initial sizes of the $T(0) - P(0)$ values of these components.

The four blocks (I, II, III, IV) correspond to four increasing values of the GO amplitude G_0 $(10, 20, 40, 80)$. The approximate invariance of termination times across components with different onset delays is indicated by the nearly equal *heights* reached by all the bars within the block. The different *lengths* of bars within each block show that less time is

needed to update those components whose onset times are most delayed. Thus, in block I, all the components terminate almost synchronously even though their onset times are staggered by as much as 26% of the total movement time. In block II, almost synchronous terminations occur even though onset times are staggered by as much as 39% of the total movement time. At very large choices of G_0 (blocks III and IV), synchrony begins to gently break down because the earliest components have executed over 50% of their trajectories before later components even begin to move. These and other results in the article suggest the critical importance of experimentally testing the existence and predicted properties of GO-DV interactions, notably the predicted correlations between the temporal evolution of the GO signal and the DV.

27. Computer Simulation of the Inverse Relation between Duration and Peak Velocity

Each curve in the simulation result depicted in Figure 24 held $T(0) - P(0)$ constant and varied G_0. In this way, a series of velocity profiles were generated whose peak velocities differed even though their trajectories traversed the same distance. The duration of each movement was computed by measuring the interval between velocity profile zero crossings. The different curves in Figure 24a used different values of the distance parameter $T(0) - P(0)$.

Figure 24

These curves mirror the data of Lestienne (1979) summarized in Figure 24b. Figure 24b plots agonist burst duration against peak velocity. The overall shapes of the plots of simulated durations (Figure 24a) and agonist burst durations (Figure 24b) as a function of peak velocity are similar. This similarity reinforces the postulate that the VITE circuit operates in agonist-antagonist muscle coordinates (Sections 3 and 20). It also suggests that the relationship between VITE circuit outputs, motoneuron inputs, and actual muscle activities might be relatively simple (Bullock and Grossberg, 1986b).

Nevertheless, two caveats deserve mention. First, were Figure 24a a plot of movement duration (MT) against *mean* velocity ($\bar{V}$), it would necessarily have the shape shown, since by definition,

$$MT = \frac{D}{\bar{V}}, \tag{10}$$

where D denotes the distance. Multiplying by different values of D generates a family of curves similar in shape to those shown in Figure 24a. The VITE model generates the curve in Figure 24a because mean velocity and peak velocity are strongly correlated in these VITE trajectories due to the duration invariance described in Section 22.

28. Speed-Accuracy Trade-off: Woodworth's Law and Fitts' Law

The VITE Model circuit predicts a speed-accuracy trade-off which quantitatively fits the classical laws of Woodworth (1899) and of Fitts (1954). The existence of a speed-accuracy trade-off *per se* can be understood by considering the role of the rate parameter α in equation (1).

Given *any* finite averaging rate α, $V(t)$ takes some time to react to changes in $P(t)$. In particular, even if $P(t) = T$ at a given time $t = t_0$, $V(t)$ will typically require some extra time after $t = t_0$ to decrease to the value 0. If α is very large, $V(t)$ can approach 0 quickly. Consequently, by (2), $V(t)$ will not allow $P(t)$ to overshoot the target value T by a large amount. On the other hand, given *any* choice of α, the *relative* amount whereby $P(t)$ overshoots the target T depends upon the size of the GO amplitude G_0. This is true because a larger value of G_0 causes $P(t)$ to increase faster, due to (2), and thus $P(t)$ can approach T faster. In contrast, $V(t)$ can only respond to the rapidly changing values of $T - P(t)$ at the constant rate α. As a result, $V(t)$ tends to be larger at a time $t = t_0$ when $P(t_0) = T$ if G_0 is large than if G_0 is small. It therefore takes $V(t)$ longer to equal 0 after $t = t_0$ if G_0 is large. Thus $P(t)$ overshoots T more if G_0 is large. This covariation of amount of overshoot with overall movement velocity is a speed-accuracy trade-off.

Fitts' Law, as described in equation (1), relates movement time (MT), distance (D),

and target width (W). The target width may be thought of as setting the criterion for what counts as an error. The law may be given two complementary readings. The first notes that for a fixed movement time, error grows in proportion to amplitude. This component of the law was discovered by Woodworth (1896). Table 1 presents simulation results based on the same parameter choices used in Figure 17. The results show that, in a parameter range where model errors do occur, the model's error also grows in proportion to amplitude. In these simulations, G_0 was held fixed and $T(0) - P(0)$ was varied.

Table 1

The second way of reading the law notes that in order to maintain a fixed absolute error size, while increasing movement distance, it is necessary to allow more time for completing the movement. In particular, every doubling of distance will add a constant amount, b, to the time needed to perform the movement with the same level of accuracy. Allowing less than b more time for a movement of twice the distance will lead to a less accurate movement.

Table 2

Table 2 presents the results of a simulation (parameters as in Figure 17) in which the rate parameter α was small enough that modest error resulted even at the smallest distance, or initial value of $T(0) - P(0)$, that was tested, namely a distance of 2 units. Then the distance $T(0) - P(0)$ was repeatedly doubled while the error level was held constant. As can be seen, movement time increased approximately linearly with each doubling of distance, as required by a logarithmic relation between MT and D. The model's striking replication of the laws of Woodworth and Fitts, together with its other successes in experimental results, increases our confidence that the VITE Model captures some of the basic neural design principles that underly trajectory generation *in vivo*.

Woodworth's Law is a consequence of duration invariance in the model. This can be seen from the mathematical analysis provided in Appendix 2. There it is proved that the

PPC value $P(t)$ can be written in the form

$$P(t) = P(0) + (T(0) - P(0)q(t) \tag{11}$$

given *any* continuous GO signal $G(t)$. In (11), $T(0) - P(0)$ represents the amount of contraction, or "distance" to be moved, that is mandated by the TPC value $T(0)$ and the initial PPC value $P(0)$. Function $q(t)$ is independent of $P(0)$ and $T(0)$. By (11), $P(t)$ approaches $T(0)$ as $q(t)$ approaches 1, and $P(t)$ overshoots or undershoots if $q(t)$ approaches a value greater or less than 1, respectively. Since $q(t)$ is multiplied by $T(0) - P(0)$, the amount of error (undershoot or overshoot), is proportional to distance, as in Woodworth's Law.

Whereas the proof of Woodworth's Law is a general consequence of duration invariance in the model, Fitts' Law has been mathematically proved in only one case as of the present time (Appendix 1), although our computer simulations demonstrate that it occurs with greater generality. In this case, the GO signal $G(t)$ switches on from value 0 at times $t < 0$ to the constant value $G_0 > 0$ at times $t \geq 0$. In addition, G_0 is chosen sufficiently large to generate overshoot errors. In particular, when $4G_0 > \alpha$,

$$MT = \frac{2}{\alpha} \log\left(\frac{T(0) - P(0)}{E}\right) \tag{12}$$

where E is the amount of overshoot error in the VITE command.

These instances of Woodworth's Law and Fitts' Law are generated by the VITE circuit itself, without the intervention of visual feedback. A number of authors have commented upon the applicability of these laws when visual feedback is unoperative. For example, Keele (1982, pp.152-153) has written: "What is the underlying nature of the movement system that yields Fitts' Law? ... One factor is the intrinsic accuracy of the motor control system when visual feedback is unavailable. When the eyes are closed during a movement (or the lights are turned off), an average movement will miss target by about 7% of the total distance moved." Schmidt (1982, pp.253-254) plotted error functions for sighted

and blind movements across four movement times. A clear speed accuracy trade-off was observed. Meyer, Keith, Smith, and Wright (1982, p.450) have reviewed data comparing the initial impulse phase of a movement, where visual feedback is unimportant, with the subsequent current-control phase, where visual feedback may be used to improve accuracy. They noted that "the initial-impulse phase was found to contribute directly to the speed-accuracy trade-off. Even when subjects had to perform with their eyes closed and relied on just this phase to execute their movements, they still produced a trade-off ... models that attempt to account for the speed-accuracy trade-off ... must include mechanisms that modulate the trade-off during the initial-impulse phase, not just during the current-control phase." The VITE circuit's ability to reproduce both Woodworth's Law and Fitts' Law as emergent properties of the PPC updating process satisfies this requirement.

It should be emphasized that the VITE circuit is also capable of generating a PPC that approaches the TPC without error in some parameter ranges (Appendix 1). In these parameter ranges, an undershoot error will occur if the GO signal is prematurely terminated. A range effect has also been reported (Georgopoulos, 1986, p.151) such that "subjects tended to overshoot the target in small movements (2.5 cm) and to undershoot in large movements (40 cm)." A number of factors may influence this result. For example, during high speed small movements, auxiliary circuits for controlling the arm's initial effects may not have a sufficient opportunity to act (Grossberg and Kuperstein, 1986, Chapters 3 and 5). During large movements, the distance to be moved may be visually underestimated, thereby leading to instatement of an incorrect TPC. The choice of GO signal amplitude as a function of target distance may contribute to the range effect. The relative importance of such factors will be easier to assess as new experiments and the theory are progressively elaborated with the aid of the quantitative VITE circuit analysis that is provided herein.

29. Computer Simulation of Peak Acceleration Data

Bizzi *et al.* (1984) measured the peak accelerations of medium-speed forearm movements by monkeys. They considered movements around the elbow that swept out 20 and 60 . A computer simulation is compared with their data in Table 3. In order to make this comparison, we scaled 1 time unit in our simulation to equal 10 msec. We then chose two values of the GO amplitude parameter G_0 which generated trajectories of duration approximately equal to 554 msec. and 692 msec., respectively. Due to duration invariance (Section 22), the same durations obtain given these choices of G_0 over a wide range of choices of the distance measure $T(0) - P(0)$. The fact that movements were 20° or 60° was translated into the constraint that the $T(0) - P(0)$ value corresponding to the smaller choice of G_0 must be chosen three times larger than the $T(0) - P(0)$ value corresponding to the larger choice of G_0. Then we searched for values of $T(0) - P(0)$ that gave the best fit to the peak acceleration data subject to this constraint.

Table 3

The result is compared in Table 3 with the data and with the fit of the Minimum-Jerk Model of Hogan (1984). The VITE Model fit these data substantially better than the Minimum-Jerk Model. The values associated with the VITE$^-$ model indicate that a perfect fit can be obtained (with Figure 17 parameters) if DV readout to the shunting stage, rather than being instantaneous, occurs over a brief interval whose length is proportional to the size of the DV.

As noted in Section 12, the Minimum-Jerk Model also erroneously predicts a symmetric velocity profile, at least at the level of the central controller. Moreover, it is hard to see how this model could explain the velocity amplification that occurs during target switching (Section 11). Finally, the Minimum Jerk Model does not contain any representation that may be compared with the existence of vector cells or with the manner in which vector cell activities are integrated into outflow movement commands (Section 13). We therefore

believe that the VITE Model provides a better foundation for developing a quantitative neurally-based theory of arm movements than does the Minimum-Jerk Model. The VITE model, in addition to the model circuits developed in Grossberg and Kuperstein (1986), also provides a mechanistic neural explanation of the types of invariant behaviors for whose analysis the task dynamics approach to motor control was developed (Saltzman and Kelso, 1983).

30. Updating the PPC using Inflow Signals during Passive Movements

Despite these successes, the VITE Model as described above is far from complete. In this section, a solution of one additional design problem is outlined. Bullock and Grossberg (1986b) suggest solutions of a number of the other design problems whereby a VITE circuit can effectively move an arm of variable mass subjected to unexpected perturbations at variable velocities through a Newtonian world.

In Section 6, we noted that inflow signals are needed to update the PPC after a passive movement terminates. Two basic problems motivate our model of PPC updating by inflow signals: First, the process of updating the PPC during passive movements must continue until the PPC registers the position coded by the inflow signals. Thus a difference vector of inflow signals minus PPC outflow signals updates the PPC during passive movements. We denote this difference vector by DV_p to distinguish it from the DV which compares TPC's with PPC's. At times when $DV_p = 0$, the PPC is fully updated. Although the DV_p is not the same as the DV which compares a TPC with a PPC, the PPC is a source of inhibitory signals, as will be seen below, in computing both difference vectors.

Second, PPC outflow signals and inflow signals may, in principle, be calibrated quite differently. We will show how corollary discharges of the PPC outflow signals are adaptively recalibrated until they are computed in the same numerical scale as the inflow signals to which they are compared. We also show that this adaptive recalibration mechanism automatically computes a DV_p which updates the PPC by just the correct amount.

Figure 25 schematizes a model circuit for adaptively computing this DV_p. We call this circuit the *passive update of position (PUP) model.* In Figure 25, the PPC sends inhibitory corollary discharge signals towards the outflow-inflow match stage where the inflow signals are registered. It is assumed that this stage is inhibited except when the movement command circuit is inactive. A simple way to achieve this property is to assume that active DV cells in the movement command circuit inhibit the outflow-inflow match stage, as in Figure 25. Thus the mismatches of outflow and inflow signals which occur during every active movement do not erroneously update the outflow-inflow match stage. In addition, these signals from the DV stage inhibit learning at the LTM traces which multiply the PPC signals on their way to the outflow-inflow match stage.

Figure 25

After a movement is over, both the outflow-inflow match stage and the LTM traces are released from inhibition. Typically, the PPC represents the same position as the inflow signals, but perhaps in a different numerical scale. The learning laws described in Appendix 3 define LTM traces which change until the PPC *times* the LTM trace equals the inflow signal. After a number of such learning trials during stable posture, $DV_p = 0$ and the PPC signals are rescaled by the LTM traces to correctly match the inflow signals.

During a passive movement, the PPC does not change, but the inflow signal may change. If the DV_p becomes positive, it causes an increase in the PPC until the DV_p decreases to 0 and the PPC is correctly updated by the inflow signals. If the DV_p becomes negative, then the DV_p of the opponent muscle can decrease the PPC until a match again occurs.

31. Concluding Remarks

The present article introduces a circuit for automatically translating a target position command into a complete movement trajectory via a mechanism of continuous vector updating and integration. A wide variety of behavioral and neural data can be quantitatively

explained by this mechanism. The model also provides a foundation for clarifying some of the outstanding classical issues in the motor control literature, highlights the relevance of learning constraints upon the design of neural circuitry, and may be viewed as a specialized version of a more general architecture for movement control.

The VITE circuit and the PUP circuit do not, however, exhaust the total neural machinery that is needed for the control of arm movements. Mechanisms for properly timed sequential read-out of TPC's in a serial motor plan, such as during reaching and grasping or during a dance (Grossberg and Kuperstein, 1986, Chapter 9), for adaptive linearization of a nonlinear muscle plant (Grossberg and Kuperstein, 1986, Chapter 5), and for automatically or predictively adapting to the inertial properties generated by variable loads and velocities (Bullock and Grossberg, 1986b) also form essential parts of the arm control system. When all of these systems are joined together, however, one can begin to understand quantitatively how the arm system achieves its remarkable flexibility and versatility, and can begin to build a new type of biologically inspired adaptive robot whose design is qualitatively different from the algorithms offered by traditional approaches to artificial intelligence.

REFERENCES

Abend, W., Bizzi, E., and Morasso, P., Human arm trajectory formation. *Brain*, 1982, **105**, 331-348.

Atkeson, C.G. and Hollerbach, J.M., Kinematic features of unrestrained vertical arm movements. *Journal of Neuroscience*, 1985, **5**(9), 2318-2330.

Beggs, W.D.A. and Howarth, C.I., The movement of the hand towards a target. *Quarterly Journal of Experimental Psychology*, 1972, **24**, 448-453.

Bernstein, N.A., **The coordination and regulation of movements**. London: Pergamon Press, 1967.

Bizzi, E., Accornero, N., Chapple, W., and Hogan, N., Arm trajectory formation in monkeys. *Experimental Brain Research*, 1982, **46**, 139-143.

Bizzi, E., Accornero, N., Chapple, W., and Hogan, N., Posture control and trajectory formation during arm movement. *Journal of Neuroscience*, 1984, **4**(11), 2738-2744.

Brody, M. and Paul, R. (Eds.), **Robotics research: The first international symposium**. Cambridge, MA: MIT Press, 1984.

Brooks, V.B., Motor programs revisited. In R.E. Talbott and D.R. Humphrey (Eds.), **Posture and movement: Perspective for integrating sensory and motor research on the mammalian nervous system**. New York: Raven Press, 1979, pp.13-49.

Brooks, V.B., **The neural basis of motor control**. New York: Oxford University Press, 1986.

Bullock, D. and Grossberg, S., Neural dynamics of planned arm movements: Synergies, invariants, and trajectory formation. Paper presented at the Symposium on Neural Models of Sensory-Motor Control at the annual meeting of the Society for Mathematical Psychology, Cambridge, MA, August 20, 1986 (a).

Bullock, D. and Grossberg, S., Neuromuscular realization of planned trajectories: Adaptive

and automatic mechanisms. In preparation, 1986 (b).

Carpenter, G.A. and Grossberg, S., A massively parallel architecture for a self-organizing neural pattern recognition machine. *Computer Vision, Graphics, and Image Processing*, in press, 1986 (a).

Carpenter, G.A. and Grossberg, S., Neural dynamics of category learning and recognition: Attention, memory consolidation, and amnesia. In J. Davis, R. Newburgh, and E. Wegman (Eds.), **Brain structure, learning, and memory**. AAAS Symposium Series, in press, 1986 (b).

Cooke, J.D., The organization of simple, skilled movements. In G.E. Stelmach and J. Requin (Eds.), **Tutorials in Motor Behavior**. Amsterdam: North-Holland, 1980, pp.199–212.

Evarts, E.V., Relation of pyramidal tract activity to force exerted during voluntary movement. *Journal of Neurophysiology*, 1968, **31**, 14–27.

Evarts, E.V. and Fromm, C., The pyramidal tract neuron as summing point in a closed-loop control system in the monkey. In J.E. Desmedt (Ed.), **Cerebral motor control in man: Long loop mechanisms**. Basel, Switzerland: Karger, 1978, pp. 56–59.

Evarts, E.V. and Tanji, J., Gating of motor cortex r flexes by prior instruction. *Brain Research*, 1974, **71**, 479–494.

Feldman, A.G., Change in the length of the muscle as a consequence of a shift in equilibrium in the muscle-load system. *Biofizika*, 1974, **19**(3), 534–538.

Fetters, L. and Todd, J., Quantitative assessment of infant reaching movements. Submitted for publication, 1986.

Fitts, P.M., The information capacity of the human motor system in controlling the amplitude of movement. *Journal of Experimental Psychology*, 1954, **47**(6), 381–391.

Fitts, P.M. and Peterson, J.R., Information capacity of discrete motor responses. *Journal of Experimental Psychology*, 1964, **67**(2), 103–112.

Flash, T. and Hogan, N., The coordination of arm movements: An experimentally confirmed

mathematical model. *Journal of Neuroscience*, 1985, **5**(7), 1688-1703.

Freund, H.-J. and Büdingen, H.J., The relationship between speed and amplitude of the fastest voluntary contractions of human arm muscles. *Experimental Brain Research*, 1978, **31**, 1-12.

Georgopoulos, A.P., On reaching. *Annual Review of Neuroscience*, 1986, **9**, 147-170.

Georgopoulos, A.P., Kalaska, J.F., Caminiti, R., and Massey, J.T., On the relations between the direction of two-dimensional arm movements and cell discharge in primate motor cortex. *Journal of Neuroscience*, 1982, **2**(11), 1527-1537.

Georgopoulos, A.P., Kalaska, J.F., Crutcher, M.D., Caminita, R., and Massey, J.T., The representation of movement direction in the motor cortex: Single cell and population studies. In G.M. Edelman, W.E. Goll, and W.M. Cowan (Eds.), **Dynamic aspects of neocortical function**. Neurosciences Research Foundation, 1984, pp.501-524.

Georgopoulos, A.P., Kalaska, J.F., and Massey, J.T., Spatial trajectories and reaction times of aimed movements: Effects of practice, uncertainty, and change in target location. *Journal of Neurophysiology*, 1981, **46**(4), 725-743.

Georgopoulos, A.P., Schwartz, A.B., and Kettner, R.E., Neuronal population coding of movement direction. *Science*, 1986, **233**, 1416-1419.

Ghez, C. and Vicario, D., The control of rapid limb movement in the cat, II: Scaling of isometric force adjustments. *Experimental Brain Research*, 1978, **33**, 191-202.

Gordon, J. and Ghez, C., EMG patterns in antagonist muscles during isometric contraction in man: Relations to response dynamics. *Experimental Brain Research*, 1984, **55**, 167-171.

Gordon, J. and Ghez, C., Control strategies determining the accuracy of targeted force impulses, I: Pulse height control. *Experimental Brain Research*, in press, 1986 (a).

Gordon, J. and Ghez, C., Control strategies determining the accuracy of targeted force impulses, II: Compensatory adjustments for initial errors in trajectory. *Experimental Brain Research*, in press, 1986 (b).

Grossberg, S., Neural pattern discrimination. *Journal of Theoretical Biology*, 1970, **27**, 291-337.

Grossberg, S., Contour enhancement, short-term memory, and constancies in reverberating neural networks. *Studies in Applied Mathematics*, 1973, **52**, 217-257.

Grossberg, S., A theory of human memory: Self-organization and performance of sensory-motor codes, maps, and plans. In R. Rosen and F. Snell (Eds.), **Progress in theoretical biology**, Vol. 5. New York: Academic Press, 1978, pp.233-374.

Grossberg, S., **Studies of mind and brain: Neural principles of learning, peception, development, cognition, and motor control**. Boston: Reidel Press, 1982.

Grossberg, S., Adaptive compensation to changes in the oculomotor plant. In E. Keller and D. Zee (Eds.), **Adaptive processes in the visual and oculomotor systems**. Pergamon Press, 1986 (a).

Grossberg, S., Cooperative self-organization of multiple neural systems during adaptive sensory-motor control. In D.M. Guthrie (Ed.), **Aims and methods in neuroethology**. Manchester University Press, 1986 (b).

Grossberg, S. (Ed.), **The adaptive brain, I: Cognition, learning, reinforcement, and rhythm**. Amsterdam: Elsevier/North-Holland, 1986 (c).

Grossberg, S. (Ed.), **The adaptive brain, II: Vision, speech, language, and motor control**. Amsterdam: Elsevier/North-Holland, 1986 (d).

Grossberg, S. and Kuperstein, M., **Neural dynamics of adaptive sensory-motor control: Ballistic eye movements**. Amsterdam: Elsevier/North-Holland, 1986.

Grossberg, S. and Stone, G.O., Neural dynamics of word recognition and recall: Attentional priming, learning, and resonance. *Psychological Review*, 1986, **93**, 46-74.

Helmholtz, H. von, **Handbuch der Physiologischen Optik**. Leipzig: Voss, 1866.

Hofsten, C. von, Development of visually directed reaching: The approach phase. *Journal of Human Movement Studies*, 1979, **5**, 160-178.

Hofsten, C. von, Eye-hand coordination in the newborn. *Developmental Psychology*, 1982, **18**(3), 450-461.

Hogan, N., An organizing principle for a class of voluntary movements. *Journal of Neuroscience*, 1984, **4**(11), 2745-2754.

Hollerbach, J.M., Computers, brain, and the control of movement. *Trends in Neuroscience*, 1982, **5**, 189-192.

Hollerbach, J.M., Dynamic scaling of manipulator trajectories. *Journal of Dynamic Systems, Measurement, and Control*, 1984, **106**, 102-106.

Hollerbach, J.M., Moore, S.P., and Atkeson, C.G., Workspace effect in arm movement kinematics derived by joint interpolation. In G. Gantchev, B. Dimitrov, and P. Gatev (Eds.), **Motor control**. Plenum Press, 1986.

Holst, E. von and Mittelstaedt, H., The reafference principle: Interaction between the central nervous system and the periphery. *Naturwissenschaften*, 1950, **37**, 464-476.

Howarth, C.I. and Beggs, W.D.A., the relationship between speed and accuracy of movement aimed at a target. *Acta Psychologica*, 1971, **35**, 207-218.

Howarth, C.I. and Beggs, W.D.A., Discrete movements. In D. Holding (Ed.), **Human skills**. New York: Wiley and Sons, 1981, pp.91-117.

Jagacinski, R.J. and Monk, D.L., Fitts' Law in two dimensions with hand and head movements. *Journal of Motor Behavior*, 1985, **17**(1), 77-95.

Jeannerod, M., The timing of natural prehension movements. *Journal of Motor Behavior*, 1984, **16**(3), 235-254.

Kalaska, J.F., Caminiti, R., and Georgopoulos, A.P., Cortical mechanisms related to the direction of two-dimensional arm movements: Relations in parietal area 5 and comparison with motor cortex. *Experimental Brain Research*, 1983, **51**, 247-260.

Keele, S.W., Behavioral analysis of movement. In V.B. Brooks (Ed.), **Handbook of physiology**, Section 1, Volume 2: *Motor Control*. Bethesda, MD: American Physiological

Society, 1981, pp.1391-1414.

Keele, S.W., Component analysis and conceptions of skill. In J.A.S. Kelso (Ed.), **Human motor behavior**. Hillsdale, NJ: Erlbaum, 1982, pp.143-159.

Kelso, J.A.S., **Human motor behavior**. Hillsdale, NJ: Erlbaum, 1982.

AKelso, J.A.S. and Holt, K.G., Exploring a vibratory systems analysis of human movement production. *Journal of Neurophysiology*, 1980, **28**, 45-52.

Kelso, J.A.S., Southard, D.L., and Goodman, D., On the nature of human interlimb coordination. *Science*, 1979, **203**, 1029-1031.

Kerr, B. and Langolf, G.D., Speed of aimed movements. *Quarterly Journal of Experimental Psychology*, 1977, **29**, 475-481.

Knight, A.A. and Dagnall, P.R., Precision in movements. *Ergonomics*, 1967, **10**, 327-330.

Lestienne, F., Effects of inertial load and velocity on the braking process of voluntary limb movements. *Experimental Brain Research*, 1979, **35**, 407-418.

Marteniuk, R.G. and MacKenzie, C.L., A preliminary theory of two-hand co-ordinated control. In G.E. Stelmach and J. Requin (Eds.), **Tutorials in motor behavior**. Amsterdam: Elsevier/North-Holland, 1980, pp.185-197.

Massey, J.T., Schwartz, A.B., and Georgopoulos, A.P., On information processing and performing a movement sequence. In C. Fromm and H. Heuver (Eds.), **Generation and modulation of action patterns**, Experimental Brain Research Supplement, 1985.

Meyer, D.E., Keith-Smith, J.E., and Wright, C.E., Models for the speed and accuracy of aimed movements. *Psychological Review*, 1982, **89**, 449-482.

Morasso, P., Spatial control of arm movements. *Experimental Brain Research*, 1981, **42**, 223-227.

Nichols, T.R., Is "the Mass-Spring Model" a testable hypothesis? *Journal of Motor Behavior*, 1985, **17**(4), 499-500.

Piaget, J., **The origins of intelligence in children**. New York: Norton, 1963.

Polit, A. and Bizzi, E., Processes controlling arm movements in monkeys. *Science*, 1978, **201**, 1235-1237.

Ruffini, A., On the minute anatomy of the neuro-muscular spindles of the cat, and on their physiological significance. *Journal of Physiology*, 1898, **23**, 190-208.

Sakitt, B., A spring model and equivalent neural network for arm posture control. *Biological Cybernetics*, 1980, **37**, 227-234.

Saltzman, E.L. and Kelso, J.A.S., Skilled actions: A task dynamics approach. Haskins Laboratories Status Report on Speech Research, 1983, SR-76, 3-50.

Schmidt, E.M., Jost, R.G., and Davis, K.K., Reexamination of the force relationship of cortical cell discharge patterns with conditioned wrist movements. *Brain Research*, 1975, **83**, 213-223.

Schmidt, R.A., **Motor control and learning**. Champaign, IL: Human Kinetics Press, 1982.

Sherrington, C.S., On the anatomical constitution of nerves of skeletal muscles; with remarks on recurrent fibres in the ventral spinal nerve-root. *Journal of Physiology*, 1894, **17**, 211-258.

Soechting, J.F. and Lacquaniti, F., Invariant characteristics of a pointing movement in man. *Journal of Neuroscience*, 1981, **1**(7), 710-720.

Sperling, G. and Sondhi, M.M., Model for visual luminance distribution and flicker detection. *Journal of the Optical Society of America*, 1968, **58**, 1133-1145.

Tanji, J. and Evarts, E.V., Anticipatory activity of motor cortex units in relation to direction of an intended movement. *Journal of Neurophysiology*, 1976, **39**, 1062-1068.

Welford, A.T., Norris, A.H., and Schock, N.W., Speed and accuracy of movement and their changes with age. In W.G. Koster (Ed.), **Attention and performance II**. Amsterdam: North-Holland, 1969, pp.3-15.

Woodworth, R.S., The accuracy of voluntary movement. *Psychological Review*, 1899, **3**, 1-114.

APPENDIX 1

Bell-Shaped Velocity Profile, Fitts' Law, and Staggered Onset Times

This Appendix solves the system of equations

$$\frac{d}{dt}V = \alpha(-V + T - P) \tag{A1}$$

$$\frac{d}{dt}P = G[V]^{+} \tag{A2}$$

under the simplifying assumption that the GO signal G is a step function. Then the system can easily be integrated to demonstrate some basic properties.

In many situations, the system starts out in an equilibrium state such that the PPC equals the TPC. Then a new TPC is switched on and the system approaches a new equilibrium. Before the new TPC is switched on, $P = T$ in (A1). Since the system is at equilibrium, $\frac{d}{dt}V = 0$. Thus, by (A1), it also follows that $V = 0$ under these circumstances.

Suppose that a new TPC value is switched on at time $t = 0$. If the system represents an agonist muscle, then $T(0) > P(0)$ so that the PPC increases when $T(0)$ turns on, thereby causing more contraction of its target muscle group. Thus by (A1),

$$V(0) = 0, \tag{A3}$$

and

$$\frac{d}{dt}V(0) = \alpha(T(0) - P(0)) > 0. \tag{A4}$$

Consequently $V(t) \geq 0$ for all $t \geq 0$, so that by (A2),

$$\frac{d}{dt}P = GV \tag{A5}$$

for all $t \geq 0$.

To solve equations (A1) and (A5), differentiate (A1) at times $t \geq 0$. Then

$$\frac{d^2}{dt^2}V = \alpha(-\frac{dV}{dt} - \frac{dP}{dt}), \tag{A6}$$

because T is constant. Substituting (A5) into (A6) yields the equation

$$\frac{d^2}{dt^2}V + \alpha\frac{d}{dt}V + \alpha GV = 0 \tag{A7}$$

subject to the initial data (A3) and (A4).

This equation can be solved by standard methods. The solution takes the form

$$V(t) = (T(0) - P(0))f(t), \tag{A8}$$

where $f(t)$ is independent of $T(0)$ and $P(0)$. Thus $V(t)$ equals the initial difference between the new TPC and the initial PPC multiplied by a function $f(t)$ which is independent of the new TPC and the initial PPC. By (A2),

$$\frac{d}{dt}P = (T(0) - P(0))g(t), \tag{A9}$$

where $g(t) = Gf(t)$. Integration of (A9) yields

$$P(t) = P(0) + (T(0) - P(0))\int_0^t g(v)dv. \tag{A10}$$

Since $\frac{d}{dt}P$ provides an estimate of the arm's velocity profile, (A9) illustrates the property of duration invariance in the special case that $G(t)$ is constant. Duration invariance is proved using a general $G(t)$ in Appendix 2. Equation (A9) also illustrates how the velocity profile can respond to a sudden switch in the TPC with a gradual increase-then-decrease in its shape, although $g(t)$ assumes a different form if $\alpha > 4G$, $\alpha = 4G$, or $\alpha < 4G$. When $\alpha > 4G$,

$$g(t) = \frac{\alpha G}{\sqrt{\alpha^2 - 4\alpha G}}e^{-\frac{\alpha}{2}t}\left[e^{\frac{t}{2}\sqrt{\alpha^2 - 4\alpha G}} - e^{-\frac{t}{2}\sqrt{\alpha^2 - 4\alpha G}}\right]. \tag{A11}$$

Term $[\exp(\frac{t}{2}\sqrt{\alpha^2 - 4\alpha G})] - [\exp(-\frac{t}{2}\sqrt{\alpha^2 - 4\alpha G})]$ in (A11) increases exponentially from the value 0 at $t = 0$, whereas term $\exp[-\frac{\alpha}{2}t]$ decreases exponentially towards the value 0

at a faster rate. The net effect is a velocity function that increases-then-decreases with an approximately bell-shaped profile. In addition, $g(t) \geq 0$ and

$$\int_0^\infty g(t)dt = 1. \tag{A12}$$

By (A10) and (A12), $P(t)$ increases towards T as t increases. Thus $P(t)$ either approaches $T(0)$ with an arbitrarily small error, or an undershoot error occurs if the GO signal is switched off prematurely.

If $\alpha = 4G$, then

$$g(t) = \alpha G t e^{-\frac{\alpha}{2}t}. \tag{A13}$$

Again the velocity profile gradually increases-then-decreases, but starts to increase linearly before it decreases exponentially. The function in (A13) also satisfies (A12), so that accurate movement or undershoot occur, depending upon the duration of the GO signal.

The case of $\alpha < 4G$ deserves special attention. In this case, the rate G with which P is updated in equation (A2) exceeds the ability of the rate α in equation (A1) to keep up. As a result, an overshoot error can occur. In particular,

$$g(t) = \frac{2\alpha G}{\sqrt{4\alpha G - \alpha^2}} e^{-\frac{\alpha}{2}t} \sin\left(\frac{\sqrt{4\alpha G - \alpha^2}}{2} t\right) \tag{A14}$$

if $0 \leq t \leq \frac{2\pi}{\sqrt{4\alpha G - \alpha^2}}$. When t exceeds $\frac{2\pi}{\sqrt{4\alpha G - \alpha^2}}$, function $g(t)$, and thus $V(t)$, becomes negative. By (A2), $V(t) = 0$ when t exceeds $\frac{2\pi}{\sqrt{4\alpha G - \alpha^2}}$, so that, by (A2), $P(t)$ stops moving at this time. The movement time in this case thus satisfies

$$MT = \frac{2\pi}{\sqrt{4\alpha G - \alpha^2}}. \tag{A15}$$

Within this time frame, the velocity profile is the symmetric function $\sin\left(\frac{\sqrt{4\alpha G - \alpha^2}}{2} t\right)$ multiplied by the decaying, hence asymmetric, function $e^{-\frac{\alpha}{2}t}$. Greater overall symmetry of $g(t)$ is achieved if the rate $\frac{\sqrt{4\alpha G - \alpha^2}}{2}$ with which the sine function changes is rapid relative to the rate $\frac{\alpha}{2}$ with which the exponential function changes, viz., if $2G \gg \alpha$.

Since $P(t)$ stops changing at time $t = \frac{2\pi}{\sqrt{4\alpha G - \alpha^2}}$, the final PPC value found from equation (A10) is

$$P\Big(\frac{2\pi}{\sqrt{4\alpha G - \alpha^2}}\Big) = P(0) + (T(0) - P(0))(1 + e^{-\frac{\alpha\pi}{\sqrt{4\alpha G - \alpha^2}}}). \tag{A16}$$

Thus an overshoot error occurs of size

$$E = (T(0) - P(0))e^{-\frac{\alpha\pi}{\sqrt{4\alpha G - \alpha^2}}}. \tag{A17}$$

In accordance with Woodworth's Law, the error is proportional to the distance $(T(0) - P(0))$. Fitts' Law can be derived by holding E constant in (A17) and varying $(T(0) - P(0))$ to test the effect on the MT in (A15). Substituting (A15) into (A17) shows that

$$E = (T(0) - P(0))e^{-\frac{\alpha MT}{2}} \tag{A18}$$

which implies Fitts' Law

$$MT = \frac{2}{\alpha}\log\Big(\frac{T(0) - P(0)}{E}\Big). \tag{A19}$$

The initial condition $V(0) = 0$ in (A3) obtains if the system has actively tracked a constant TPC until its PPC attains this TPC value. Under other circumstances, $V(0)$ may be negative. When this occurs, $\frac{d}{dt}P$ in (A2) may remain 0 during an initial interval while $V(t)$ increases to nonnegative values. Thus P begins to change only after a staggered onset time. Some properties of staggered onset times are derived below.

A negative initial value of $V(0)$ may obtain if a particular muscle group has been passively moved to a new position either by an external force or by the prior active contraction of other muscle groups. In such a situation, $P(t)$ may be changed by the PUP circuit (Section 30) even if $T(t) = 0$, and $V(t)$ may track $P(t)$ via equation (A1) until a new equilibrium is reached. Under these circumstances, (A1) implies that

$$0 = \frac{d}{dt}V = \alpha(-V + 0 - P). \tag{A20}$$

If we assume that this equilibrium value obtains at time $t = 0$, then

$$V(0) = -P(0) < 0. \tag{A21}$$

and equation (A2) implies that

$$\frac{d}{dt}P = G[V]^+ = 0. \tag{A22}$$

Thus P remains constant until V becomes positive. If a new TPC is switched on at time $t = 0$ to an agonist muscle which satisfies (A21), then $T(0) > P(0)$. By (A1), V increases according to the equation

$$\frac{d}{dt}V + \alpha V = \alpha(T(0) - P(0)), \tag{A23}$$

where $\alpha(T(0) - P(0))$ is a positive constant, until the time $t = t_1$ at which $V(t_1) = 0$. Thereafter $[V]^+ = V > 0$ so that V and P mutually influence each other through equations (A1) and (A5).

Time t_1 is computed by integrating equation (A10). We find

$$V(t) = V(0)e^{-\alpha t} + (T(0) - P(0))(1 - e^{-\alpha t}) \tag{A24}$$

for $0 \leq t \leq t_1$. By (A21),

$$V(t) = -P(0) + T(0)(1 - e^{-\alpha t}). \tag{A25}$$

Thus

$$t_1 = \frac{1}{\alpha} ln \left[1 - \left(\frac{P(0)}{T(0)}\right)\right]^{-1}. \tag{A26}$$

By (A26), t_1 is a function of the ratio of the initial PPC value to the new TPC value.

For times $t \geq t_1$, equations (A1) and (A5) can be integrated just as they were in the preceding case. Indeed,

$$V(t_1) = 0 \tag{A27}$$

by the definition of t_1, and

$$\frac{d}{dt}V(t_1) = \alpha(T(0) - P(0)) \tag{A28}$$

by (A23) and (A28). The initial data (A27) and (A28) are the same as the initial data (A3) and (A4) except for a shift of t_1 time units. Consequently if the GO signal onset time is also shifted by t_1 time units, then it follows from (A8) that at times $t \geq t_1$,

$$V(t) = (T(0) - P(0))f(t - t_1). \tag{A29}$$

An estimate of such a velocity profile is found by piecing together (A24) and (A29). Thus

$$\frac{d}{dt}P = \begin{cases} 0 & \text{for } 0 \leq t < t_1 \\ G(T(0) - P(0))f(t - t_1) & \text{for } t_1 \leq t \end{cases}. \tag{A30}$$

Equation (A30) illustrates how a velocity profile with a staggered onset time can occur if $V(0) < 0$. As shown in Section 26, the VITE command to a muscle group can compensate for a staggered onset time if its DV is multiplied by the same GO signal as other muscles in the synergy. In this case, the GO signal onset time is not shifted to match the onset time of each component of the VITE command.

APPENDIX 2

Synchrony and Duration Invariance

Consider equations (A1) and (A2) under the influence of an arbitrary nonnegative and continuous GO function $G(t)$. As in Appendix 1, let

$$V(0) = 0 \tag{A3}$$

and $P = T$ before T is switched to a new value. Suppose for definiteness that $T(t)$ switches from the value T_0 to T_1 at time $t = 0$, and that

$$T_1 > T_0 = P(0). \tag{A31}$$

Consequently, equations

$$\frac{d}{dt}V = \alpha(-V + T - P) \tag{A1}$$

and

$$\frac{d}{dt}P = GV \tag{A5}$$

hold for $t \geq 0$. Define the new PPC variable

$$Q(t) = P(t) - T_0 \tag{A32}$$

and the new target position constant

$$T_2 = T_1 - T_0. \tag{A33}$$

Then (A1) and (A5) can be replaced by equations

$$\frac{d}{dt}V = \alpha(-V + T_2 - Q) \tag{A34}$$

and

$$\frac{d}{dt}Q = GV \tag{A35}$$

for $t \geq 0$. By (A31),

$$Q(0) = 0. \tag{A36}$$

Thus by (A3) and (A36), both V and Q start out with 0 values at $t = 0$.

Now define new variables

$$v(t) = \frac{V(t)}{T_2} \tag{A37}$$

and

$$q(t) = \frac{Q(t)}{T_2}. \tag{A38}$$

By (A34) and (A35), these variables obey the equations

$$\frac{d}{dt}v = \alpha(-v + 1 - q) \tag{A39}$$

and

$$\frac{d}{dt}q = Gv. \tag{A40}$$

In addition,

$$v(0) = q(0) = 0 \tag{A41}$$

by (A3) and (A36). It is obvious that a unique solution of (A39)-(A41) obtains no matter how T_2 and T_1 are chosen, if $T_2 > T_1$.

By combining (A31), (A32), (A33), and (A38), we find that

$$P(t) = P(0) + (T_1 - P(0))q(t), \tag{A42}$$

where $q(t)$ is independent of T_1 and $P(0)$. Equation (A42) proves duration invariance given a general GO function $G(t)$. Indeed, differentiating (A42) yields

$$\frac{d}{dt}P = (T_1 - P(0))\frac{d}{dt}q(t) \tag{A43}$$

which shows that function $\frac{d}{dt}q$ generalizes function $g(t)$ in equation (A9).

APPENDIX 3

Passive Update of Position

Mathematical equations for a PUP circuit are described below. As in our description of a VITE circuit, equations for the control of a single muscle group will be described. Opponent interactions between agonist and antagonist muscles also exist and can easily be added once the main ideas are ur lerstood.

The PUP circuit supplements the equation

$$\frac{d}{dt}P = G[V]^+ \tag{A42}$$

whereby the PPC integrates DV's through time. A PUP circuit obeys equations

Present Position Command

$$\frac{d}{dt}P = G[V]^+ - G_p[M]^+. \tag{A44}$$

Outflow-Inflow Interface

$$\frac{d}{dt}M = -\beta M + \gamma P - zI. \tag{A45}$$

Adaptive Gain Control

$$\frac{d}{dt}z = \delta G_p(-\epsilon z + [M]^+). \tag{A46}$$

The match function M in (A45) rapidly computes a time-average of the difference between outflow (γP) and gated inflow (zI) signals. Thus

$$M \simeq \frac{1}{\beta}(\gamma P - zI). \tag{A47}$$

If the outflow signal γP exceeds the gated inflow signal zI, then $[M]^+ > 0$ in (A47). Otherwise $[M]^+ = 0$. The *passive gating function* G_p in (A44) is positive only when the

muscle is in a passive, or postural, state. In particular, $G_p > 0$ only when $[V]^+ \simeq 0$ in the VITE circuit. If both G_p and $[M]^+$ are positive in (A44), then $\frac{d}{dt}P < 0$. Consequently, P decreases until $M = 0$; that is, until the outflow signal γP equals the gated inflow signal zI. At such a time, the PPC is updated to match the position attained by the muscle during a passive movement. To see why this is true, we need to consider the role of function z in (A45) and (A46).

Function z is a long term memory (LTM) trace, or associative weight, which adaptively recalibrates the scale, or gain, of inflow signals until they are in the same scale as outflow signals. Using this mechanism, a match between inflow and outflow signals accurately encodes a correctly updated PPC. Adaptive recalibration proceeds as follows.

In equation (A46), the learning rate parameter δ is chosen to be a small constant to assure that z changes much more slowly than M or P. Ths passive gating function G_p also modulates learning, since z can change only at times when $G_p > 0$. At such times, term $-\epsilon z$ describes a very slow forgetting process which prevents z from getting stuck in mistakes. The forgetting process is much slower than the process whereby z grows when $[M]^+ > 0$. Since function M reacts quickly to its inputs γP and $-Iz$, as in (A47), term $[M]^+ > 0$ only if

$$\gamma P > Iz. \tag{A48}$$

Function I is an inflow signal which is multiplied, or gated, by z on its way to the match interface where M is computed (Figure 24).

Because z changes only when the muscle is in a postural, or a passive state, terms γP and I typically represent the same position, or state of contraction, of the muscle group. Then inequality (A48) says that the scale γP for measuring position P using outflow signals is larger than the scale zI for measuring the same position using inflow signals. When this happens, z increases until $M = 0$; viz., until outflow and inflow measurement scales are equal.

On an occasion when the arm is passively moved by an external force, the outflow signal γP may momentarily be greater than the inflow signal zI. Due to past learning, however, the gated inflow signal satisfies

$$zI = \gamma P^*, \tag{A49}$$

where P^* is the outflow command that is typically associated with I. Thus by (A47),

$$M \simeq \frac{\gamma}{\beta}(P - P^*). \tag{A40}$$

By (A44) and (A50), P quickly decreases until it equals P^*. Thus, after learning occurs, P approaches P^*, and M approaches 0, so quickly that spurious new learning due to the passive movement has little opportunity to occur, since z changes slowly through time. What small deviations may occur tend to average out due to the combined action of the slow forgetting term $-\epsilon z$ in (A46) and opponent interactions.

Equations (A45) and (A46) use the same formal mechanisms as the *head-muscle interface* (HMI) described by Grossberg and Kuperstein (1986). The HMI adaptively recodes a visually activated target position coded in head coordinates into the same target position coded in agonist-antagonist muscle coordinates. Such a mechanism for adaptive matching of two measurement scales may be used quite widely in the nervous system.

TABLE 1

MT	DISTANCE	ERROR
.56	10	.084
.56	20	.170
.56	40	.349
.56	80	.700

FOR FIXED DURATION (MT), ERROR GROWS IN PROPORTION TO DISTANCE.

TABLE 2

ERROR	DISTANCE	MT
.059	2	.39
.057	4	.49
.058	8	.59
.059	16	.70
.057	32	.80
.059	64	.91

FOR FIXED ERROR LEVEL, DURATION (MT) GROWS LINEARLY WITH DISTANCE DOUBLING.

TABLE 3

DISTANCE	MT	PEAK $\ddot{P}$	PEAK $\ddot{P}$ SOURCE
20	.554	$397°/sec^2$	Bizzi *et al.* (1984)
60	.692	$1130°/sec^2$	(experimental data)
20°	.554	$376°/sec^2$	Minimum-jerk model
60°	.692	$722°/sec^2$	(simulation)
20°	.554	$394°/sec^2$	VITE model
60°	.692	$854°/sec^2$	(simulation)
20°	.554	$396°/sec^2$	VITE$^+$ model
60°	.692	$1127°/sec^2$	(simulation)

COMPARISON OF THREE MODELS' ABILITY TO PREDICT DATA ON PEAK ACCELERATION.

FIGURE CAPTIONS

Figure 1. Consequences of two motor-control schemes. Dashed lines: Movement paths generated when a synergist producing vertical motion and a synergist producing horizontal motion contract in parallel and at equal rates to effect movements from various beginning points (Bs) to the common endpoint E. Solid lines: Movement paths generated when the synergists' contraction rates are adjusted to compensate for differences in the lengths of the vertical and horizontal components of the movement.

Figure 2. Both outflow and inflow signals contribute to the brain's estimate of the limb's present position, but in different ways.

Figure 3. Curves for subjects' approach to various targeted force levels. Targeted (peak) levels are reached at nearly the same time, indicating duration invariance across different force "distances". Only the initial part of each curve represents active movement. Post-peak portions represent passive relaxation back to base-line. Reprinted with permission from Freund and Büdingen (1978).

Figure 4. Overshooting (gray curve), hitting (black curve), and undershooting (dashed line) a force-level target (horizontal line) in an isometric task. Reprinted with permission from Gordon and Ghez (1986b).

Figure 5. Duration invariance across three force target levels. Oblique lines indicate an inverse relation between rise time (duration) and peak acceleration across trials with the same force target level. These trends overlay a direct relation between target level and peak acceleration. Reprinted with permission from Gordon and Ghez (1986b).

Figure 6. Monkeys seamlessly transformed a movement initiated toward the 2 o'clock target into a movement toward the 10 o'clock target when the latter target was substituted 50 or 100 msec after activation of the 2 o'clock target light. Reprinted with permission from Georgopoulos *et al.* 1981.

Figure 7. Velocity profiles from movements of similar duration are approximately superimposable following velocity and time axis rescaling. Reprinted with permission from Atkeson and Hollerbach (1984).

Figure 8. A match interface within the motor command channel continuously computes the difference between the target position and present position, and adds the difference to the present position command.

Figure 9. Quick buildup and gradual decline of activity in motor-cortical vector cells. Reprinted with permission from Georgopoulos *et al.* (1982).

Figure 10. Directional tuning curve for a motor-cortical cell exhibiting peak activity during a 90° (forward from body) arm movement. Dotted line indicates control period discharge rate. Thus this cell is inhibited when movement direction falls outside the 180° hemisphere of movements to which it can contribute a positive motion component. Reprinted with permission from Kalaska *et al.* (1983).

Figure 11. A comparison of the population vector of 241 directionally tuned cells (upper figure) with the velocity vector of the hand (lower figure), each measured at 20 msec. intervals during the reaction time and during movement. Note the asymmetry (longer right tail) in both. Reprinted with permission from Georgopoulos *et al.* (1984).

Figure 12. (A): The time course of each trial in the push-or-pull task used by Evarts and Tanji (1974). (B): Operating characteristics of two motor-cortical cells. Solid arrows indicate increases (upward arrow) or decreases (downward arrow) in cell discharge rates. Hollow arrows indicate a push-(upward arrow) or pull-(downward arrow) related event: either the push/pull priming signal, a push/pull movement, or the push/pull perturbation that also served as the release signal.

Figure 13. Learning in sensory-motor pathways is gated by a DV process which matches TPC with PPC to prevent incorrect associations from forming between eye-head TPC's and hand-arm TPC's.

Figure 14 A GO signal gates execution of a primed movement vector and regulates the rate at which the movement vector updates the present position command.

Figure 15 Opponent interactions among channels controlling agonists and their antagonists enable coordinated, automatic updating of their PPC's.

Figure 16 Network variables employed in computer simulations. See text equations 2 and 3.

Figure 17 The simulated time course of the neural network activities V, G, and P during an 1100 msec movement. The variable T (not plotted) had value 0 at $t < 0$, and value 20 thereafter. The derivative of P is also plotted to allow comparison with experimental velocity profiles. Parameters for equations (2), (3), (6): $\alpha = 30$, $n = 1.4$, $\beta = 1$, $\gamma = 0$.

Figure 18. With equal GO signals, movements of different size have equal durations and perfectly superimposable velocity profiles after velocity axis rescaling. (A, B): GO signals and velocity profiles for 20 and 60 unit movements lasting 560 msec. (See Figure 17 caption for parameters.)

Figure 19. (A, B, C): Velocity profiles associated with a slow, medium, and fast performance of a 20 unit movement. Each SR value gives the trajectory's *symmetry ratio*: that is, the time taken to move half the distance, $.5(T(0) - P(0))$, divided by the total movement duration, MT. These ratios indicate progressive symmetrization at higher speeds. (D): The velocity profiles shown in (A), (B), and (C) are not perfectly superimposable. (See Figure 17 for parameters.)

Figure 20. (A, B): Velocity profiles for a slow and a fast movement with a slower-than-linear $g(t)$: $\alpha = 30$, $n = 1$, $\beta = 1$, $\gamma = 1$. (C, D): Velocity profiles for a slow and a fast movement with a linear $g(t)$: $\alpha = 30$, $n = 1$, $\beta = 1$, $\gamma = 0$.

Figure 21. Simulated time course of neural network activities and $\frac{dP}{dt}$ for a 35 msec movement. Note the S-shaped growth in G (sigmoid GO signal). Parameters as in

AD-A179 501 WORKSHOP SYMPOSIUM ON NEURAL MODELS OF SENSORY-MOTOR CONTROL HELD IN CAMB.. (U) BOSTON UNIV MA CENTER FOR ADAPTIVE SYSTEMS D BULLOCK ET AL. 06 MAR 87 2/3

UNCLASSIFIED AFOSR-TR-87-0457 AFOSR-86-0228 F/G 5/10 NL

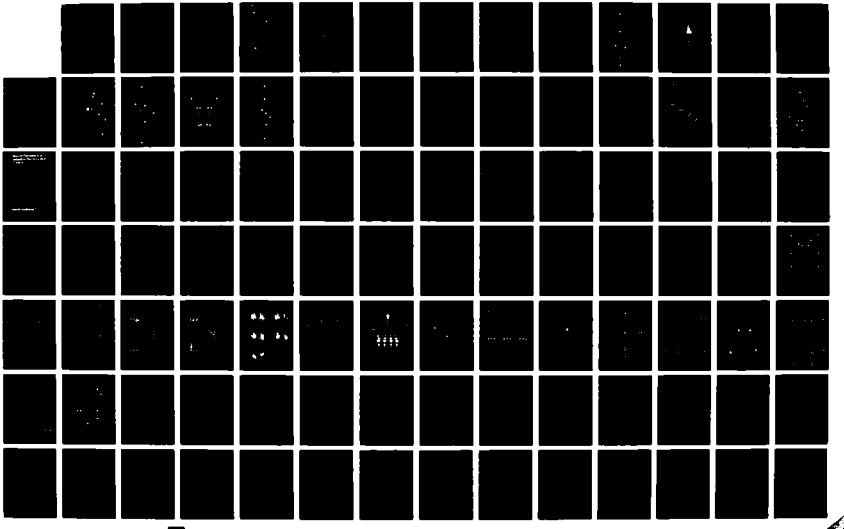

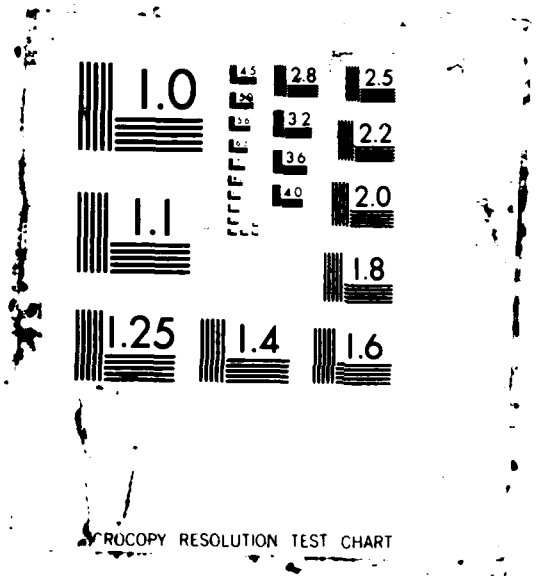
1.0
1.1
1.25
1.4
1.6
2.8
3.2
3.6
4.0
2.5
2.2
2.0
1.8
ROCOPY RESOLUTION TEST CHART

equations (2), (3), (8), (9): $\alpha = 25$, $A = 1$, $B = 25$.

Figure 22. A much higher peak velocity is predicted by the model whenever a target is activated after the GO signal has already had time to grow. (A): The control condition, in which T and the GO signal growth process are activated synchronously. (B): Same T as in (A), but here T was activated after $G(t)$ had been growing for 300 msec. (See Figure 17 for parameters.)

Figure 23. Simulation results showing automatic VITE circuit compensation for contraction-onset-time staggering across components of a synergy. Each block (I, II, III, IV) shows results for a different value (10, 20, 40, and 80, respectively) of the GO signal scalar, G_0. (See Figure 17 for parameters.)

Figure 24. (A): Simulation of movement duration (sec) as a function of peak velocity (deg/sec) for a 30° (lower curve) and a 60° (upper curve) movement. (See Figure 17 for parameters.) (B): Data on agonist burst duration (squares) and antagonist burst onset-time (dots) as a function of peak velocity (rad/sec) for a 60° movement. Reprinted with permission from Lestienne (1979).

Figure 25. A passive update of position (PUP) circuit. An adaptive pathway $PPC \rightarrow DV_P$ calibrates PPC-outflow signals in the same scale as inflow signals during intervals of posture. During passive movements, output from DV equals zero. Hence the passive difference vector DV_P updates the PPC until it equals the new position caused by any passive movements that may occur due to the application of external forces.

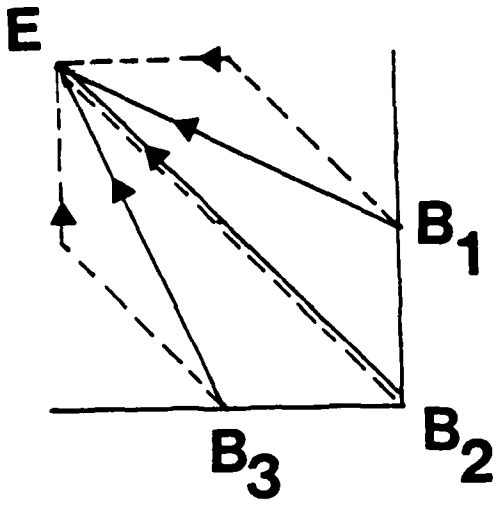

Figure 1

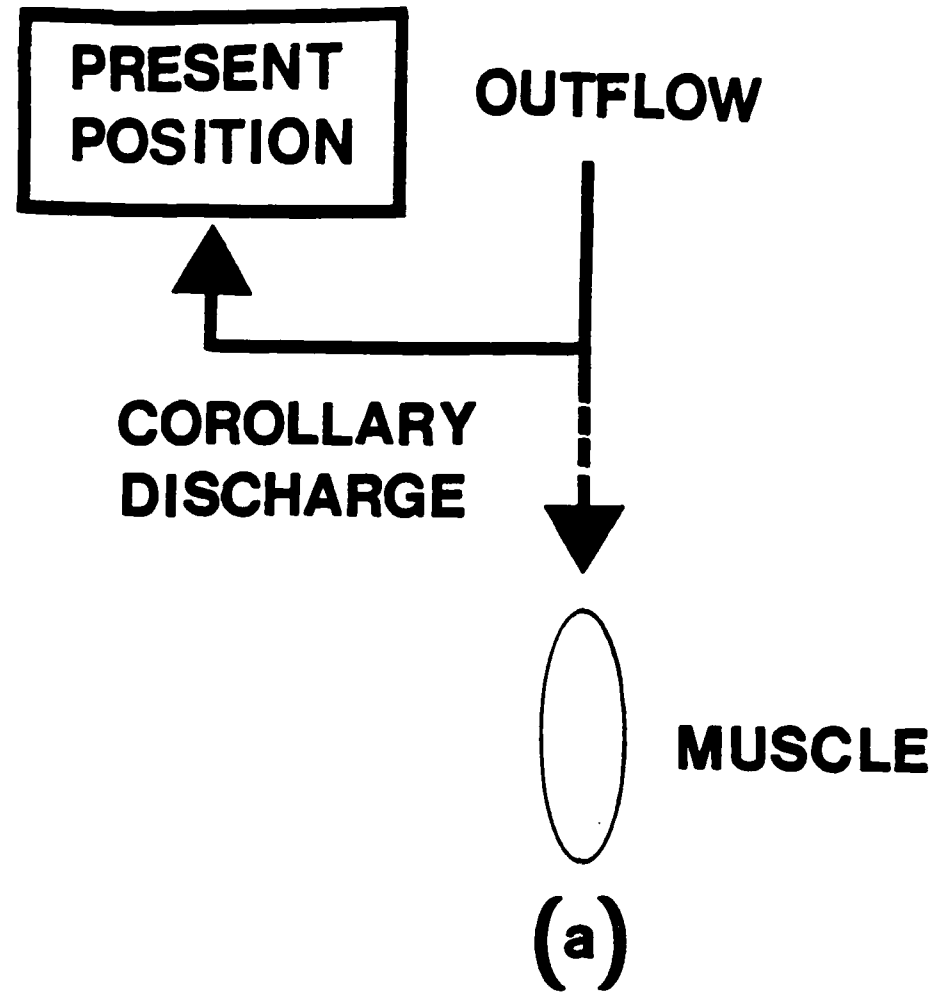
PRESENT POSITION
OUTFLOW
COROLLARY DISCHARGE
MUSCLE
(a)

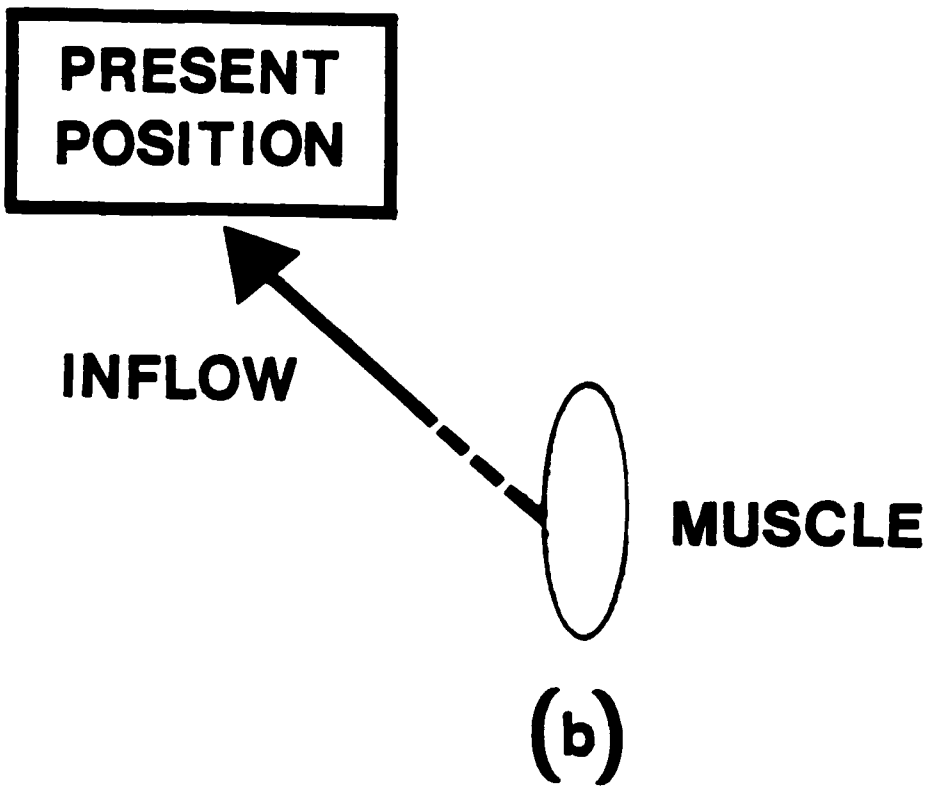
PRESENT POSITION
INFLOW
MUSCLE
(b)

Figure 2

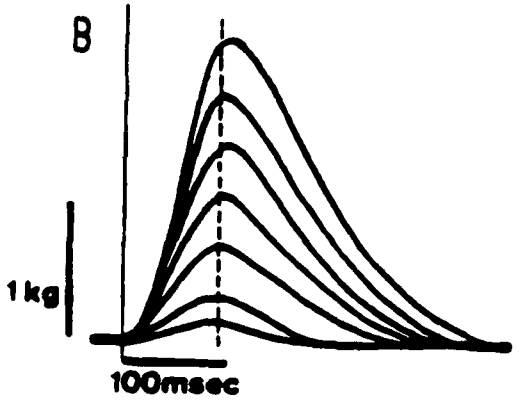

Figure 3

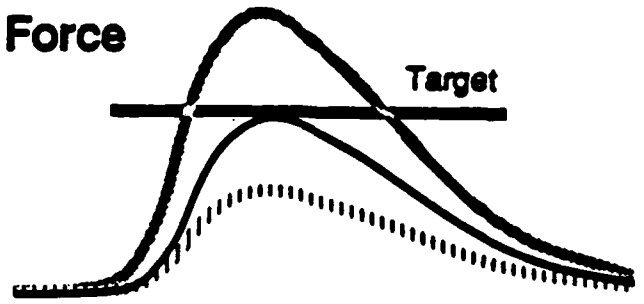

Figure 4

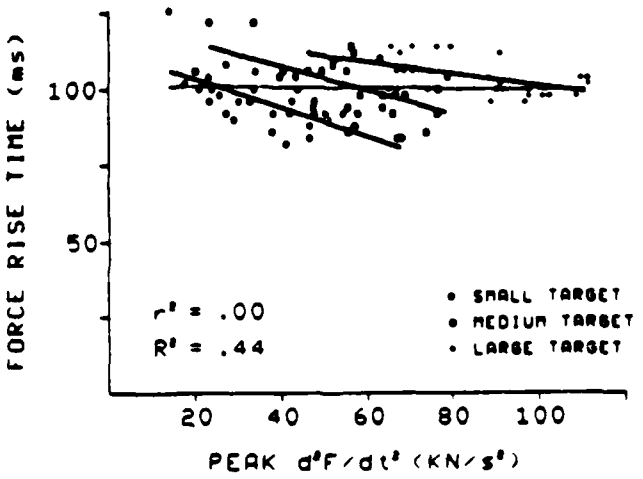
FORCE RISE TIME (ms)
100
50
20
40
60
80
100
PEAK d³F/dt³ (KN/s³)
r² = .00
R² = .44
• SMALL TARGET
• MEDIUM TARGET
• LARGE TARGET

Figure 5

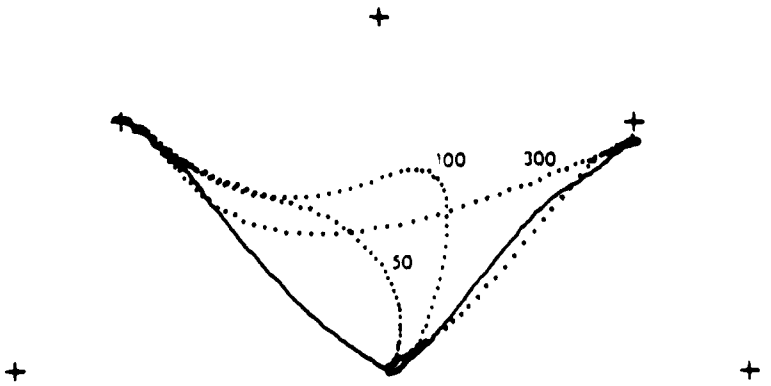

Figure 6

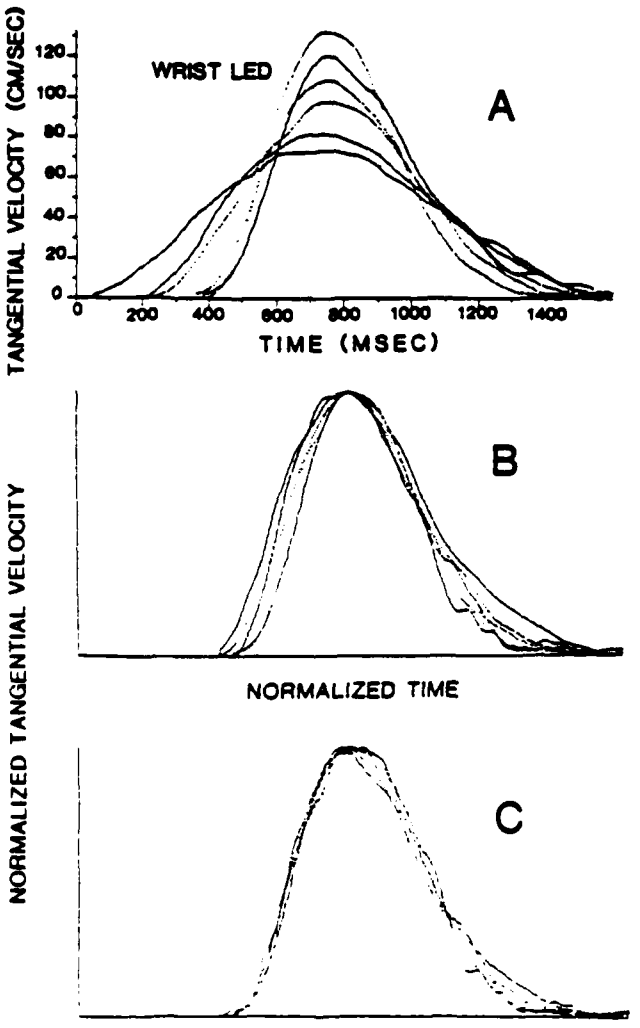
TANGENTIAL VELOCITY (CM/SEC)
WRIST LED
A
120
100
80
60
40
20
0
0
200
400
600
800
1000
1200
1400
TIME (MSEC)
B
NORMALIZED TANGENTIAL VELOCITY
NORMALIZED TIME
C

Figure 7

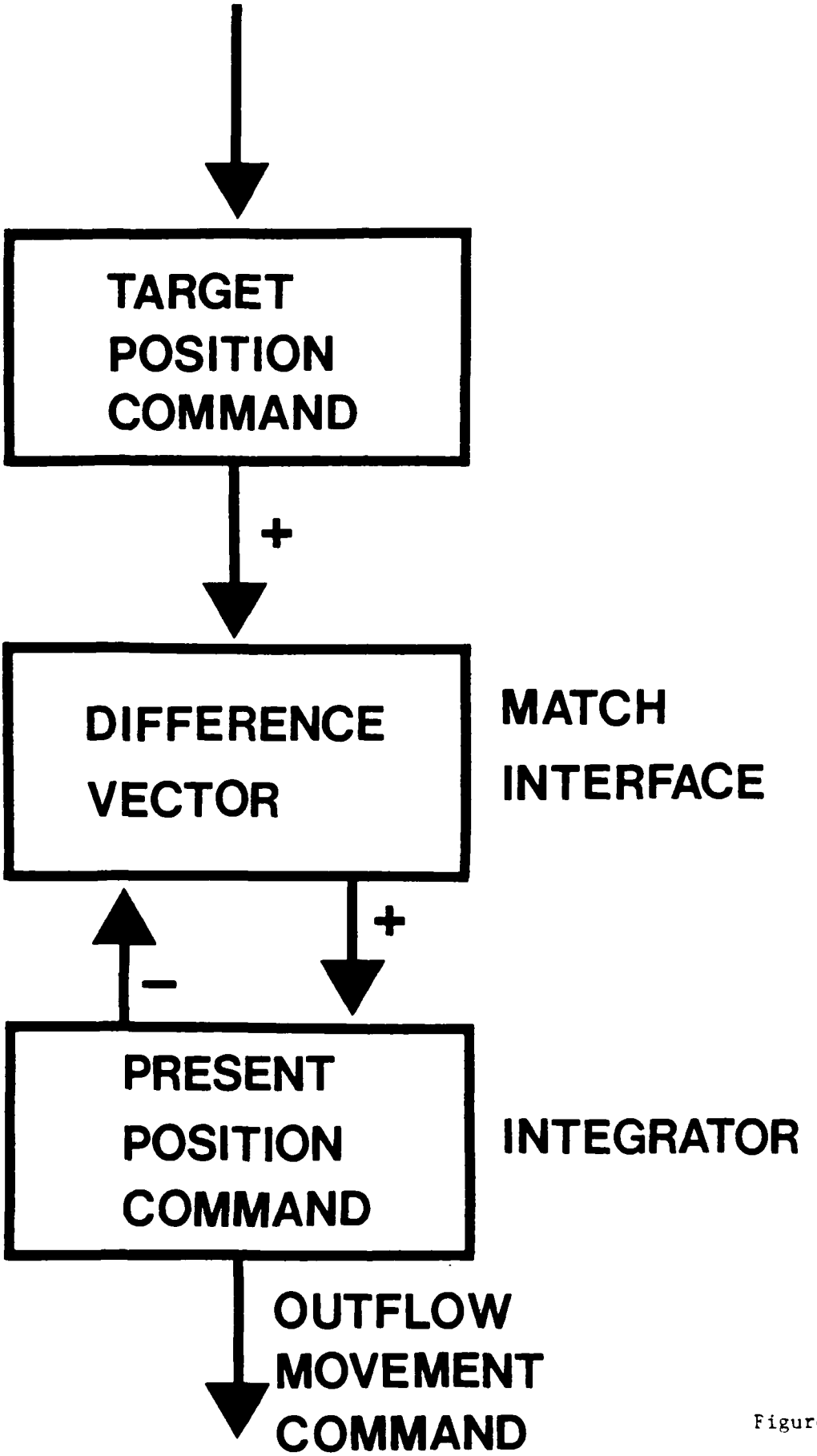
TARGET
POSITION
COMMAND
+
DIFFERENCE
VECTOR
MATCH
INTERFACE
+
−
PRESENT
POSITION
COMMAND
INTEGRATOR
OUTFLOW
MOVEMENT
COMMAND

Figure 8

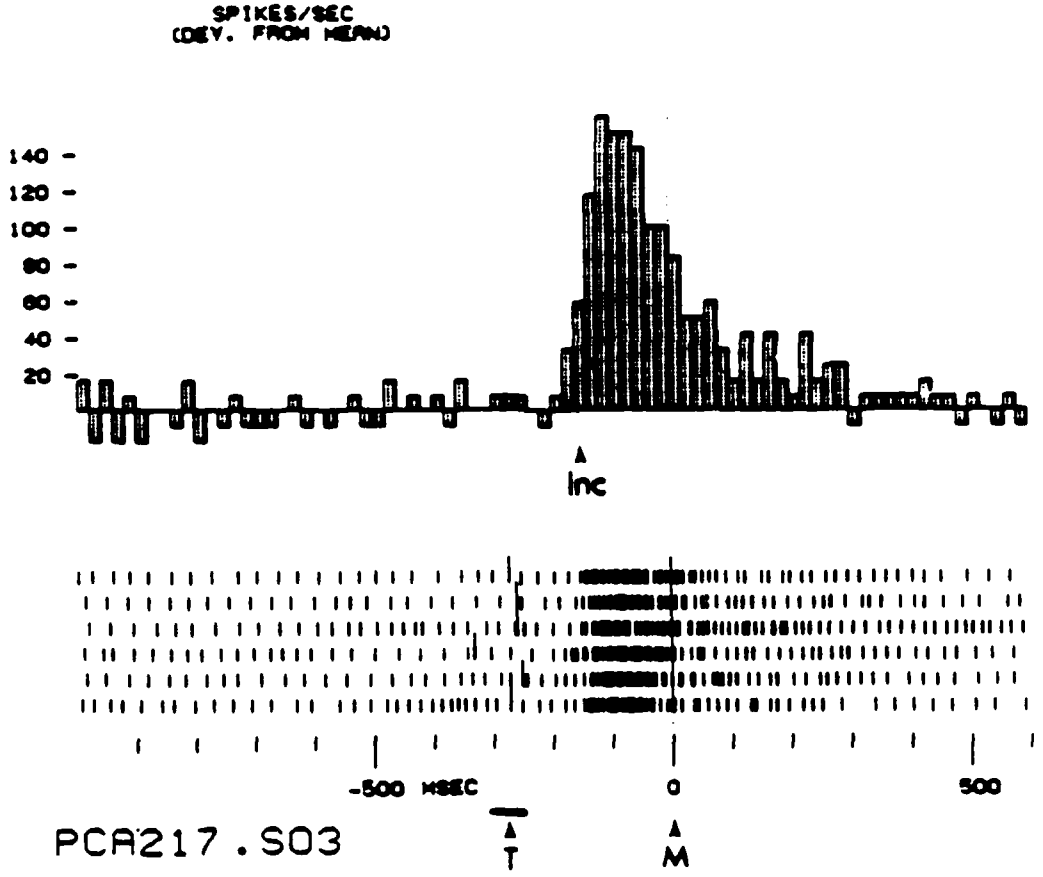
SPIKES/SEC
(DEV. FROM MEAN)
140
120
100
80
60
40
20
Inc
-500 MSEC
0
500
PCA217.S03
T
M

Figure 9

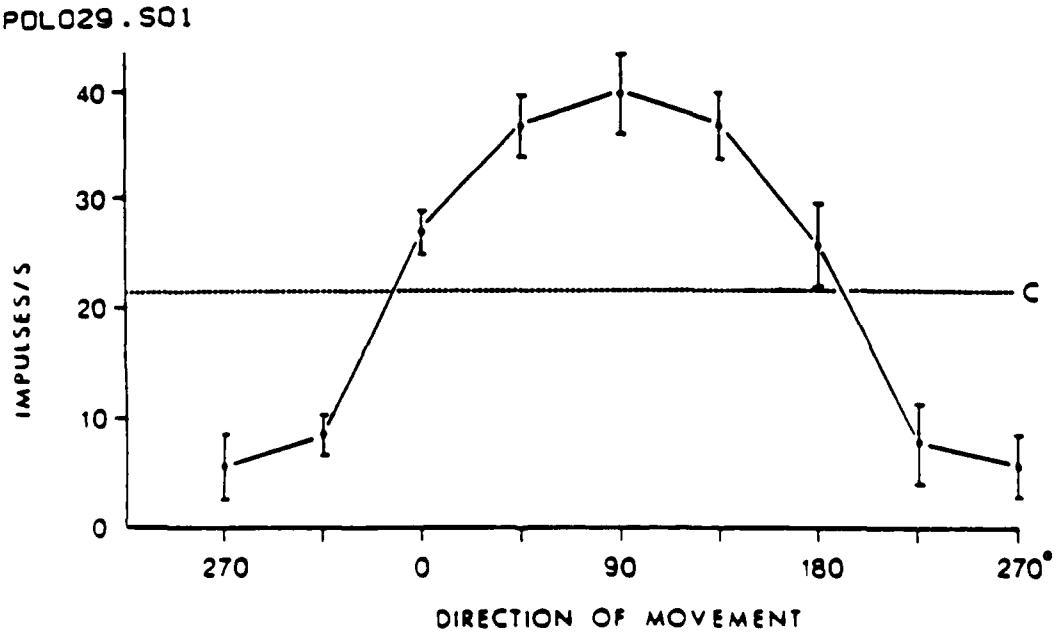
POL029.S01
40
30
20
10
0
IMPULSES/S
C
270
0
90
180
270°
DIRECTION OF MOVEMENT

Figure 10

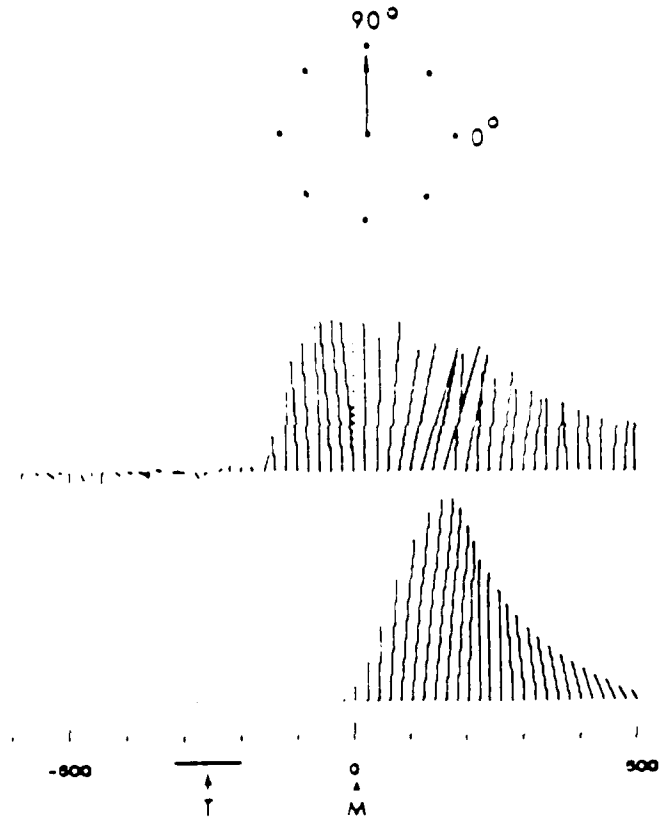

Figure 11

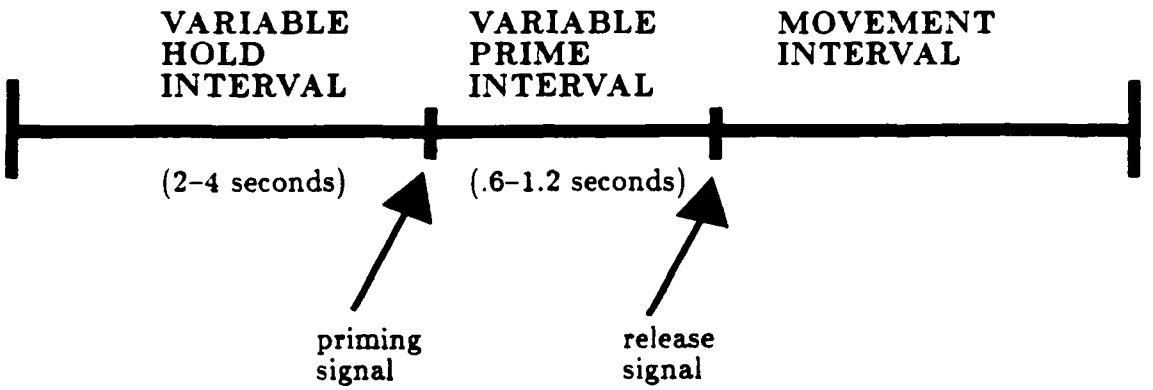

(A)

CELL 1 OPERATING CHARACTERISTICS

⇑ priming signal	produced	↑ activity
⇓ priming signal	produced	↓ activity
⇑ movement	produced	↓ activity
⇑ prime + ⇓ perturbation	produced	greater ↑ activity
⇑ prime + ⇑ perturbation	produced	less ↑ activity

CELL 2 OPERATING CHARACTERISTICS

⇓ priming signal	produced	↑ activity
⇑ priming signal	produced	↓ activity
⇓ movement	produced	↓ activity
⇓ prime + ⇑ perturbation	produced	greater ↑ activity
⇓ prime + ⇓ perturbation	produced	less ↑ activity

(B)

Figure 12

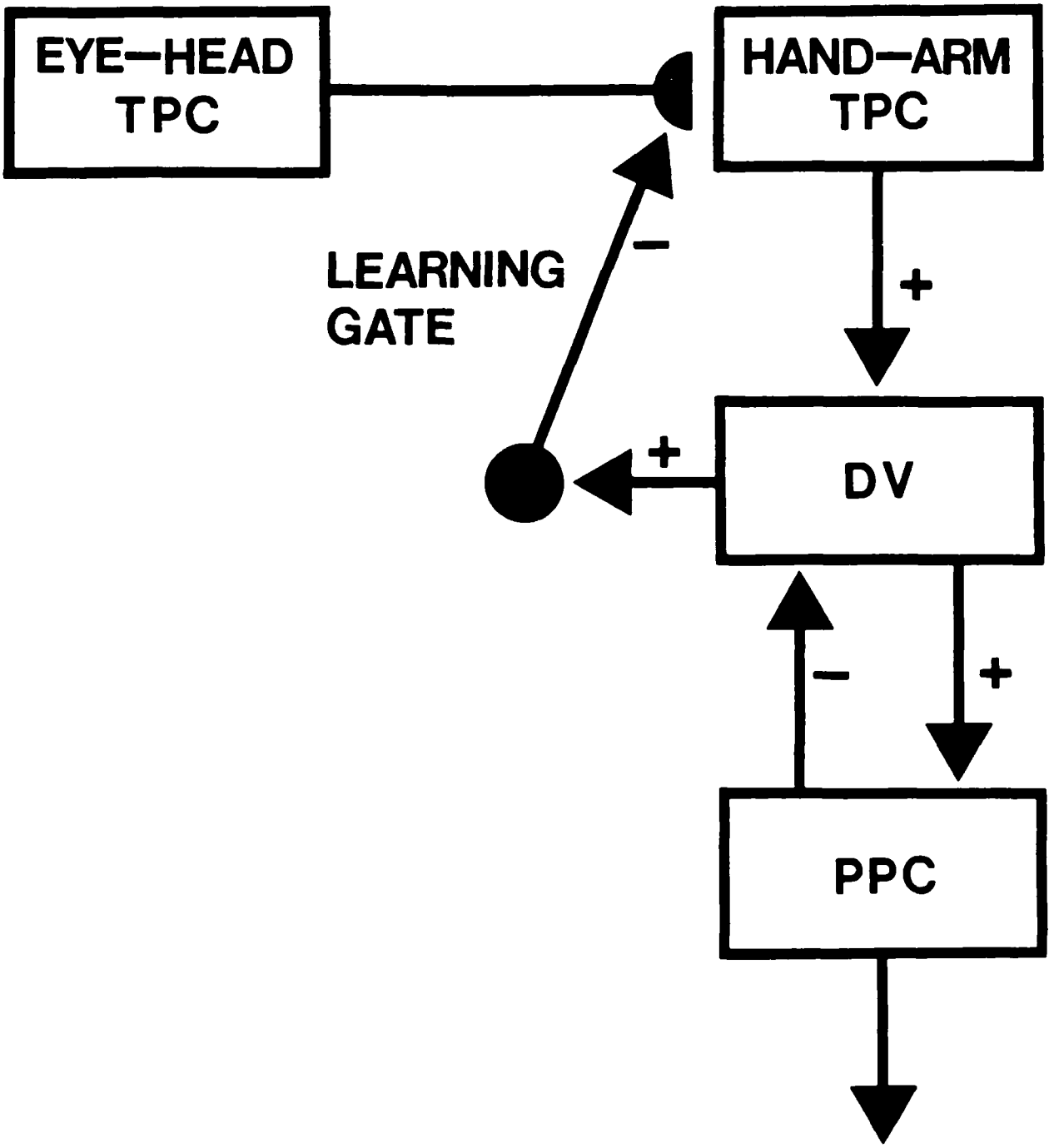

Figure 13

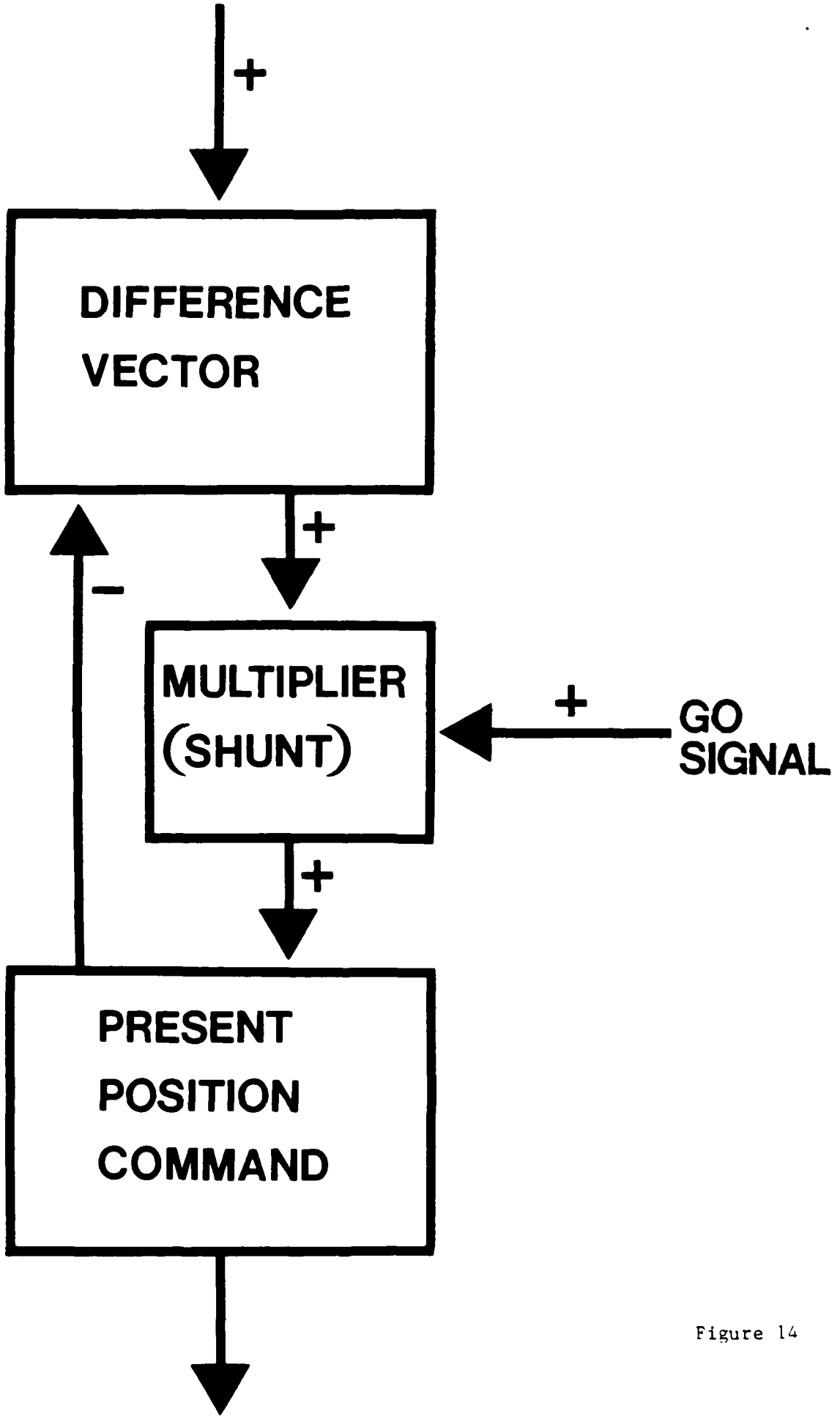
+
DIFFERENCE
VECTOR
+
−
MULTIPLIER
(SHUNT)
+
GO
SIGNAL
+
PRESENT
POSITION
COMMAND

Figure 14

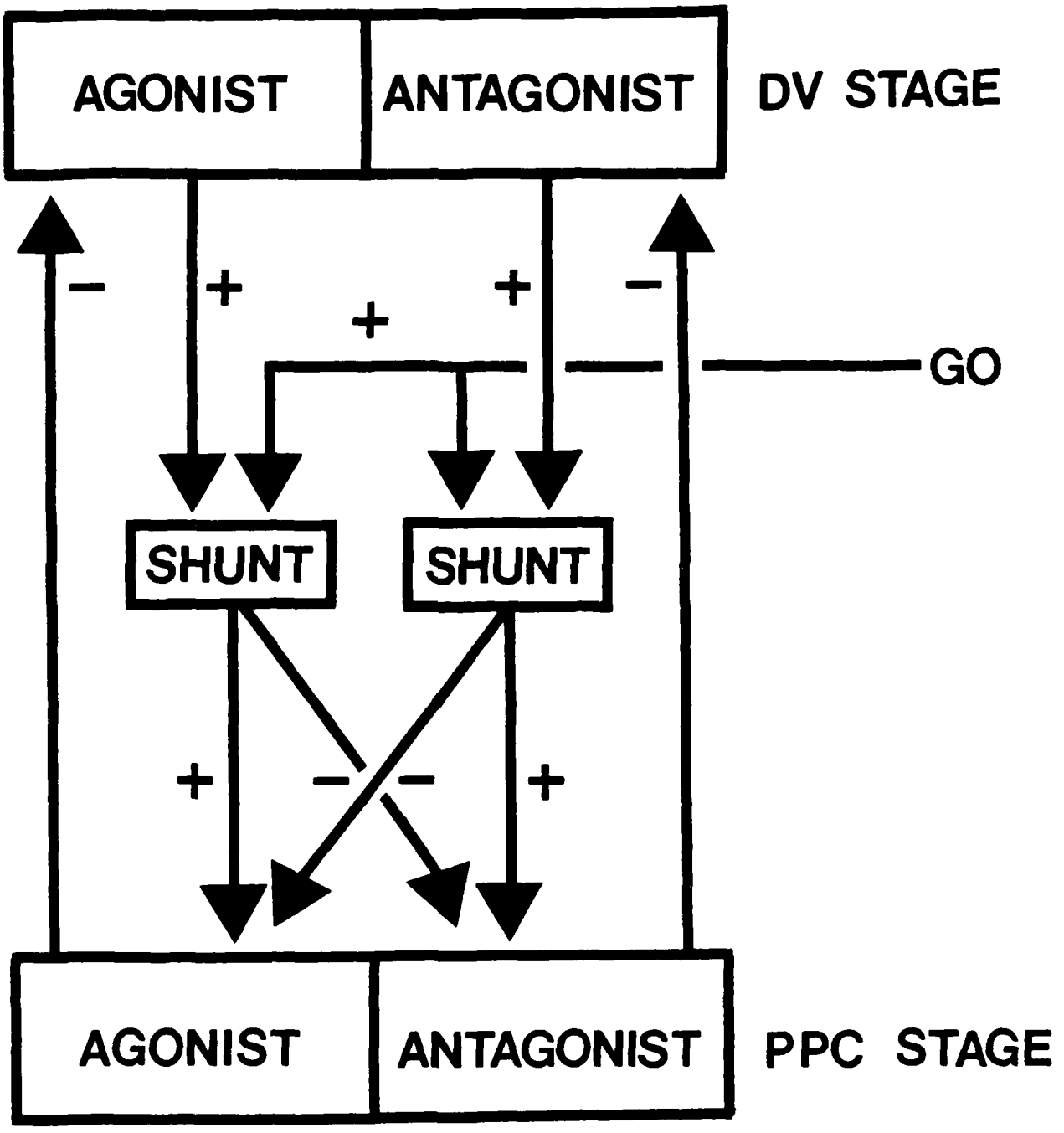
AGONIST
ANTAGONIST
DV STAGE
GO
SHUNT
SHUNT
AGONIST
ANTAGONIST
PPC STAGE

Figure 15

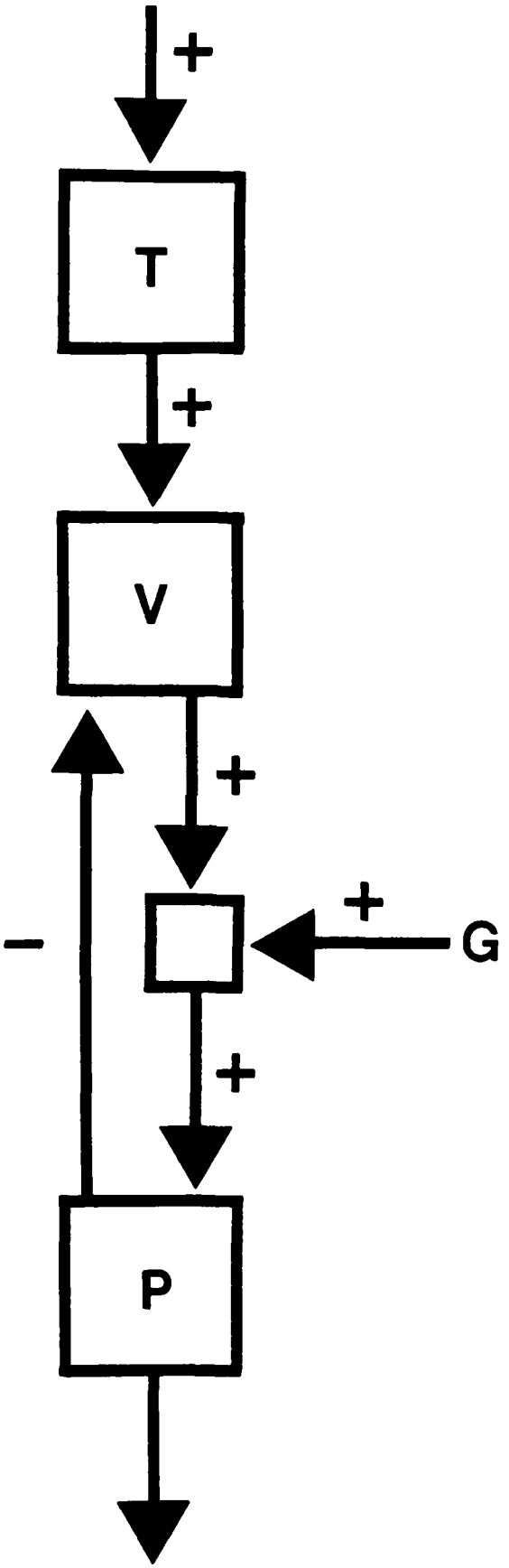

Figure 16

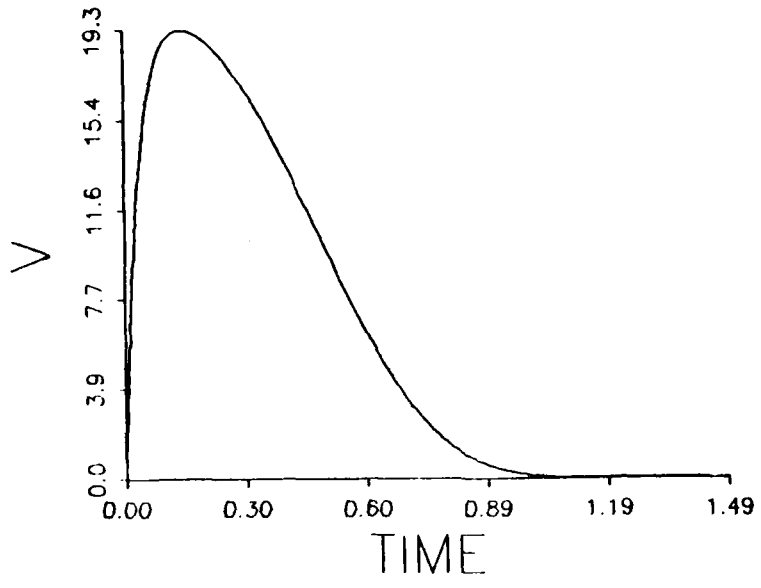
V
0.0
3.9
7.7
11.6
15.4
19.3
0.00
0.30
0.60
0.89
1.19
1.49
TIME

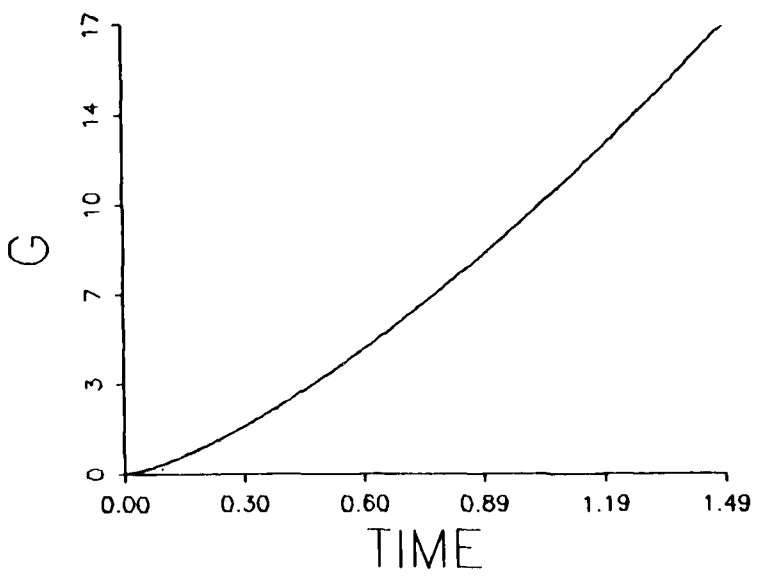
G
0
3
7
10
14
17
0.00
0.30
0.60
0.89
1.19
1.49
TIME

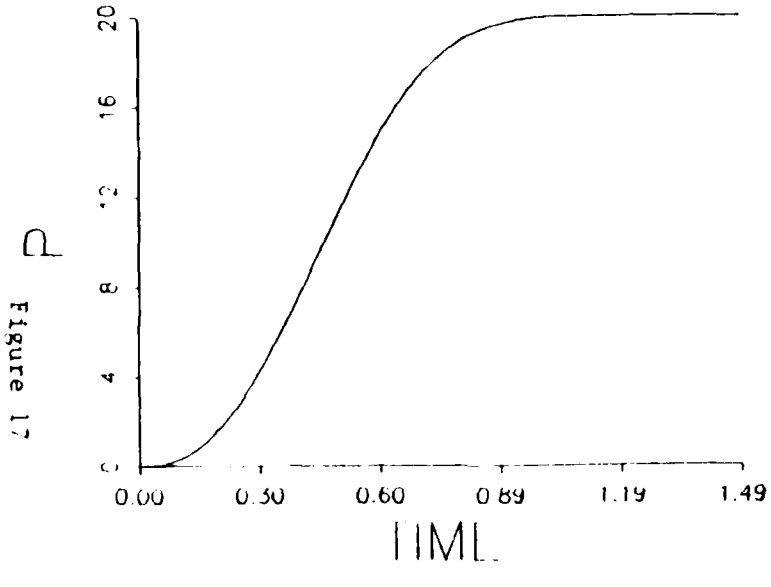
P
0
4
8
12
16
20
0.00
0.30
0.60
0.89
1.19
1.49
TIME

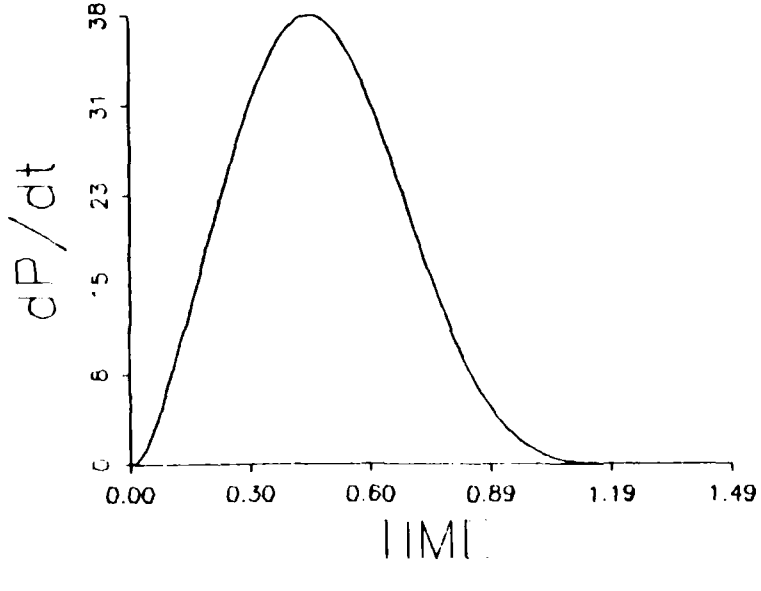
dP/dt
0
6
15
23
31
38
0.00
0.30
0.60
0.89
1.19
1.49
TIME

Figure 17

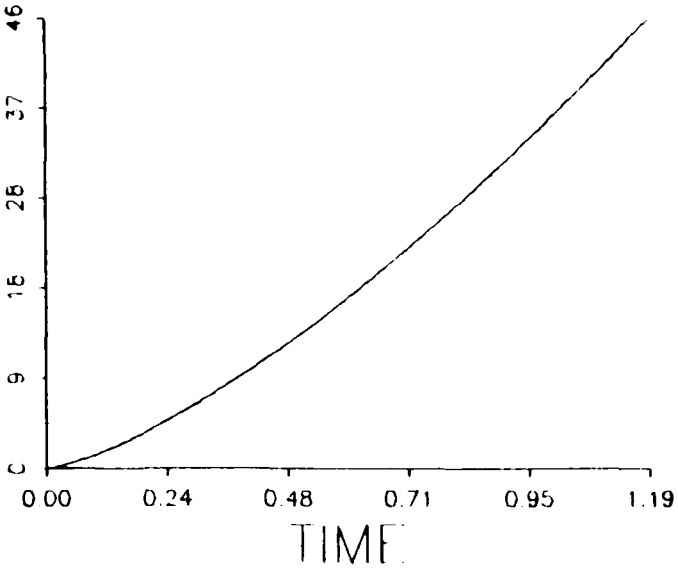
G
0
9
18
28
37
46
0.00
0.24
0.48
0.71
0.95
1.19
TIME

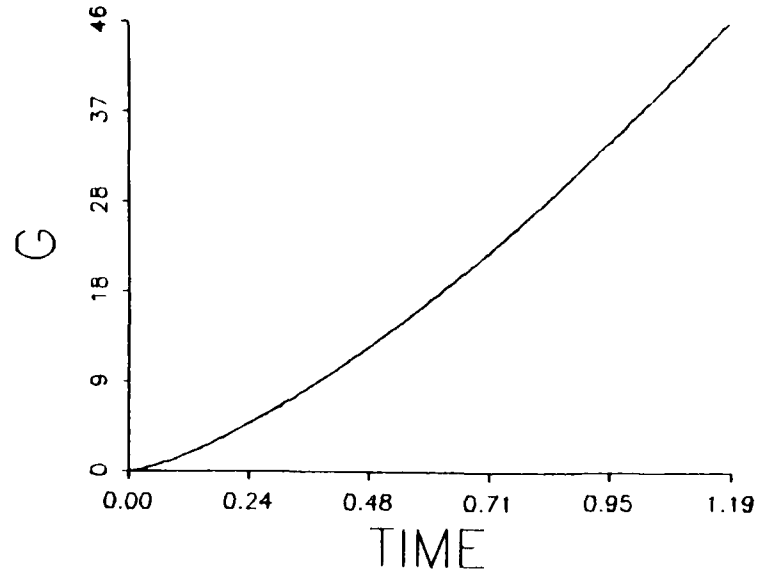
G
0
9
18
28
37
46
0.00
0.24
0.48
0.71
0.95
1.19
TIME

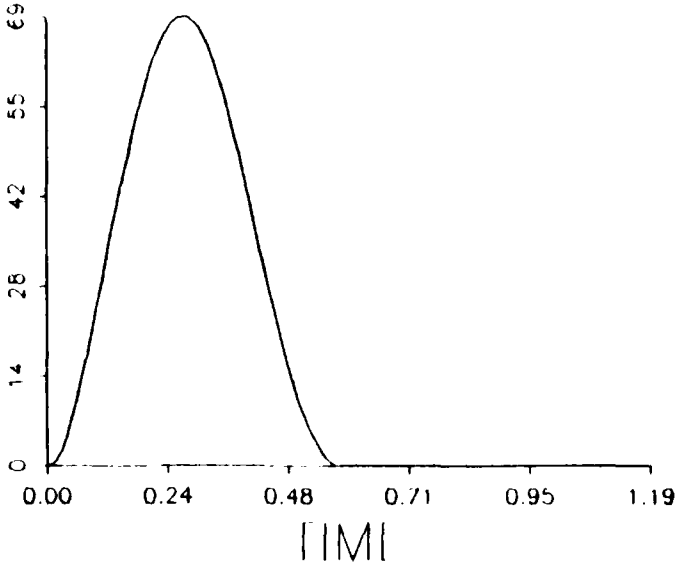
dP/dt
0
14
28
42
55
69
0.00
0.24
0.48
0.71
0.95
1.19
TIME

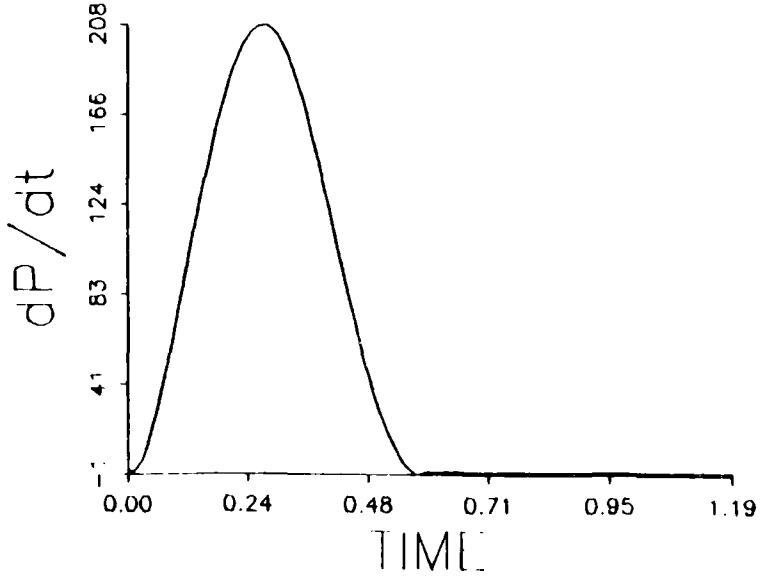
dP/dt
41
83
124
166
208
0.00
0.24
0.48
0.71
0.95
1.19
TIME

Figure 18

(A)

(B)

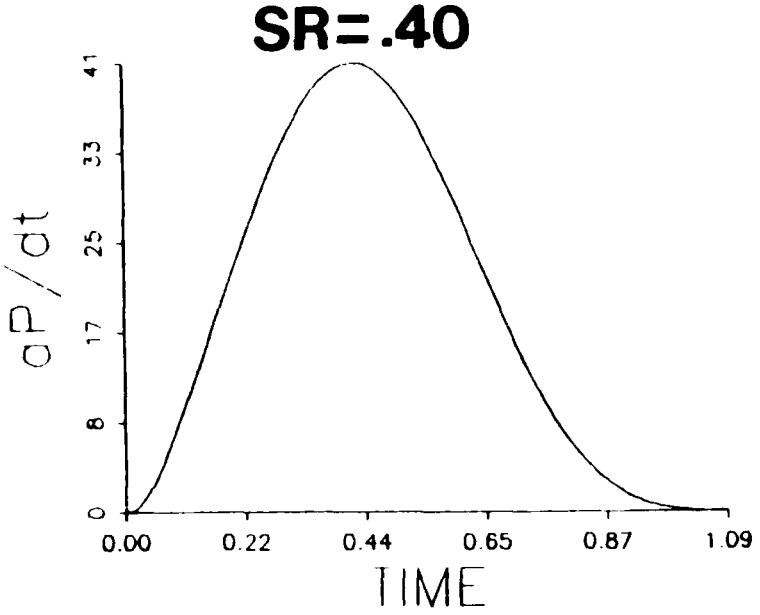

(A)

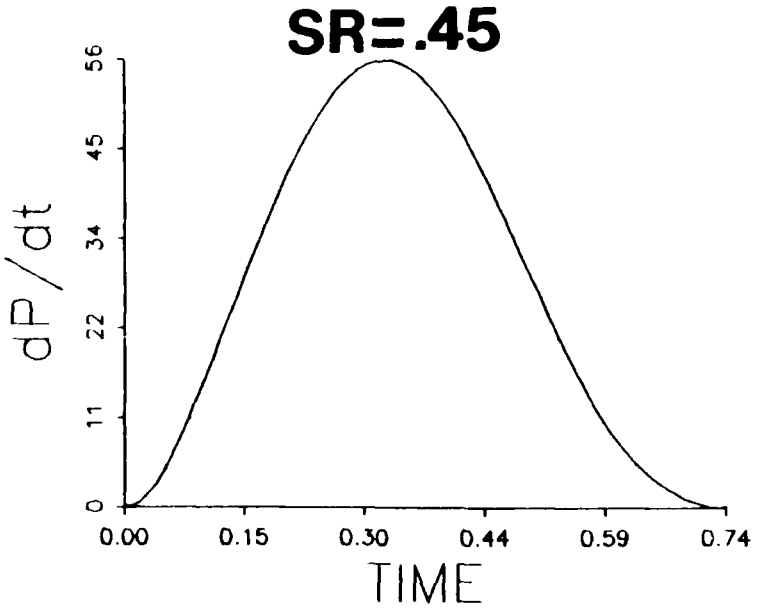

(B)

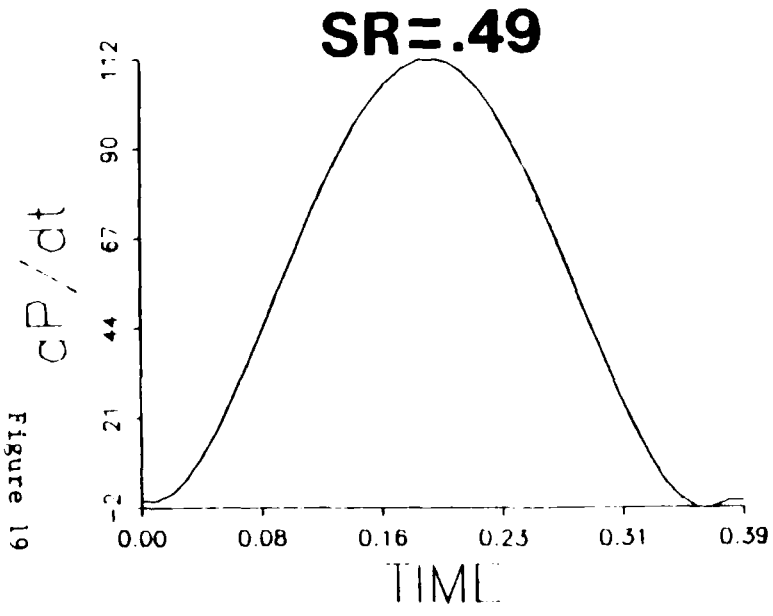

(C)

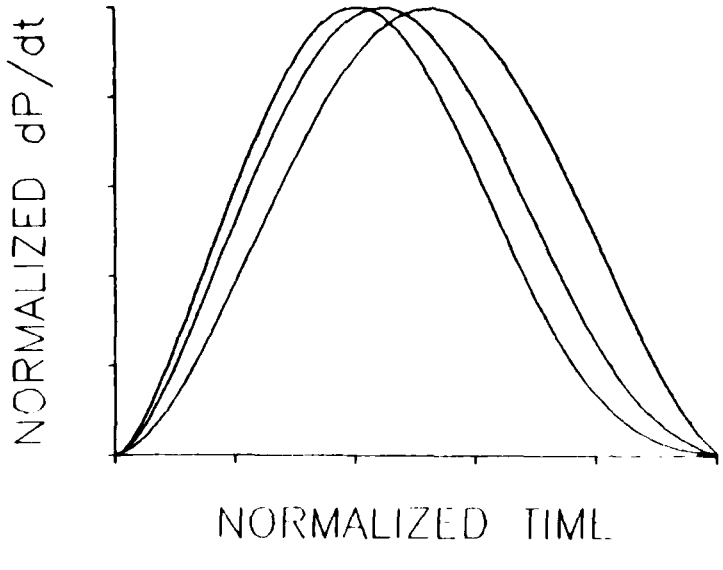

(D)

Figure 19

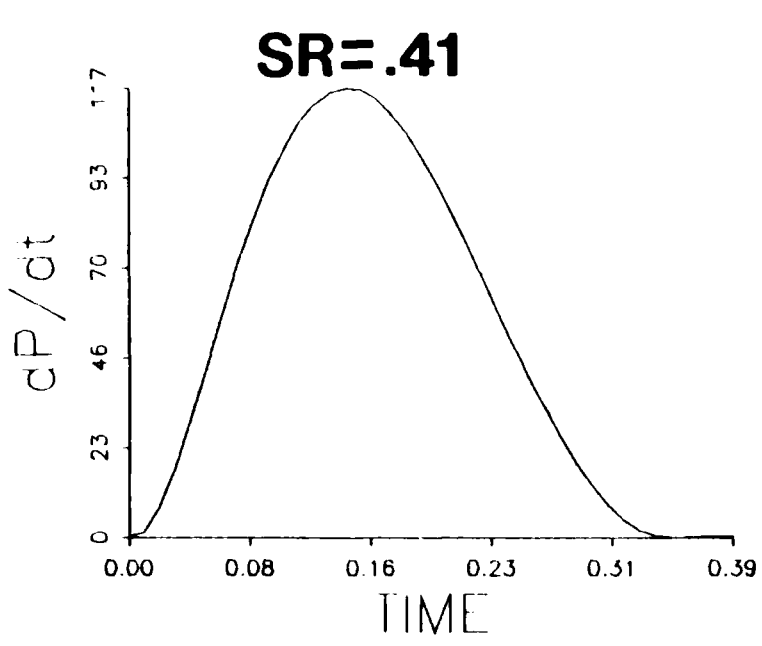

(A)

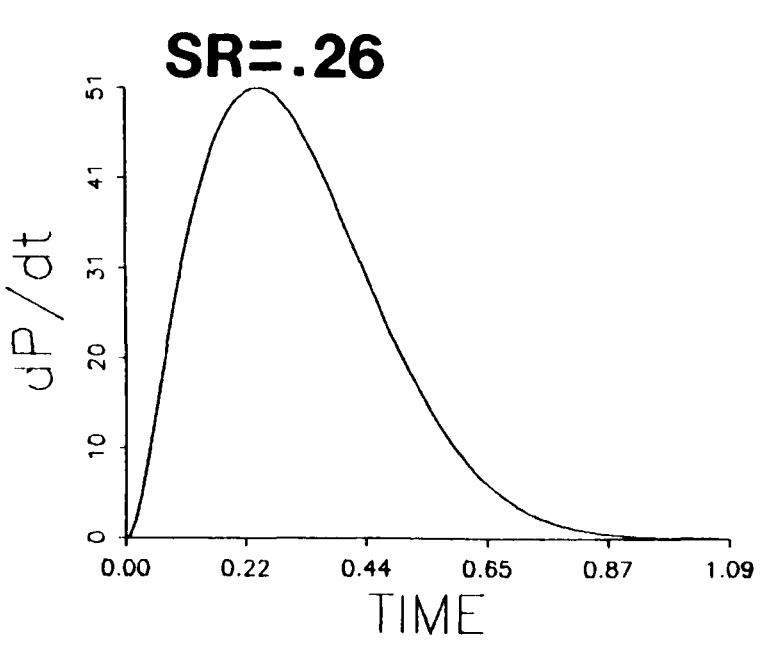

(B)

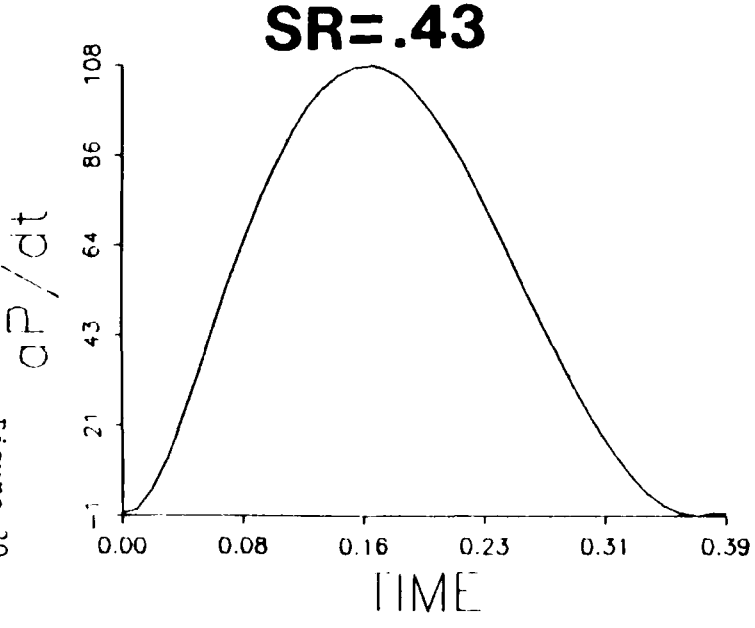

(C)

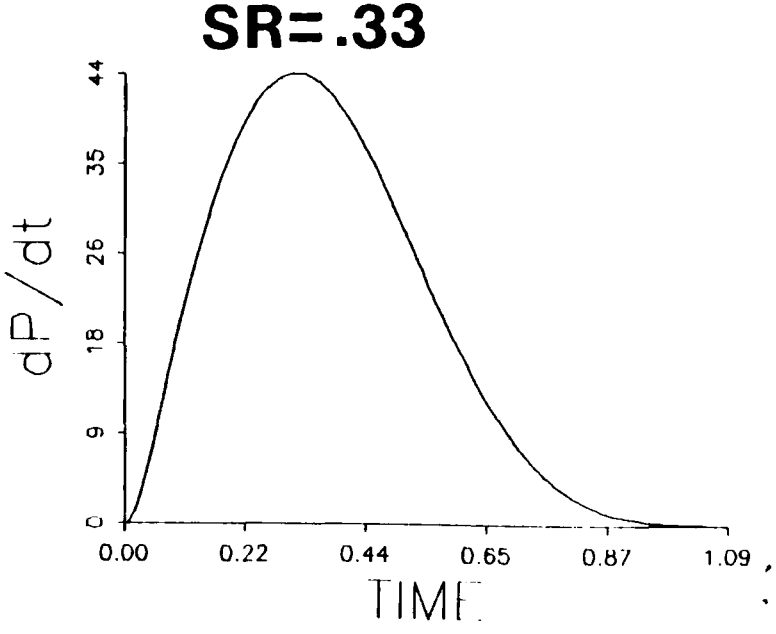

(D)

Figure 20

C
0
4
8
12
16
20
0.00
0.08
0.16
0.23
0.31
0.39
TIME

dP/dt
0
25
51
77
103
128
0.00
0.08
0.16
0.23
0.31
0.39
TIME

V
1.1
2.6
6.3
10.1
13.8
17.5
0.00
0.08
0.16
0.23
0.31
0.39
TIME

P
0
4
9
13
17
21
0.00
0.08
0.16
0.23
0.31
0.39
TIME

Figure 21

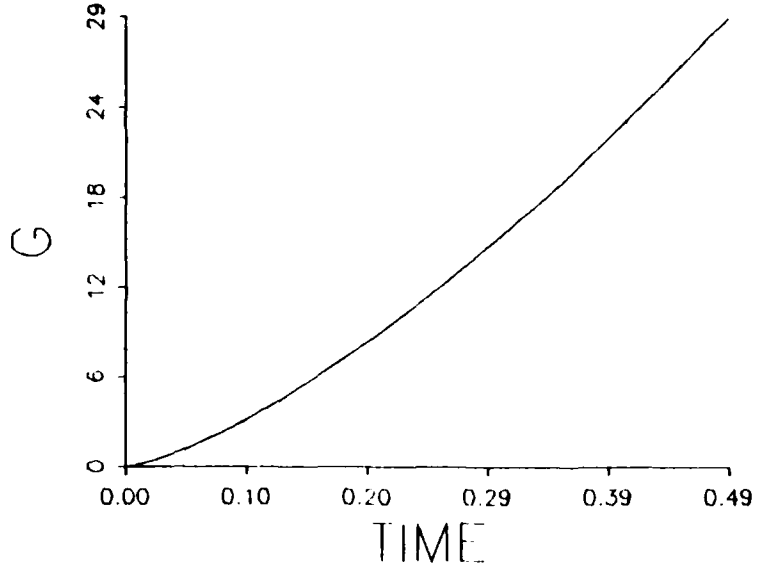
G
0
6
12
18
24
29
0.00
0.10
0.20
0.29
0.39
0.49
TIME

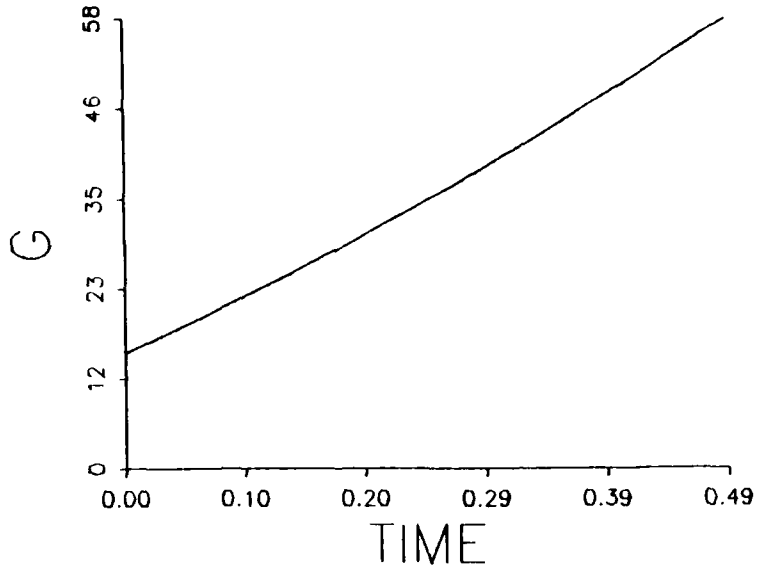
G
0
12
23
35
46
58
0.00
0.10
0.20
0.29
0.39
0.49
TIME

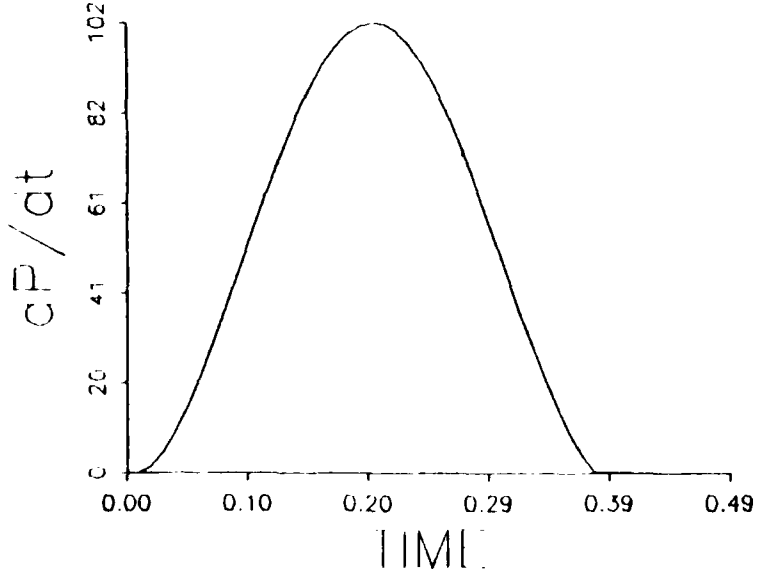
dP/dt
0
20
41
61
82
102
0.00
0.10
0.20
0.29
0.39
0.49
TIME

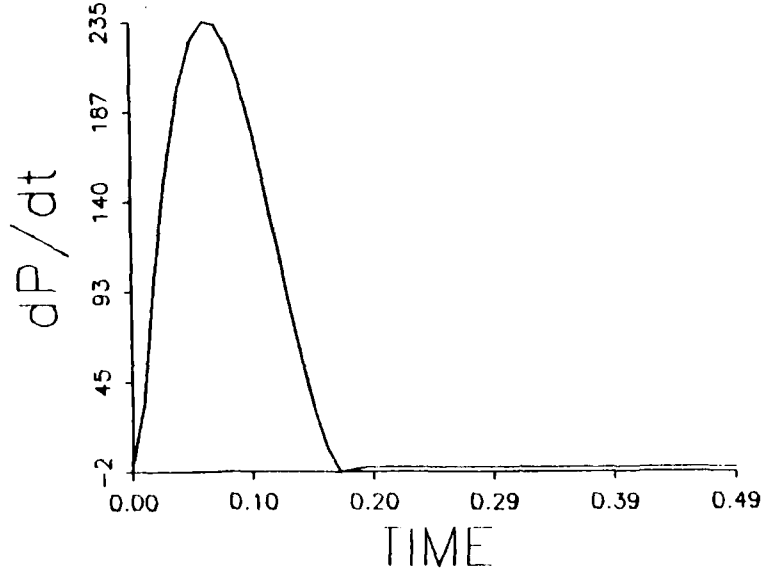
dP/dt
-2
45
93
140
187
235
0.00
0.10
0.20
0.29
0.39
0.49
TIME

Figure 22

(A)

(B)

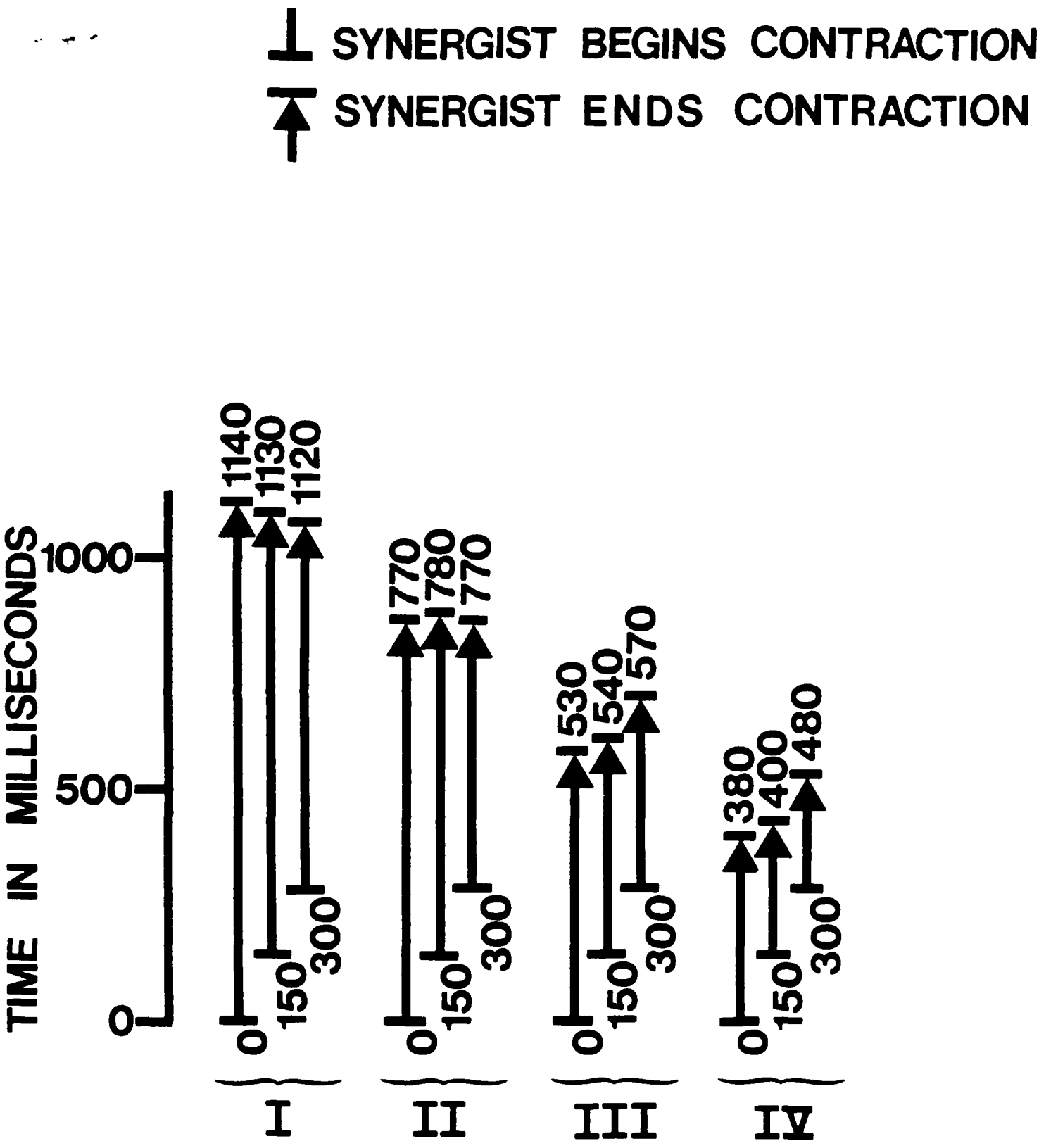
SYNERGIST BEGINS CONTRACTION
SYNERGIST ENDS CONTRACTION
TIME IN MILLISECONDS
1000
500
0
1140
1130
1120
770
780
770
530
540
570
380
400
480
0
150
300
I
II
III
IV

Figure 23

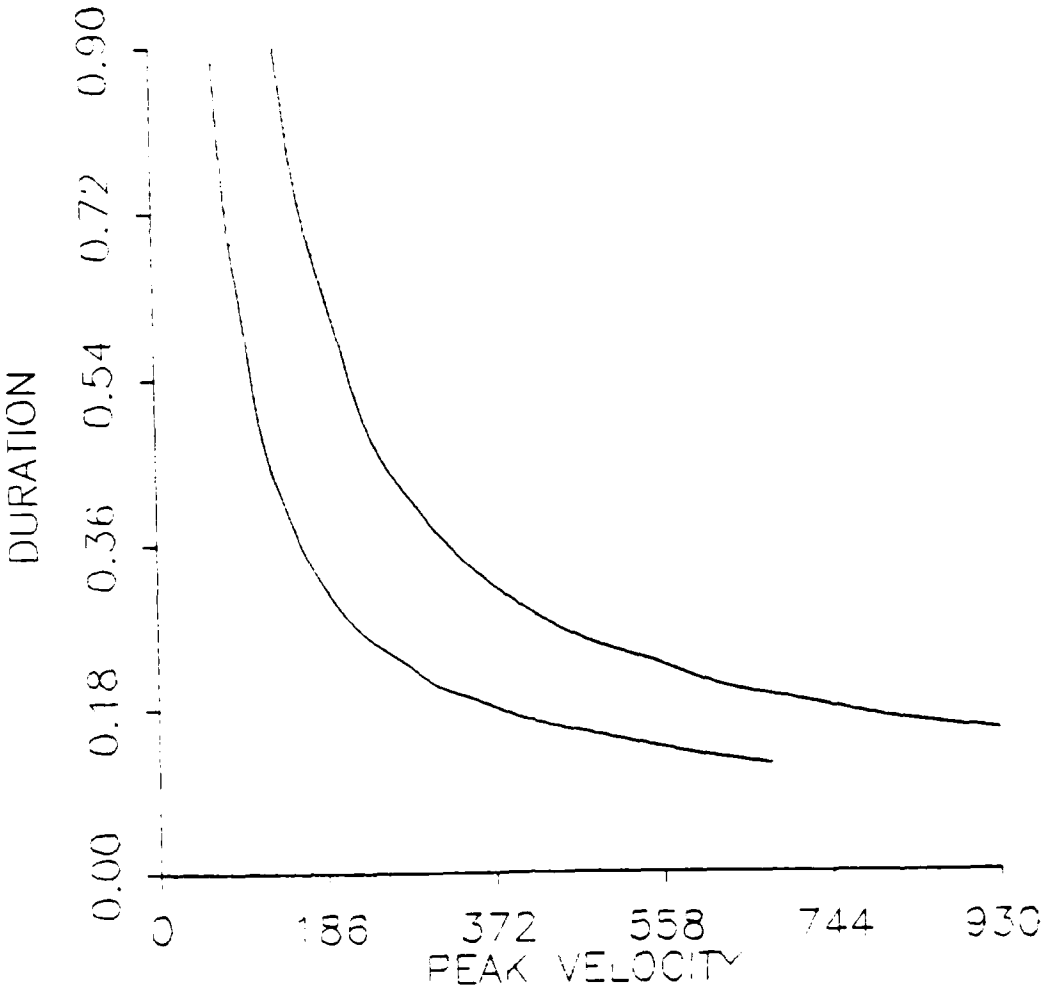
DURATION
0.00
0.18
0.36
0.54
0.72
0.90
0
186
372
558
744
930
PEAK VELOCITY

(A)

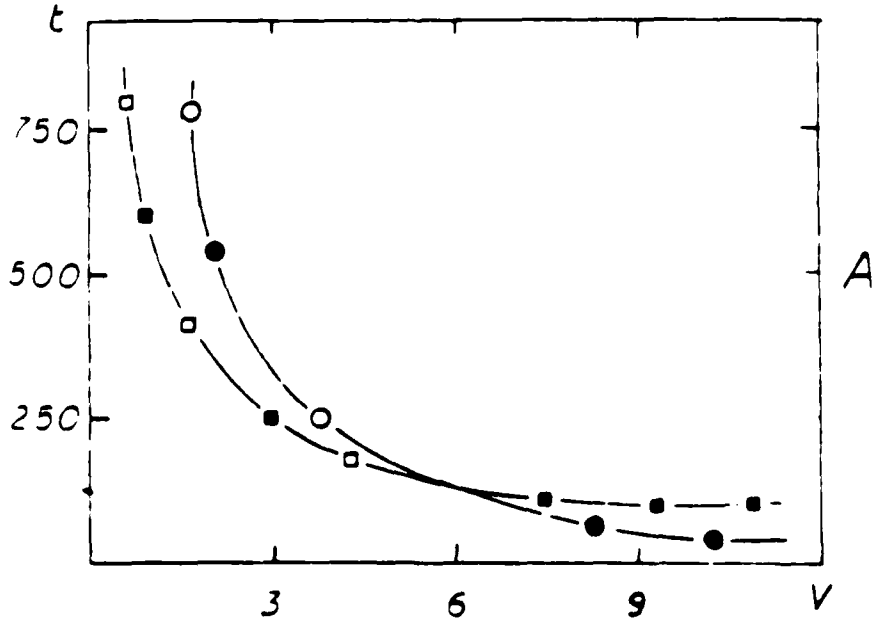
t
750
500
250
A
3
6
9
V

(B)

Figure 24

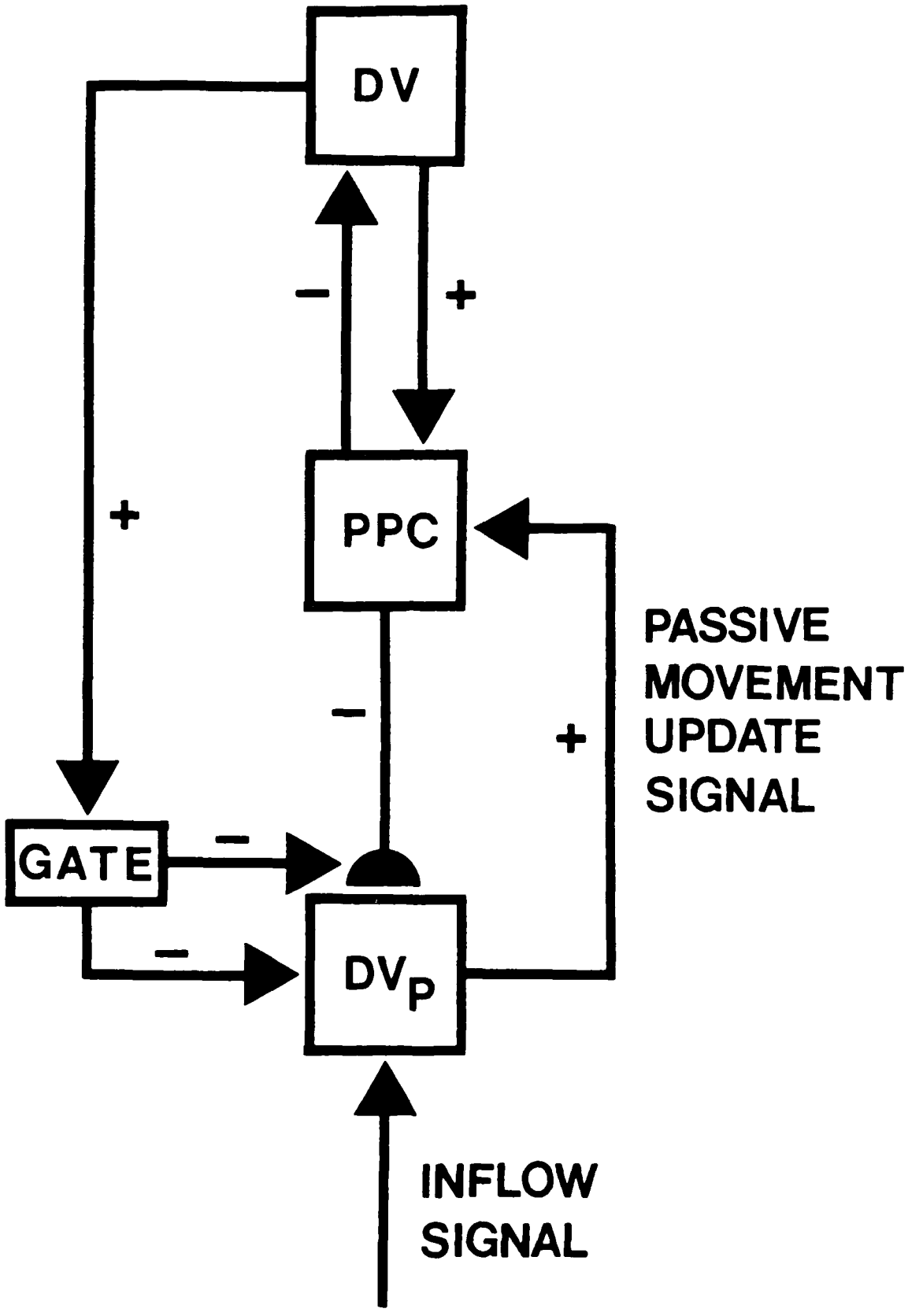
DV
PPC
GATE
DVP
PASSIVE MOVEMENT UPDATE SIGNAL
INFLOW SIGNAL
+
−
+
−
+
−
−

Figure 25

Neural Dynamics of Adaptive Sensory-Motor Control

Ballistic Eye Movements

By STEPHEN GROSSBERG, *Center for Adaptive Systems, Boston University, Boston, MA, USA, and* MICHAEL KUPERSTEIN, *Department of Biology, Wellesley College, Wellesley, MA, USA*

ADVANCES IN PSYCHOLOGY, Volume 30

1986. xvi + 336 pages. US $74.00/Dfl. 200.00 ISBN 0-444-87929-3

The book provides a functional and mechanistic theory of a complex sensory-motor system, the saccadic eye movement system. It shows that learning constraints are rate-limiting in determining the neural circuits of this system. This system solves adaptive problems which are shared with other sensory-motor systems, as well as with other brain learning systems. The results of this investigation suggest new designs for self-calibrating robots.

Forthcoming:

The Adaptive Brain

Vol. 1: Cognition, Learning, Reinforcement, and Rhythm

Vol. 2: Vision, Speech, Language, and Motor Control

Editor: S. GROSSBERG

These two volumes integrate interdisciplinary data, rigorously developing basic adaptive neural circuits used in vision, speech, cognitive self-organization, conditioning, reinforcement, attention, biological rhythms, and motor control. The results are a contribution not only to psychology and neurobiology, but also to artificial intelligence, adaptive control theory and engineering.

north-holland

IN THE U.S.A. AND CANADA:
ELSEVIER SCIENCE PUBLISHING CO., INC.
P.O. BOX 1663
GRAND CENTRAL STATION
NEW YORK, NY 10163, USA

IN ALL OTHER COUNTRIES:
ELSEVIER SCIENCE PUBLISHERS
BOOK ORDER DEPT.
P.O. BOX 211
1000 AE AMSTERDAM
THE NETHERLANDS

US $ prices are valid only in the USA and Canada. In all other countries the Dutch Guilder prices is definitive. Customers in the Netherlands, please add 5% B.T.W. In New York State applicable sales tax should be added. All prices are subject to change without prior notice.

NH/PSY/BK/2198

COOPERATIVE SELF-ORGANIZATION OF MULTIPLE NEURAL SYSTEMS DURING ADAPTIVE SENSORY-MOTOR CONTROL

by

Stephen Grossberg[+]
Center for Adaptive Systems
Boston University
Boston, Massachusetts 02215

To appear in
Aims and Methods in Neuroethology, D.M. Guthrie (Ed.)
Manchester University Press, 1986

Revised Version
April, 1986

[+] Supported in part by the Air Force Office of Scientific Research (AFOSR 85-0149 and AFOSR F49620-86-C-0037), the Army Research Office (ARO DAAG-29-85-K-0095), and the National Science Foundation (NSF IST-84-17756).

Acknowledgements: Thanks to Cynthia Suchta for her valuable assistance in the preparation of the manuscript and illustrations.

TABLE OF CONTENTS

1. Environment, Behavior, and Brain: The Central Role of Adaptive Mechanisms

A thorough ethological analysis of behavior requires the simultaneous consideration of several interacting factors: the environment with which an organism interacts, the behaviors which are generated in that environment, and the neural mechanisms which control and are modified by these environmental-behavioral interactions. The remarkable multiplicity of behaviors, of levels of behavioral and neural organization, and of experimental paradigms and methods for probing this complexity present a formidable challenge to all serious theorists of mind. The challenge is, quite simply, to discover unity behind this diversity by characterizing a small set of theoretical principles and mechanisms capable of unifying and predicting large and diverse data bases as manifestations of fundamental processes.

My colleagues and I have repeatedly found that such fundamental processes can best be discovered by analysing how the behavior of individuals successfully adapts in real-time to constraints imposed by the environment. Such an analysis requires that one identify the functional level on which an individual's behavioral success is defined. This is not the level of individual nerve cells. Rather it is the level of neural systems, properly defined. My chapter will describe several examples of adaptive mechanisms of sensory-motor control to illustrate the fact that one cannot, in principle, determine the properties which govern behavioral success from an analysis of individual cells alone. An analysis of individual cells is insufficient because key behavioral properties are often emergent properties due to interactions among cells. Different types of specialized neural circuits govern different combinations of emergent properties.

On the other hand, it is equally incorrect to assume that the properties of individual cells are unimportant, as many proponents of artificial intelligence have incessantly done to promote the untenable claim that human intelligence can be understood through an analysis of Von Neumann computer architectures. Carefully designed single cell properties are joined to equally carefully designed neural circuits to generate the subtle relationships among emergent behavioral properties which are characteristic of living organisms. Indeed, on a finer level of analysis, single cells can also be represented by interactive networks of still finer components. Remarkably, formal network mechanisms on different levels of behavioral organization often recapitulate one another (Carpenter and Grossberg, 1983; Cohen and Grossberg, 1983; Grossberg, 1978a, 1980).

In summary, the present approach analyses how brain systems are designed to form an adaptive relationship with their environment. Instead of limiting consideration to a few performance characteristics of a behaving organism, we consider the developmental and learning problems that a brain system as a whole must solve before accurate performance can be achieved. Accurate performance is not taken for granted. Rather the dynamical mechanisms whereby it is achieved and maintained are analysed. Such an analysis is necessary if only because an analysis of performance *per se* does not impose sufficiently many constraints to determine underlying control mechanisms. The unifying power of such theoretical work is due, we believe, to the fact that principles of adaptation—such as the laws governing development and learning—are fundamental in determining the design of behavioral mechanisms.

2. A Comparative Neuroethological Analysis of Ballistic Movement Systems

A wide variety of behaviors and their neural substrates have been subjected to this type of modelling approach. Included are analyses of sensory processing, cognitive recognition codes, reinforcement, attention, motivation, biological rhythms, and the interfacing of these processes with mechanisms for the control of planned motor behavior. Many of these results are brought together in several recent books (Grossberg, 1982, 1986a, 1986b; Grossberg and Kuperstein, 1986). In this chapter, theoretical issues and results are described about

visually guided motor behavior. These results are relevant to such central neuroethological issues as localization, orienting, sensorimotor interfacing, and the design of motor pattern generating circuitry (Evert, Capranica, and Ingle, 1981). They also clarify the types of sensory-motor transformations that are modulated by sensory recognition, attentional, and motivational mechanisms during the synthesis of a behavioral act. In fact, models of how such modulatory mechanisms interface with sensory-motor mechanisms have been developed hand-in-hand with the sensory-motor mechanisms themselves, and each class of models has provided additional constraints upon the other's development.

The need for a sustained investigation of sensory-motor designs is illustrated by two quotations from the important neuroethological proceedings that were summarized in Evert, Capranica, and Ingle (1981). Scheich (1981, pp.7-8) wrote that

> "sensorimotor interfacing covers functional and structural mechanisms of the brain which mediate between sensory and motor maps ... since much less is known about the motor-organization of species-specific behaviors and almost nothing is known about interfacing it is apparent that the state of the art in neuroethology of vertebrates is hardly beyond the stage of a comparative neurobiology of sensory systems."

In their analysis of frog prey capture behavior, Grobstein, Comer, and Kostyk (1981, p.344) wrote that

> "while a given retinal and tectal region corresponds to a single direction in an eye-centered co-ordinate frame, they in fact correspond to a set of directions in a body-centered or movement co-ordinate frame. Conversely, a given point in a movement co-ordinate frame in fact corresponds to a set of points in an eye-centered co-ordinate frame such as the retina or the tectum. We are intrigued by the possibility that between the tectum and the pattern generating circuitry there may be an intermediate level of circuitry into which space is represented in a body-centered or movement co-ordinate frame. Because of the many to one and one to many character of the transformation in going from an eye-centered to a body-center or movement co-ordinate frame, disturbances of circuitry involved in this transformation might be expected to result not in disconnection of particular tectal regions from pattern generating circuitry but rather in an alteration in the particular output associated with activation of given tectal regions."

These remarks illustrate the critical importance of understanding the computations whereby sensory inputs generate motor actions. To the extent that one cannot characterize these sensory-motor transformations, understanding of the state-dependent mechanisms which modulate them is correspondingly weakened. For example, unless one can say how a motor trajectory is planned and executed, one cannot adequately understand how shifts in reinforcement, attentional distractors, or other types of environmental feedback can alter these planning mechanisms before or during the execution of a motor trajectory. Understanding how a motor trajectory is planned and executed is also needed to characterize how the neural mechanisms which encode *what* a stimulus is interact with the mechanisms which compute *where* it is to plan how to reach it.

In the present analysis, as in all neuroethological analyses, I illustrate some general organizational principles and mechanisms through an analysis of a single sensory-motor system, the mammalian saccadic eye movement system. Saccadic eye movements are ballistic movements of great speed and accuracy in humans and many other mammals. Toads do not make involuntary saccadic eye movements (Autrum, 1959; Evert, Burghagen, and Schürg-Pfeiffer, 1981). On the other hand, a number of vertebrates, including toads, do make ballistic snapping movements which involve tectal interactions (Evert, Capranica,

and Ingle, 1981). The tectum is a homolog of the mammalian superior colliculus, which is involved in the generation of ballistic eye movements (Hikosaka and Wurtz, 1983; Mays and Sparks, 1980; Schiller and Stryker, 1972; Sparks, 1978; Sparks and Mays, 1981). As in the control of ballistic snapping behavior by the frog tectum (Grobstein, Comer, and Kostyk, 1981), the monkey superior colliculus generates ballistic eye movements which have been recoded from retinal coordinates into egocentric coordinates (Mays and Sparks, 1980, 1981; Schiller and Sandell, 1983). The mammalian saccadic eye movement system thus offers neuroethology a useful source of insights for comparative analysis with systems which have traditionally been subjected to a neuroethological analysis.

3. Hierarchical Resolution of Informational Uncertainty: Relating Anatomy to Adaptive Function

A central theme running through an analysis of real-time adaptive behavior concerns the manner in which neural subsystems are interconnected to solve a behavioral problem which is incompletely specified at any one stage of neural processing. As mentioned in Section 2, all the examples described in this chapter concern saccadic, or ballistic, eye movements in mammals. Although saccadic eye movements are a relatively simple type of motor behavior, a large number of brain regions are utilized to control them. These regions include retina, superior colliculus, visual cortex, parietal cortex, frontal cortex, cerebellum, peripontine reticular formation, and the oculomotor nuclei (Baker and Berthoz, 1977; Fuchs and Becker, 1981; Ito, 1984; Keller and Zee, 1986; Zuber, 1981).

Our analysis of saccadic movements has identified a series of distinct learning problems that its control system needs to solve in order to achieve and maintain accurate performance characteristics (Grossberg and Kuperstein, 1986). We have hereby translated an anatomical multiplicity of brain regions into a functional multiplicity of learning problems. Each brain region can then be discussed as a real-time circuit realization that is capable of solving a class of functionally characterized problems. Several sensory-motor control systems can all send circuits through a single brain region because these circuits all need to solve a similar functional problem. Such an analysis suggests, for example, a single model of the cerebellum which can be used by several sensory-motor circuits that all require a certain type of conditionable gain control property. In each of these circuits, the internal architecture of the cerebellar model is the same. Only the input pathways and output pathways that are connected to the model are changed. Thus, once one has used adaptive constraints on one type of behavior to characterize a neural design, one can then utilize this design to help discover how functionally related adaptive behaviors are organized. For his reason, our work on eye movements has provided a basis for developing an analysis of arm movements (Bullock and Grossberg, 1986).

4. Planned versus Reactive Movements: The Problem of Infinite Regress

Once the primacy of adaptive constraints is granted, the problem of infinite regress cannot be avoided. On what firm computational foundation can adaptive calibrations be based? If parameters in several subsystems can all change due to learning, then what prevents learning in one subsystem from undoing the learning in a different subsystem? What prevents a global inconsistency from developing due to the very fact that individual subsystems, by needing to be specialized to deal with part of an adaptive problem, cannot have complete information about the problem as a whole?

We have found that infinite regress can be avoided through a mechanistically characterized developmental sequence. In it, obligatory saccadic movements to flashing or moving lights on the retina are supplemented by attentionally mediated movements towards motivationally interesting or intermodal (e.g., auditory) sensory cues. These movements are supplemented once again by predictive saccades which form part of planned sequences of

complex movement synergies capable of ignoring the sensory substrate on which they are built.

The distinction between reactive movements and planned movements illustrates the subtlety of the infinite regress problem. In our theory, as in the data, the analysis of these two types of movements implicates both the superior colliculus and the frontal eye fields (Bruce and Goldberg, 1984; Buchtel and Guitton, 1980; Goldberg and Bushnell, 1981; Hikosaka and Wurtz, 1983; Mays and Sparks, 1980, 1981; Schiller, Sandell, and Maunsell, 1984; Schiller, True, and Conway, 1979; Sparks and Mays, 1981). Although patients with discrete frontal lobe removals for intractable epilepsy produce obligatory saccades to visual stimuli (Buchtel and Guitton, 1980; Goldberg and Bushnell, 1981), normal humans have a remarkable capacity to override the influence of sensory cues (Murphy, Haddad, and Steinman, 1974; Steinman, 1965). Steinman (1976, p.121) has, for example, written: "Perhaps the most striking aspect of human oculomotor performance is its independence from stimulus variables. By this I mean that a normal human adult can look about in his visual world and attend whatever region catches his fancy undisturbed by ... light on his retina, or, in perceptual terms, the way the visual world looks at a particular movement." Thus, when a human generates a planned eye movement, he or she does so by suppressing the influence of lights on the retina that would otherwise have caused a reactive eye movement.

When one considers how an accurate planned movement can be learned, however, it becomes clear that visual error signals, although not the only type of error signals, are the final arbiter of movement accuracy. The planned movement system, no less than the reactive movement system, requires visual error signals to tune its movement commands. Yet during a planned movement, sensitivity to visual signals is suppressed. How can the planned movement system both suppress sensitivity to visual signals in order to generate a planned movement at all, yet benefit from visual signals to learn how to generate *accurate* planned movements? In particular, how are movement parameters that are learned by the reactive movement system used to enable accurate planned movements to be learned, thereby avoiding the problem of infinite regress? This issue, although critical to discovering how reactive and planned movement systems are designed and interact, is invisible to an analysis that is based entirely on movement performance. The same is true of many neural designs that we have discovered during our analyses of sensory-motor data.

5. Learned Coordinate Transforms: Comparing Target Position with Present Position to Gate Intermodal Learning

Many of the learning problems which are solved by an adaptive sensory-motor system take the form of learned transformations between different coordinate systems, or neural maps. Several of these learned transformations are summarized herein to illustrate major issues in sensory-motor control. A good place to begin this discussion is with the central problem of how, when an observer looks at an object, the observer's hand knows where to move in order to touch the object? I will discuss this issue from the perspective of eye-hand coordination in a mammal, but the issues that are raised, as well as the conclusions that are drawn, generalize to many other species and sensory-motor systems.

How is a transformation learned between the parameters of the eye-hand system and the hand-arm system so that an observer can touch a visually fixated object? Following Piaget (1963), let us imagine that an infant's hand makes a series of unconditional movements, which the infant's eyes unconditionally follow. As the hand occupies a variety of positions that the eye fixates, a transformation is learned from the parameters of the hand-arm system to the parameters of the eye-head system. A *circular reaction*, or reverse transformation, is also learned from parameters of the eye-head system to parameters of the hand-arm system. This reverse transformation enables an observer to intentionally move its hand to a visually fixated position.

How do these two sensory-motor systems know what parameters are the correct ones to map upon each other? This question raises the fundamental problem that many neural signals, although large, are unsuitable for being incorporated into behavioral maps and commands. They are "functional noise" to the motor learning process. The learning process needs to be actively modulated, or gated, against learning during inappropriate circumstances.

In the present instance, not all positions which the eye-head system or the hand-arm system assume are the correct positions to associate through learning. For example, suppose that the hand briefly remains at a given position and that the eye moves to foveate the hand. An infinite number of positions are assumed by the eye as it moves to foveate the hand. Only the final, intended, or expected position of the eye-head system is a correct position to associate with the position of the hand-arm system.

Learning of an intermodal motor map must thus be prevented except when the eye-head system and the hand-arm system are near their intended positions. Otherwise, all possible positions of the two systems coud be associated with each other, which would lead to behaviorally disastrous consequences. Several important conclusions follow from this observation (Grossberg, 1978b; Grossberg and Kuperstein, 1986).

(1) All such adaptive sensory-motor systems compute a representation, or map, of target position (also called expected position, or intended position).

(2) All such adaptive sensory-motor systems also compute a representation of present position.

(3) During movement, target position is matched against present position. Intermodal map learning is prevented except when target position approximately matches present position (Figure 1). A *gating*, or modulator, signal is thus controlled by the network at which target position is matched with present position. This gating signal enables learning to occur when a good match occurs and prevents learning from occurring when a bad match occurs.

(4) In order to compare target positions with present positions, both types of data must be computed in the same coordinate system. Present eye position is computed with respect to head coordinates. Thus there is an evolutionary pressure to encode target position in head coordinates.

Figure 1

6. Trajectory Formation Using Neural Vectors: Automatic Compensation for Present Position

The above discussion of how *intermodality* sensory-motor transformations are learned also sheds light upon how *intramodality* movement trajectories are formed. Intermodality transformations associate target positions because only such transformations can avoid the multiple confusions that could arise through associating arbitrary positions along a movement trajectory. Target position commands are not, however, sufficient to generate intramodality movement trajectories. In response to the same target position command, an eye, arm, or leg must move different distances and directions depending upon its present position when the target position is registered.

Present position signals can be used to convert a single target position command into many different movement trajectories. Computation of the difference between target position and present position at the match interface in Figure 1 generates a movement *vector* that automatically compensates for present position. Such automatic compensation accomplishes a tremendous reduction in the memory load that is placed upon an adaptive sensory-motor system. Instead of having to learn whole movement trajectories, the system only has to learn intermodality maps between target positions. The neural vectors which

are computed from target positions and present positions at the match interface automatically generate the movement commands from which the trajectory is formed. In summary, consideration of the types of information that can be learned during motor development leads to general conclusions about how movement trajectories are formed, and thus about the way in which other neural systems can influence the planning of such trajectories.

In the saccadic eye movement system, there is now convincing experimental evidence that a critical stage in the generation of a movement command consists in the computation of a neural vector (Bruce and Goldberg, 1984, 1985; Hallett and Lightstone, 1976; Mays and Sparks, 1980, 1981; Schiller and Sandell, 1983; Sparks and Mays, 1981; Zee, Optican, Cook, Robinson, and Engel, 1976), and that such vectors are manipulated both by the superior colliculus and the frontal eye fields. As in the general discussion above, such a vector computation compares a target position with a present position to generate a movement command. In the case of eye movements, the target position is derived from the position of a light on the retina (Figure 2). The present position is derived from a position of the eye in the head. Subtraction of present position from target position generates a difference vector that represents how far the eye must move in order to foveally fixate a target. Before discussing the learned transformations which need to be carried out in order to realize this ostensibly simple computation, I will pause to further emphasize some of its conceptual implications.

Figure 2

Computation of movement vectors is a radically different approach to generating a trajectory than are traditional computations based upon a Newtonian analysis of movement kinematics. In a Newtonian analysis, every position within the trajectory is assumed to be explicitly controlled (Atkeson and Hollerbach, 1985; Brody and Paul, 1984; Hogan, 1984; Hollerbach, 1984). Such computations rapidly lead to a combinatorial explosion which is hard to reconcile with the rapidity of biological movement generation in real-time. In a vector computation, the entire trajectory is never explicitly planned. Instead, a target position is computed which determines where the movement expects, or intends, to terminate. The subtraction of present position is an automatic process which compensates for the variability of the starting position. The vector which is hereby computed can generate an accurate movement without ever explicitly computing a planned sequence of trajectory positions for the whole movement. In a typical saccadic movement, a single vector may generate the entire movement. In arm movements, by contrast, a continuous comparison of a fixed target position with the present positions achieved during the movement is often made (Bullock and Grossberg, 1986). All of these compensations for present position changes are automatically registered, and therefore place no further burden whatsoever upon the computation of planned movement parameters. In addition, such automatic compensations for present position spontaneously generate the major invariants of arm movements that have been discovered to date. Thus the general problem of how neural vectors are computed is a central one for the understanding of trajectory formation in several movement systems.

7. Learned Transformation of Target Position from Retinotopic to Head Coordinates: A Many-To-One, Invariant, Self-Regulating Target Position Map

Despite the apparent simplicity of the difference vector concept, its actual computation in an adaptive system requires the solution of several important problems. All of these problems derive from the fact that target position and present position are computed using different kinds of information. One thus cannot compare them unless they can first be made dimensionally consistent.

In particular, a light on the retina is computed in a *retinotopic* coordinate system, because lights hit the retina. Present eye position is computed in a *head-centered*, or

egocentric, coordinate system because the eyes move in the head. In order to show how target position and present position become dimensionally consistent, Kuperstein and I analysed how the position of a light on the retina can be transformed from a retinotopic coordinate system, or frame, into a head coordinate system, or frame. Once target positions are computed in a head frame they can be compared with present positions which are also computed in a head frame, as in Figure 1. Neurophysiological data suggest that one place where a target position map in a head frame is computed is the posterior parietal cortex (Anderson, Essick, and Siegel, 1984; Hyvärinen, 1982; Lynch, 1980; Motter and Mountcastle, 1981).

In order to convert the position of a light on the retina into a target position in head coordinates, one needs to join together information about the light's retinotopic position with information about present position of the eye in the head (Figure 3). We suggest that this type of transformation is learned. Otherwise, the retinotopic system and the present position system—which are widely separated in the brain and designed according to different internal constraints—would also have to be pre-wired with perfectly chosen parameters for interaction with yet another brain system. We have shown how to avoid precise pre-wiring. Indeed, we have shown how a transformation can be learned even if parameters are coarsely chosen initially and if significant portions of either system are damaged or even destroyed. This type of learning exhibits properties which are of general interest in other movement systems and also in cognitive psychology. I will therefore describe its major elements here.

Figure 3

The most important properties of this transformation are that it is many-to-one, invariant, and self-regulating. As Figure 3 illustrates, many combinations of retinal position and eye position correspond to a single target position with respect to the head, as Grobstein *et al.* (1981) have also emphasized in their study of frog tectum. When a single representation in the brain is activated by all of these possible combinations, the transformation is said to be invariant (Figure 4). The key difficulty in understanding how such an invariant transformation is learned arises from its many-to-one property. The

Figure 4

many-to-one property implies that each retinal position and each eye position can activate many target positions in head coordinates (Figure 5). Even after learning takes place, each pair of retinal and eye positions can activate many target positions in head coordinates, but only the correct target position receives the maximal total activation.

Figure 5

What prevents learning due to one pair of retinal and eye positions from contradicting learning due to a different pair of positions? In particular, if pairing retinal position R_1 with eye position E_1 strengthens the pathways from these positions to target position T_1, then why does not future pairing of R_1 with a different eye position E_2 continue to maximally excite T_1 instead of the correct target position corresponding to R_1 and E_2? How is a *globally consistent rule* learned by a network, despite the fact that all computations in the network are local? How can a target position map be *implicitly* defined, such that each eye position and retinal position, taken separately, activates a large number of target positions, yet in combination always maximally activate the correct target position?

Finally, the property of self-regulation means that the map can correct itself even if a large fraction of the retinal positions and/or eye positions are destroyed, or if their parameters are otherwise altered through time. Destruction of a single retinal position eliminates all the combinations which that position made with all eye positions to activate

target positions. In a similar fashion, destroying a single eye position can disrupt all target positions with which it was linked. A self-regulating map must thus be able to reorganize *all* of its learned changes to maintain its global self-consistency after removal of any of its components.

The self-regulation property is illustrated by the computer simulation summarized in Figure 6. Each row in Figure 6 depicts learning of target positions corresponding to a different number of retinal and eye positions. More combinations of positions are represented in each successive row. The first column in each row depicts an intermediate learning stage, and the second column depicts a late learning stage. The abscissa plots topographic positions across the retinal and eye positions maps, whereas the ordinate plots the sizes of the adaptive path strengths, or learned long term memory (LTM) traces, in the pathways from these maps to the target position map (TPM). Such a TPM refines the concept of target position map that is schematized in Figure 1. The LTM traces were randomly chosen before learning began. A comparison of panels (b), (d), and (f) shows that the LTM traces can reorganize themselves when more combinations of positions are associated in such a way as to (approximately) preserve that part of the map which was learned when fewer combinations of positions were associated. This self-regulation property also holds when more combinations are replaced by fewer combinations, or if the initial LTM traces are not randomly chosen.

Figure 6

8. Autoreceptors: Presynaptic Competition for Long Term Memory

The complete theory of how an invariant self-regulating target position map (TPM) can be learned, as well as variants of this theory, are developed in Grossberg and Kuperstein (1986). Herein I emphasize three key points about the theory that are especially relevant from an ethological perspective: (i) the need to specialize the laws for individual cells to enable them to interact effectively in a specialized network to achieve a prescribed functional capability; (ii) the need to recognize these specialized laws as evolutionary variations of general dynamical principles; and (iii) the need to solve the problem of infinite regress.

(i) The specialization in question achieves the invariance and self-regulation properties of the TPM. How do *all* the LTM traces whose pathways project to a single TPM cell readjust themselves in a compensatory fashion when any one of these LTM tracs changes due to learning (Figure 3)? We suggest that the synaptic endings in which these LTM traces are computed contain autoreceptors (Cubeddu, Hoffmann, and James, 1983; Dubocovich and Weiner, 1982; Groves and Tepper, 1983; Groves, Fenster, Tepper, Nakamura, and Young, 1981; Niedzwiecku, Mailman, and Cubeddu, 1984; Siever and Sulser, 1984; Tepper, Young, and Groves, 1984). Then when transmitter is released by one synaptic ending, a portion of it can undergo reuptake via the autoreceptors of other active and nearby synaptic endings. Reuptake has an inhibitory effect on the LTM trace of each synaptic ending. Thus autoreceptors help to realize a type of presynaptic competition among all the LTM traces whose pathways converge upon the same cell within the TPM.

Such an LTM trace obeys an equation of the form

$$\frac{d}{dt} z_{ij} = \epsilon S_i \Big[-F z_{ij} + G x_j - H \sum_{k=1}^{n} S_k z_{kj} \Big]. \tag{1}$$

In (1), z_{ij} is the LTM trace in the pathway from the ith cell in the retinotopic map or eye position map to the jth cell in the TPM; S_i is the signal emitted by the ith cell into this pathway; and x_j is the activity, or short term memory (STM) trace, of the jth TPM cell. The terms ϵ, F, G, and H are constants. Equation (1) says that reuptake via autoreceptors

of a fraction of released transmitter, as in term $-H \sum_{k=1}^{n} S_k z_{kj}$, inhibits the growth of the corresponding LTM trace.

Although autoreceptors are well known to occur in certain transmitter systems, notably catecholaminergic systems, this is the first time that they have been used to explain such a high-order functional property as formation of an invariant, self-regulating TPM. If this TPM is indeed to be found in posterior parietal cortex and if the autoreceptors are catecholaminergic, then the theory suggests that experimentalists search for catecholaminergic autoreceptors in those regions of the posterior parietal cortex that are used to build up a TPM in head coordinates.

9. Invariant Map Formation by Associative Learning

(ii) There are several senses in which equation (1) is a specialization of a general learning law. For one, the type of learning which is used to generate a TPM is a variant of the simplest type of associative learning, namely classical conditioning. The events controlled by the external environment do not include an explicit conditioned stimulus (CS) and unconditioned stimulus (US). However, a combination of externally delivered inputs and *internally* generated signals *functionally* act like a CS and a US. The CS is a combination of an externally delivered retinal input and an internally generated eye position signal. This eye position signal computes the *initial* eye position *before* the movement occurs (Figure 3). The US is also an internally generated eye position signal. This eye position signal computes the *final* eye position *after* the movement is over. The retinotopic position and the initial eye position act together like a composite CS which is capable of learning a final eye position US.

There is a second sense in which learning of an invariant TPM is a special case of a more general learning scheme. Removing the autoreceptor term in equation (1) by setting $H = 0$ converts the equation into a learning law which has been used to explain a variety of data about classical conditioning, instrumental conditioning, list learning, and learning of perceptual and cognitive recognition codes (Carpenter and Grossberg, 1986a, 1986b, 1986c; Grossberg, 1976, 1982a, 1982b, 1982c, 1984; Grossberg and Levine, 1986; Grossberg and Stone, 1986; Kohonen, 1982, 1983). Thus processes such as invariant map formation and list learning, which appear to be quite unrelated when described using lay language, can now be studied as variations of general dynamical laws using a formal language whereby adaptive designs can be mechanistically characterized. Such linkages help to discover a mechanistic unity behind the remarkable behavioral diversity that I noted at the beginning of this chapter.

The example of TPM formation also illustrates how the problem of infinite regress (Section 4) enters an analysis of adaptive systems. Each composite CS learns a US that represents the final eye position after a movement terminates. Map learning is invariant because *all* composite CS's which are associated with a single final eye position are capable of learning this position, due to the self-regulation property. However, the task of the system is to learn a *target* position, not just any final eye position. The final eye position equals the target position only if the eye movement is accurate.

In the complete theory, such accuracy is due to the fact that the visually reactive movement system is sensitive to visual error signals (Section 13), and uses these error signals to improve the accuracy of its movements until visually reactive saccades become accurate. The theory assumes that learning of an invariant TPM takes place while the system is in its visually reactive mode. Thus an invariant TPM can be learned because the (distinct) visually reactive system can correct its movement errors. Once an invariant TPM is learned, it stimulates further learning within the attentionally modulated and predictive movement systems of which it forms a part. As a consequence of this learning, these movement systems can compete effectively with the visually reactive system for control of overt movements. I now discuss some of the other functional problems which the system

as a whole needs to solve to realize this developmental progression, and whose solution is triggered by the self-organization of a TPM.

10. Associative Transformation of Target Positions into Motor Coordinates: Automatic Computation of Vectors

The transformation of target position from retinotopic coordinates into head coordinates needs to be followed by further learned transformations. One such learned transformation is necessary in order to compute a movement command vector by subtracting present position from target position (Section 6). Target position, whether in retinotopic or head coordinates, is determined by a *visual* input. In contrast, present position is computed in *motor* coordinates, since the position of each eye in the head is determined by the relative lengths of six muscles that are organized into three agonist-antagonist pairs. Before present position can be subtracted from target position, the two types of information must be made dimensionally consistent. Only then can a vector be computed by subtraction.

To solve this problem, we suggest how a target position in head coordinates can be recoded, by a learned transformation, into a target position in motor coordinates (Figure 7). Then present position in motor coordinates can be subtracted from target position in motor coordinates to compute a vector in motor coordinates. A surprising conclusion of this analysis is that the same network region which learns to transform target position into motor coordinates also automatically computes a vector in motor coordinates. Thus what appeared to be two distinct problems can be solved by a single properly specialized network. This network is called the *head-muscle interface*, or HMI. The HMI is the match interface that was schematically represented in Figure 1.

Figure 7

Figure 8 shows a macrocircuit which relates the HMI to its sources of target position and present position signals. When a population within the TPM is activated by a retinal light, the population sends inhibitory signals along conditionable pathways to all the cells

Figure 8

of the HMI. The HMI also receives present position signals, which are computed in motor coordinates. These present position signals are corollary discharges that are derived from outflow signals to the eye muscles (Figure 9). As in the learning of a TPM (Figure 4) and in the learning of an intermodality associative transform between TPM's (Figure 1), learning within the HMI is prevented from occurring by a learning gate, or modulator, except after an eye movement is over. The visually reactive system guarantees that the corollary discharges which the TPM-activated inhibitory pathways learn after a movement terminates are actually target positions. Thus, transforming target position from head coordinates into motor coordinates is also a specialized type of associative learning.

Figure 9

Each target position in motor coordinates is encoded by the LTM traces of the inhibitory pathways that are activated by that target position from the TPM. Thereafter, when that TPM population is activated, it reads out these LTM values, as inhibitory signals, into the HMI. Present position signals are also read into the HMI, but as excitatory signals. The differences between these target position and present position signals generate an STM activity pattern across HMI cells that encodes a vector in motor coordinates.

These properties of HMI dynamics are succinctly summarized by the following network equations:

Short Term Memory

$$\frac{d}{dt}x_j = -Ax_j + G(\sum_i S_i)(-\sum_i S_i z_{ij} + I_j). \tag{2}$$

Long Term Memory

$$\frac{d}{dt}z_{ij} = \epsilon P S_i(-z_{ij} + B[x_j]^+). \tag{3}$$

Vector

$$V = ([x_1]^+, [x_2]^+, \ldots, [x_6]^+). \tag{4}$$

where

$$G(\sum_i S_i) = \begin{cases} 1 & \text{if } \sum_i S_i > 0 \\ 0 & \text{if } \sum_i S_i \leq 0 \end{cases} \tag{5}$$

$$[x_j]^+ = \begin{cases} x_j & \text{if } x_j > 0 \\ 0 & \text{if } x_j \leq 0 \end{cases} \tag{6}$$

and P is a Now Print signal that becomes positive only after a movement is over. As in equation (1), x_j is an STM trace; in particular, x_j is the activity of the jth HMI population. Function z_{ij} is the LTM trace from the ith TPM population to the jth HMI population. A comparison of the learning equations (1) and (3) shows that both equations are specializations of a more general learning process. Equation (1) contains autoreceptors. Equation (3) contains a movement-sensitive Now Print signal. As the discussion subsequent to equation (1) noted, such Now Print modulation of learning is also needed when equation (1) is specialized within a TPM-learning network.

The vector V in (4) is simply the pattern of output signals generated by the activities $(x_1, x_2, \ldots, x_6)$ of the HMI cells. This output signal pattern also determines the LTM pattern that is learned via equation (3). A complete analysis of how the HMI recodes target positions into motor coordinates and reads out vectors in motor coordinates is provided in Grossberg and Kuperstein (1986).

11. Vectors in Motor Coordinates Are Adaptively Transformed into Retinotopic Coordinates

A vector in motor coordinates must itself be further transformed before it can effectively generate accurate movements. This is true because the final test of an eye movement command's accuracy is whether or not the command enables the eye to foveate a target light. Such a test can only be carried out using visual error signals; in particular, using a measure of how far the target light is from the fovea after the movement is over. This fact suggests that the vector in motor coordinates must be recoded into a retinotopic coordinate system so that it can benefit from visual error signals that are also computed in a retinotopic coordinate system. Thus, after converting visual information into motor coodinates in order to compute a vector command, the movement system then reconverts motor coodinates back into retinotopic coordinates to utilize the error-correcting properties of visual error signals.

The properties of the HMI are essential for carrying out this transformation. Target positions in either head or motor coordinates cannot, in principle, be directly transformed into a retinotopic frame, because the eye can move with respect to the head. On the other hand, the HMI automatically transforms target positions into vectors. Vectors in motor

coordinates can be transformed into retinotopic coordinates, because a vector compensates for initial eye position.

12. Distinct Vectors Activate Distinct Movement Command Pathways Using Interactions Between Adaptive Filter and Competition Mechanisms

Two problems must be solved before a vector in motor coodinates can generate movement commands capable of benefitting from visual error signals. The first problem is to show how distinct vectors in motor coodinates, which all activate a common set of HMI cells, can activate distinct movement command pathways. The second problem is to show how each distinct movement command pathway can correct its movement command using visual error signals. Due to the parsing of vectors into distinct movement command pathways, altering the command controlled by one pathway will not disrupt the movement commands that are controlled by other pathways.

A solution to the first problem is schematized in Figure 10. The problem is to parse vectors so that each vector maximally activates a distinct cell population at the next processing stage. Expressed more generally, such a parsing process recodes distinct spatial patterns into distinct locations in a topographically organized map. Then each location can activate its own movement command pathway.

Figure 10

Several closely related models of this type of transformation are developed in Grossberg and Kuperstein (1986). Figure 11 illustrates a computer simulation of how such a topographic map recodes a vector in motor coordinates into a unimodal focus of maximal activity.

Figure 11

A model capable of realizing such a transformation through learning combines conditionable pathways from the HMI to the topographic map with competition, or lateral inhibition, between the populations of this map. The conditionable pathways are said to form part of an *adaptive filter*. Combinations of adaptive filter and competition mechanisms are ubiquitous in neural models of map formation. See Banquet and Grossberg (1986), Carpenter and Grossberg (1986a, 1986b, 1986c), Cohen and Grossberg (1986), and Grossberg and Stone (1986) for some recent examples of such models in the learning of cognitive recognition codes. Thus the problem of recoding vectors into locations is a special case of a more general theory of code learning. The mechanistic unity achieved by this theory can be clearly appreciated only by using a formal language capable of rigorously characterizing its adaptive design principles.

The model of how an invariant TPM is learned (Section 7) may also be included in this coding theory. Such a model also uses a combination of adaptive filter and competition mechanisms. In forming an invariant TPM, competition is presynaptically mediated by autoreceptors at the synaptic terminals of adaptive filter pathways. In forming a topographic map, competition is postsynaptically mediated by the target cells of the adaptive filter.

13. Automatic Gain Control of Movement Commands by Visual Error Signals: Cerebellar Learning

The second problem concerns the manner in which each movement command pathway can individually benefit from visual error signals to generate a more accurate movement in the future. This analysis leads to a model of learning by the cerebellum which significantly extends earlier models of cerebellar learning (Albus, 1971; Brindley, 1964; Fujita, 1982a, 1982b; Grossberg, 1964, 1969, 1972; Ito, 1974; Marr, 1969; McCormick and Thompson, 1984). I emphasize two key properties of this model herein: (i) the dual action of each

light; and (ii) the learning of a motor synergy. The remainder of this section considers the dual processing issue.

Each light on the retina which is chosen to generate a movement command is processed in parallel along distinct pathways (Figure 12). One pathway—labelled 1 in Figure 12—generates a movement command. The other pathway—labelled 2 in Figure 12—generates an error signal. The movement command is registered and stored in short term memory before the eye moves and can lead to an overt movement. The error signal is registered after the eye moves and provides an error measure of how far the target light still deviates from the fovea. Each movement pathway is, in turn, broken up into two parallel components: an unconditioned pathway and a conditioned pathway. The unconditioned pathway can generate a movement command even before movements become accurate through learning. This pathway creates the occasions for registering visual error signals and thereby learning a more accurate command. Thus learning by this system operates through a perform-and-test-scheme. Such a scheme realized a type of instrumental conditioning, because behaviors are emitted and the consequences of these behaviors, in the form of error signals, shape their future accuracy. The actual conditioning law is, however, again a variant of a general classical conditioning mechanism.

Figure 12

Conditioning in this system takes place in the Adaptive Gain Stage, or AG stage (Figure 12). The AG stage is identified with the cerebellar vermis, based upon data which show that this brain region controls modification of a saccade's *pulse gain* (Optican and Robinson, 1980). The conditioned movement pathway generates sampling signals which pass through the AG stage and add a conditionable movement signal to the total movement command. An error signal acts to change the size, or gain, of the conditionable movement signal. Thus the AG stage is a region where automatic gain control of the total movement command takes place.

All the movement commands are feedforward commands in Figure 12. Feedback influences the system by controlling the size of the error signals which change the gain of future movement commands. In Figure 12, feedback is *externally* mediated: a feedforward movement command elicits a movement which generates feedback in the form of a visual error signal. In other circuits which use the AG stage, feedback can be internally mediated (Section 13).

14. Learning a Motor Synergy: Opponent Processing of Error Signals

The second key property of the AG stage concerns its ability to convert visual error signals, which individually activate only a *single* retinal position, into correct and synchronous movement commands to *all* the muscles which move the eye. This property is realized by preprocessing the error signals several times before they can be sampled by the conditioned movement pathway. Two processing constraints conceptualize these preprocessing stages: (a) the Opponent Processing constraint, and (b) the Equal Access constraint. The need for Opponent Processing—which is a new feature of our model—can be seen as follows.

Each eye is moved by three pairs of agonist and antagonist muscles. One pair moves the eye horizontally. The other two pairs move the eye obliquely, and together can generate vertical movements (Figure 13a). I now indicate why an *increase* in the gain of an agonist muscle command must generate a *decrease* in the gain of the corresponding antagonist muscle command, and conversely. In other words, each visual error signal has antagonistic, or opponent, effects on the conditionable gains of the muscle commands which it changes.

Figure 13

In order to realize the Opponent Processing constraint, suppose that the retina is topographically transformed from retinotopic coordinates into a motor map containing

six sectors (Figure 13a). Each pair of agonist-antagonist muscles—(α^+, α^-), (β^+, β^-), (γ^+, γ^-)—is represented by opposite sectors in the sector map. A visual error signal which falls within a prescribed sector increases the conditioned gain of the corresponding muscle and decreases the conditioned gain of the antagonistic muscle. This scheme can correct undershoot, overshoot, and skewed movement errors as follows.

Suppose that a light activates the retinal position labelled 1 in Figure 13b and thereby causes a saccade. Suppose that, after movement, the light activates position 2. Such a movement defines an undershoot error: the eye does not move far enough toward the right to foveate the light. If the error signal increases the gain of muscle β^+ and decreases the gain of muscle β^-, then the eye will move further toward the right the next time that position 1 is activated, thereby tending to correct the undershoot error.

The need for opponent processing can be seen by considering the case of an overshoot error in Figure 13c. Here a light to position 1 moves the eye in such a way that the error signal activates a position 2 on the opposite side of the fovea. In other words, the eye moves too far to the right. Due to opponent processing, the error signal increases the gain of muscle β^- *and* decreases the gain of muscle β^+, thereby tending to correct the overshoot error the next time position 1 is activated. A similar analysis shows how opponent processing of error signals corrects skewed errors, as in Figure 13d.

15. The Equal Access Constraint

Figure 13 emphasizes the fact that, before learning occurs, a light to a fixed retinal position (1) can cause undershoot, overshoot, or skewed errors. The system cannot *a priori* predict which type of error will occur as a result of its inadequately tuned parameters. In order to correct any possible error, each position must be able to activate a conditioned movement pathway that is capable of sampling error signals delivered to *any* of the motor sectors. This is the Equal Access constraint, which was first articulated in a formal model of cerebellar learning by Grossberg (1964, 1969).

In order to realize the Equal Access constraint, we assume that the motor sectors are mapped, via a complex logarithmic map (Schwartz, 1980), into motor strips (Figure 14).

Figure 14

Then a single conditioned movement pathway can sample gain changes due to error signals which activate any motor strip. Figure 15 describes two variants of this design. Each variant realizes both the Opponent Processing constraint and the Equal Access constraint.

Figure 15

The most obvious, and by now classical, cerebellar interpretation of this anatomy is that the sampling signals are carried by parallel fibers through the dendrites of Purkinje cells, whereas the error signals are carried by climbing fibers to the Purkinje cell dendrites (Albus, 1971; Grossberg, 1964, 1969; Marr, 1969).

In summary, visual error signals are mapped from retinotopic coordinates into motor sector coordinates and then into motor strip coordinates, so that they can all be sampled by individual movement command pathways which can supply conditioned gain signals to their corresponding muscles.

16. Adaptive Linearization of the Muscle Plant: Error Signals from Outflow-Inflow Mismatches

All of the above constraints have been implemented using a variant of the associative equation (3) in which x_j is replaced by a visual error signal. Then perfect learning is achieved if the muscle plant responds linearly to the total movement signal, which is a

sum of unconditioned and conditioned components (Figure 12). Figure 16A describes the outcome of a computer simulation that demonstrates perfect learning. Unfortunately the muscle plant is known to be nonlinear (Robinson, 1970; Schiller, 1970). When the muscle plant is nonlinear, a single retinotopically coded source of conditioned pathways cannot adequately learn to correct foveation errors using visual error signals. Figure 16B describes the outcome of a computer simulation that illustrates this failure when the muscle plant exhibits a slower-than-linear, or saturating, nonlinearity.

Figure 16

This failure raises one of the classical issues about sensory-motor control: How does the brain compensate for changes in muscle plant gains and nonlinearities that may occur throughout life due to normal development, aging, minor muscle tears, or changes in blood supply? How does the brain continue to generate accurate movement commands despite the fact that the muscles which execute these commands change their response characteristics through time? In particular, how does the brain compensate for these changes without altering the entire hierarchy of learned transformations that are used to move the muscles? In Grossberg and Kuperstein (1986), a detailed analysis and solution of this problem is offered. Herein I discuss some main points that are relevant to an ethological perspective.

Outflow signals give rise to corollary discharges which provide information about present position (Figure 9). However, the laws that goven the muscle plant are not known *a priori* to the outflow source. It is not known how much the muscle will contract in response to an outflow signal of fixed size. Even if the outflow source somehow possessed this information at one time, it might turn out to be the wrong information at a later time, since the muscle plant characteristics can change through time.

In order to use an outflow signal as a reliable source of present position information, the movement system as a whole must guarantee that the muscle plant reacts linearly, and with a reasonable gain, to outflow signals, even if the muscle plant is nonlinear. Once a linear muscle response is achieved, perfect learning using visual error signals (Figure 16A) will also be possible.

The relationship between the size of an outflow command and the amount of muscle contraction is, in principle, undeterminable without some type of inflow information from the muscle itself concerning its state of contraction. We suggest that a brain region exists wherein comparisons between outflow and inflow signals are used for this purpose. This region is called the *outflow-inflow interface*, or OII, and forms a part of a larger circuit called the Muscle Linearization Network, or MLN (Figure 17).

Figure 17

We suggest how spatial patterns of outflow signals are matched against spatial patterns of inflow signals at the OII. Good matches imply that the muscles are responding linearly, and with a reasonable gain, to outflow signals. Bad matches must be able to adjust muscle plant gain as well as muscle plant nonlinearities. This is accomplished as follows. Mismatches within the OII generate error signals to the AG stage that can change the size of the total outflow signal to the muscle plant (Figure 17). The conditionable part of the total outflow signal adds or subtracts the correct amount of signal to make the muscle react *as if* it is a linear muscle plant with a reasonable gain. Thus, in response to changes in the muscle plant, automatic gain control signals compensate for these changes through learning. If the muscle plant changes due to aging or accidents, mismatches are caused within the OII and trigger new learning. The gain control signals automatically alter the total outflow command until the muscle again reacts linearly. Thus the linearization of the muscle plant is a learning process that takes place on a slower time scale than registration of a corollary discharge. We have used this model of the MLN, and its microcircuit

refinements, to suggest explanations of diverse neurophysiological and clinical data, such as data about strabismus and dysmetria (Ron and Robinson, 1973; Steinbach and Smith, 1981; Vilis, Snow, and Hore, 1983).

The error signals from the OII are assumed to reach the AG stage, or cerebellum, just as in the circuit of Figure 12. In Figure 12, the error signals are visual error signals that are mediated by feedback from the external environment. In Figure 17, the error signals are due to outflow-inflow mismatches that are mediated by feedback pathways internal to the brain. In both cases, the same AG stage model is employed, although different cells of the AG stage are used in the two distinct circuits. In particular, Ron and Robinson (1973) have reported data which indicate that the dentate nucleus of the cerebellum may form part of the AG stage cells that are used by the MLN. A comparison of Figures 12 and 17 illustrates the following general conclusions:

Once a single functional processor, such as the AG stage, is successfully invented by the evolutionary process, its functional capability can be used by several sensory-motor circuits that may be invented or specialized at later evolutionary stages.

Solution of a single functional problem can provide the foundation for an adaptive solution of several other functional problems. For example, adaptive linearization of the muscle plant both enables corollary discharges to be used as present position signals *and* enables visual error signals to effectively correct foveation errors.

Different types of present position information are available to the brain, but each type is used in only certain ways. For example, I have already described four ways in which outflow signals are used: to unconditionally move the eye (Figure 9), to modify the unconditional movement command with a conditionable movement command through the AG stage, to generate corollary discharges at the HMI (Figure 8), and to generate error signals from the OII to the AG stage (Figure 17). Inflow signals, by contrast, have only been used during my discussion to generate error signals from the OII to the AG stage (Figure 17). Thus, although inflow signals are essential to determine how the eyes will move, their role is indirect: They do not tell the system where the eyes are pointing, but instead can initiate a learning process which enables the eyes to point where outflow signals tell them to point.

The controversy about the role of outflow signals versus inflow signals as a source of present position information is a classical one (Helmholtz, 1962; Ruffini, 1898; Sherrington, 1894). A mechanistic refinement of classical ideas, in the manner proposed above, seems to be clarifying some of the core difficulties by introducing qualitatively new ideas, such as the concept of a separate Muscle Linearization Network.

17. Attentionally Modulated Choices, Stable Postures, and Planned Movement Sequences

The above discussion outlines some of the problems which need to be solved by a neural and a computational theory of how a complex sensory-motor system adapts to its environment. This list of problems does not, however, exhaust the problems which such a system must solve. In addition, one must discover how an attentionally modulated movement system, which bases its movement commands upon vectors (Section 6), can benefit from the conditioned gains that are learned by a visually reactive movement system (Section 13), yet can also suppress reactive movements in favor of attentionally salient movements. One must analyse how a postural system can adaptively balance opponent muscle forces to maintain stable postures in any of the positions to which a movement may lead. One must characterize how a predictive movement system can encode a sequence of movement commands, learn to group these commands into a unitized movement plan, and read-out these commands in a manner that can override the momentary demands of sensory cues. One must decide how intermodal cues, such as visual and auditory cues,

can compete in a dimensionally consistent coordinate system to choose an overt movement command.

Detailed neural models of all these processes have been suggested in the domain of ballistic eye movements (Grossberg and Kuperstein, 1986) and are presently being developed in the domain of continuous arm movements and eye-hand coordination (Bullock and Grossberg, 1986). The generality of the organizational principles and neural mechanisms embodied within these models has begun to reveal a mechanistic unity behind the rich diversity of behavioral and neural data about mammalian sensory-motor control, and a still more far-reaching mechanistic unity between mechanisms of sensory-motor control, perception, and cognition. These unifying principles and mechanisms have all been derived from an analysis of how the real-time behavior of individual organisms adapts to complex environments. Although a systematic comparative analysis of how such principles and mechanisms are specialized across species will require an enormous amount of future work, the theoretical framework which has already been articulated reaffirms the usefulness of a neuroethological approach to the analysis of behavior.

REFERENCES

Albus, J.S., A theory of cerebellar function. *Mathematical Biosciences*, 1971, **10**, 25-61.

Anderson, R.A., Essick, G.K., and Siegel, R.M., The role of eye position on the visual response of neurons in area 7A. *Society for Neuroscience Abstracts*, 1984, **10**, 274.11.

Atkeson, C.G. and Hollerbach, J.M., Kinematic features of unrestrained vertical arm movements. *Journal of Neuroscience*, 1985, **5**, 2318-2330.

Autrum, H., Das Fehlen unwillkürlicher Augenbewegungen beim Frosch. *Naturwissenschaften*, 1959, **46**, 436.

Baker, R. and Berthoz, A., **Control of gaze by brain stem neurons: Developments in neuroscience**, Vol. 1. Amsterdam: Elsevier/North-Holland, 1977.

Banquet, J.-P. and Grossberg, S., Structure of event-related potentials during learning: An experimental and theoretical analysis. Submitted for publication, 1986.

Brindley, G.S., The use made by the cerebellum of the information that it receives from sense organs. *International Brain Research Organization Bulletin*, 1964, **3**, 80.

Brody, M. and Paul, R. (Eds.), **Robotics research: The first international symposium**. Cambridge, MA: MIT Press, 1984.

Bruce, C.J. and Goldberg, M.E., Physiology of the frontal eye fields. *Trends in Neurosciences*, 1984, **7**, 436-441.

Bruce, C.J. and Goldberg, M.E., Primate frontal eye fields, I: Single neurons discharging before saccades. *Journal of Neurophysiology*, 1985, **53**, 603-635.

Buchtel, H.A. and Guitton, D., Saccadic eye movements in patients with discrete unilateral frontal-lobe removals. *Society for Neuroscience Abstracts*, 1980, **6**, 316.

Bullock, D. and Grossberg, S., Neural dynamics of planned arm movements: Invariants, synergies, and trajectory formation. Submitted for publication, 1986.

Carpenter, G.A. and Grossberg, S., Dynamic models of neural systems: Propagated signals, photoreceptor transduction, and circadian rhythms. In J.P.E. Hodgson (Ed.), **Oscillations in mathematical biology**. New York: Springer-Verlag, 1983, 102-196.

Carpenter, G.A. and Grossberg, S., Neural dynamics of category learning and recognition: Attention, memory consolidation, and amnesia. In J. Davis, R. Newburgh, and E. Wegman (Eds.), **Brain structure, learning, and memory**. AAAS Symposium Series, in press, 1986 (a).

Carpenter, G.A. and Grossberg, S., Neural dynamics of category learning and recognition: Structural invariants, reinforcement, and evoked potentials. In M.L. Commons, S.M. Kosslyn, and R.J. Herrnstein (Eds.), **Pattern recognition and concepts in animals, people, and machines**. Hillsdale, NJ: Erlbaum, 1986 (b).

Carpenter, G.A. and Grossberg, S., A massively parallel architecture for a self-organizing neural pattern recognition machine. Submitted for publication, 1986 (c).

Cohen, M.A. and Grossberg, S., Absolute stability of global pattern formation and parallel memory storage by competitive neural networks. *I.E.E.E. Transactions on Systems, Man, and Cybernetics*, 1983, **SMC-13**, 815-826.

Cohen, M.A. and Grossberg, S., Adaptive tuning of unitized perceptual groupings: Neural association, competition, and modulation. Submitted for publication, 1986.

Cubeddu, L.X., Hoffmann, I.S., and James, M.K., Frequency-dependent effects on neuronal uptake inhibitors on the autoreceptor-mediated modulation of dopamine and acetylcholine release from the rabbit striatum. *Journal of Pharmacology and Experimental Therapeutics*, 1983, **226**, 99-94.

Dubocovich, M.L. and Weiner, N., Modulation of the stimulation-evoked release of 3H-dopamine through activation of dopamine autoreceptors of the D-2 subtype in the isolated

rabbit retina. In M. Kohsaka *et al.* (Eds.), **Advances in the biosciences, Vol. 37: Advances in dopamine research**. New York: Pergamon Press, 1982.

Evert, J.-P., Burghagen, H., and Schürg-Pfeiffer, E., Neuroethological analysis of the innate releasing mechanism for prey-catching behavior in toads. In J.-P. Evert, R.R. Capranica, and D.J. Ingle (Eds.), **Advances in vertebrate neuroethology**. New York: Plenum Press, 1981.

Evert, J.-P., Capranica, R.R., and Ingle, D.J. (Eds.), **Advances in vertebrate neuroethology**. New York: Plenum Press, 1981.

Fuchs, A.F. and Becker, W., **Progress in oculomotor research: Developments in neuroscience**, Vol. 12. New York: Elsevier/North-Holland, 1981.

Fujita, M., Adaptive filter model of the cerebellum. *Biological Cybernetics*, 1982, **45**, 195–206 (a).

Fujita, M., Simulation of adaptive modification of the vestibulo-ocular reflex with an adaptive filter model of the cerebellum. *Biological Cybernetics*, 1982, **45**, 207–214 (b).

Goldberg, M.E. and Bushnell, M.C , Role of the frontal eye fields in visually guided saccades. In A.F. Fuchs and W. Becker (Eds.), **Progress in oculomotor research**. New York: Elsevier/North-Holland, 1981, 185–192.

Grobstein, P., Comer, C., and Kostyk, S.K., Frog prey capture behavior: Between sensory maps and directed motor output. In J.-P. Evert, R.R. Capranica, and D.J. Ingle (Eds.), **Advances in vertebrate neuroethology**. New York: Plenum Press, 1981.

Grossberg, S., **The theory of embedding fields with applications to psychology and neurophysiology**. New York: Rockefeller Institute for Medical Research, 1964.

Grossberg, S., On learning of spatiotemporal patterns by networks with ordered sensory and motor components, I: Excitatory components of the cerebellum. *Studies in Applied Mathematics*, 1969, **48**, 105–132.

Grossberg, S., Neural expectation: Cerebellar and retinal analogs of cells fired by learnable or unlearned pattern classes. *Kybernetik*, 1972, **10**, 49–57.

Grossberg, S., Adaptive pattern classification and universal recoding, I: Parallel development and coding of neural feature detectors. *Biological Cybernetics*, 1976, **23**, 121–134.

Grossberg, S., Communication, memory, and development. In R. Rosen and F. Snell (Eds.), **Progress in theoretical biology**, Vol. 5. New York: Academic Press, 1978 (a).

Grossberg, S., A theory of human memory: Self-organization and performance of sensory-motor codes, maps, and plans. In R. Rosen and F. Snell (Eds.), **Progress in theoretical biology**, Vol. 5. New York: Academic Press, 1978 (b).

Grossberg, S., Biological competition: Decision rules, pattern formation, and oscillation. *Proceedings of the National Academy of Sciences*, 1980, **77**, 2338–2342.

Grossberg, S., Processing of expected and unexpected events during conditioning and attention: A psychophysiological theory. *Psychological Review*, 1982, **89**, 529–572 (a).

Grossberg, S., A psychophysiological theory of reinforcement, drive, motivation, and attention. *Journal of Theoretical Neurobiology*, 1982, **1**, 286–369 (b).

Grossberg, S., **Studies of mind and brain: Neural principles of learning, perception, development, cognition, and motor control**. Boston: Reidel Press, 1982 (c).

Grossberg, S., Some psychophysiological and pharmacological correlates of a developmental, cognitive, and motivational theory. In R. Karrer, J. Cohen, and P. Tueting (Eds.), **Brain and information: Event related potentials**. New York: New York Academy of Sciences, 1984.

Grossberg, S. and Kuperstein, M., **Neural dynamics of adaptive sensory-motor control: Ballistic eye movements**. Amsterdam: North-Holland, 1986.

Grossberg, S. and Levine, D.S., Neural dynamics of attentionally modulated Pavlovian conditioning: Blocking, inter-stimulus interval, and secondary reinforcement. Submitted for publication, 1986.

Grossberg, S. and Stone, G.O., Neural dynamics of word recognition and recall: Attentional priming, learning, and resonance. *Psychological Review*, 1986, **93**, 46–74.

Groves, P.M., Fenster, G.A., Tepper, J.M., Nakamura, S., and Young, S.T., Changes in dopaminergic terminal excitability induced by amphetamine and haloperidol. *Brain Research*, 1981, **221**, 425–431.

Groves, P.M. and Tepper, J.M., Neuronal mechanisms of action of amphetamine. In I. Creese (Ed.), **Stimulants: Neurochemical, behavioral, and clinical perspectives**. New York: Raven Press, 1983, 81–129.

Hallett, P.E. and Lightstone, A.D., Saccadic eye movements to flashes targets. *Vision Research*, 1976, **16**, 107–114.

Helmholtz, H.L.F. von, **Treatise on physiological optics**, J.P.C. Southall (Trans.). New York: Dover, 1962.

Hikosaka, O. and Wurtz, R.H., Effects on eye movements of a GABA agonist and antagonist injected into monkey superior colliculus. *Brain Research*, 1983, **272**, 368–372.

Hogan, N., An organizing principle for a class of voluntary movements. *Journal of Neuroscience*, 1984, **4**, 2745–2754.

Hollerbach, J.M., Dynamic scaling of manipulator trajectories. *ASME Journal of Dynamic Systems Measurement Control*, 1984, **106**, 102–106.

Hyvärinen, J., Posterior parietal lobe of the primate brain. *Physiological Review*, 1982, **62**, 1060–1129.

Ito, M., The control mechanisms of cerebellar motor systems. In F.O. Schmitt and F.G. Worden (Eds.), **The neurosciences third study program**. Cambridge, MA: MIT Press, 1974, 293–303.

Ito, M., **The cerebellum and neural control**. New York: Raven Press, 1984.

Keller, E. and Zee, D. (Eds.), **Adaptive processes in visual and oculomotor systems**. New York: Pergamon Press, 1986.

Kohonen, T., A simple paradigm for the self-organized formation of structural feature maps. In S. Amari and M.A. Arbib (Eds.), **Competition and cooperation in neural networks**. New York: Springer-Verlag, 1982.

Kohonen, T., Representation of information in spatial maps which are produced by self-organization. In E. Basar, H. Flohr, H. Haken, and A.J. Mandell (Eds.), **Synergetics of the brain**. New York: Springer-Verlag, 1983.

Lynch, J.C., The functional organization of posterior parietal association cortex. *Behavioral and Brain Sciences*, 1980, **3**, 485–534.

Marr, D., A theory of cerebellar cortex. *Journal of Physiology (London)*, 1969, **202**, 437–470.

Mays, L.E. and Sparks, D.L., Saccades are spatially, not retinocentrically, coded. *Science*, 1980, **208**, 1163–1165.

Mays, L.E. and Sparks, D.L., The localization of saccade targets using a combination of retinal and eye position information. In A.F. Fuchs and W. Becker (Eds.), **Progress in oculomotor research**. New York: Elsevier/North-Holland, 1981, 39–47.

McCormick, D.A. and Thompson, R.F., Cerebellum: Essential involvement in the classically conditioned eyelid response. *Science*, 1984, **223**, 296–299.

Motter, B.C. and Mountcastle, V.B., The functional properties of the light-sensitive neurons of the posterior parietal cortex studied in waking monkeys: Foveal sparing and opponent vector organization. *Journal of Neuroscience*, 1981, **1**, 3–26.

Murphy, B.J., Haddad, G.M., and Steinman, R.M., Simple forms and fluctuations in the line of sight: Implications for motor theories of form processing. *Perception and Psychophysics*, 1974, **16**, 557–563.

Niedzwiecki, D.M., Mailman, R.B., and Cubeddu, L.X., Greater potency of mesoridazine and sulforidazine compared with the parent compound, thioridazine, on striatal dopamine autoreceptors. *Journal of Pharmacology and Experimental Therapeutics*, 1984, **228**, 636-639.

Optican, L.M. and Robinson, D.A., Cerebellar-dependent adaptive control of primate saccadic system. *Journal of Neurophysiology*, 1980, **44**, 1058–1076.

Robinson, D.A., Oculomotor unit behavior in the monkey. *Journal of Neurophysiology*, 1970, **35**, 393–404.

Ron, S. and Robinson, D.A., Eye movements evoked by cerebellar stimulation in the alert monkey. *Journal of Neurophysiology*, 1973, **36**, 1004–1021.

Ruffini, A., On the minute anatomy of the neuro-muscular spindles of the cat, and on their physiological significance. *Journal of Physiology*, 1898, **23**, 190–208.

Schiller, P.H., The discharge characteristics of single units in the oculomotor and abducens nuclei of the unanesthetized monkey. *Experimental Brain Research*, 1970, **10**, 347–362.

Schiller, P.H. and Sandell, J.H., Interactions between visually and electrically excited saccades before and after superior colliculus and frontal eye field ablations in the rhesus monkey. *Experimental Brain Research*, 1983, **49**, 381–392.

Schiller, P.H., Sandell, J.H., and Maunsell, J.H.R., The effect of superior colliculus and frontal eye field lesions on saccadic latency in the monkey. *Society for Neuroscience Abstracts*, 1984, **10**, 21.9.

Schiller, P.H., True, S.D., and Conway, J.L., Paired stimulation of the frontal eye fields and the superior colliculus of the rhesus monkey. *Brain Research*, 1979, **179**, 162–164.

Sherrington, C.S., On the anatomical constitution of nerves of skeletal muscles, with remarks on recurrent fibres in the ventral spinal nerve-root. *Journal of Physiology*, 1894, **17**, 211–258.

Siever, L. and Sulser, F., Regulations of amine neurotransmitter systems: Implication for the major psychiatric syndromes and their treatment. *Psychopharmacology Bulletin*, 1984, **20**, 500–504.

Sparks, D.L. and Mays, L.E., The role of the monkey superior colliculus in the control of saccadic eye movements: A current perspective. In A.F. Fuchs and W. Becker (Eds.), **Progress in oculomotor research**. New York: Elsevier/North-Holland, 1981.

Steinbach, M.J. and Smith, D.R., Spatial localization after strabismus surgery: Evidence for inflow. *Science*, 1981, **213**, 1407–1408.

Steinman, R.M., Effect of target size, luminance, and color on monocular fixation. *Journal of the Optical Society of America*, 1965, **55**, 1158–1165.

Steinman, R.M., The role of eye movements in maintaining a phenomenally clear and stable world. In R.A. Monty and J.M. Senders (Eds.), **Eye movements and psychological processes**. Hillsdale, NJ: Erlbaum, 1976.

Tepper, J.M., Young, S.T., and Groves, P.M., Autoreceptor-mediated changes in dopaminergic terminal excitability: Effects of increases in impulse flow. *Brain Research*, 1984, **309**, 309–316.

Vilis, T., Snow, R., and Hore, J., Cerebellar saccadic dysmetria is not equal in the two eyes. *Experimental Brain Research*, 1983, **51**, 343–350.

Zee, D.S., Optican, L.M., Cook, J.D., Robinson, D.A., and Engel, W.K., Slow saccades in spinocerebellar degeneration. *Arch. Neurol.*, 1976, **33**, 243–251.

Zuber, B.L., **Models of oculomotor behavior and control**. Boca Raton, FL: CRC Press, 1981.

FIGURE CAPTIONS

1. Learning intermodal circular reactions: Learning is gated by signals which are sensitive to how well target position matches present position within each modality. The vectors which compare target position with present position are also used to generate movement trajectories that automatically compensate for present position within each modality.

2. A fixed target light excites a different retinal position wherever the eye assumes a different position in the head. The difference between retinal position and eye position provides a measure of how far the eye must move to foveate the target.

3. Many combinations of retinal position and eye position can encode the same target position.

4. When the many combinations of retinal position and eye position that correspond to each fixed target position all activate the same internal representation of that target position in head coordinates, the ensemble of such head coordinate representations is said to form an invariant map.

5. Every eye position and retinal position can send signals to many target position representations.

6. Expansion of LTM maps due to an increase in the number of retinotopic positions and eye positions that are combined to form target positions in head coordinates: (a) Intermediate stage of learning using 40 positions of each type; (b) Final stage of learning using 40 positions; (c) Intermediate stage of learning using 80 positions of each type; (d) Final stage of learning using 80 positions; (e) Intermediate stage of learning using 160 positions of each type; (f) Final stage of learning using 160 positions. Initial values of LTM traces are chosen randomly between 0 and 1. (Reprinted with permission from Grossberg and Kuperstein, 1986.)

7. Target position is adaptively transformed from retinotopic coordinates into head coordinates, and then into motor coordinates, so that it can be used to compute a vector in motor coordinates at the head-muscle interface, or HMI.

8. Recoding of a target position map (TPM) into muscle coordinates at a head muscle interface (HMI): The LTM traces at the ends of the conditioned pathways learn an "adaptive inhibitory efference copy" from the corollary discharges that they are allowed to sample when the learning gate is active between movements. When the efference copy equals the sampled corollary discharges, learning ceases. On a future perfomance trial, read-out of the target position subtracts from corollary discharge present position signals to activate a vector in motor coordinates across the HMI cells. (Reprinted with permission from Grossberg and Kuperstein, 1986.)

9. The outflow pathway generates present position information via corollary discharge signals. (Reprinted with permission from Grossberg and Kuperstein, 1986.)

10. Distinct vectors in (a), (b), and (c) can activate the same populations of HMI cells. In order for distinct vectors to activate distinct movement command pathways, they are transformed into activations of distinct locations within a topographic map.

11. Computer simulation of a transformation from a vector in motor coordinates at the HMI into a unimodal peak of activation within a topographic map. Difference vectors map into distinct activation peaks. (Reprinted with permission from Grossberg and Kuperstein, 1986.)

12. The representation of the chosen first light gives rise to an unconditioned movement signal and a conditioned movement signal. The unconditioned signal causes movements that are corrected by the conditioned movement signal via learning. The conditioned pathway carries sampling signals whose strength can be altered by second-light mediated

error signals. These sampling signals give rise to the conditioned movement signal. The representation of the first light must be stored until after the end of the saccade, so that the second-light mediated error signal can act. The AG stage at which learning occurs is identified with the cerebellum. (Reprinted with permission from Grossberg and Kuperstein, 1986.)

13. (a) Motor sectors corresponding to agonist muscles $(\alpha^+, \beta^+, \gamma^+)$ and antagonist muscles $(\alpha^-, \beta^-, \gamma^-)$ of one eye. The position of the light before movement (labelled 1) activates a movement command pathway. The position of the light after movement (labelled 2) generates an increase in the gain of the muscle in whose sector it falls, and a decrease in the gain of the antagonist muscle. (b) An undershoot error. (c) An overshoot error. (d) A skewed undershoot error. (Reprinted with permission from Grossberg and Kuperstein, 1986.)

14. Logarithmic map from sensory sectors into motor strips: Each sensory hemifield $(\alpha^+, \beta^+, \gamma^+)$ and $(\alpha^-, \beta^-, \gamma^-)$ maps into a row of parallel motor strips. In this fractured somatotopy, the strips of agonist-antagonist pairs (α^+, α^-), (β^+, β^-), and (γ^+, γ^-) are juxtaposed, much as in the case of ocular dominance columns in the striate cortex. A pair of motor strip maps is depicted, one in each AG stage hemisphere. Outputs from all agonist-antagonist pairs compete before the net outputs add to the total movement command. This circuit works even if only agonist muscles $(\alpha^+, \beta^+, \gamma^+)$ receive excitatory error signals in one hemifield and antagonist muscles $(\alpha^-, \beta^-, \gamma^-)$ receive excitatory error signals in the other hemifield. An excitatory error signal to the α^+ strip can weaken the net α^- output of the contiguous strip via competition of the outputs, but cannot strengthen the α^+ output signal. An excitatory error signal to the α^+ strip of the other hemifield can strengthen the net α^+ output. (Reprinted with permission from Grossberg and Kuperstein, 1986.)

15. Two ways to achieve opponent conditioning of agonist-antagonist muscles: (a) An error signal increases the conditioned gain at the agonist muscle strip and decreases the conditioned gain at the antagonist muscle strip; (b) An error signal increases the conditioned gain at the agonist muscle strip. Competition between agonist and antagonist muscle strip outputs cause the decrease in the net antagonist output. A single sampling signal can learn the gain changes appropriate to all the muscles, and can synchronously read out these learned gains due to the rapidity with which the sampling signal traverses the motor strips. (Reprinted with permission from Grossberg and Kuperstein, 1986.)

16. Computer simulation of saccadic error correction model. (A) Linear Muscle Plant: (a) Topographic distribution of learned gains across the sampling pathways. (b) Muscle response function used during the simulation. (c) Errors in 100 trials before learning begins and 100 trials after learning ends. Negative values correspond to undershoots and positive values correpond to overshoots. Learning is perfect. (B) Slower-than-Linear Muscle Plant: Learning improves performance but cannot correct an unacceptable error size. (Reprinted with permission from Grossberg and Kuperstein, 1986.)

17. Some main features of the muscle linearization network, or MLN: The outflow-inflow interface (OII) registers matches and mismatches between outflow signals and inflow signals. Mismatches generate error signals to the adaptive gain (AG) stage. These error signals change the gain of the conditioned movement signal to the motoneurons (MN). Such an MLN adaptively linearizes the responses of a nonlinear muscle plant to outflow signals. The outflow signals can therefore also be used as a source of accurate corollary discharges of present eye position. (Reprinted with permission from Grossberg and Kuperstein, 1986.)

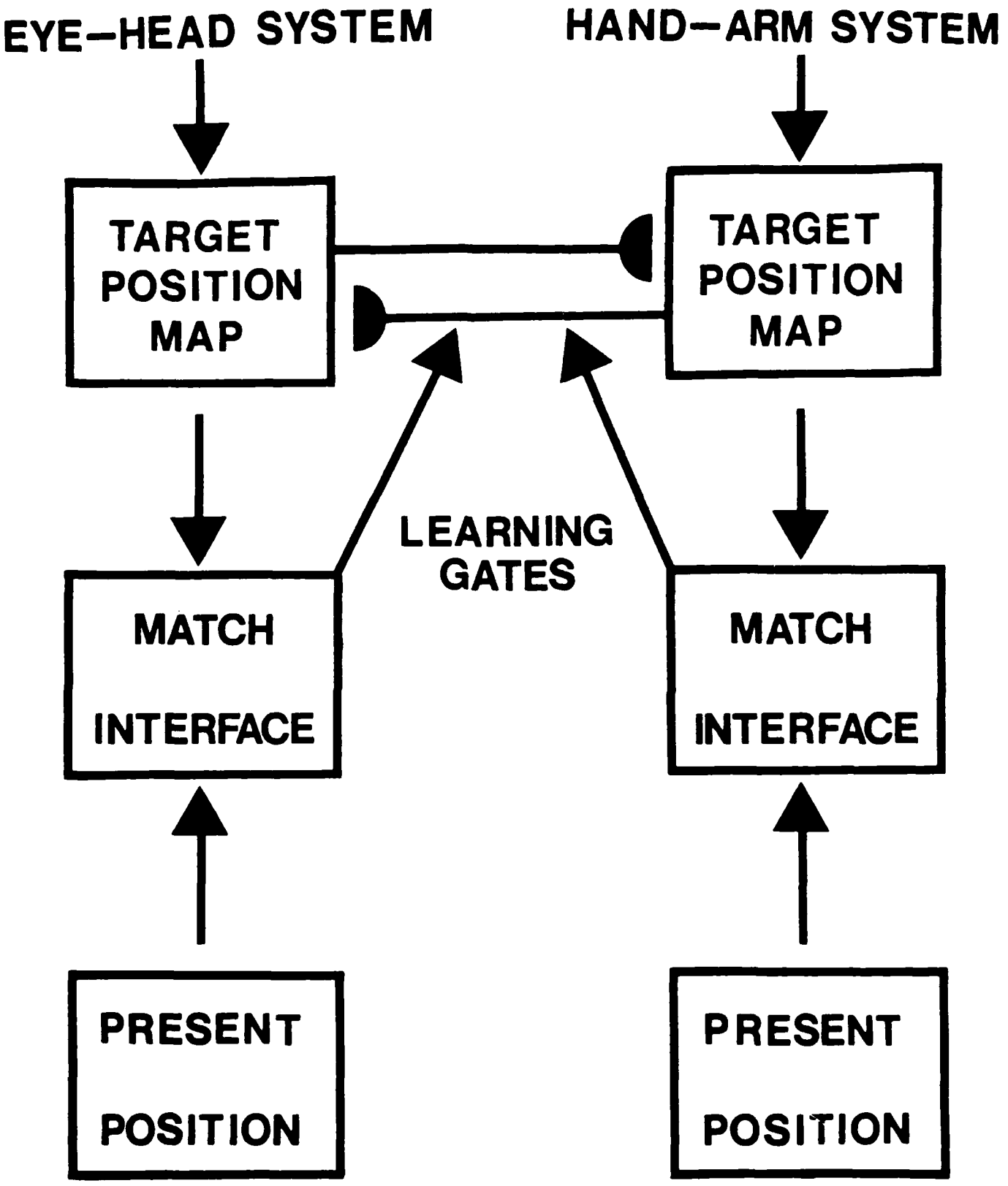
EYE–HEAD SYSTEM
HAND–ARM SYSTEM
TARGET POSITION MAP
TARGET POSITION MAP
LEARNING GATES
MATCH INTERFACE
MATCH INTERFACE
PRESENT POSITION
PRESENT POSITION

Figure 1

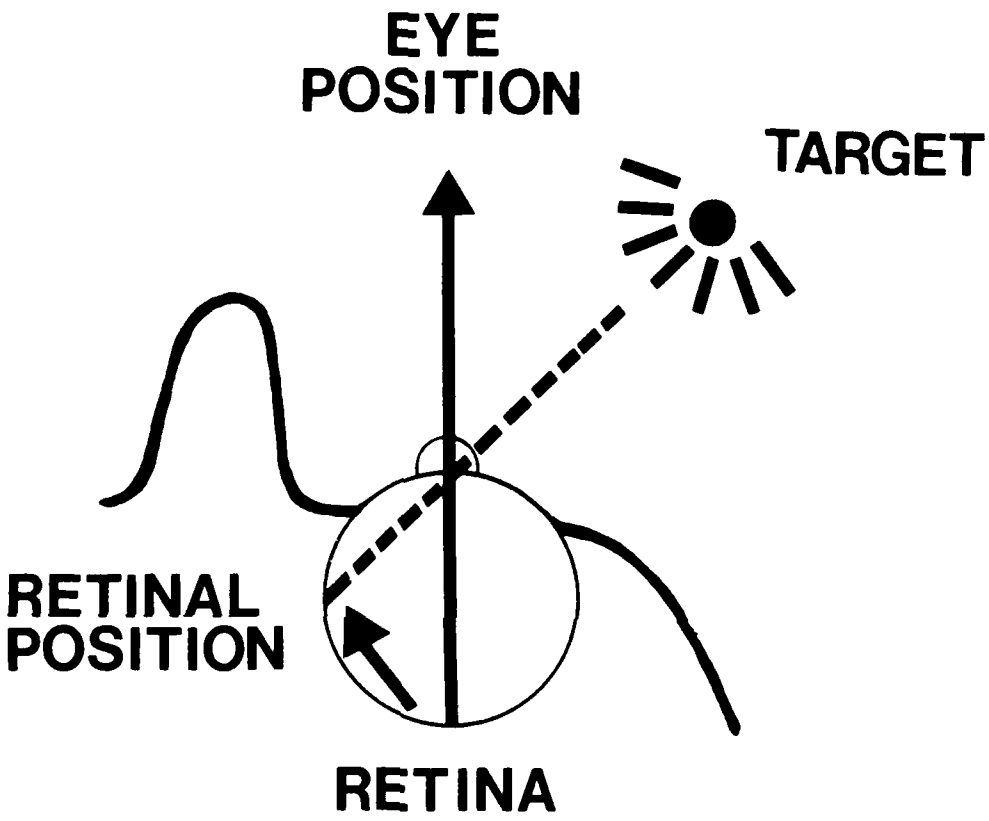

Figure 2

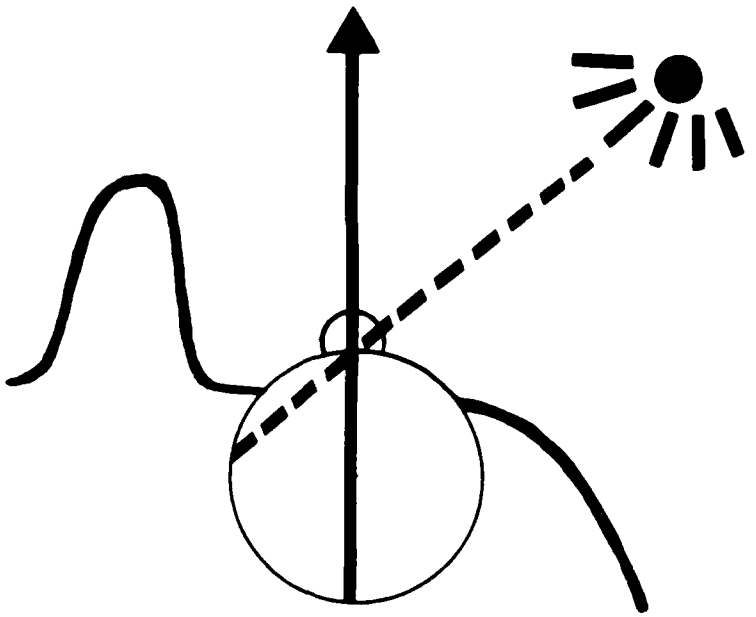

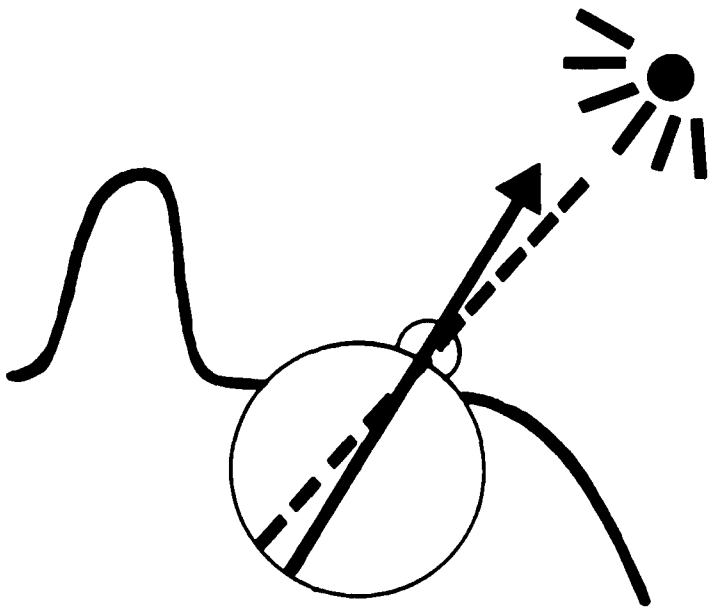

Figure 3

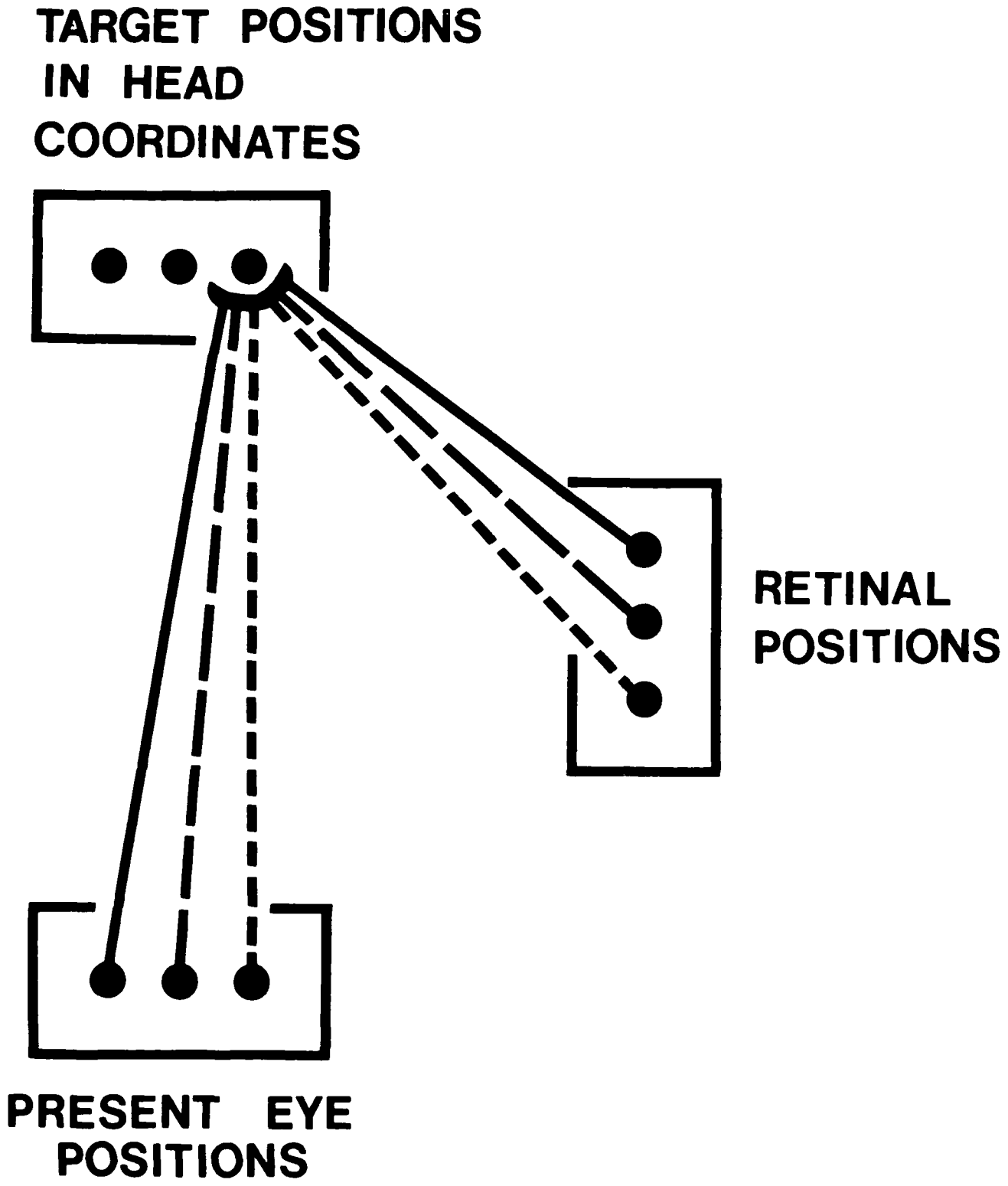
TARGET POSITIONS
IN HEAD
COORDINATES
RETINAL
POSITIONS
PRESENT EYE
POSITIONS

Figure 4

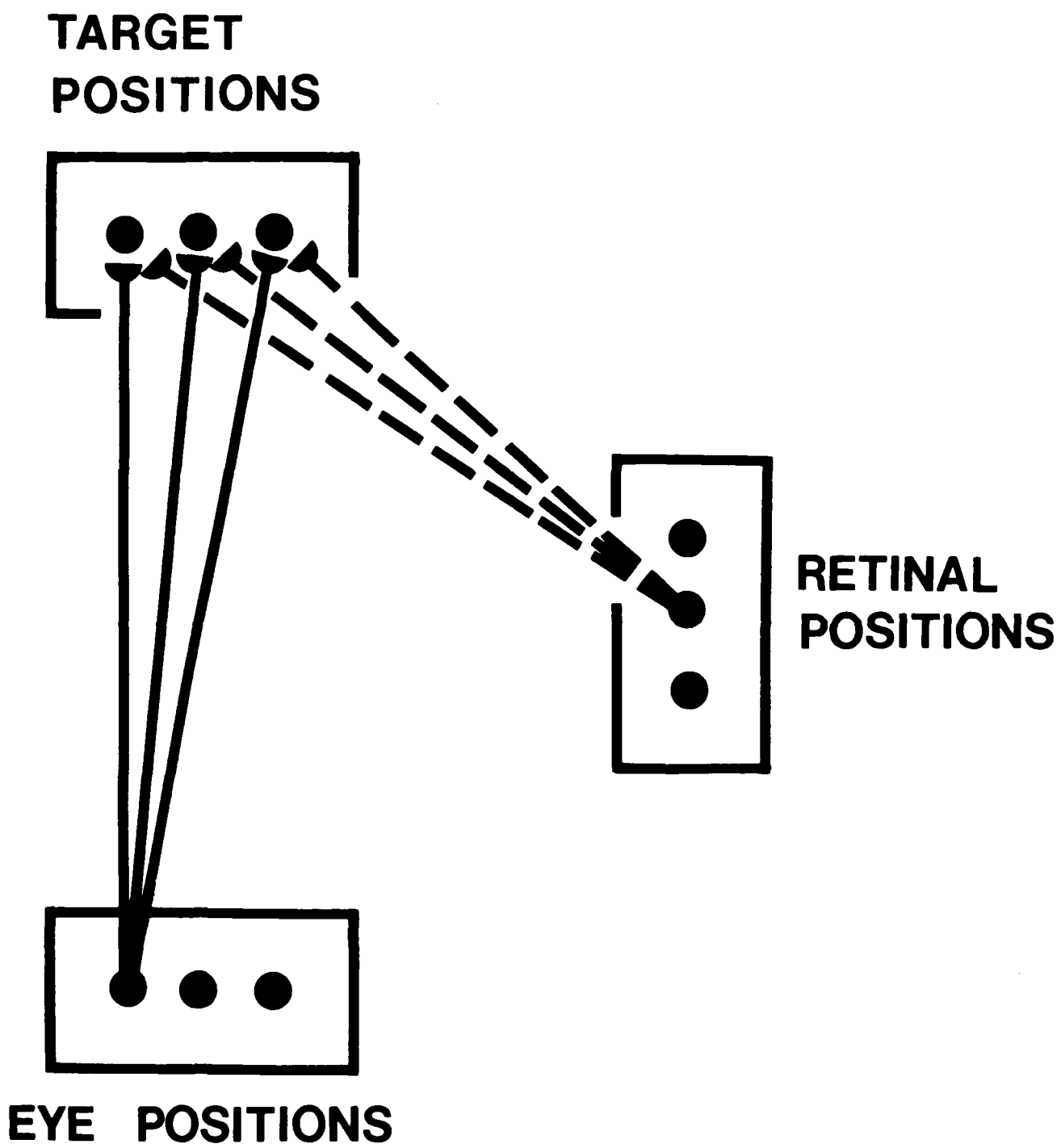

Figure 5

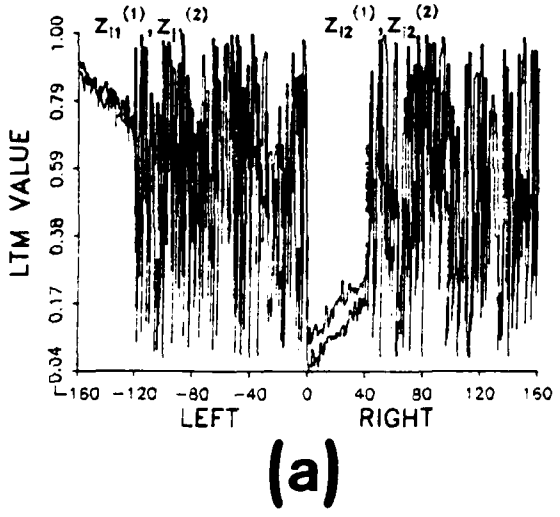

(a)

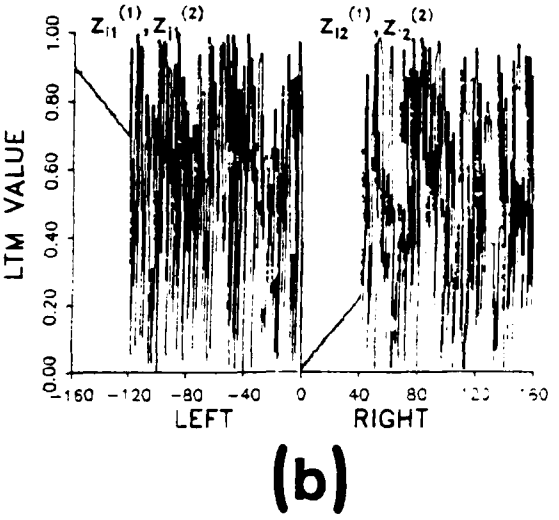

(b)

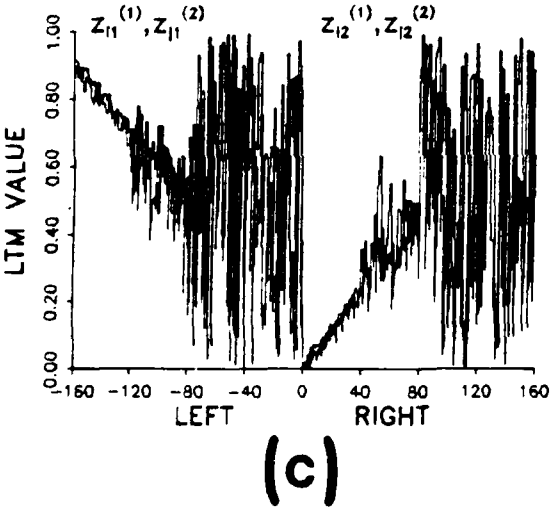

(c)

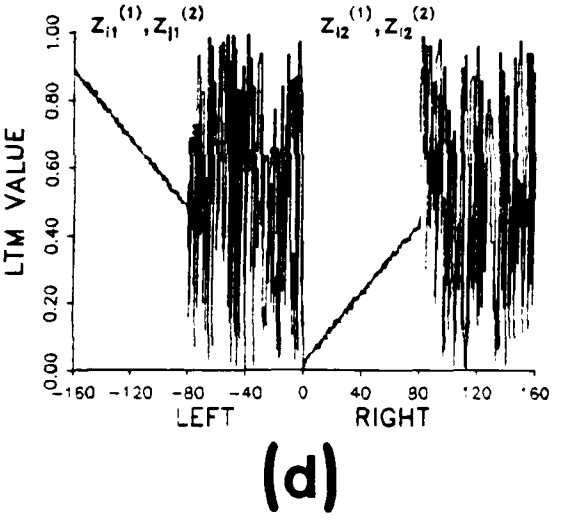

(d)

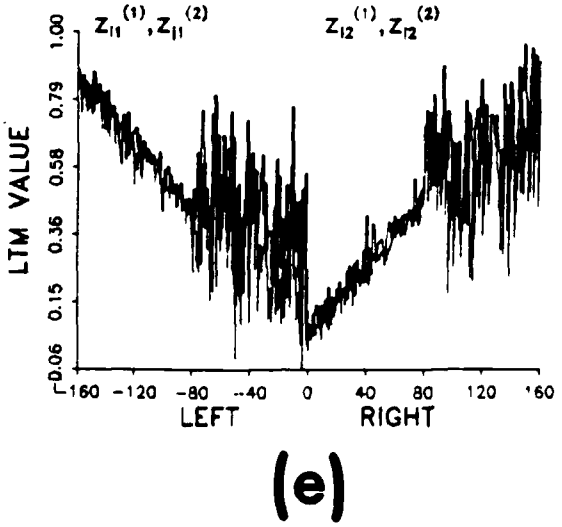

(e)

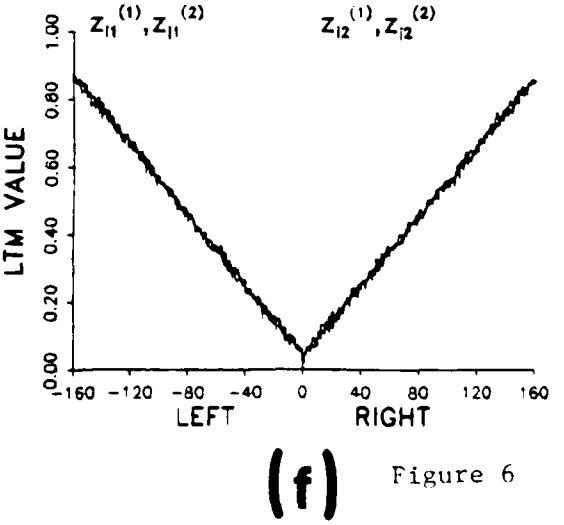

(f)

Figure 6


TARGET POSITION (RETINOTOPIC)
TARGET POSITION (HEAD)
TARGET POSITION (MOTOR)


VECTOR (MOTOR)
TARGET POSITION (MOTOR)
PRESENT POSITION (MOTOR)

Figure 7

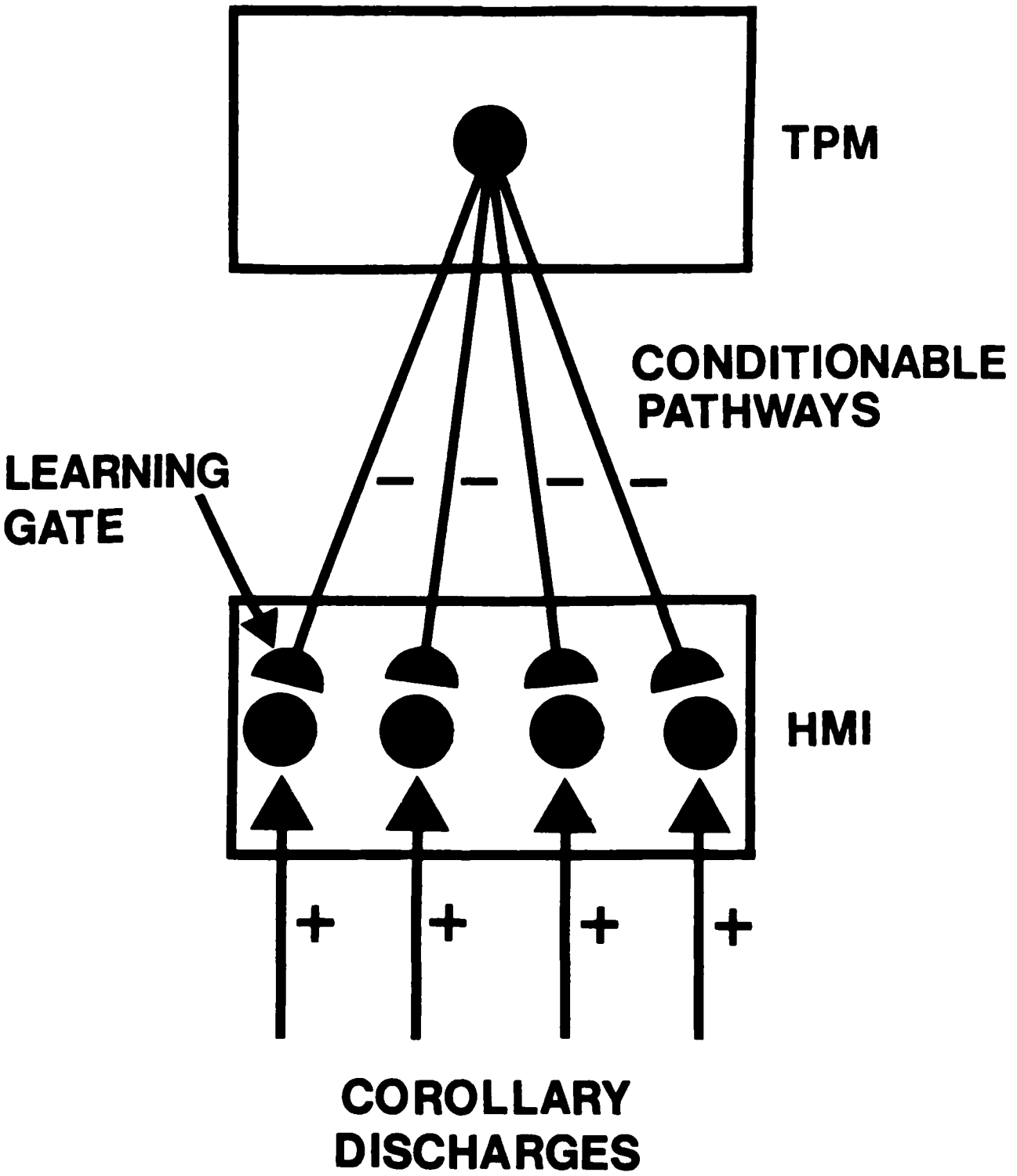
TPM
CONDITIONABLE
PATHWAYS
LEARNING
GATE
HMI
COROLLARY
DISCHARGES

Figure 8

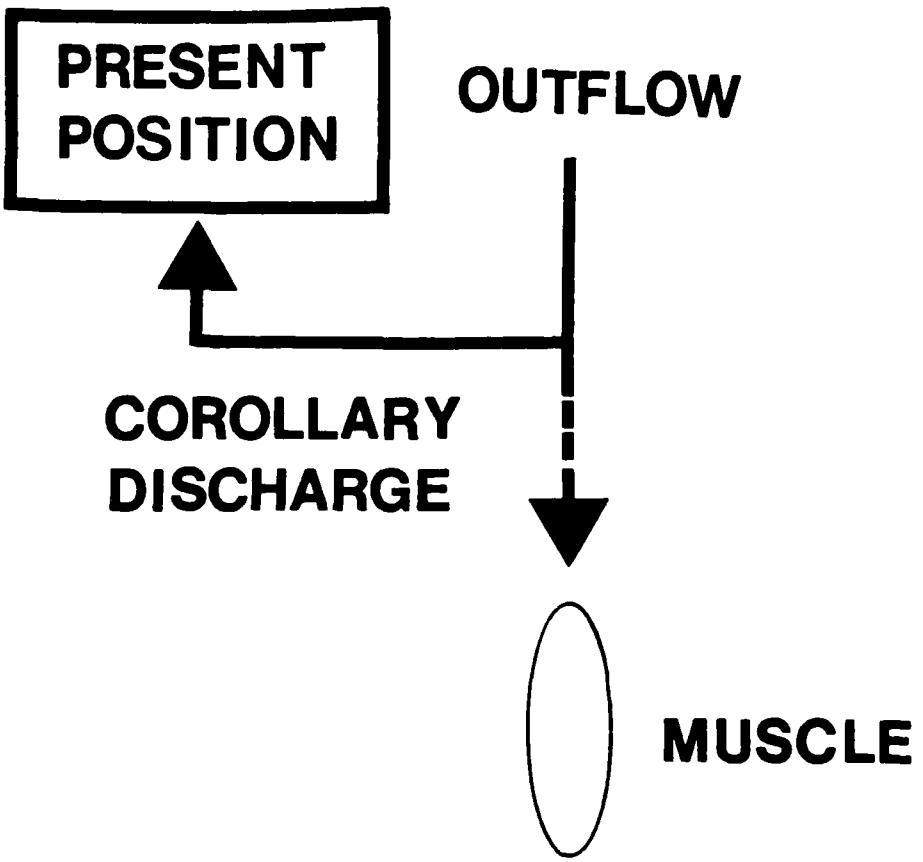

Figure 9

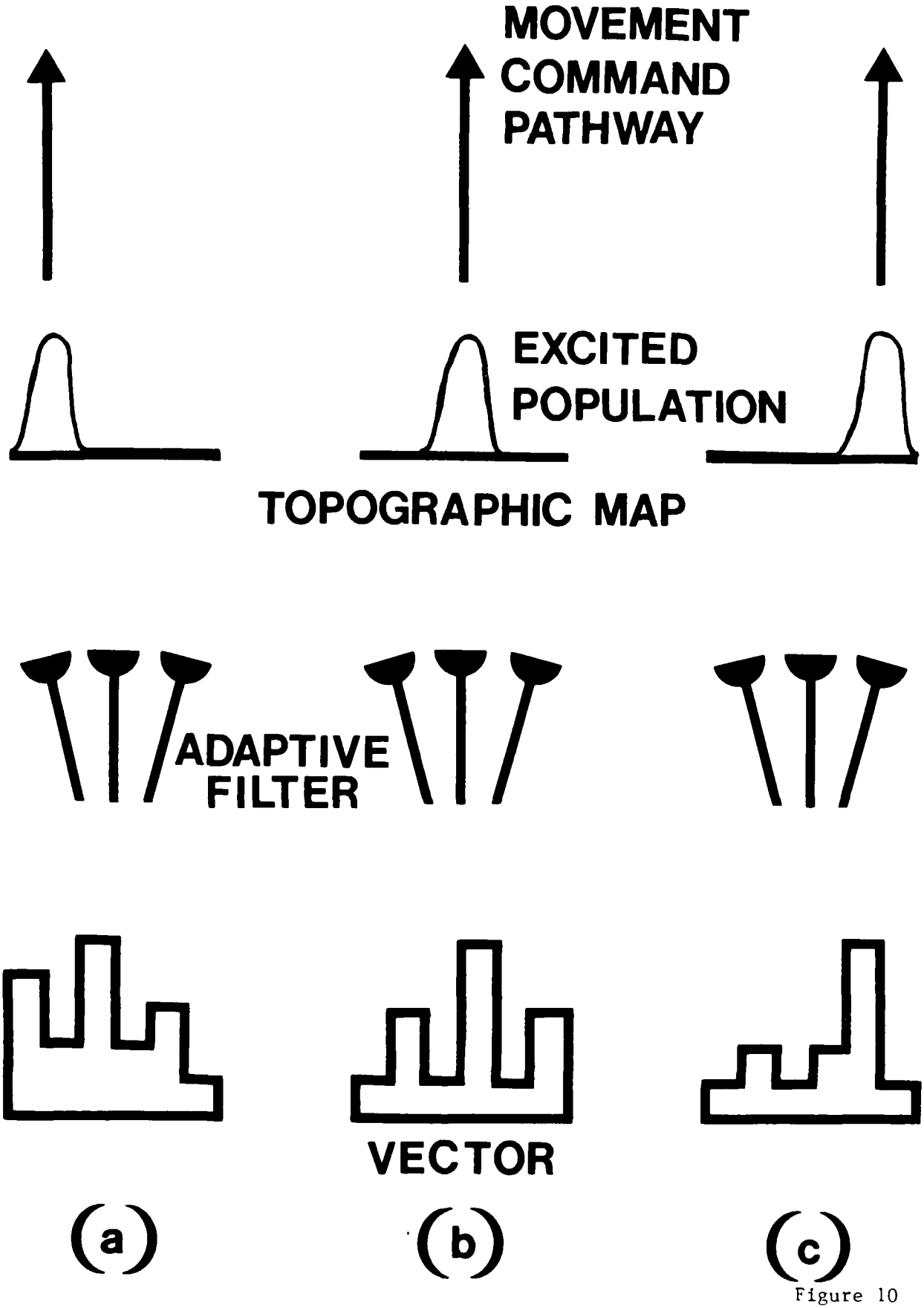
MOVEMENT
COMMAND
PATHWAY
EXCITED
POPULATION
TOPOGRAPHIC MAP
ADAPTIVE
FILTER
VECTOR
(a)
(b)
(c)

Figure 10

TOPOGRAPHIC MAP

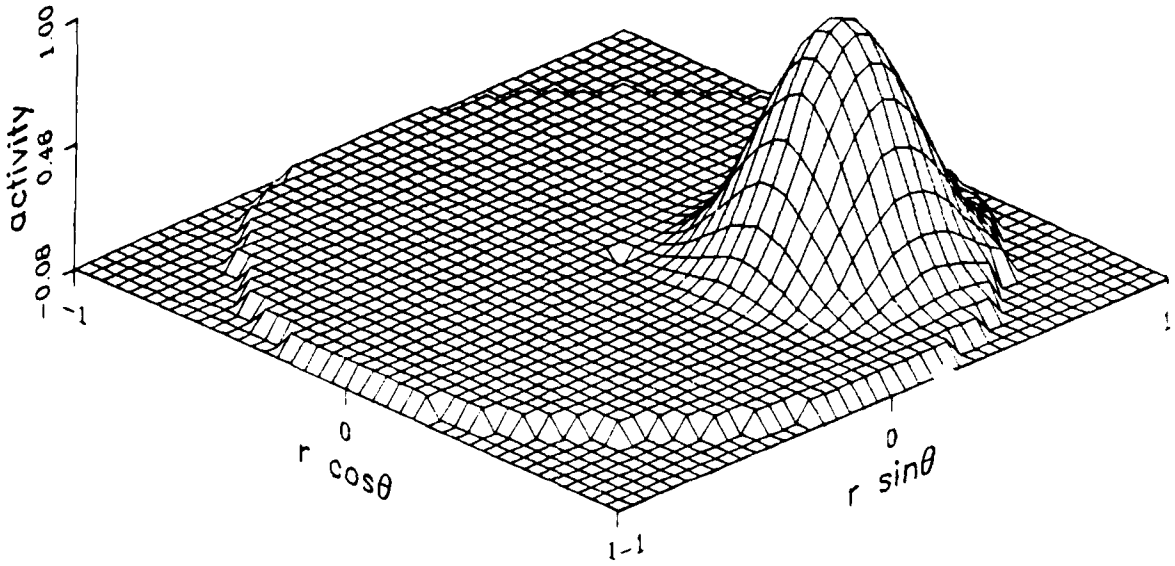

HEAD-MUSCLE INTERFACE

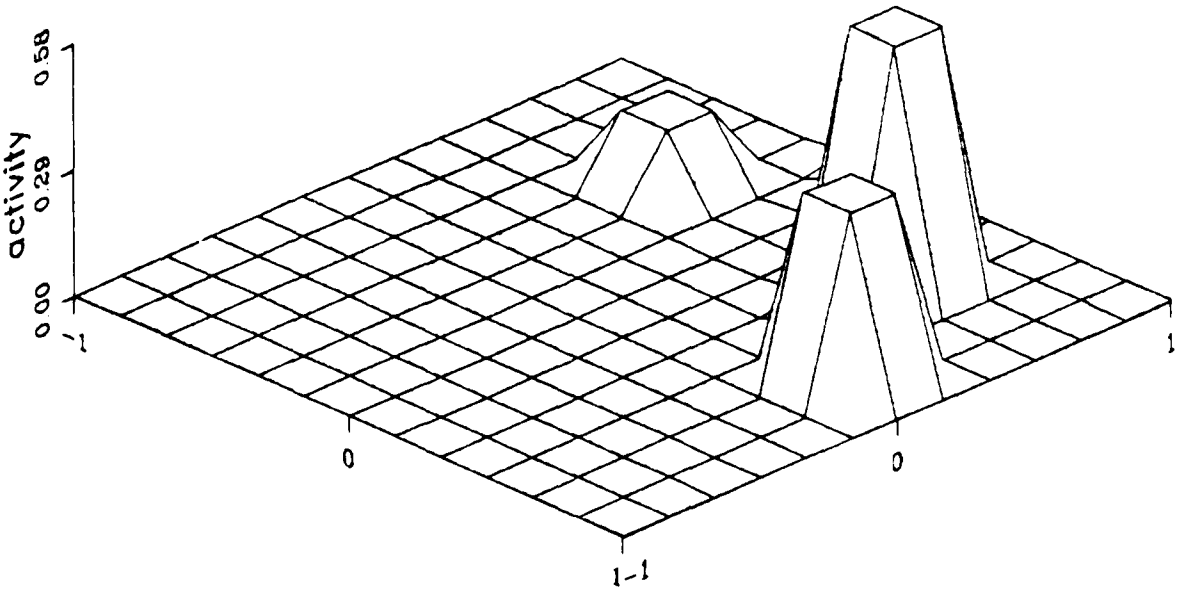

Figure 11

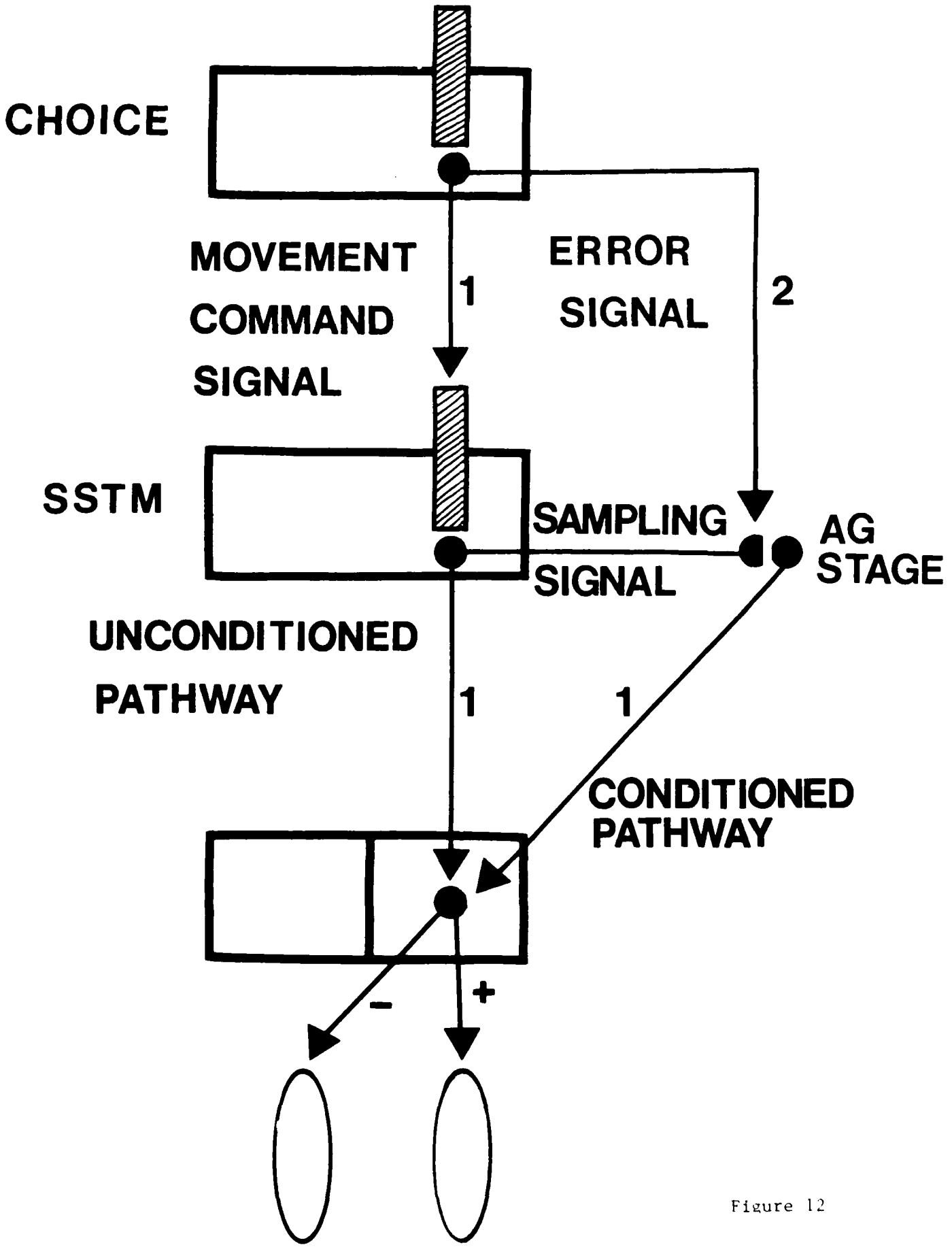
CHOICE
MOVEMENT
COMMAND
SIGNAL
1
ERROR
SIGNAL
2
SSTM
SAMPLING
SIGNAL
AG
STAGE
UNCONDITIONED
PATHWAY
1
1
CONDITIONED
PATHWAY
−
+

Figure 12

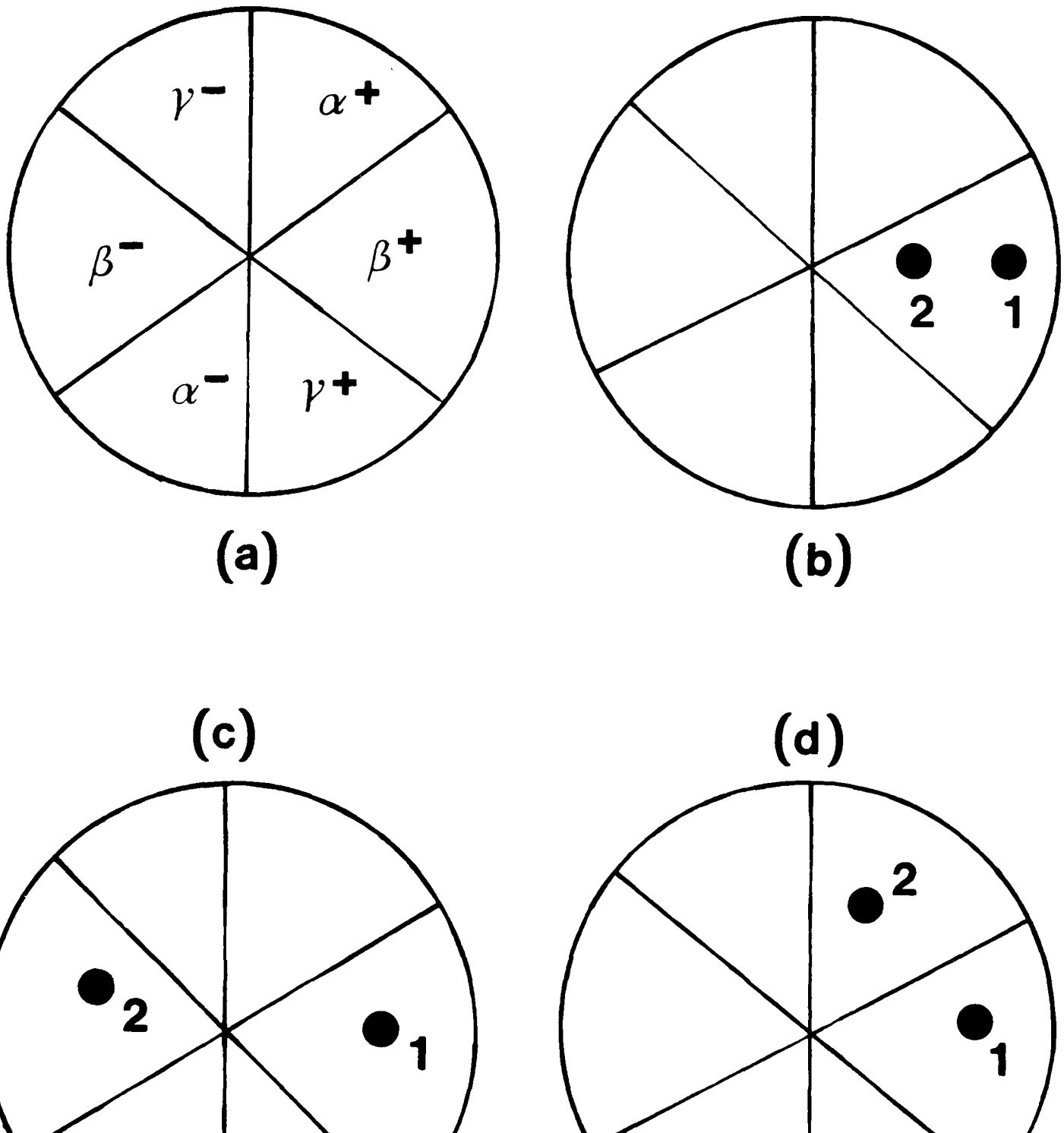

Figure 13

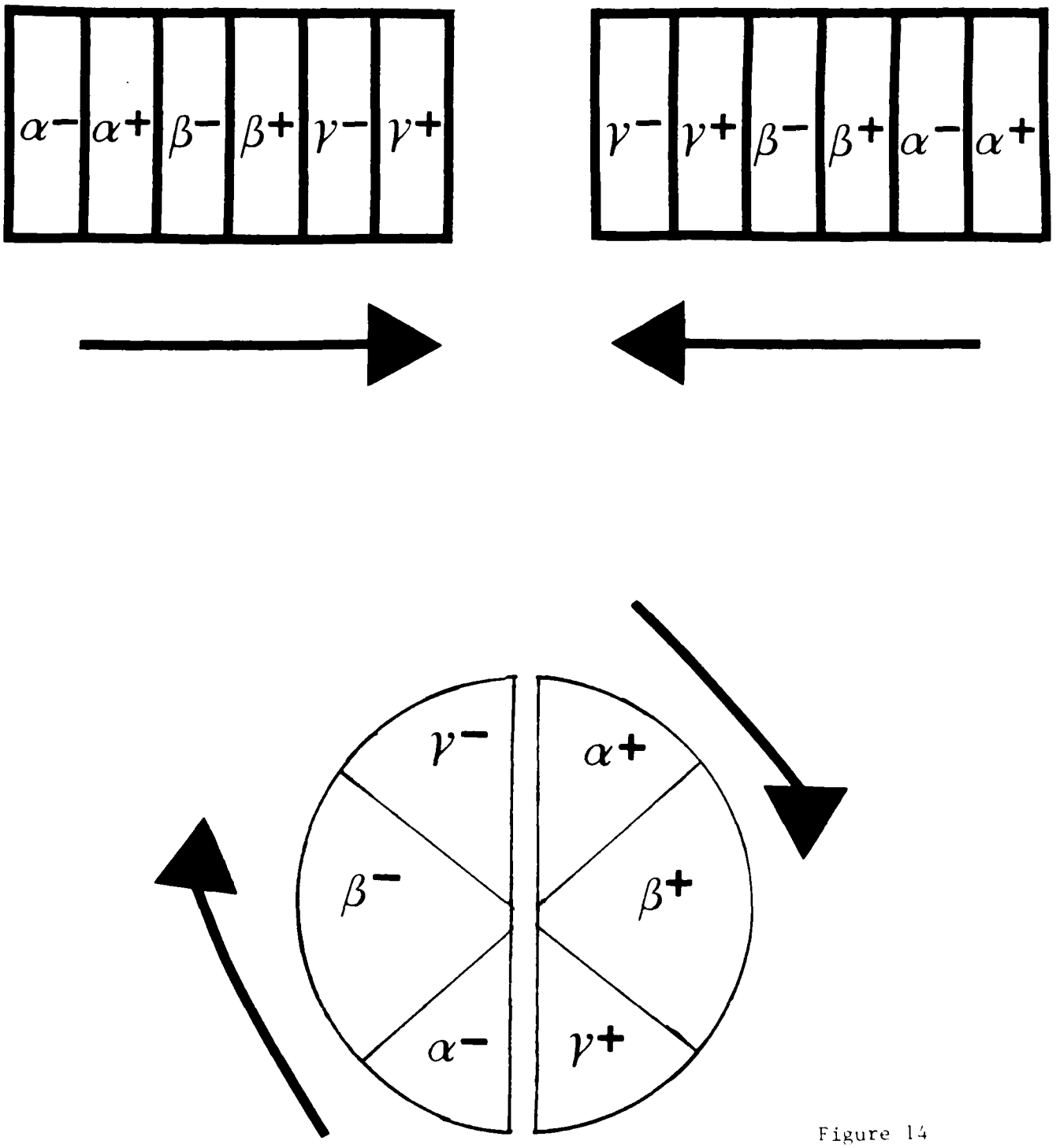

Figure 14

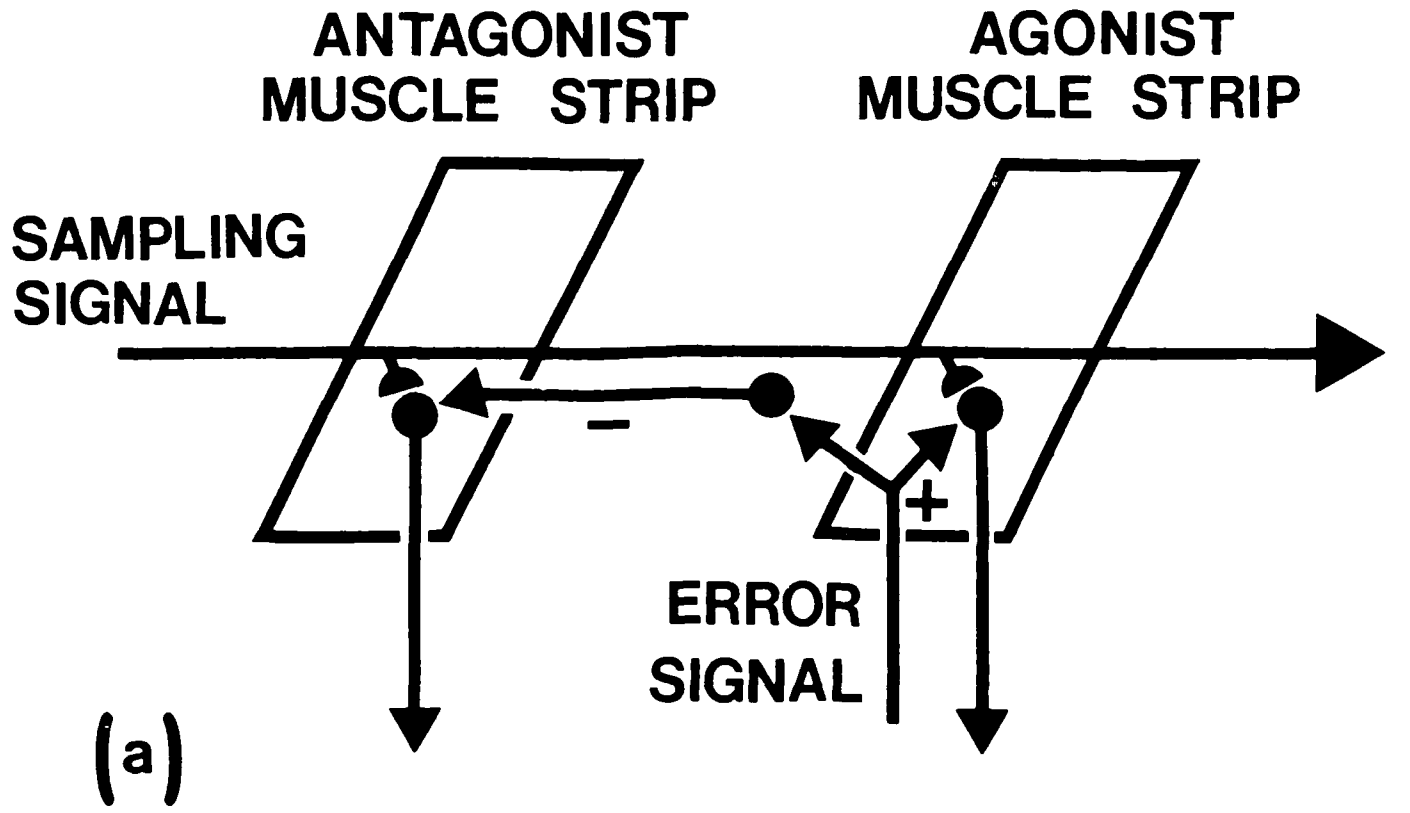
ANTAGONIST
MUSCLE STRIP
AGONIST
MUSCLE STRIP
SAMPLING
SIGNAL
−
+
−
ERROR
SIGNAL
(a)

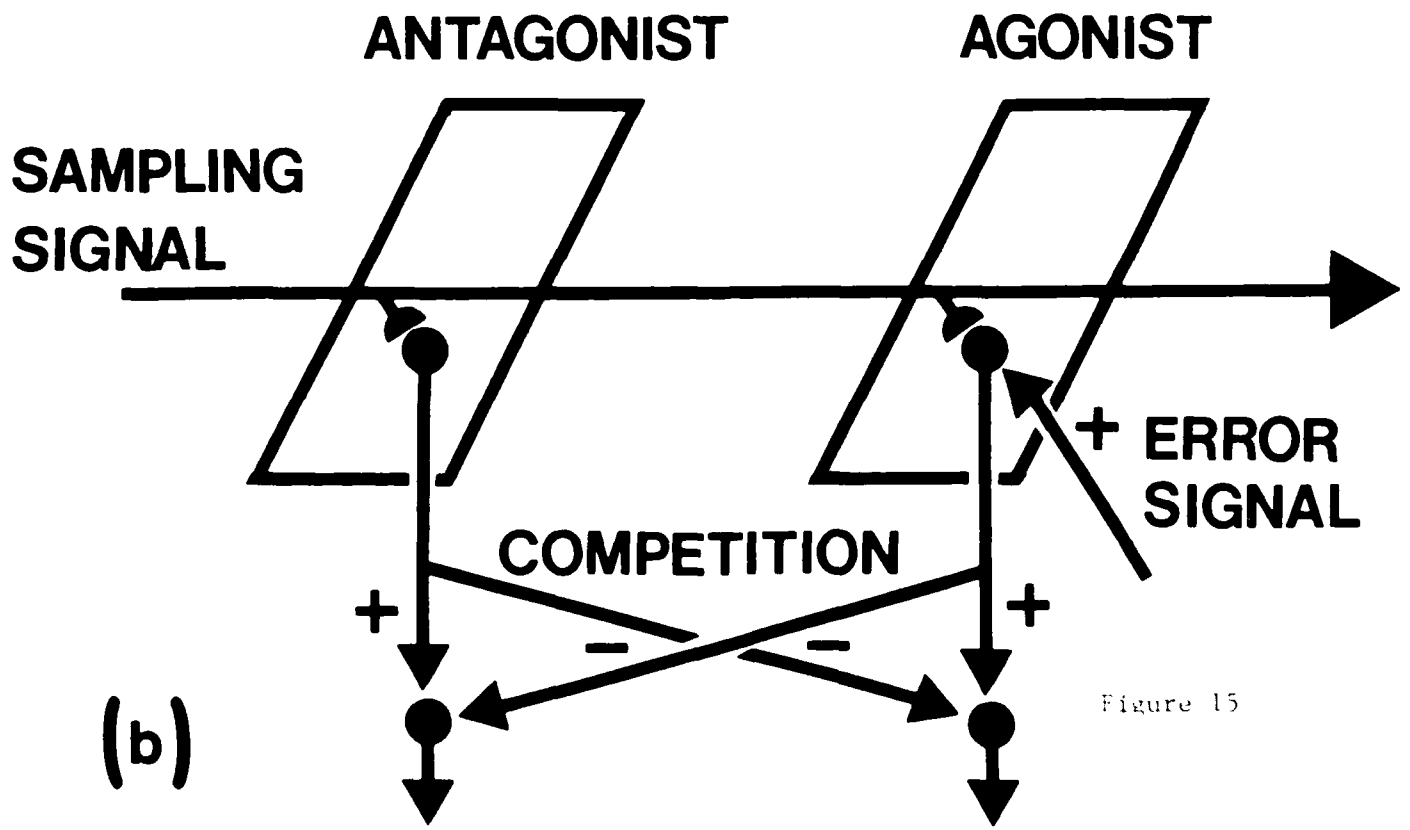
ANTAGONIST
AGONIST
SAMPLING
SIGNAL
+ ERROR
SIGNAL
COMPETITION
+
−
−
+
(b)

Figure 15

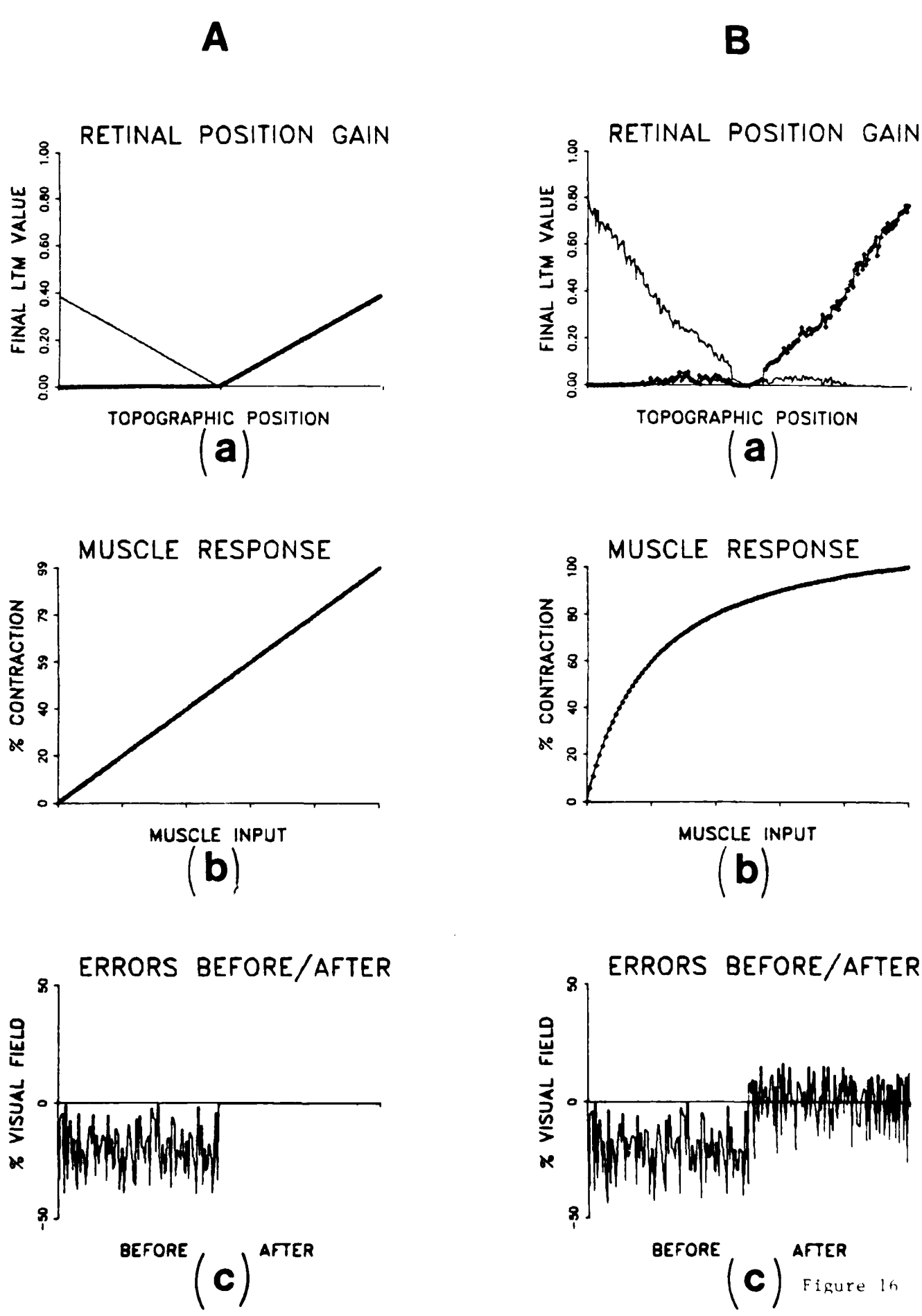
A
B
RETINAL POSITION GAIN
FINAL LTM VALUE
0.00
0.20
0.40
0.60
0.80
1.00
TOPOGRAPHIC POSITION
(a)
MUSCLE RESPONSE
% CONTRACTION
0
20
40
59
79
99
MUSCLE INPUT
(b)
ERRORS BEFORE/AFTER
% VISUAL FIELD
50
0
-50
BEFORE
AFTER
(c)

Figure 16

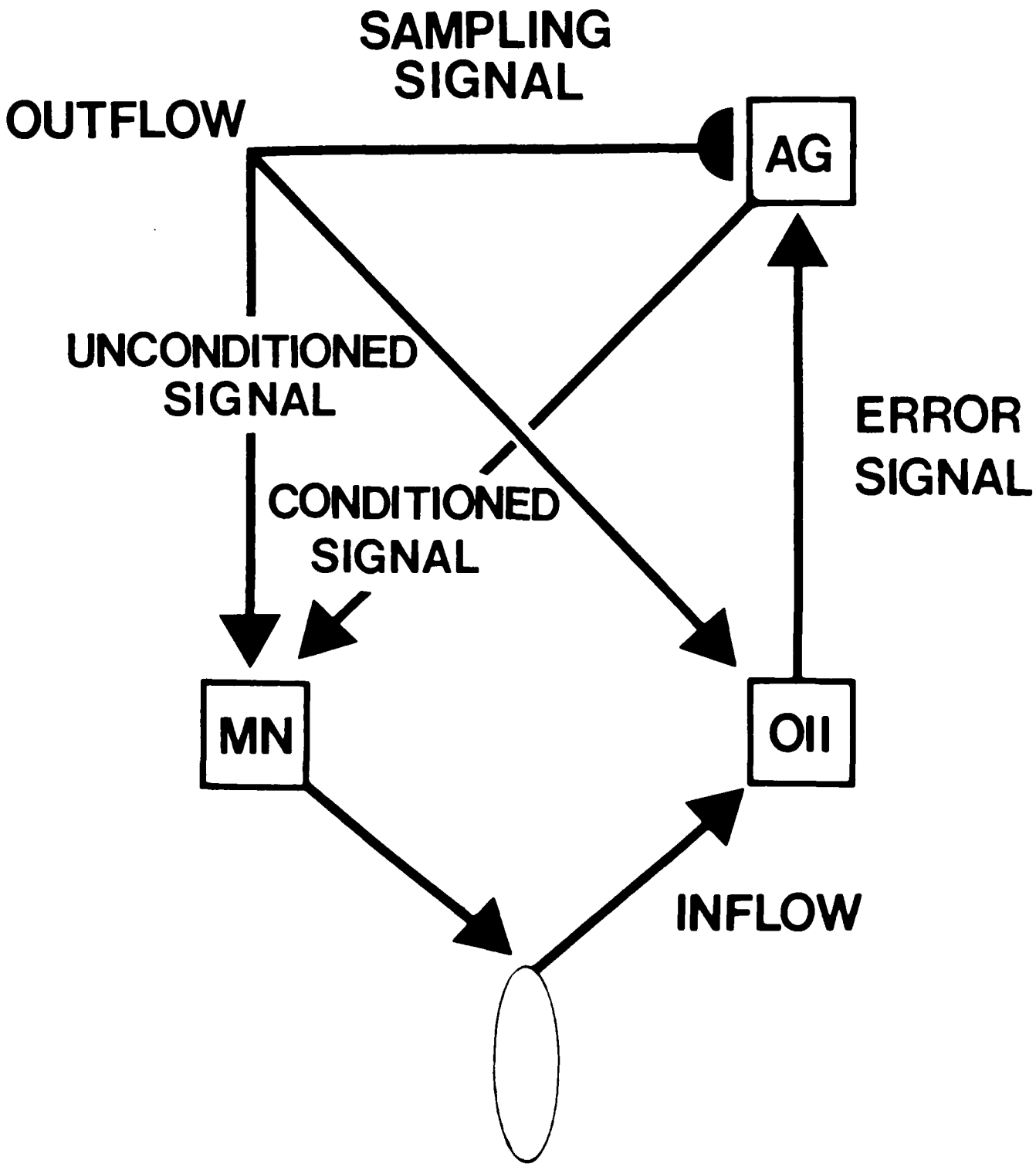
SAMPLING
SIGNAL
OUTFLOW
AG
UNCONDITIONED
SIGNAL
ERROR
SIGNAL
CONDITIONED
SIGNAL
MN
OII
INFLOW

Biol. Cybern., submitted.

Deducing Planning Variables from Experimental Arm Trajectories: Pitfalls and Possibilities

J.M. Hollerbach and C.G. Atkeson

Massachusetts Institute of Technology
Center for Biological Information Processing
and
Artificial Intelligence Laboratory

Address correspondence to:
John M. Hollerbach
MIT Artificial Intelligence Laboratory
545 Technology Square
Cambridge, Mass. 02139
USA

Abstract

This paper investigates whether endpoint Cartesian variables or joint variables better describe the planning of human arm movements. For each of the two sets of planning variables, a coordination strategy of linear interpolation is chosen to generate possible trajectories, which are to be compared against experimental trajectories for best match. Joint interpolation generates curved endpoint trajectories called N-leaved roses. Endpoint Cartesian interpolation generates curved joint trajectories, which however can be qualitatively characterized by joint reversal points.

Though these two sets of planning variables ordinarily lead to distinct predictions under linear interpolation, three situations are pointed out where the two strategies may be confused. One is a straight line through the shoulder, where the joint trajectories are also straight. Another is any trajectory approaching the outer boundary of reach, where the joint rate ratio always appears to be approaching a constant. A third is a generalization to staggered joint interpolation, where endpoint trajectories virtually identical to straight lines can sometimes be produced. In examining two different sets of experiments, it is proposed that staggered joint interpolation is the underlying planning strategy.

1 Introduction

A major approach towards studying biological motor control rests on the premise that one can infer representations used by the brain from regularities in observed behavior. External observations of movement patterns may lead to a set of variables that most concisely describes them. It is then hypothesized that these descriptive variables are used internally by the motor control system during movement planning to generate the observed trajectories.

This paper investigates this approach by presuming that there is a distinct geometric planning level for the whole movement. The whole motion evolves as a result of controlled relations among kinematic variables, and any dynamic effects due to joint torque production, muscle activation, and reflexes are subservient to the kinematic goals. An alternative is to suppose that only the endpoints of movement have a determined geometrical relationship, and that intermediate trajectory points are dynamically determined through interaction of dynamic effects, muscle properties, and reflexes.

One argument to support the presumption that there is a kinematic representation of the whole movement is that the geometry of the external world is more simply captured. With dynamically determined trajectories, the location of a moving limb is hard to predict or control and may violate environmental constraints (Hildreth and Hollerbach, 1986). Another argument derives from studies showing that the path of arm movement and the tangential velocity profile along the path are not altered when the speed of movement is changed or when the hand holds a weight (Atkeson and Hollerbach, 1985). This indicates that dynamic effects are subservient to kinematic invariances. Yet the final support must come from the success in locating a set of kinematic variables that concisely describes movement.

Two obvious choices for kinematic planning variables that have been frequently made are hand position and joint angles. Support for hand position in terms of endpoint Cartesian coordinates derives from experimental observations of path shape (Morasso, 1981; Viviani and Terzuolo, 1982), theoretical analysis of optimization strategies (Flash and Hogan, 1985), and teleological arguments about interfacing to the geometry of the external world (Hollerbach, 1985). One disadvantage with endpoint planning is that an inverse kinematics solution is required, i.e., the conversion to corresponding joint coordinates. Fortunately, the human arm has the correct kinematic structure that would allow this computation to be done relatively efficiently (Hollerbach, 1985).

although the computation is not trivial. Support for joint variable planning derives from experimental studies of Kots and Syrovegin (1966), Soechting and Lacquaniti (1981), and Soechting et al. (1985). While an inverse kinematics computation is not required, and hence joint variable planning is evidently a simpler strategy, the price paid is some loss of endpoint control.

In this paper, we examine possibilities in terms of the kinds of trajectories that can be produced utilizing either endpoint variables or joint variables. The eventual goal is to find the best match of predicted trajectories to experimental trajectories. To proceed after a choice of variables in order to generate trajectories, a coordination strategy must be hypothesized. We examine the simplest and most commonly proposed coordination strategy, simple linear interpolation, in both endpoint variables and joint variables.

More complex planning strategies variables are of course possible. Hollerbach (1981) suggested that in handwriting each Cartesian variable described an oscillatory motion, with adjustable relative phase and frequency relationships. Morasso and Mussa-Ivaldi (1982) suggested that elemental strokes were overlapped in time to form the letters in handwriting. Viviani and Terzuolo (1982) and Lacquaniti et al. (1983) suggested functional relationships between curvature, tangential velocity, and angular velocity of the path. Nevertheless, the movement goals in these curved motions are more complex than the simpe point-to-point reaching movements considered here, and this paper is restricted to the commonly proposed coordination strategy of linear interpolation.

At the same time this paper identifies some pitfalls in this approach. There may be situations where alternative strategies lead to nearly indistinguishable behavior. We identify one such situation in this paper when movement approaches the edge of the workspace. This approach is also sensitive to assumptions either in the details of the variables chosen or in the coordination strategy chosen. We demonstrate an intermediate strategy between the proposed extremes that sometimes looks like one alternative and sometimes like the other.

In the present study, the characterization of interpolated movements and the identification of possible pitfalls will serve as the basis for analyzing two different experimental studies of human arm movement in a vertical plane. In the first of these, Soechting and Lacquaniti (1981) noted that joint rate ratios in the deceleratory phases of the movements they studied appeared to approach a constant. In the second study, Atkeson and Hollerbach (1985) noted both curved and straight endpoint Cartesian trajectories. We examine the possibility that the intermediate strategy alluded to above is in effect in

both studies.

2 Linear Interpolation

In the subsequent discussion the human arm will be represented by a two-link planar manipulator (Figure 1A). Although the human arm is of course easily capable of three-dimensional movement, many experimental studies have confined the arm motion to a plane. Two-link kinematics is sufficiently complex to develop principles of coordination, and the results prove useful in more general analyses. For this two-joint arm, θ_1 represents the shoulder angle and θ_2 represents the elbow angle. No motion of the wrist is assumed, and the length of the hand is included in the forearm length. The upper arm length l_1 is assumed equal to the forearm plus hand length l_2, which is a good approximation for the human forearm plus hand relative to the upper arm (Hollerbach and Flash, 1982). For convenience, both lengths are set to 1.

The shoulder angle θ_1 corresponds to one of the psychophysical variables determined by Soechting and Ross (1984). For a vertical arm movement the shoulder angle corresponds to the second pitch shoulder rotation, while for a horizontal arm movement it corresponds to the first shoulder yaw rotation. The elbow angle is the relative elbow angle, as normally defined in robotics. Though the relative elbow angle is physiologically the most meaningful, Soechting and Ross (1984) suggest that the absolute forearm inclination in the vertical plane is the most relevant psychophysical parameter. Nevertheless, in the section on joint interpolation the results are equivalent whether relative or absolute elbow angle is used.

This section begins by developing the mathematics for linear interpolation in terms of endpoint Cartesian coordinates and in terms of joint angles. Three equivalent mathematical forms are given that are useful in subsequent analysis, namely straight line, interpolation, and constant velocity ratio.

2.1 Straight-Line Form

Conceptually the simplest strategy in terms of any planning variables is a straight line, equivalent to a linear interpolation between initial and final points. In terms of endpoint Cartesian variables (x, y), the familiar form for a straight line is (Figure 2A):

$$\frac{y(t) - y(t_0)}{x(t) - x(t_0)} = \frac{y(t_f) - y(t_0)}{x(t_f) - x(t_0)} \tag{1}$$

or equivalently,

$$y(t) = mx(t) + b \tag{2}$$

where $m = (y(t_f) - y(t_0))/(x(t_f) - x(t_0))$ and $b = y(t_0) - mx(t_0)$. Here the initial point at time t_0 is given by $(x(t_0), y(t_0))$ and the final point at time t_f by $(x(t_f), y(t_f))$.

Cartesian coordinates are of course not the only possible variables describing endpoint position, as the polar coordinates r and ϕ (Figure 1B) are one of many possible alternatives. Nevertheless, Cartesian coordinates have been primarily emphasized in the literature, and have so far proven the most useful. Hence our attention will be restricted to them.

A straight line in terms of joint variables is also the conceptually simplest planning strategy. Such a straight-line motion is described by (Figure 2B):

$$\frac{\theta_1(t) - \theta_1(t_0)}{\theta_2(t) - \theta_2(t_0)} = \frac{\theta_1(t_f) - \theta_1(t_0)}{\theta_2(t_f) - \theta_2(t_0)} \tag{3}$$

or equivalently,

$$\theta_1(t) = K\theta_2(t) + \phi_0 \tag{4}$$

where $K = (\theta_1(t_f) - \theta_1(t_0))/(\theta_2(t_f) - \theta_2(t_0))$ and $\phi_0 = \theta_1(t_0) - K\theta_2(t_0)$.

During a straight-line motion in joint space, there is no particular control of the endpoint position, which evolves incidentally according to the characteristics of this coordination strategy. At the movement ends, however, there must of course exist the knowledge of the joint angles that correspond to the desired targets. Section 2.4 discusses the inverse kinematic relation between the fixed Cartesian endpoints $(x(t_0), y(t_0))$ and $(x(t_f), y(t_f))$, and the beginning and final joint angles $(\theta_1(t_0), \theta_2(t_0))$ and $(\theta_1(t_f), \theta_2(t_f))$.

2.2 Interpolation Form

The straight-line forms just developed do not explicitly indicate how time evolves during the trajectory. This dependency is made clear in the interpolation form, by introducing a common time function $f(t)$ that parameterizes each variable.

$$\begin{aligned} x(t) &= (x(t_f) - x(t_0))f(t) + x(t_0) \\ y(t) &= (y(t_f) - y(t_0))f(t) + y(t_0) \end{aligned} \tag{5}$$

Rearrangement and division easily converts (5) into (1). In terms of joint variables, the interpolation form is:

$$\theta_1(t)=(\theta_1(t_f)-\theta_1(t_0))f(t)+\theta_1(t_0)$$
$$\theta_2(t)=(\theta_2(t_f)-\theta_2(t_0))f(t)+\theta_2(t_0) \tag{6}$$

The time function starts and stops appropriately ($f(t_0) = 0$ and $f(t_f) = 1$), and does not reverse direction ($\dot{f}(t) \geq 0$). Later, considerable emphasis will be given to this property of the interpolation form, namely that the trajectory cannot double back on itself, although the trajectory may stop momentarily.

It is important that exactly the same time function $f(t)$ be used for each variable; otherwise a straight line would not result. The time function is most conveniently cast in terms of rates $\dot{f}(t)$, so that in the case of joint velocities obtained by differentiating (6):

$$\dot{\theta}_1(t)=\Delta\theta_1\dot{f}(t)$$
$$\dot{\theta}_2(t)=\Delta\theta_2\dot{f}(t) \tag{7}$$

where $\Delta\theta_1 = (\theta_1(t_f) - \theta_1(t_0))$ and $\Delta\theta_2 = (\theta_2(t_f) - \theta_2(t_0))$ are the total angle displacements through which each joint is interpolated. Figure 3A shows hypothetical joint velocity profiles. Note once again that the joints execute the same time profile $f(t)$ in lockstep, starting and stopping together. The only difference is the amplitude of joint displacement.

2.3 Velocity Ratio Form

A third equivalent form is a constant velocity ratio. In the case of joint angles, the joint velocity ratio may be derived from (7):

$$\frac{\dot{\theta}_1}{\dot{\theta}_2} = \frac{\Delta\theta_1}{\Delta\theta_2} = K \tag{8}$$

where K is a constant because the total joint displacements are fixed. We point out again that this ratio is a constant precisely because each joint is executing the same time profile, which cancels out in the division.

To show the equivalence in the other direction, suppose the joint rate ratio is a constant K. Then by the chain rule:

$$\frac{\dot{\theta}_1}{\dot{\theta}_2} = \frac{d\theta_1}{dt}\frac{dt}{d\theta_2} = \frac{d\theta_1}{d\theta_2} \tag{9}$$

Integration of the equation $d\theta_1 = K d\theta_2$ yields the straight-line equation (2). Thus the following three forms have been demonstrated equivalent:

1. Joint interpolation,
2. Straight line in joint space, and
3. Constant joint rate ratio.

2.4 Kinematics

To decide whether a given trajectory has been executed under one or the other set of coordinates, a description of the trajectory must be given in terms of each set of coordinates. Direct kinematics derives the endpoint Cartesian coordinates from the joint angles. From Figure 1A:

$$\begin{aligned} x &= l_1 \cos\theta_1 + l_2 \cos(\theta_1 + \theta_2) \\ y &= l_1 \sin\theta_1 + l_2 \sin(\theta_1 + \theta_2) \end{aligned} \tag{10}$$

Inverse kinematics derives the joint angles from the endpoint position, and is more computationally complex than the direct kinematics. From Figure 1B, since the link lengths are assumed equal ($l_1 = l_2 = 1$), an isosceles triangle is formed with the radial line r to the endpoint. From the half-angle formula, each of the two equal interior angles is half the exterior angle θ_2. Thus

$$\cos(\theta_2/2) = r/2 = \sqrt{x^2 + y^2}/2 \tag{11}$$

where the perpendicular from the elbow bisects the radial line of length $r = \sqrt{x^2 + y^2}$ from shoulder to endpoint. The shoulder angle θ_1 is simply the difference between the polar angle $\phi = \tan^{-1}(y/x)$ and the interior angle $\theta_2/2$:

$$\theta_1 = \tan^{-1}(y/x) - \theta_2/2 \tag{12}$$

The time parameter (t) has been left out for convenience.

In examining the kinematics, the transcendental functions relating joint angles to endpoint positions would lead one to expect complex curves in one set of coordinates corresponding to simple curves or straight lines in the other set of coordinates. The following two sections investigate the joint angle trajectories corresponding to endpoint

straight lines, and then the endpoint trajectories corresponding to joint angle straight lines.

2.5 Trajectories under Endpoint Interpolation

The exact relationship between endpoint Cartesian variables and joint variables is highly specific to the workspace region occupied by the straight line. To analyze this relationship, it proves useful to focus on joint reversal points. Figure 4A shows a hypothetical vertical straight-line motion. Points 1 and 4 correspond to maximum reach, when the elbow joint is straight out. When the forearm is perpendicular to the straight line, the shoulder joint reverses direction. This corresponds to point 2: both an upward and a downward motion from this point causes the shoulder joint to rotate counterclockwise. When the endpoint is closest to the shoulder, the elbow joint reverses direction. This point 3 can also be characterized as the normal intersection from the shoulder to the straight line. Motion either upward or downward from point 3 causes clockwise rotation at the elbow joint.

Figure 4B shows the joint angle plot, where the specific joint angles are identified corresponding to the four endpoints of Figure 4A. As can be seen, in general the joint angle profile is curved. The extent of curvature depends on the portion of the curve traversed, as determined by the exact start and stop points chosen along the straight line. When the start and stop points do not cross a joint reversal point, the joint curves are a bit simpler. This comprises motion within target pairs 1 and 2, 2 and 3, and 3 and 4. A motion crosses exactly one joint reversal point when, for the case of shoulder reversal, one target is between 1 and 2 and the other target is between 2 and 3, and for the case of elbow reversal, when one target is between 2 and 3 and the other is between 3 and 4. These single-joint reversal trajectories will be somewhat more complex than the former trajectories. Finally for long enough motions, both joints can reverse: one target is between 1 and 2 and the other between 3 and 4. These motions will yield the most complex joint angle plots.

This analysis covers all straight-line motions. First, if the straight line is at a different inclination, the coordinate system can be rotated so that the line will appear vertical. Second, if the straight line is at a different normal distance from the shoulder, the topology of the joint reversal points remains the same. The elbow joint reversal point 3 will remain on the x axis, while the shoulder joint reversal point 2 will move up as the

straight line moves away from the shoulder.

2.6 Trajectories under Joint Interpolation

When the link lengths for the two-link planar manipulator are the same, endpoint trajectories arising from straight lines in joint space can be succinctly expressed using polar coordinates. Letting r be the radial distance from the shoulder to the arm tip and ϕ the angle the radial line makes at the shoulder (Figure 1B):

$$\begin{aligned} \phi &= \theta_1 + \theta_2/2 \\ r &= 2\cos(\theta_2/2) \end{aligned} \tag{13}$$

Given the straight line in joint coordinates (4) and substituting above,

$$r = 2\cos\left(\frac{\phi - \phi_0}{2K+1}\right) \tag{14}$$

When the link lengths are substantially different, such a simple expression does not arise.

This class of polar coordinate curves is known as an *N-leaved rose* (Burlington, 1942), presumably because each complete curve looks like a rose petal, with the thickness determined by some slope N. Figure 5 illustrates some straight-line joint paths (5A) and the corresponding endpoint Cartesian paths (5B). The straight-line joint paths chosen here all pass through the origin, corresponding to both angles at 0 degrees when the arm is perfectly straight and horizontal, and are numbered 1 through 13. The endpoint Cartesian paths corresponding to them are also numbered from 1 to 13. Arrows in both diagrams indicate the direction of travel in each. The endpoint Cartesian curves are symmetrical, although only half of each curve has been presented because of elbow joint limits. As can be seen in Figure 5B, N-leaved roses tend to be strongly curved, especially for movements that are not primarily radial movements through the shoulder.

As mentioned earlier, Soechting and Ross (1984) argue that the relevant psychological variable for the elbow is the absolute forearm orientation $\theta_1 + \theta_2$, rather than the relative elbow angle θ_2. It is easily shown that joint interpolation using the absolute forearm orientation also yields an N-leaved rose, and hence the results will not change.

2.7 Distinguishing Endpoint from Joint Interpolation

Summarizing the last two sections, straight lines in one space generally yield curved lines in the other space. Hence interpolation in joint variables generally yields trajectories readily distinguishable from straight-line hand paths.

There is one important special case where the two planning strategies can be confused — any Cartesian straight line through the shoulder. Then $y/x = m$, $b = 0$, and from (12):

$$\theta_1 = \tan^{-1} m - \theta_2 . 2 \tag{15}$$

In terms of joint variables θ_1 and θ_2 the trajectory is also straight. This is the only circumstance in which there can be a straight line simultaneously in endpoint Cartesian variables and joint variables. In Figure 5, this would correspond to trajectory 4 (a rose petal of zero width in 5A).

Past studies have provided evidence for both alternatives. Morasso (1981) investigated horizontal planar arm movements with a pantograph experimental apparatus. In all cases the movements appeared to be Cartesian straight lines, while the joint angle profiles were quite varied, even involving joint reversal. Given the manifest simplicity of the endpoint trajectories and the greater complexity of the joint angle profiles, he argued that the planning variables were Cartesian coordinates.

In an intriguing set of experiments, Soechting and Lacquaniti (1981) presented data that apparently indicate simultaneous straight lines in both spaces for a large class of movements. Sagittal plane arm motions were studied, with an initial starting posture of a horizontal forearm and a vertical upper arm. Movements were made unidirectionally from this starting point towards six different targets near the workspace boundary, located along a vertical line. Their data is reproduced in Figure 6. The endpoint trajectories (A) appear to be straight lines. Their joint angles in (B) are defined differently than the conventions of this paper. Their shoulder angle $\theta = \theta_1 - 90°$ differs from θ_1 in terms of the zero position. Their elbow angle $\phi = \pi - \theta_2$ is the interior angle ϕ between the upper arm and forearm instead of the exterior angle θ_2 between the upper arm extension and the forearm. Thus $\dot{\phi} = -\dot{\theta}_2$.

The joint angle plots (B) are generally curved, but the last half of the plots appear straight and parallel. This is more clearly seen in the joint velocity diagrams (C)-(H), corresponding to trajectories 1 through 6, respectively. In these diagrams, the motion is

counterclockwise along the curves. In the last half, or deceleratory phase of the motion, it appears that the joint velocity ratio is approaching the same straight line. These motion phases are plotted in (I).

Since a constant joint rate ratio is equivalent to a straight line in joint space, it thus appears that the last half of motion is characterized by simultaneous straight lines in both spaces. The analysis at the beginning of this section has shown that the only case where this can strictly be true is for a straight line through the shoulder joint. Only trajectory 6 and perhaps trajectory 5 can be explained this way. The other four trajectories cannot be explained on the basis of what has been presented so far, and appear to run counter to the expectation that joint interpolation generally yields curved trajectories readily distinguishable from straight lines in endpoint Cartesian variables. The next section is entirely devoted towards explaining this discrepancy.

3 The Boundary Artifact

To proceed with the analysis, a simulation is set up in Figure 7 to capture the main features of Figure 6. In the simulation, movements are straight lines with approximately the same starting and target points as in Figure 6A. Link lengths are taken from a human subject, and the tangential velocity profiles are minimum jerk (Hogan, 1984; Flash and Hogan, 1985). The simulated straight-line paths are shown in (7A); the shoulder point is indicated by a circle, and the arm is shown in the starting position. The six targets are located near the workspace boundary, represented by the quarter-circle arc. The joint angle plots appear in (7B), and the joint velocity plots in (7C).

The simulated joint velocities (7C) do indeed indicate that in the last half of the trajectories the joint rate ratio approaches a constant for all movements. Thus the simulation verifies the observation of Soechting and Lacquaniti, and can serve as a representation of their data for further discussion. This simulation also disproves the possibility that the small deviations from hand-space straight lines seen in the data are significant and explain the constant joint rate ratio asymptote.

3.1 Joint Interpolation

Since the last half of the joint angle trajectories appear to be straight lines, we analyze first the shape of the trajectories if the whole joint angle trajectories were straight. There is a unique N-leaved rose between any two endpoints, and Figure 8A shows the simulated Cartesian straight lines and corresponding N-leaved roses for the higher trajectories. Clearly the N-leaved roses are significantly curved relative to the Cartesian straight line, and hence joint interpolation by itself cannot explain these trajectories. Also the joint angle plots (7B) are clearly curved as well.

3.2 Mixed Interpolation Strategies

Another possibility is to take this data at face value, namely that in the first half of the trajectory there is a straight line in endpoint Cartesian variables and in the last half there is a straight line in joint variables. There is, after all, no reason that the motor control system needs to plan movements only in terms of one set of variables. Perhaps endpoint Cartesian control is used when demanded by the task, and joint variable control is used in less restrictive situations. Presumably endpoint control is harder for

the motor control system to accomplish, and the simpler joint variable control is reverted to when it suffices. Even a mixing of joint variables and endpoint Cartesian variables in the same trajectory is conceivable. Below we investigate the path that results when a trajectory starts with interpolation in endpoint Cartesian coordinates and finishes with interpolation in joint coordinates.

At the junction point, we impose a continuity condition in terms of the slopes. Given the beginning and endpoints of the total movement, there is one free variable left to be specified. This will be specified as the fraction of the distance covered by the straight-line trajectory, and in particular by explicitly specifying the x coordinate at the junction point and solving for the y coordinate. The relation between Cartesian coordinates and polar coordinates of the endpoint is:

$$\begin{aligned} x &= r\cos\phi \\ y &= r\sin\phi \end{aligned} \tag{16}$$

The slope of the N-leaved rose at the junction point is found from the chain rule:

$$m = \frac{dy}{dx} = \frac{dy}{d\phi}\,\frac{d\phi}{dx} \tag{17}$$

Elements of this relation can be obtained by differentiating (14) and (16):

$$\begin{aligned} \frac{dy}{d\phi} &= \frac{dr}{d\phi}\sin\phi + r\cos\phi = \frac{y}{r}\,\frac{dr}{d\phi} + x \\ \frac{dx}{d\phi} &= \frac{dr}{d\phi}\cos\phi - r\sin\phi = \frac{x}{r}\,\frac{dr}{d\phi} - y \\ \frac{dr}{d\phi} &= -\frac{2}{2K+1}\sin\left(\frac{\phi-\phi_0}{2K+1}\right) \end{aligned} \tag{18}$$

Spliced trajectories for the same movement endpoints as in Figure 8A are shown in Figure 8B. For a given set of endpoints, five spliced trajectories with the Cartesian straight-line portion comprising 50, 55, 60, 65, and 70% of the total distance are shown. It can be seen that the movements still have a significant curvature, particularly at the end of the joint interpolated portion. Hence this explanation must be ruled out.

3.3 Joint Rate Ratio near Full Reach

The seeds for an explanation are planted in Figure 9A, which replots the joint velocities of Figure 7C as $\arctan(-\dot{\theta}_2/\dot{\theta}_1)$ versus normalized movement distance (the distance

traveled so far divided by the total distance). Evidently the joint rate ratios are approaching a constant, but they are not yet there. Extending the trajectories all the way to the workspace boundary yields the plots in (9B), and the joint rate ratios are seen to converge to a point at 65°.

Figure 9B leads to a suspicion that there is something peculiar about movements near the workspace boundary. To develop this idea, we will solve for the joint velocity ratio for a trajectory approaching the workspace boundary. Endpoint Cartesian velocities are related to joint velocities by differentiating (10):

$$\begin{aligned} \dot{x} &= -\dot{\theta}_1 l_1 \sin\theta_1 - (\dot{\theta}_1 + \dot{\theta}_2) l_2 \sin(\theta_1 + \theta_2) \\ \dot{y} &= \dot{\theta}_1 l_1 \cos\theta_1 + (\dot{\theta}_1 + \dot{\theta}_2) l_2 \cos(\theta_1 + \theta_2) \end{aligned} \tag{19}$$

Conversely, the joint velocities can be found in terms of the endpoint Cartesian velocities by solving the equations above:

$$\begin{aligned} \dot{\theta}_1 &= \frac{1}{2 l_1 l_2 \sin\theta_2} \left(\dot{x} l_2 \cos(\theta_1 + \theta_2) + \dot{y} l_2 \sin(\theta_1 + \theta_2) \right) \\ \dot{\theta}_2 &= -\frac{1}{2 l_1 l_2 \sin\theta_2} \left(\dot{x} \left(l_1 \cos\theta_1 + l_2 \cos(\theta_1 + \theta_2) \right) + \dot{y} \left(l_1 \sin\theta_1 + l_2 \sin(\theta_1 + \theta_2) \right) \right) \end{aligned} \tag{20}$$

At the edge of the workspace the elbow becomes straight, i.e., $\theta_2 = 0$. Taking the limit of the joint rate ratio at the workspace boundary,

$$\lim_{\theta_2 \to 0} \frac{\dot{\theta}_2}{\dot{\theta}_1} = \lim_{\theta_2 \to 0} \frac{\dot{x} \left(l_1 \cos\theta_1 + l_2 \cos(\theta_1 + \theta_2) \right) + \dot{y} \left(l_1 \sin\theta_1 + l_2 \sin(\theta_1 + \theta_2) \right)}{\dot{x} l_2 \cos(\theta_1 + \theta_2) + \dot{y} l_2 \sin(\theta_1 + \theta_2)} = -\frac{l_1 + l_2}{l_2} \tag{21}$$

Surprisingly, the joint rate ratio is a constant, dependent only on the link lengths. The constancy holds for any point on the workspace boundary and for any trajectory that approaches the boundary. This explains the convergence to the particular 65° point in Figure 9B; all joint velocity ratios approach the same constant value, although in different ways.

Another way of viewing this phenomenon is presented in Figure 9C, which is a contour map of constant $\arctan(-\dot{\theta}_2/\dot{\theta}_1)$ lines connecting the shoulder point to the movement starting point. Overlayed onto this contour map are the extended straight-line hand-space movements of Figure 2. As these movements traverse towards the boundary, they approach the boundary value of 65°. Each movement, however, crosses the contours at different rates, so that while in the limit the joint rate ratios are the same, in detail the approaches to this limit differ.

3.4 Apparent Constancy of Joint Rate Ratios

Thus an insidious property of two-link kinematics at the outer boundary of the workspace makes it appear that any trajectory approaching the boundary has been executed by a strategy of joint interpolation, whether this is the case or not. The data of Soechting and Lacquaniti therefore cannot be taken by itself as evidence for planning in terms of joint variables. Before the workspace boundary, the joint rate ratios are not constant despite appearances. It is critical to distinguish the statements *is a constant* versus *tending towards a constant*. The trajectories do tend towards a constant, but in a different manner for each trajectory. Therefore this data does not actually demonstrate a constant joint rate ratio in the deceleratory phase, and there is no contradiction with the trajectory features of hand-space straight-line paths.

What this analysis shows is that if one is interested in the question of joint-space versus hand-space planning, then one should stay away from the workspace boundary. Movements near the boundary will always appear to have a constant joint rate ratio, and there is not a clear enough distinction from hand-path trajectories. The experimental movements in Figure 6A are an unfortunate choice because of the misleading invariances they seem to compel. If the movements were made bidirectionally, then for the movements from the boundary to the starting point the joint rate ratio would have appeared constant in the first half of the trajectory. If both the start and stop points were well interior to the workspace boundary, then possibly neither of these observations would hold.

Hence a knowledge of path shape between targets in other parts of the workspace would be desirable. The trajectories in Figure 6A all correspond to one particular region of a straight line, namely between points 3 and 4 of Figure 4A. It would be of interest to know the trajectory shapes when targets are placed along different parts of this prototype straight line, particularly to encompass joint reversal points. In the next section, a different set of experiments are described that lead to new insights into differentiating endpoint Cartesian variable planning from joint variable planning.

4 Staggered Joint Interpolation

In another set of experiments examining unrestricted arm movements in a sagittal plane, Atkeson and Hollerbach (1985) noticed that curved movements occurred in certain portions of the workspace, while in other parts of the workspace the movements were straight. In Figure 10A-D, four different movements are shown, represented by vertical plane traces of markers on the fingertip, wrist, either side of the elbow, and shoulder. These markers allow the construction of shoulder and elbow joint angles, depicted in Figures 10E-H respectively.

Trajectories 10A-B are straight, and take place in workspace regions roughly represented by trajectories 1 and 5 in the data of Soechting and Lacquaniti (Figure 6A). That is to say, they take place betweeen points 3 and 4 of the prototype straight-line motion 4A. Thus both experiments agree on the kinematic features of these trajectories.

Trajectories 10C-D are curved, and are in workspace regions not represented by the studies of Soechting and Lacquaniti. Trajectory 10C spans the elbow reversal point 3 of Figure 4A, and moves between vertical endpoints. Targets happened to be placed so that the beginning and final elbow joint angles were the same, and joint angle plot 10G shows that the subject chose to move only the shoulder joint. Thus trivially this is an example of joint interpolation, and the endpoint naturally follows a circular arc caused by swinging of the whole arm through the shoulder. Trajectory 10D spans both the shoulder and elbow reversal points 2 and 3, respectively. One endpoint is low and out from the body, the other high and in, almost above the head. The joint angle plot 10H clearly shows that this trajectory is represented by a straight line in joint space.

While the straight lines in 10A-B seem to indicate a strategy of interpolation in endpoint Cartesian coordinates, the straight lines in the joint angle plots 10G-H indicate a strategy of joint interpolation for trajectories 10C-D. Superficially, it thus appears that the coordination strategy depends on the workspace region the movement is executed in. On the other hand, a reexamination of trajectory 10A shows that it a straight line nearly through the shoulder, and the joint angle plot of Figure 10E verifies the simultaneous straight line in joint space. Thus this trajectory could just as well have been interpreted as evidence for joint interpolation. This would leave only trajectory 10B as not explainable by joint interpolation, since its joint angle plot 10F is clearly curved. The next section proposes a slight generalization of joint interpolation that explains trajectory 10B and unifies all results.

4.1 A New Joint Coordination Strategy

In joint interpolation both joints execute the same time profile. Suppose instead that one joint is staggered in onset relative to the other by a time offset δ and that its time profile $f(t)$ is scaled uniformly by a factor c (Figure 3B) The new time profile is $f(ct - \delta)$, yielding from (6):

$$\begin{aligned} \theta_1(t) &= (\theta_1(t_f) - \theta_1(t_0))f(t) + \theta_1(t_0) \\ \theta_2(t) &= (\theta_2(t_f) - \theta_2(t_0))f(ct - \delta) + \theta_2(t_0) \end{aligned} \tag{22}$$

Again, the same time profile is kept for both joints, but that for joint 2 is merely shifted relative to the joint 1 time profile and uniformly expanded or compressed. The scaling is needed so that joint 2 can end at the same time as joint 1 if its start is different, or joint 2 can start at the same time as joint 1 if its finish is different. Given that one of these two conditions holds, this strategy has only one free variable δ since the other can be determined by $c = 1 - \delta/(t_f - t_0)$.

Figure 11A-B simulates the upward and outward diagonal movement 10B and 10F. The solid line in 11A represents a perfect straight line in Cartesian coordinates, and the solid line in 11B the inverse kinematic joint angle solution. The outer dotted line in 11A represents the endpoint trajectory resulting from simple joint interpolation; this corresponds in 11B to the dotted straight-line joint path. The remaining dotted lines are staggered joint interpolations with increasing relative joint offset. Finally an offset value is found that generates a trajectory nearly indistinguishable from the Cartesian straight-line paths. It is hard to see in the Figure because the overlap is so good. Thus all trajectories in Figure 10 can be explained in terms of joint variable planning, when the coordination strategy is generalized to staggered interpolation.

4.2 Limitations of Staggered Joint Interpolation

Since staggered joint interpolation made trajectory 10B straight, could not this strategy be used to make trajectories 10C-D straight as well? Why this cannot be done is answered by the simulations in Figures 11C and 11E, which represent trajectories 10C and 10D respectively. The nearly vertical movement 11C requires a substantial amount of elbow joint reversal in 11D. For the upward and inward diagonaling movement 11E, reversal is required in both joints (11F). By definition interpolation does not allow a reversal in any variable. Thus staggered joint interpolation is incapable of

approximating a Cartesian straight line whenever a substantial amount of joint reversal is required. This means that whenever points 2 or 3 of the prototytpe straight line 4A are spanned by targets, a curved line should result because staggered joint interpolation breaks down. Movements within the joint reversal zones, namely between points 1 and 2, 2 and 3, and 3 and 4 of Figure 4A do not require joint reversal, and hence can be made fairly straight by straggered joint interpolation.

Even though a Cartesian straight line does not result, sometimes staggered joint interpolation can make trajectories straighter than they might be otherwise. Though trajectory 11E requires a reversal in both elbow and shoulder joint movement 11F to produce a straight line, by increasing the delay in relative joint onset a series of curves is produced that eventually makes the joint-interpolated path straighter. The dotted straight line in joint space 11F corresponds to the substantially curved outer dotted line in 11E. As the shoulder motion is increasingly offset from the elbow motion, curves intermediate in straightness are generated. From 11F it can be seen that the best strategy would be an almost complete decoupling in the joint movements to approximate the theoretical joint angle plotted as a solid line. The elbow should move alone, generating a straight vertical line, and then the shoulder should move alone, generating a straight horizontal line. Apparently such a strategy was occasionally used in some of the experimental movements reported in (Hollerbach et al., 1986). For endpoints similar to Figure 10D for a different subject, Figure 12 shows a large degree of decoupling between elbow and shoulder joints. This subject therefore was able to make this motion much straighter than the subject in Figure 10D.

On the other hand, staggering has no effect on the trajectories in 11C. The beginning and final elbow joint angles are nearly the same, and there is hardly any elbow joint displacement during joint interpolation. Hence introducing an offset in the elbow joint motion has almost no effect on the trajectory, as seen by the clustering of the dotted lines. Staggered joint interpolation cannot make the vertical movement of Figure 10C straighter because the elbow joint is not moving, and substantial elbow joint reversal is required to achieve a perfect Cartesian straight line.

4.3 A Unifying Explanation

In keeping with our definition of joint interpolation, subjects in the experiments of (Atkeson and Hollerbach, 1985) almost never reversed a joint motion, either in the shoulder

or in the elbow joints. We speculate that the planning goal of subjects is to execute a straight-line Cartesian motion, but that this goal is limited by the restrictions of joint interpolation. Figure 11 has already indicated when joint interpolation breaks down in terms of realizing the straight-line goal, namely workspace regions where joint reversal would be required. All subjects executed curved motions in these workspace regions, ostensibly through joint interpolation. When joint reversal is not required, subjects achieve a very good approximation to a straight line through staggered joint interpolation. Even for trajectories requiring joint reversal to achieve a Cartesian straight line, some subjects were able to make these trajectories straighter by decoupling the joints through staggered joint interpolation.

Staggered joint interpolation is an intriguing explanation for the experiments of Soechting and Lacquaniti (1981). The endpoints in 6A do not require joint reversal (Figure 6B) to execute a straight line exactly. Hence they are candidates for close approximation by staggered joint interpolation. The velocity space diagram in Figure 6C for trajectory 1 definitely shows an offset, with the shoulder joint moving before the elbow joint. Smaller offsets are seen in 6D-E, and practically none in 10F. Staggered joint interpolation is not a perfect explanation for this data, which is a little irregular. To proceed with the analysis, the time function must be known because the joint rate ratio is now definitely dependent on the exact time profile as well as on the path. Differentiating (22):

$$\frac{\dot{\theta}_1}{\dot{\theta}_2} = \frac{\Delta\theta_1}{\Delta\theta_2} \frac{\dot{f}(t)}{c\dot{f}(ct+\delta)} \tag{23}$$

where $\Delta\theta_i = \theta_i(t_f) - \theta_i(t_0)$. Unlike regular joint interpolation, the time functions do not cancel out in the joint rate ratio.

Joint interpolation could be generalized further by adding more adjustable parameters, and conceivably a better ability to achieve approximate endpoint goals would be achieved. Nevertheless, after a certain point such generalizations become no less complex than solving the inverse kinematics problem.

5 Discussion

In this paper we have compared trajectories derived from endpoint variables and from joint variables under a coordination strategy of linear interpolation. The straight lines consequent from endpoint interpolation ordinarily are associated with complex joint-variable curves. The endpoint trajectories consequent from joint interpolation are associated with a class of polar coordinate curves known as N-leaved roses. Thus distinct predictions are derived from these two possibilities, and ordinarily the matching to experimental data should not result in any overlap or confusion. Nevertheless, situations do exist that blur the distinction.

Linear interpolation in joint variables and in endpoint variables are merely two simple extremes of a continuum of coordination possibilities, and intermediate strategies may exist that provide a better match to the data. In particular, a strategy of staggered joint interpolation has been identified that can generate nearly straight Cartesian trajectories in certain portions of the workspace. Thus data described by Cartesian straight lines do not automatically support planning in terms of these variables, and the distinction between joint variable planning and endpoint Cartesian variable planning is not clear cut.

Labeling a path as *straight* requires extracting metric features from a trajectory. Since no trajectory is likely to be perfectly straight, one can only speak of degrees of straightness. But then there may be other coordination strategies that yield approximately straight lines within a reasonable statistical measure, such as the staggered joint interpolation mentioned above. The departure from linearity may be small but significant, and not detectable within experimental error.

Straightness may also result from a limiting process. A peculiar property of planar two-link kinematics has been identified that causes all trajectories approaching the outer workspace boundary to appear to be planned by simple joint interpolation. The joint angle plots are close to being straight, but are not actually straight except in the limit at the workspace boundary. Again, the departures from linearity will be slight but highly significant.

Lastly, there is a danger of overgeneralizing from too little data. Studying an overly restricted set of movements may prove misleading in terms of the invariance that appear to emerge. If one studied only movements directed towards the workspace boundary, then it would always appear that a strategy of joint interpolation was in effect. Kine-

matic features of horizontal planar movement may differ from those in vertical planar movement. Free arm trajectories may differ from trajectories constrained by a measurement apparatus.

5.1 Staggered Joint Interpolation

In the last section, it was proposed that staggered joint interpolation may be the underlying coordination strategy in the experiments of (Soechting and Lacquaniti, 1981; Atkeson and Hollerbach, 1985). A main feature of staggered joint interpolation is that there is no joint reversal, and that the resultant endpoint curvature can be mitigated by staggering the relative joint onsets. Thus it is proposed that joint variables are used by the motor control system in planning movement, but in a relatively flexible way. In movement regions where joint reversal is not required to execute a Cartesian straight-line motion, as in the studies of (Soechting and Lacquaniti, 1981), a fairly good approximation to the straight line can be obtained. In movement regions where joint reversal would be required, as in the studies of (Atkeson and Hollerbach, 1985), curved endpoint motions result.

The observation that in the motions of (Atkeson and Hollerbach, 1985) no joint reversals were seen is not a universal result. Morasso (1981) observed joint reversal in horizontal arm movements measured with a planar pantograph. One may speculate as to why subjects may choose to avoid joint reversal. In robotics, minimum-time trajectories tend to be close to joint-interpolated motions (Sahar and Hollerbach, 1986). Intuitively, it seems that reversing the direction of limb motion would be energetically inefficient. There may also be some analogy with zones of muscle synergies in posture (Nashner and McCollum, 1985). Nashner and McCollum propose that postural adjustments are made so that switches in synergies are not required, presumably simplifying the control of leg and trunk musculature. For arm movement, avoiding joint reversal would also presumably simplify the control of the arm musculature.

5.2 Conclusion

This paper has hopefully shown that kinematics is a deep subject, and its understanding is fundamental in designing experiments and interpreting results. At the outset, the goal was to determine which set of planning variables under linear interpolation, namely endpoint Cartesian variables or joint variables, best described human arm movement.

It was found that this group of planning strategies was inadequate and that a generalization of the coordination strategy to staggered interpolation for [illegible] described existing data.

Along the way, it was shown that there are pitfalls in attempting to match these planning strategies to experimentally recorded trajectories. A boundary artifact was identified that makes all trajectories approaching full extension appear to be planned by joint interpolation. Thus experiments attempting to ascertain the planning strategy should specify trajectories that stay away from the boundary. Near straight lines in Cartesian coordinates can be generated by staggered joint interpolation, so that apparent linearity does not imply linear planning.

Acknowledgments

This research was supported by NIH Grant AM26710 and by a grant from the Whitaker Health Sciences Fund. This paper was produced using facilities of the Artificial Intelligence Lab, partially supported by DARPA contract N00014-80-C-0505.

References

Abend W, Bizzi E, Morasso P (1982) Human arm trajectory formation. *Brain* 105: 331-348

Atkeson CG, Hollerbach JM (1985) Kinematic features of unrestrained vertical arm movements. *J Neurosci* 5: 2318-2330

Bernstein N (1967) *The Coordination and Regulation of Movements.* Pergamon Press Oxford

Bishop A, Harrison A (1977) Kots and Syrovegin (1966) - a demonstration of modular units in motor programming?. *J Human Movement Studies* 3: 99-109

Bizzi E, Chapple W, Hogan N (1982) Mechanical properties of muscles: implications for motor control. *Trends Neurosci* 5(11): 395-398

Bizzi E, Accornero N, Chapple W, Hogan N (1984) Posture control and trajectory formation during arm movement. *J Neurosci* 4: 2738-2745

Brady JM (1982) Trajectory planning. In: Brady JM, Hollerbach JM, Johnson TL, Lozano-Perez T, Mason MT (ed) *Robot Motion: Planning and Control.* MIT Press Cambridge, MA, pp 221-243

Burlington RS (1942) *Handbook of Mathematical Tables and Formulas.* Handbook Publ Inc Sandusky, Ohio

Flash T, Hogan N (1985) The coordination of arm movements: an experimentally confirmed mathematical model. *J Neurosci* 5: 1688-1703

Hildreth EC, Hollerbach JM (1986) Artificial Intelligence: a computational approach to vision and motor control. In: Plum F (ed) *Handbook of Physiology.* American Physiological Society, in press

Hogan N (1984) An organizing principle for a class of voluntary movements. *J Neurosci* 4: 2745-2754

Hollerbach JM (1981) An oscillation theory of handwriting. *Biol Cybern* 39: 139-156

Hollerbach JM (1985) Computers, brains, and the control of movement. In: Evarts EV, Wise SP, Bousfield D (ed) *The Motor System in Neurobiology.* Elsevier Biomedica Press Amsterdam, pp 140-146

Hollerbach JM (1985) Optimum kinematic design for a seven degree of freedom manipulator. In: Hanafusa H, Inoue H (ed) *Robotics Research: The Second International Symposium.* MIT Press Cambridge, MA, pp 215-222

Hollerbach JM, Atkeson CG (1986) Characterization of joint-interpolated arm movements. In: Heuer H, Fromm C (ed) *Generation and Modulation of Action Patterns.* Springer-Verlag New York, in press

Hollerbach JM, Flash T (1982) Dynamic interactions between limb segments during planar arm movement. *Biol Cybern* 44: 67-77

Kots YM, Syrovegin AV (1966) Fixed set of variants of interaction of the joints used in the execution of simple voluntary movements. *Fiziol*

Lacquaniti F, Terzuolo CA, Viviani P (1983) The law relating the kinematic aspects of drawing movements. *Acta Psycologica* 54

Morasso P (1981) Spatial control of arm movements. *Exp*

AD-A179 501 WORKSHOP SYMPOSIUM ON NEURAL MODELS OF SENSORY-MOTOR CONTROL HELD IN CAMB..(U) BOSTON UNIV MA CENTER FOR ADAPTIVE SYSTEMS D BULLOCK ET AL. 06 MAR 87 3/3

UNCLASSIFIED AFOSR-TR-87-0457 AFOSR-86-0228 F/G 5/10 NL

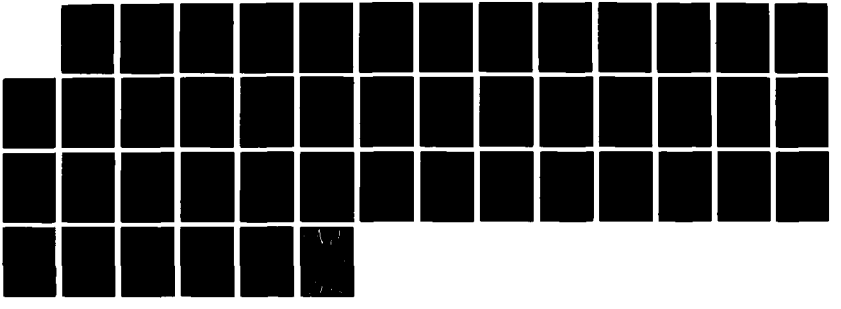

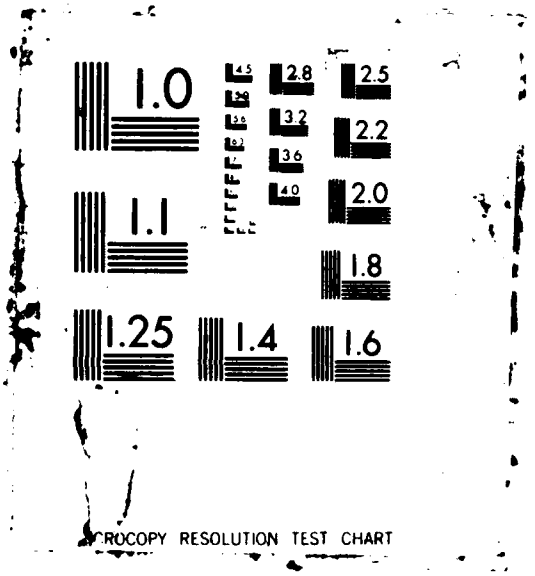
1.0
1.1
1.25
1.4
1.6
2.8
3.2
3.6
4.0
2.5
2.2
2.0
1.8
CROCOPY RESOLUTION TEST CHART

Morasso P, Mussa Ivaldi FA (1982) Trajectory formation and handwriting: a computational model. *Biol Cybern* 45: 131-142

Nashner LM, McCollum G (1985) The organization of human postural movements: a formal basis and experimental synthesis. *Behavioral and Brain Sciences* 8: 135-172

Polit A, Bizzi E (1979) Characteristics of motor programs underlying arm movements in monkeys. *J Neurophysiol* 42: 183-194

Sahar G, Hollerbach JM (1986) Planning of minimum-time trajectories for robot arms. *Int J Robotics Research* 5(3):

Soechting JF, Lacquaniti F (1981) Invariant characteristics of a pointing movement in man. *J Neurosci* 1: 710-720

Soechting JF, Lacquaniti F, Terzuolo CA (1985) Coordination of arm movements in three-dimensional space. Sensorimotor mapping during drawing movement. *Neurosci*:

Soechting JF, Ross B (1984) Psychophysical determination of coordinate representation of human arm orientation. *Neurosci* 13: 595-604

Viviani P, Terzuolo C (1982) Trajectory determines movement dynamics. *Neurosci* 7: 431-437

Legends

1. (A) A planar two-link arm, with endpoint position described by the Cartesian coordinates x, y. θ_1 and θ_2 are the joint angles, and l_1 and l_2 are the link lengths. (B) The case of equal length links, with $l_1 = l_2 = 1$. The endpoint position is now described by the polar coordinates (r, ϕ).

2. Straight-line trajectories in terms of endpoint Cartesian coordinates (A) and joint coordinates (B).

3. (A) Joint velocity profiles have the same shape under joint interpolation. (B) Under staggered joint interpolation, the joint 2 velocity profile has been delayed and scaled.

4. (A) A vertical straight-line motion with extremal points 1 and 4, and joint reversal points 2 and 3 for the shoulder and elbow, respectively. (B) Corresponding joint angle plot, with joint angles identified for endpoints 1 to 4.

5. (A) A sampling of the straight lines in joint space from the origin. (B) The corresponding endpoint trajectories, belonging to the class of polar coordinate curves known as *N-leaved roses.*

6. Data reproduced from the experiments of (Soechting and Lacquaniti, 1981). The endpoint coordinates are shown in (A), the joint coordinates in (B). The joint velocities are plotted in (C)-(H), corresponding to trajectories 1 through 6 respectively. In (I) the deceleratory phases are compared.

7. (A) Simulation of the six movements of Figure 6A. The movements are displaced and reversed in direction due to different coordinate system conventions. (B) The corresponding paths in joint space, which match Figure 6B. (C) The normalized joint velocity-space trajectories, which match Figures 6C-I.

8. (A) Joint-interpolated trajectories between the same endpoints as for the upper straight-line hand space movements depicted in Figure 7. (B) Spliced trajectories between the same endpoints. The Cartesian straight-line portions are illustrated by solid lines, the joint interpolated portions by dotted lines.

9. (A) The simulated joint rate ratios (in angular form) for each movement plotted as the $\arctan(-\dot{\theta}_2/\dot{\theta}_1)$ of the points in velocity space versus normalized movement distance. (B) A similar plot, but for movements extended to the workspace boundary. (C) A contour map with the simulated movements shown extended to the edge of the workspace. Each contour represents an N-leaved rose from the starting point to the shoulder, corresponding to a particular joint rate ratio (in terms of $\arctan(-\dot{\theta}_2/\dot{\theta}_1)$).

10. (A)-(D) LED trajectories in the sagittal target plane for the four experimental movements. In each plot the traces for each of the five LEDs attached to the arm

are shown. Six movements are superimposed in each panel, three in one direction and three in the reverse direction. Except for (A), the upward movements are indicated by dotted lines, where the dots are equally spaced in time, and the downward movements are indicated by solid lines. In (A) the outward movements are indicated by dotted lines. (E)-(H) Joint angle plots of shoulder pitch angle θ_1 versus elbow angle θ_2 corresponding to plots (A)-(D) respectively.

11. (A) Simulation of Figure 10B. The solid line represents a theoretical straight line, the dotted lines represent various staggered joint interpolations. (B) The corresponding joint angle plots. The solid line corresponds to the straight line in (A). The straight dotted line represents simple joint interpolation, and generates the outer curve in (A). Increased staggering of relative joint onset produces a sequence of curves that approaches the theoretical straight-line motion. (C) Simulation of Figure 10C. The theoretical straight line in (C) (solid line) requires a significant amount of elbow joint reversal, as seen by the solid line in (D). Since the beginning and final elbow joint angles are nearly the same, joint interpolation results in almost no elbow movement, even when staggered (dotted lines in (D) and the corresponding endpoint trajectories in (C)). (E) Simulation of Figure 10D. The theoretical straight line in (E) requires reversal in both shoulder and elbow joints in (F). The more decoupled the elbow joint motion is from the shoulder joint motion, the closer is the approximation to a straight line.

12. (A) An inward and upward diagonal movement for a different subject. (B) The joint angle plot. (C) The joint velocity plot.

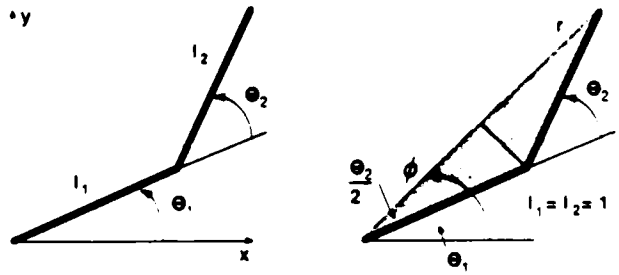
y
l_2
Θ_2
l_1
Θ_1
x
(A)
r
Θ_2
$\frac{\Theta_2}{2}$
ϕ
$l_1 = l_2 = 1$
Θ_1
(B)

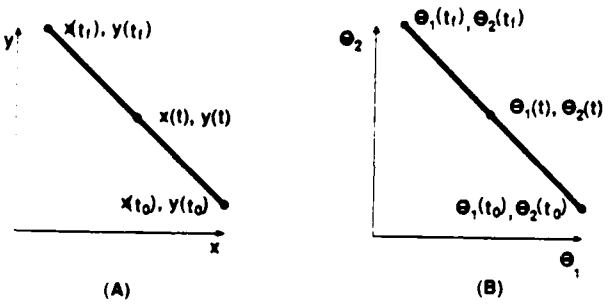
y
x(t_f), y(t_f)
x(t), y(t)
x(t_0), y(t_0)
x
(A)
θ_2
θ_1(t_f), θ_2(t_f)
θ_1(t), θ_2(t)
θ_1(t_0), θ_2(t_0)
θ_1
(B)

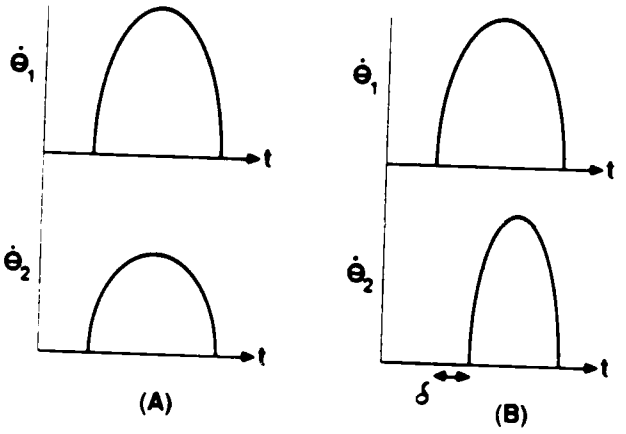
$\dot{\theta}_1$
t
$\dot{\theta}_2$
t
(A)
$\dot{\theta}_1$
t
$\dot{\theta}_2$
t
δ
(B)

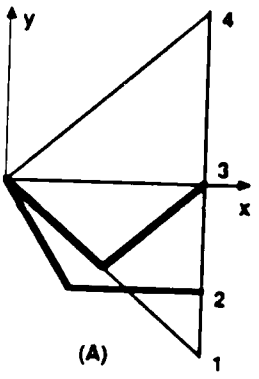

(A)

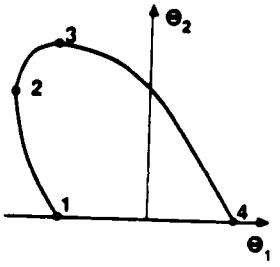

(B)

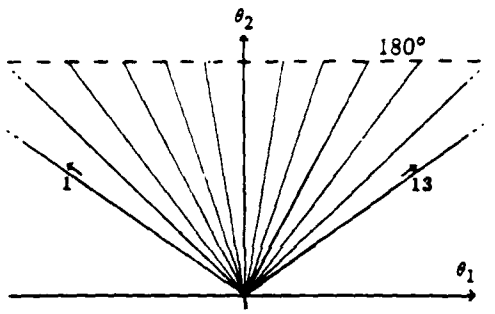

A

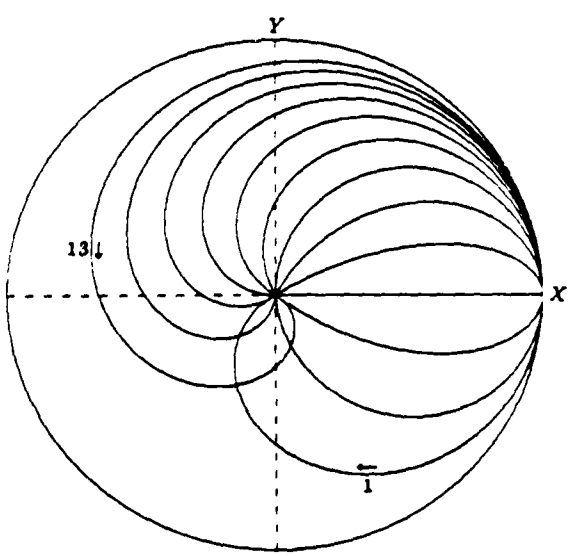

B

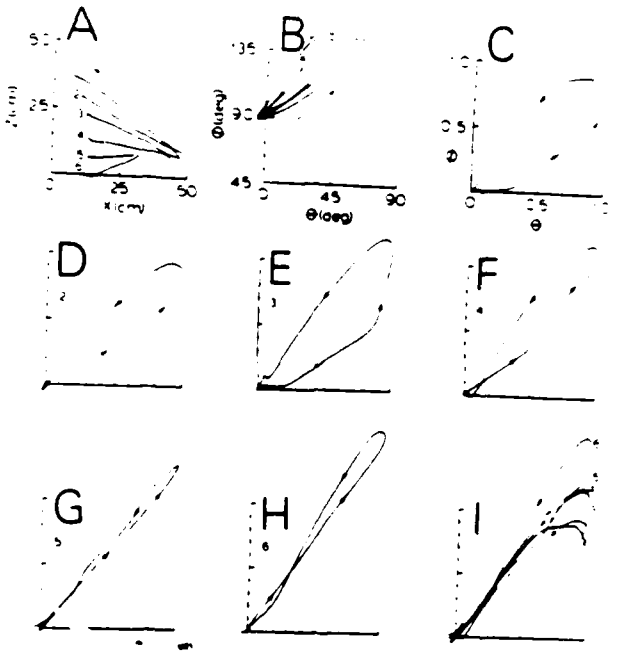
A
B
C
D
E
F
G
H
I
25
50
45
90
0.5

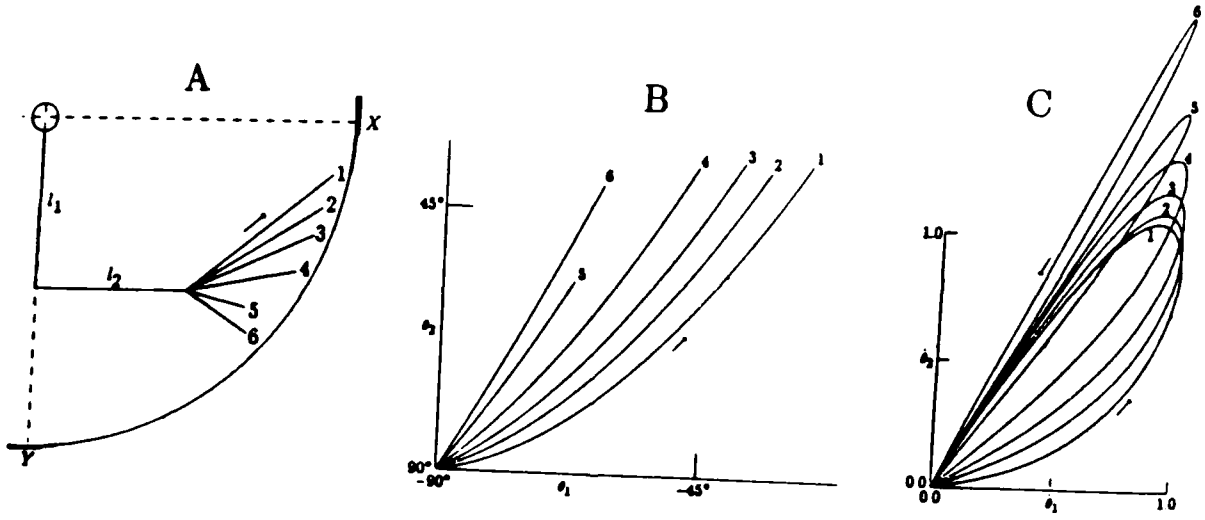
A
B
C
X
Y
l_1
l_2
1
2
3
4
5
6
45°
90°
-90°
-45°
θ_1
θ_2
1.0
0.0

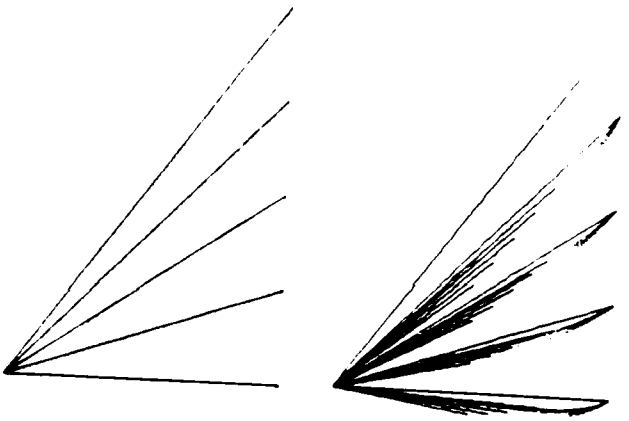

A B

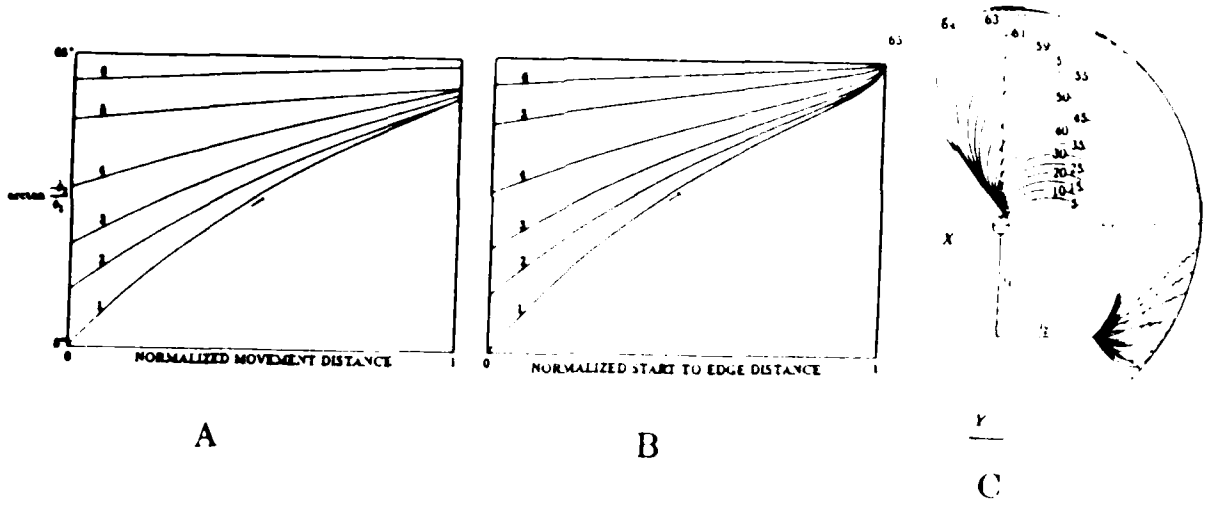
NORMALIZED MOVEMENT DISTANCE
NORMALIZED START TO EDGE DISTANCE
X
Y

A B C

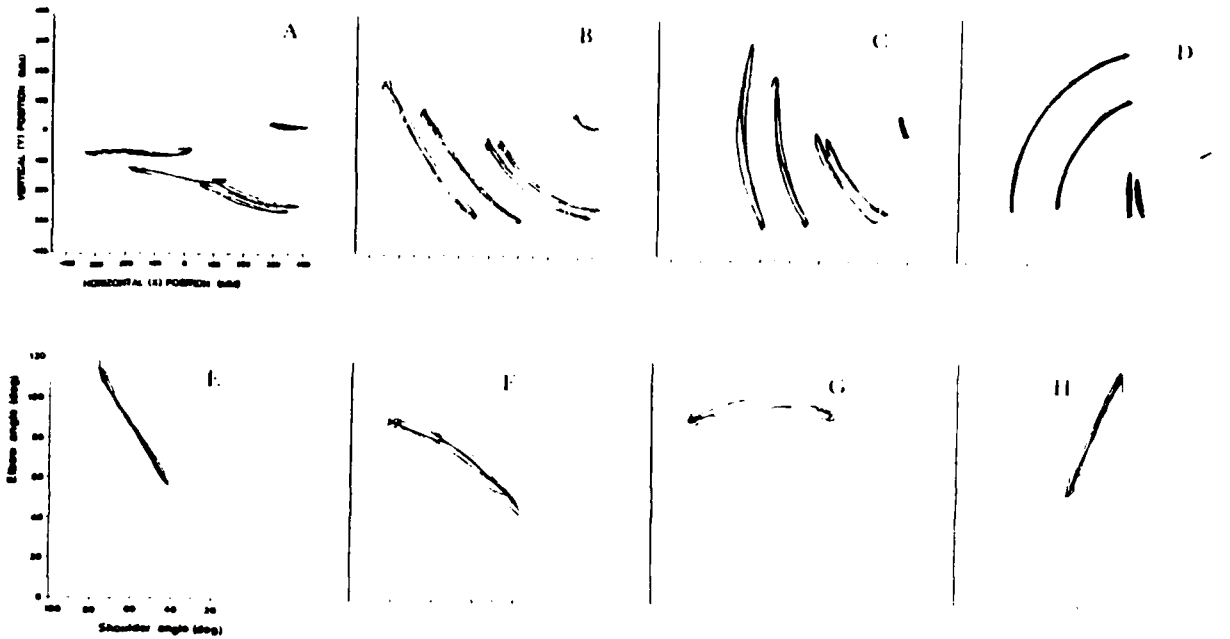
A
B
C
D
E
F
G
H

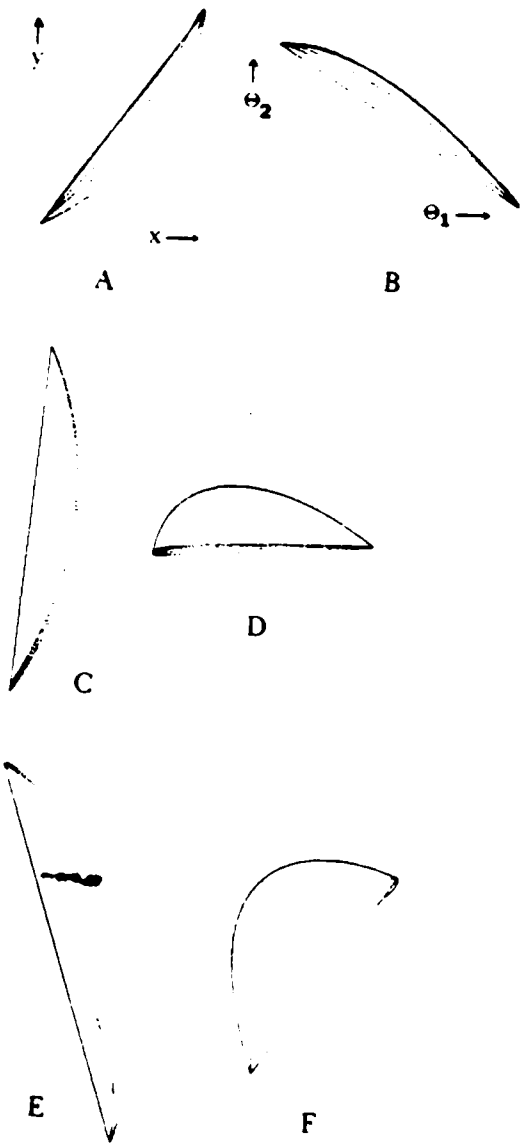
y
Θ_2
Θ_1
x
A
B
C
D
E
F

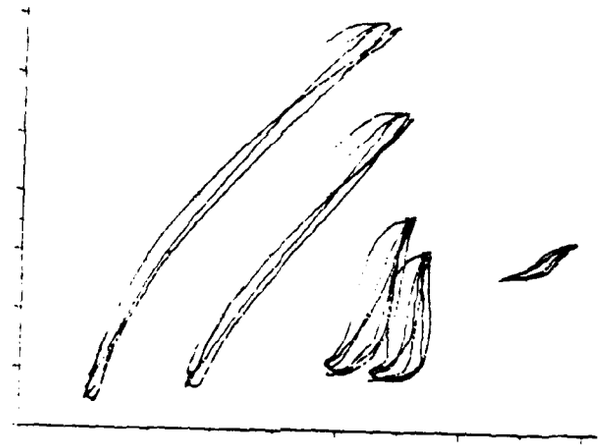

A

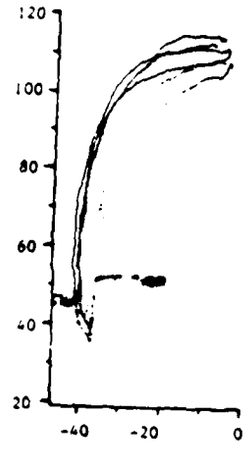

B

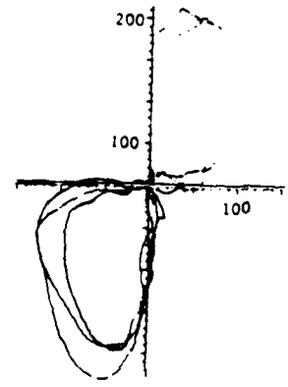

C

J. A. S. Kelso*†, G. Schöner*, J. P. Scholz* and H. Haken*

Physica Scripta Vol 34, 000-000, 1986

Phase-Locked Modes, Phase Transitions and Component Oscillators in Biological Motion

J. A. S. Kelso, G. Schöner, and J. P. Scholz

*Center for Complex Systems, Florida Atlantic University, Boca Raton, FL 33431, U.S.A., †Haskins Laboratories, New Haven, CT 06511, U.S.A.
‡Institut für theoretische Physik, Universität Stuttgart, Stuttgart, F.R. of Germany

Received August 29, 1986; accepted September 10, 1986

Abstract

We review the results of joint experimental and theoretical work on coordinated biological motion demonstrating the close alliance between our observations and other nonequilibrium phase transitions in nature (e.g., the presence of critical fluctuations, critical slowing down). Order parameters are empirically determined and their (low-dimensional) dynamics used in order to explain specific pattern formation in movement, including stability and loss of stability leading to behavioral change, phase-locked modes and entrainment. The system's components and their dynamics are identified and it is shown how these may be coupled to produce observed cooperative states. This "phenomenological synergetics" approach is minimalist and operational in strategy, and may be used to understand other systems (e.g., speech), other levels (e.g., neural) and the linkage among levels. It also promotes the search for additional forms of order in multi-component, multi-stable systems.

1. Introduction

One may well ask: What role might the theoretical and experimental study of coordinated movement play in a conference on the Physics of Structure and Complexity? There are at least two reasons for its inclusion. One is that the movements of animals and people are *ordered spatiotemporal structures* that arise in a system composed of very many neural, muscular and metabolic components that operate on different time scales. The order is such that we are often able to classify it, like the gaits of a horse, for example, or the limited number of basic sounds (the so-called phonemes), that are common to all languages. Structure, then, emerges from complexity in a fashion reminiscent of the spontaneous formation of structure in open, nonequilibrium systems (e.g., [1, 2]).

A second reason for allying movement to a physics of complexity is that biological systems are *behaviorally complex*. They are multifunctional in the sense that they are capable of producing a wide variety of behaviors often using the same set of anatomical components (e.g., speaking and chewing). In certain cases, this behavioral complexity may, nevertheless, have a common basis. For example, common to many creatures – vertebrate and invertebrate – is the ability to generate *rhythmical* acts such as walking, flying and feeding. Since rhythmic behaviors are supported by such a diversity of neural processes, they may be a good starting place to look for laws underlying behavioral complexity.

How then is order in biological coordination to be characterized? Ideally, one would like to have a model system that affords the analysis of pattern and change in pattern, both in terms of experimental data and theoretical tools. Here we describe an ongoing program of research in which theory and experiment have gone (literally), hand in hand, and whose main aims are to understand: (1) The formation of ordered, cooperative states in biological motion; (2) The stability of these observed states; and (3) The conditions that give rise to switching cooperative states. Although our experimental paradigms are concerned with movement control, we believe they might also offer a window into stability and change in general, in a biological system whose real-time behavior can be monitored continuously. We start with some basic facts obtained by ourselves and others. Then we map these observations onto an explicit model that in turn predicts additional aspects which are also studied.

2. Phase transitions in biological movement

Our experiments deal with rhythmical finger (or hand) movements in human subjects. We monitor the kinematic characteristics of these movements using infrared light-emitting diodes attached to the moving parts. The output of these diodes is detected by a *Selspot* optoelectronics camera systems. On occasion, we also record from relevant muscles using surface or fine-wire platinum electrodes as the occasion demands (see, e.g., [3]). Thus the behavioral phenomena can be examined at both kinematic and neuromuscular levels. All data are recorded on a 14-channel FM recorder for later off-line digitization at 200 samples/sec., and consequent computer analysis.

Following a paradigm introduced by Kelso [4, 5], subjects oscillate their index fingers bilaterally in the transverse plane (i.e., abduction-adduction) in one of two patterns (in-phase or anti-phase). In the former pattern, homologous muscles contract simultaneously; in the latter, the muscles contract in an alternating fashion. Using a pacing metronome, the frequency of oscillation is systematically increased from 1.25 Hz to 3.50 Hz in 0.25 Hz steps every 4 sec (see [3, 6]).

Data from the last 3 sec of each frequency plateau (600 data samples) are used for the calculation of averages to secure stationarity. Figure 1 shows a time series when the system is prepared initially in the anti-phase mode. Obviously, at a certain critical frequency the subject switches spontaneously into the in-phase mode. No such switching occurs when the subject starts in the in-phase mode. Thus, while there are two stable patterns for low frequency values, only one pattern remains stable as frequency is scaled beyond a critical region. This transition behavior can be monitored by calculating the relative phase between the two fingers. A *point estimate* of relative phase is the latency of one finger with respect to the other finger's cycle, as determined from peak-to-peak displacement. A *continuous estimate* of relative phase (i.e., at the sampling rate of 200 Hz) can be obtained from the phase plane trajectories of both fingers. (The velocities are obtained by a central difference numerical differentiation procedure). Normalizing the finger oscillations to the unit

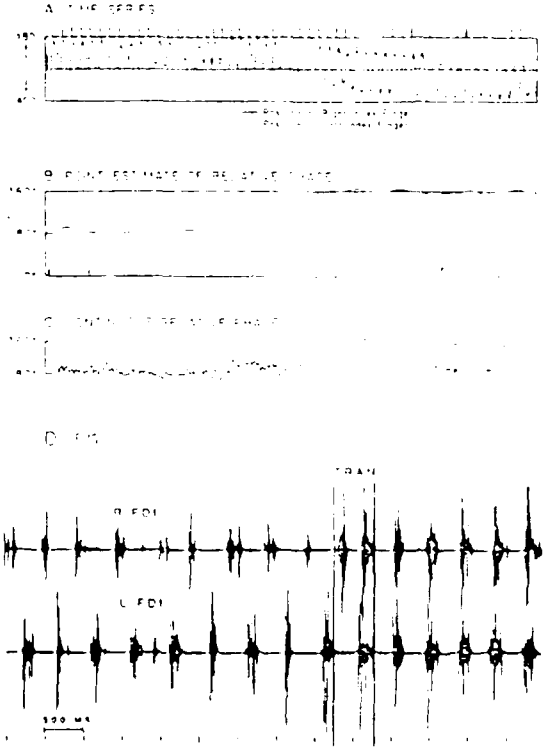

Fig. 1. (A) Time series of left and right finger position. (B) Point estimate of the relative phase. (C) Continuous relative phase. (D) The EMG record of FDI from right and left index finger movements (see text for details).

circle, the phases of the individual fingers can be obtained simply from the arctan $(\dot{x}/x)$ if x is normalized finger position (see [7]). Relative phase is then just the difference between these individual phases. In figure 1 the relative phase fluctuates before the transition and stabilizes thereafter (cf. [3, 5, 6]).

3. Dynamical modeling

In order to understand temporal order and the observed change of such order in terms of dynamics, we need to address the following questions: First, what are the essential variables (order parameters) and how can their dynamics be characterized? Second, what are the 'control' parameters, that move the system through its collective states? Third, given a model, what new observations does the model predict? In a first step, relative phase, ϕ may be considered a suitable collective variable that can serve as order parameter. The reasons are as follows: (1) relative phase, ϕ characterizes the observed, coordinative modes; (2) ϕ changes abruptly at the transition and is only weakly dependent on parameters outside the transition; (3) ϕ has very simple dynamics in which the ordered phase-locked states are characterized by fixed point attractors. Since the prescribed frequency of oscillation, manipulated during the experiment, is followed very closely, frequency does not appear to be system dependent and can be considered the control parameter.

It is thus possible to determine the dynamics of ϕ from a few basic postulates. (1) The observed states, [illegible] at 0deg and ± 180deg, are modeled as point attractors. The dynamics are then assumed to be purely [illegible] a minimality strategy in which only the simplest [illegible] type (point attractor) appears in the model. (2) The model must reproduce the observed bifurcation diagram, [illegible] in a certain parameter regime, monostable [illegible] parameter regime). (3) Pursuing again a minimality strategy, only the point attractors, [illegible] appear. (4) Due to the angular character of ϕ, the [illegible] have to be 2π-periodic. (5) From the [illegible] found in the data, the model is required [illegible] under the transformation $\phi \to -\phi$. The most general [illegible] obeying (1) to (5) is

$$\dot{\phi} = -\frac{\mathrm{d}H(\phi)}{\mathrm{d}\phi},$$

where

$$H(\phi) = -a\cos(\phi) - b\cos(2\phi)$$

(cf. [8]). This is an explicit model of the dynamics of the relative phase with two parameters, a and b. Haken, Kelso and Bunz ([8], Fig. 5) show that equations (1) and (2) indeed capture the bifurcation diagram which has minima at $\phi = 0$ and $\phi = \pm 180$deg for $a/b < 4$ with the latter minimum turning into a maximum for $a/b > 4$. The order parameter dynamics (1) and (2) for ϕ can be derived from nonlinear oscillator equations for the two hands with a nonlinear coupling between them ([8]). We shall postpone discussion of the individual component's dynamics to Section 7.

A chief strategy of the foregoing dynamical analysis is to map the reproducibly observed states of the system onto attractors of a corresponding dynamical model. Thus, *stability* is a central concept, not only as a characterization of the two attractor states, but also because it is *loss of stability* that plays a chief role in effecting the transition. Stability can be measured in several ways. (1) If a small perturbation applied to a system drives it away from its stationary state, the time for the system to return to its stationary state is independent of the size of the perturbation (as long as the latter is sufficiently small). The "local relaxation time", t_{rel}, (i.e., local with respect to the attractor) is therefore an observable system property that measures the stability of the attractor state. The smaller t_{rel} is, the more stable is the attractor. The case $t_{rel} \to \infty$ corresponds to a loss of stability.

(2) A second measure of stability is related to noise sources. Any real system, described by low dimensional dynamics will be composed of, and be coupled to, many subsystems. These act to a certain degree as *stochastic forces* on the collective variables (cf. [1], Section 6.2 and references therein). The presence of stochastic forces and hence of *fluctuations* of the macroscopic variables, is not merely a technical issue, but of both fundamental and practical importance (cf. [1], Section 7.3). In the present context, the stochastic forces act as continously applied perturbations and therefore produce deviations from the attractor state. The size of these fluctuations as measured, for example, by the variance or SD of ϕ around the attractor state, is a metric for the stability of this state. The more stable the attractor, the smaller the mean deviation from the attractor state for a given strength of stochastic force. Let us see how these stability measures behave in experiment.

4. Critical fluctuations: loss of stability

5.

4.2. Critical slowing down

Direct evidence of critical slowing down has been obtained from perturbation experiments carried out recently by Scholz [10] as part of his Ph.D. dissertation under the direction of the first author. The basic experimental paradigm consisted of perturbing one of the index fingers with a torque pulse (50 ms duration) as subjects performed in the two basic coordinative modes [11]. The apparatus consisted of a freely rotating support for each index finger that allowed flexion and extension about the metacarpophalangeal joint in the horizontal plane (see [12] for description). Electronics provided for the direct transduction of position, velocity and acceleration, and for the application of a predetermined magnitude of torque to either of the index fingers. In Scholz's experiment, only the right index finger was perturbed at random times during a trial and the torque onset was electronically timed to the peak flexion velocity of that finger. Torque magnitude was set individually for each subject in order to produce readily observable displacement of the finger into extension. Subjects ($N = 5$) were asked to move their fingers rhythmically in one of two modes of coordination: in-phase (relative phase ≈ 0 deg.), and anti-phase (relative phase ≈ 180 deg.). Scaling trials consisted of increasing the frequency of oscillation in nine 0.2 Hz steps every 10 sec starting at 1.0 Hz. When scaling began in the anti-phase mode of coordination a transition invariably occurred to the in-phase mode.

Relaxation time was operationally defined as the time from the offset of the perturbation until the continuous relative phase – calculated from the difference between each hand's phase plane trajectory – returned to its previous steady-state value. Except for the lowest movement frequencies (e.g., 1.0 to 1.2 Hz), relaxation time of the anti-phase

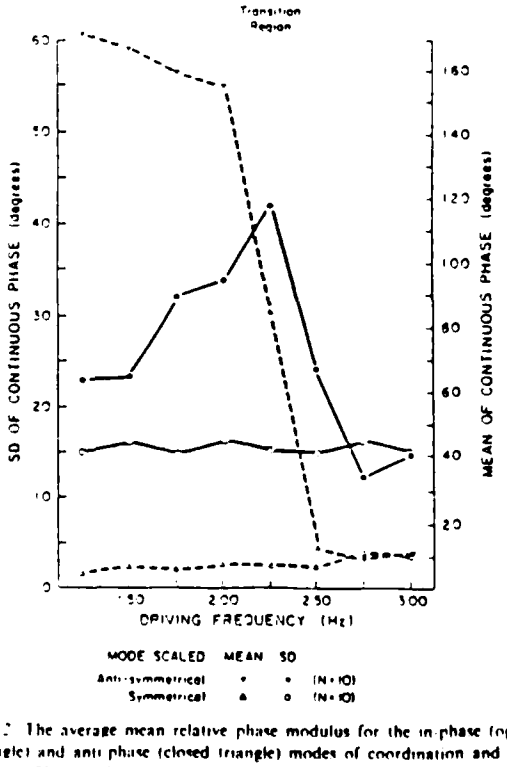

Fig. 2. The average mean relative phase modulus for the in-phase (open triangle) and anti-phase (closed triangle) modes of coordination and the average SD (in-phase = open circles, anti-phase = closed circles) as a function of driving frequency (in Hz) for a set of 10 experimental runs. On a given run, the mean and SD were calculated for the last 3 s (600 samples) at a given frequency (from Scholz and Schöner, in press).

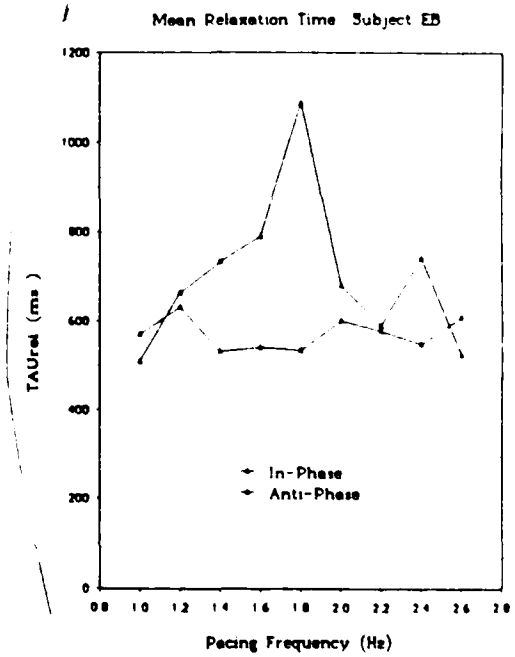

Fig. 3. The mean relaxation time (in ms) as a function of pacing frequency for the two coordinative modes, in-phase (closed triangles) and anti-phase (open triangles). Most of the transitions occur for this subject at 1.8 Hz. Each triangle contains at least 10 observations.

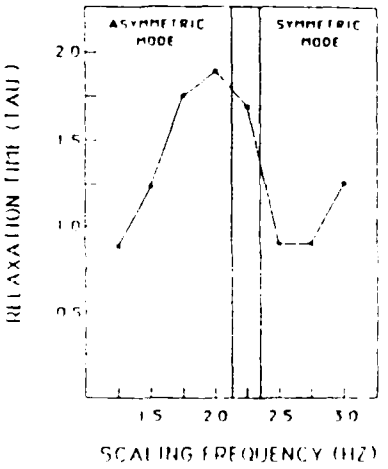

Fig. 4. Plot of mean relaxation time, calculated as the inverse of the line width of the power spectra of relative phase at half power, versus the scaling frequency. One subject's data averaged across 10 trials. Power spectra calculated for 3 s of data (600 points) on each trial at each value of the scaling frequency.

mode was significantly longer than that of the in-phase mode for all five subjects. Furthermore, as the critical frequency for mode transition was approached, the relaxation time increased monotonically. The result is revealed by a significant positive correlation between the pacing frequency and relaxation time up to the transition ($p < 0.001$). No such increase occurred when scaling was carried out over the same frequency range beginning in the in-phase mode. Here, either no relationship existed between pacing frequency and relaxation time ($N = 3,5$), or relaxation time actually decreased with increasing frequency of movement ($N = 2,5$; $p < 0.001$). The results of one of the subjects are presented in Fig. 3.

Additional, though more preliminary evidence for critical slowing down has also been found (see [13]). The method for determining relaxation time in this case uses the power spectrum of the continuous relative phase calculated for the stationary portion of each frequency plateau. Due to the Wiener–Khinchin theorem, this function is just the Fourier transform of the relative phase autocorrelation function. It has a low frequency peak that reflects the relaxational dynamics of relative phase. Stochastic theory (see [9]) tells us that the line width of this low frequency peak is a measure of relaxation rate (the reciprocal of relaxation time). Figure 4 is a plot of relaxation time, τ_{rel}, as determined from the line width of the power spectrum of relative phase for one subject (the same data as shown in Fig. 2).

The strong enhancement of τ_{rel} before the transition can be clearly seen. Nevertheless, a lot of work remains to be done on this topic: an algorithm for determing the line shape of the relative phase spectral density function has to be developed. Detailed modelling is necessary to compare theory and experiment with respect to relaxation time in a quantitative fashion.

5. Stochastic model of the phase transition

With respect to the previously discussed features of the phase transition the model (1), (2) is as yet incomplete because it lacks a representation of fluctuations. Including fluctuations in the model allows us to (1) test the consistency of the dynamical model experimentally (via time scales relations), (2) determine model parameters quantitatively, and (3) make non-trivial predictions that can be further tested experimentally. The latter point aims at finding lawful relations on the level of dynamics rather than a mere redescription of observations.

To account for fluctuations, and again guided by several reasonable assumptions, we add a stochastic force to eq. (1). We assume (1) the source of the noise consists of many, weakly interacting degrees of freedom (e.g., on the neuromuscular level), (2) the noise sources are correlated over short times compared to the observed macroscopic dynamics (otherwise they are included in the deterministic part of equation (1)), and (3) the noise sources are regular during the transition. These assumptions imply that stochastic forces can be modeled as additive, gaussian, white noise ξ,

$$\dot{\phi} = -\frac{dV(\phi)}{d\phi} + \sqrt{Q}\,\xi_t \qquad (3)$$

with

$$\langle \xi_t \rangle = 0; \quad \langle \xi_t\, \xi_{t'} \rangle = \delta(t - t') \qquad (4)$$

where the parameter Q measures the noise strength [9]. This stochastic model is still incomplete, however. In order to solve eq. (3) and compare its solution to experimental data, we have to furnish initial conditions. Finding the appropriate initial conditions requires a discussion of several relevant *time scales* of the present system. Because this is an important point for modeling biological dynamics in many situations, we will be somewhat more general here.

To characterize the state of a biological system within a stochastic dynamical description three types of time scales are relevant. The first is the typical time scale on which the system is *observed*, τ_{obs} (i.e., how long the experimeter observes the system in a given preparation). The second is the previously discussed local relaxation time τ_{rel} (cf. Section 3), that is specific to a given attractor. The third one is the so-called *equilibration time* (or global relaxation time), τ_{equ}, which is defined as the time it takes the system to achieve the stationary probability distribution from a typical initial distribution. In a bistable situation like ours, below the transition τ_{equ} is determined mostly by the typical time it takes to cross the potential hill (see, e.g., [14]).

If these time scales fulfill the following relation

$$\tau_{rel} \ll \tau_{obs} \ll \tau_{equ} \qquad (5)$$

then the interpretation of observed states as attractor states is consistent. That is, the system has relaxed to a stationary state on the observed time scale, but is not yet distributed over all coexisting attractors according to the stationary probability distribution. When stationary states in an experiment are referred to, what is meant is that the time scale relation (5) is obeyed.

It is important to realize that much of the work in dynamical modeling of biological systems uses deterministic models only and thus implicitly makes the assumption that (5) holds (see, for instance, the contributions to the 1982 Conference on Nonlinearities in Brain Function [15] for typical examples). To neglect fluctuations and assume (5) throughout is dangerous, however, because (a) the relation (5) breaks down at critical points, (b) fluctuations are an important feature of

bifurcation phenomena, and (c) fluctuations are essential in bringing about transitions. Let us examine these three points in more detail.

In our system (3), as the transition is approached (i.e., the anti-phase mode loses its stability), the local relaxation time (with respect to the anti-phase mode) increases, while the global relaxation time decreases (because the potential hill between 0 and 180 deg vanishes). At the critical point however both are of the same order as the observed time and one can see the transition. Thus, at the transition point, the time scales relation (5) is violated and an additional time scale assumes importance, namely the *time scale of parameter change* $\dot{\alpha}$. This reflects the fact that in our system (as often in biological systems) the control parameter that brings about the instability is itself changed in time. The relation of the time scale of parameter change to the other system times plays a decisive role in predicting the nature of the phase transition. If, for example,

$$\tau_{\text{relax}} \ll \tau_{\dot{\alpha}} \ll \tau_{\text{relax}} \tag{6}$$

then the system changes only as the old state actually becomes unstable. This transition behavior is sometimes referred to as a *second order phase transition* (because of an analogy with equilibrium phase transitions, see [1], [1983a], Section 6.7). In that case features of critical phenomena (such as critical fluctuations or critical slowing down, see below) are predicted. If, on the other hand

$$\tau_{\text{relax}} \ll \tau_{\text{relax}} \ll \tau_{\dot{\alpha}} \tag{7}$$

then the system, with overwhelming probability, always seeks out the lowest potential minimum. It therefore switches state before the old state actually becomes unstable. Jumps and hysteresis (among other features) are generally predicted. This behavior is also called a *first order transition*, again in reference to equilibrium phase transitions. [Note: In catastrophe theory, these two different transition behaviors are sometimes referred to as conventions, although they can, of course, be derived from the experimentally accessible relations (6) and (7). It is the failure to treat fluctuations that renders catastrophe theory incomplete in this respect].

Following these more general remarks, let us return to the concrete stochastic model (3). Because $\tau_{\dot{\alpha}}$ and τ_{relax} are of the same order in the experiment, we expect time scales relation (6) to hold up to the transition. At the transition all time scales may then be of the same order. This requires us to differentiate two parameter regimes: (a) The noncritical regime, where the system is stationary in the sense of (5); and (b) The critical regime, where the system exhibits transient behavior. In these regimes one can now solve the stochastic equation (3) via the corresponding Fokker-Planck equation ([9]). For the noncritical regime, stationary probability distributions of local models (that have only one stationary state at either 0 or 180 deg) can be determined. From these the standard deviation (SD) as a measure of the width of the distribution can be calculated. As the transition is approached, the SD of the local model of the anti-phase mode increases, reflecting the enhancement of fluctuations. Using the experimental information on the local relaxation time and the SD in the noncritical regime, one can determine all model parameters a, b, and Q ([9]). In the critical regime the full Fokker-Planck equation can now be solved numerically, using an appropriate distribution from the pre-transitional regime as an initial condition. Without further adjustable parameters the model accounts nicely for the transient behavior [9].

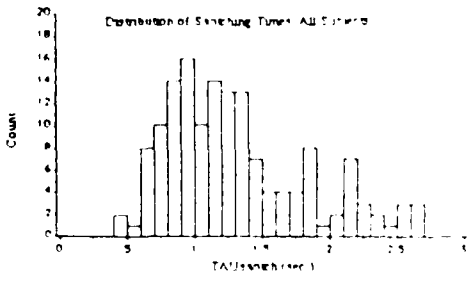

Fig. 5. The distribution of switching times for all subjects in Scholz's phase transition experiment (see text for details).

The stochastic model contains another feature that can be compared with experiments. This is the duration of the transient from the anti-phase state to the in-phase state – which we call the *switching time*. The basic idea is that during the transition the probability density of relative phase – initially concentrated at $\phi \approx \pm 180$ deg – flows to $\phi \approx 0$ deg and accumulates there until the "new" peak at $\phi \approx 0$ deg is dominant and stationary. The model predicts the duration of this process both in terms of its distribution and its mean [9]. These switching times have been extracted from the experimental data described in Section 4.2 above. In most cases they were easy to calculate as the time between the relative phase value immediately before the transition and the value assumed immediately following the transition. The distribution of switching times for all five subjects is shown in Fig. 5. The match between theoretical prediction (cf. [9] Fig. 11) and empirical data is impressive, to say the least, even to the shapes of the switching time distributions. This new aspect is particularly interesting, because it shows that the switching process itself is quite closely captured by the stochastic dynamics of (3). Using the language of phase transitions may thus be adequate to understand the present phenomenon – even beyond the more superficial level of analogy.

6. Phase-locked modes: the "sea gull effect"*

In our discussion so far we have always assumed that the system has only two phase-locked patterns – in-phase and anti-phase – at its disposal. Is this assumption really valid? The experiments described in Sections 2 and 4 probe only these two states and their local environment (local in relative phase).

We shall now discuss experiments [16, 17], that allow us to establish the stabilities of all relative phase values, thus affording a view of the whole "potential landscape".

In Tuller and Kelso's experiment [16], the subject's task was simply to tap with the left index finger every time a light for the left hand flashed, and to tap with the right index finger every time a light for the right hand flashed. The set of

* The reason we dub this the "sea gull effect" is obvious from the shape of the function shown in Fig. 6 (bottom). Perhaps our proximity to the Atlantic Ocean played a role in naming it the way we did (for another example, see [17], Fig. 2).

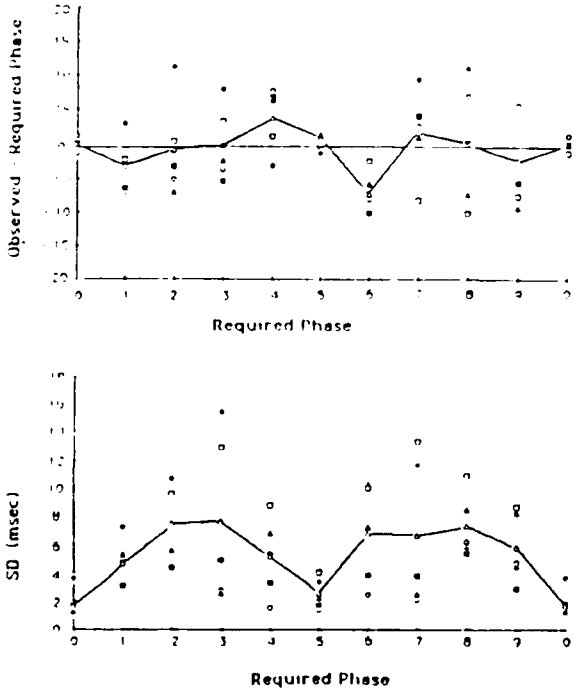

Fig. 6. Top. The phase of the pacing lights specifying the required phase plotted against the mean difference between the phase required and the phase actually produced. A negative number means that the required phase was underestimated. Each symbol represents an individual subject's mean computed over $N > 80$ movements. *Bottom.* Standard deviation of the phase produced plotted against the required phase. Symbols same as above.

conditions involved different lag times between onsets of the two lights varying in 100 ms steps from synchrony to a 500 ms lag (or 0.5 out-of-phase) and back to synchrony. The cycle time for the lights was constant at 1 sec. The phases of the lights did not change within a trial. Four 24-sec trials of each ten phase conditions were presented randomly.

The top portion of Fig. 6 shows the mean deviation from required relative phase as a function of the required phase difference. The bottom portion of Fig. 6 shows the standard deviation (SD) of the observed relative phase between the hands as a function of the required relative phase. The different symbols refer to different subjects and the open triangles connected by straight lines are the means across subjects. Obviously in-phase (at zero) and anti-phase (at 0.5) movements are the most stably produced. (This is the case in both musicians and non-musicians as well as in split-brain patients [16]). Moreover, the top portion of Fig. 6 shows how these two states attract neighboring states – the difference between observed and required phase passes through 0.0 and 0.5 with a negative slope. These findings are highly consistent with our basic modeling assumption, namely, that in-phase and anti-phase are the two basic stable phase-locked patterns. To make the implications of this experiment more stringent, however, we have to generalize our model to include the externally imposed required phase. A simple way to include the external pacing in the equation (3) for relative phase is to alter the potential. The potential (2) represents the system's intrinsic cooperativity. We assume that this remains valid under the paced conditions. Thus, we represent the required phase by adding a term to the potential that attracts the 'intrinsic' relative phase toward the required phase. The simplest function that does this (while conforming to certain periodicity requirements, see [18] for details) is $\cos(\phi - \psi)$, where ψ is the required phase.

The new potential thus reads:

$$V_\psi(\phi) = -a\cos\phi - b\cos(2\phi) - c\cos\left(\frac{\phi - \psi}{2}\right) \quad (8)$$

(Note that the new term breaks the $\phi \to -\phi$ symmetry as the pacing does in the experiment). The zero of this potential are the new stationary states. [Unfortunately the corresponding transcendental equation cannot be solved analytically. We determine the stationary states numerically, using for parameters a and b values similar to those previously established to account for experimental data [9], and choosing c sufficiently large to see an effect of the new term. No systematic attempt to optimize parameters has yet been made, however.] In the top portion of Fig. 7 the deviation of the stationary solution for relative phase from the required phase ($\phi_{stat} - \psi$) is plotted as a function of required phase, ψ. Obviously our model captures the attractivity of the two basic modes. To determine the stochastic properties we proceed as in the previously discussed case of noncritical properties for the model (3) (cf. Section 5; [9]): Expanding the potential about its stationary solution and determining the stationary probability distribution of the resulting local model allows us to calculate the SD in this approximation. The *bottom portion* of Fig. 7 shows the SD as a function of required phase ψ (where a, b and c are as in the top portion and Q is chosen as in the model for the phase transition [9]). Obviously this function captures the qualitative features of the experimental data (although it is a somewhat edgy "see gull"[!]). Our modeling here acquires additional credibility through the fact that the potential (8) can again be derived from a model of the oscillatory components of the system, in which the external pacing has been incorporated. This is briefly discussed in the

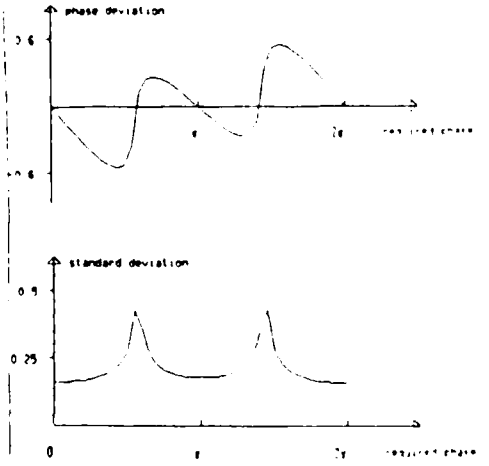

Fig. 7. Top. The deviation of relative phase from required phase as a function of required phase as calculated from the minima of V_ψ [eq. (8)]. The parameters were $a = 1$ Hz, $b = 1$ Hz, $c = 20$ Hz. *Bottom.* The standard deviation as determined from a local model around the minima of V_ψ. The parameters a, b, c were as above and $Q = 0.5$ Hz.

following section. A more detailed analysis of these models will be published elsewhere [18]. In summary, the global stability measurement performed in this experiment together with a theoretical model shows the consistency of our conceptual approach. We consider this continued close match of theory and experiment to be quite remarkable.

7. Modeling the subsystems

A key feature of the approach thus far has been to characterize coordinated states entirely in terms of the dynamics of macroscopic, collective variables (in this case relative phase is an order parameter). Here we address the nature of the subsystems themselves and how these can be coupled so as to produce coordinated states. We start at the next level down, as it were, which is the individual hands themselves. Experimentally, the behavior of the individual hands is observed as finger position x and velocity $\dot{x}$. The stable and reproducible oscillatory performance of each hand is modeled as an attractor in the phase plane $(x, \dot{x})$, in this case a limit cycle. Several experimental features constrain the modeling. Kinematic relationships, such as those between amplitude, frequency and peak velocity, have been measured ([19]). Figure 8 (from [19]) shows the amplitude-frequency relation for oscillatory movements of only one hand. The observed monotonic decrease of amplitude with frequency can be modeled by a combination of the well-known van der Pol and Rayleigh oscillators [8, 19]:

$$\ddot{x} + f(x, \dot{x}) = 0 \tag{9}$$

with

$$f(x, \dot{x}) = \alpha x + \beta \dot{x}^3 + \gamma x \dot{x}^2 + \omega^2 x. \tag{10}$$

In mapping the observed oscillatory state onto a limit cycle the notion of stability is, once again, a key feature of our theory. This can again be tested by measuring the relaxation time after a perturbation of the hand in a fashion similar to that described in Section 4. Such experiments have been recently performed by Kay under the direction of the first author ([20]). Along with the observed kinematic relations, relaxation time measures allow one to determine all parameters in eqs. (9) and (10).

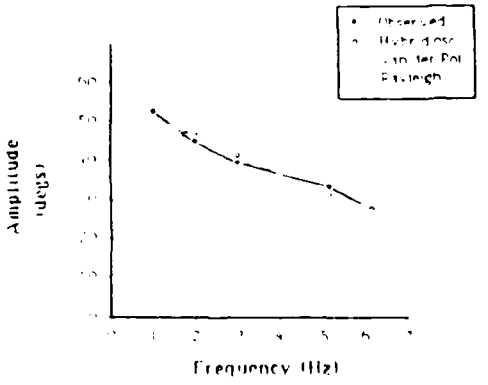

Fig. 8. Amplitude versus frequency for rhythmical movements of a single hand. The experimental points (full circles) are means over subjects, experimental sessions and trials. The (hybrid) oscillator of eqs. (9) and (10) was fitted to the data (least squares). For illustration purposes fits of the van der Pol and the Rayleigh oscillators alone are also shown.

Another assumption implicit in eqs. (9) and (10) is that the oscillation is essentially autonomous. This can be experimentally tested in the perturbation paradigm by phase resetting techniques (see, e.g., [21]). The basic idea is that the phase of an autonomous oscillator is marginally stable, unlike that of a driven oscillator which is locked to the driving function. This assumption has also been checked in Kay's experiment. Preliminary results show that the oscillation is indeed autonomous (in the absence of external pacing).

How can the components with their dynamics (9) and (10) give rise to the phase-locked coordinative modes? Obviously their dynamics have to be coupled. Haken, Kelso and Bunz [8] have determined coupling structures that can account for the observed phase-lockings. The simplest model that achieves this is a van-der-Pol-like coupling of the form

$$\ddot{x}_1 + f(x_1, \dot{x}_1) = (\dot{x}_1 - \dot{x}_2)\{A + B(x_1 - x_2)^2\} \tag{11}$$

$$\ddot{x}_2 + f(x_2, \dot{x}_2) = (\dot{x}_2 - \dot{x}_1)\{A + B(x_2 - x_1)^2\} \tag{12}$$

where f is the oscillator function (10) and A and B are coupling constants. The experimental observation that the kinematic relations (e.g., amplitude frequency relation) are not significantly different between the coordinative modes and the single hand movements show that the coupling constants A, B are small compared to the corresponding coefficients α, γ of the oscillator function (10) [19]. In spite of this the coupling structure (11) and (12) gives rise to the two phase-locked states. Indeed Haken, Kelso and Bunz [8] were able to derive the equation for relative phase (1), (2) from eqs. (11) and (12) using the slowly varying amplitude and rotating wave approximations. These results not only provide further support for the dynamical model on the collective variable level, but also establish in a rigorous fashion the relation of the two levels of description.

Finally, we indicate briefly how the pacing of both hands in the "sea-gull effect" (Section 6) may be incorporated into the model at the component level. The basic idea is similar to that used to determine the potential (8). We assume that the system's intrinsic dynamics are still intact and the pacing acts as an additional external force. For the oscillator equations this can be done by adding a periodic driving force to their oscillator function, e.g., as

$$\ddot{x}_1 + f(x_1, \dot{x}_1) = (\dot{x}_1 - \dot{x}_2)\{A + B(x_1 - x_2)^2\} + F\cos(\omega t), \tag{13}$$

$$\ddot{x}_2 + f(x_2, \dot{x}_2) = (\dot{x}_2 - \dot{x}_1)\{A + B(x_2 - x_1)^2\} + F\cos(\omega t + \psi) \tag{14}$$

Here F is the coupling constant of the driving force and ψ the required relative phase. For convenience we have chosen the natural frequency of the oscillators as identical to the driving frequency. In fact, the ability of the subjects to entrain their rhythmic movements without a phase lag to the external pacing lights is an interesting subject in its own right and deserves further theoretical and experimental study. Using again the slowly varying amplitude and the rotating wave approximations we were able to derive the following equations for the relative phase ϕ and the phase sum θ:

$$\dot{\phi} = -\frac{\partial V(\phi, \theta)}{\partial \phi} \tag{15}$$

$$\dot{\theta} = -\frac{\partial V(\phi, \theta)}{\partial \theta} \tag{16}$$

with a potential

$$V(\phi, \theta) = -a\cos\phi - b\cos 2\phi - c\sin\left(\frac{\theta - \psi}{2}\right)\cos\left(\frac{\phi - \psi}{2}\right) \quad (17)$$

where

$$a = -4 - 2B\hat{\omega}, \quad b = \tfrac{1}{2}B\hat{\omega} \text{ and } c = F(\omega r_0)$$

with amplitude

$$r_0 = \sqrt{\tfrac{1}{2}(3B\hat{\omega} + 2)}$$

If one assumes the phase sum to have relaxed to its stationary value $\theta = -\pi + \psi$ the resulting equation for relative phase is exactly

$$\dot{\phi} = -\frac{dV(\phi)}{d\phi} \quad (18)$$

with the potential V_ϕ of eq. (8). Thus again we have derived the collective variable dynamics from the component level. The details of these calculations will be published elsewhere ([18]).

8. Conclusions: "phenomenological synergetics"

The laws governing the dynamic patterns produced by complex, biological systems that possess very many degrees of freedom (such as the human brain which has $\sim 10^{14}$ neurons and neuronal connections) are, in general, not known. Unlike certain physical systems, the path from the microscopic dynamics to the collective order parameters – as in Haken's *slaving* principle – is not readily accessible to theoretical analysis. Here we suggest that an understanding of biological order may still be possible via an alternative approach, namely one in which the nature and dynamics of the (low-dimensional) order parameters are first empirically determined, particularly near nonequilibrium phase transitions (or bifurcations). Then the relevant subsystems and their dynamics can be identified. This approach, which we may call "phenomenological synergetics", has provided the conceptual framework for the empirical studies of spatiotemporal order in bimanual coordination that we have reported here. Parenthetically, we have preliminary, but exciting evidence that the approach is useful for understanding another system, namely the multiple articulator movements that structure the sounds of speech ([7]). A similar strategy has been successfully applied to "muscle streaming" by Shimizu and Haken [22, 23].

"Understanding" is sought, in the present approach, not through some privileged scale of analysis, but within the abstract level of the essential (collective) variables and their dynamics, *regardless of scale or material substrate*. Not only may the language of dynamics be appropriate at the behavioral level (e.g., in the patterns among muscles and kinematic events), but also, we hypothesize, at the more microscopic scale of neurons and neuronal assemblies. Many of the dynamical features we have observed and modeled in our experiments, for example, synchronization, phase-locking, switching, etc., can also be observed in the neuronal behavior of even the lowliest creatures, e.g., in the buccal ganglion of the snail, *Helisoma* (as in Kater and colleagues' work, cf. [24] for review) or in the motoneuronal firing patterns of *Pleurobranchaea* during feeding (cf. [25]). Thus the long sought-for link between neuronal activities (microscopic events) and behavior (macroscopic events) may actually reside in the coupling of dynamics on different levels (cf. Section 7 above). Relatedly, the classical dichotomy in biology between structure and function may be one of appearance only. The present theory promotes a unified treatment, with the two processes separated only by the time scales on which they live.

Finally, we want to stress – after Bridgeman [26] and Haken [27] – the operational nature of the present approach. That is, dynamics are formulated for observable variables only and predictions are made that can be experimentally tested. As much as possible, a minimality strategy is followed in which all consequences of a theoretical formulation are checked for their empirical validity. Insight is not necessarily gained by increasingly accurate quantitative descriptions of data, or by using increasingly complicated dynamical equations. Rather, we seek to account for a larger number of experimental features with a smaller number of theoretical concepts.

Acknowledgements

The work reported here was supported, in large part, by Contract No. N00014-83-K0083 from the U.S. Office of Naval Research (H. Hawkins, Scientific Officer) and by NINCDS Grants NS-13617 and BRS Grant RR-05596. G. Schöner was supported by a Forschungsstipendium of the Deutsche Forschungsgemeinschaft, Bonn, FRG.

References

1. Haken, H., *Synergetics – An Introduction*, Springer-Verlag, Heidelberg (3rd ed.) (1983).
2. Haken, H., Advanced Synergetics, Springer-Verlag, Heidelberg (1983).
3. Kelso, J. A. S. and Schöner, J. P., Cooperative Phenomena in Biological Motion, In H. Haken (Ed.) Complex Systems: Operational Approaches in Neurobiology, Physical Systems and Computers, Springer-Verlag, Berlin, (1985).
4. Kelso, J. A. S., Bulletin of the Psychonomic Society 18, 63 (1981).
5. Kelso, J. A. S., Am. J. Physiol. Reg. Int. Comp. Physiol. 15, R1000 (1984).
6. Kelso, J. A. S., Scholz, J. P., and Schöner, G., *Phys. Lett.* (in press).
7. Kelso, J. A. S., Saltzman, E. L., and Tuller, B., J. Phonetics 14, 29 (1986).
8. Haken, H., Kelso, J. A. S., and Bunz, H., Biological Cybernetics 51, 347 (1985).
9. Schöner, G., Haken, H., and Kelso, J. A. S., Biological Cybernetics 53, 247 (1986).
10. Scholz, J. P., Ph.D. Dissertation, University of Connecticut, Storrs, CT (1986).
11. Kelso, J. A. S., Holt, P. G., Rubin, P., and Kugler, P. J. Motor Behav. 13, 226 (1981).
12. Kelso, J. A. S. and Holt, K. G., J. Neurophysiology 43, 1183 (1980).
13. Kelso, J. A. S., Schöner, G., Scholz, J. P., and Haken, H., Non-equilibrium Phase Transitions in Coordinated Movement Involving Many degrees of Freedom. In: Perspectives in Biological Dynamics and Theoretical Medicine. Annals of the New York Academy of Sciences (in press).
14. Gardiner, C. W., Handbook of Stochastic Methods for Physics, Chemistry and the Natural Sciences, Springer-Verlag, New York (1983).
15. Garfinkel, A. and Walter, D. O. (Eds.), Am. J. Physiol. Reg. Int. Comp. Physiol. 14, R450 (1983).
16. Tuller, B. and Kelso, J. A. S., Coordination in Normal and Split Brain Patients. Paper presented at *Psychonomic Society*, Boston, MA (1985).
17. Yamanishi, J., Kawato, M., and Suzuki, R., Biological Cybernetics 37, 219 (1980).
18. Schöner, G., Kelso, J. A. S., and Tuller, B. (forthcoming).
19. Kay, B. A., Kelso, J. A. S., Saltzman, E., and Schöner, G., J. Exp.

Psych. Human Perception and Performance (in press)
20. Kay, B. A. Ph.D. Dissertation, University of Connecticut, Storrs, Conn. (1986)
21. Winfree, A. T. The Geometry of Biological Time. Springer Verlag, New York (1980)
22. Shimizu, H. In Haken, H. (Ed.) Evolution of Order and Chaos in Physics, Chemistry and Biology. Springer Verlag, Berlin, Heidelberg, New York (1982)
23. Shimizu, H. and Haken, H. J. Theoret. Biol. 104, 261 (1983)
24. Kater, S. B. Dynamic Regulators of Neuronal Form and Connectivity in the Adult Snail Helisoma. In Model Neural Networks and Behavior (Edited by Allen I. Selverston. Plenum (1985)
25. Mpitsos, G. J. and Cohan, C. S. J. Neurobiology (in press)
26. Bridgeman, P. W. The Nature of Physical Theory. Dover Pub. (1953)
27. Haken, H. Cooperational Approaches to Complex Systems. An Introduction. In Haken, H. (Ed.) Complex Systems — Operational Approaches in Neurobiology, Physics and Computers. Springer Verlag, Berlin, Heidelberg, New York (1985)

22. Landauer, R. and Wo[illegible], J. F., In Rice, S.A., Freed, K.F. and [illegible] Statistical Mechanics: New Concepts, New Problems, New Applications, University of Chicago Press, Chicago, 1972

2 J. A. S. Kelso, G. Schöner and J. P. Scholz

Phase-Locked Modes, Phase Transitions and Component Oscillators in Biological Motion 3

4 J. A. S. Kelso, G. Schöner and J. P. Scholz

Phase-Locked Modes, Phase Transitions and Component Oscillators in Biological Motion 5

6 J. A. S. Kelso, G. Schöner and J. P. Scholz

Phase-Locked Modes, Phase Transitions and Component Oscillators in Biological Motion 7

8 J. A. S. Kelso, G. Schöner and J. P. Scholz

Phase-Locked Modes, Phase Transitions and Component Oscillators in Biological Motion 9

10 J. A. S. Kelso, G. Schöner and J. P. Scholz

Phase-Locked Modes, Phase Transitions and Component Oscillators in Biological Motion 11

NOTES ADDED IN PROOF

1. Regarding the experiments decribed in Section 2, Professor H. Swinney (University of Texas, Austin) has inquired about additional bifurcations. In fact, as frequency is scaled to even higher values, a further bifurcation has been observed (cf. [3]) in which the fingers shift from a symmetrical abduction-adduction pattern to a symmetrical flexion-extension pattern (see [3] Fig. 10 and Sect. 6.7). We do not discuss this bifurcation further here, however, because it has not been studied in any detail as yet. Nevertheless, the increase in mean relaxation time at 3 Hz seen in the present Fig. 4 may be because this new bifurcation is observed near that value.

2. The analogy of the observed transition with equilibrium second order phase transitions refers to the presence of critical fluctuations and critical slowing down. The origin of these critical phenomena in the present case, however, is different from the equilibrium situation. In particular, symmetry breaking does not occur. It is only due to the time scales relation (6) that criticality is seen in what one might rather call--following a suggestion of Professor R. Landauer (IBM)--a limiting case of a first order transition. We would like to thank Profs. Swinney and Landauer for raising these points with us.

JOURNAL OF NEUROPHYSIOLOGY
Vol. 54, No. 4, October 1985 Printed in U.S.A.

Visually Induced Adaptive Changes in Primate Saccadic Oculomotor Control Signals

L. M. OPTICAN AND F. A. MILES

Laboratory of Sensorimotor Research, National Eye Institute; and Laboratory of Neurophysiology, National Institute of Mental Health, National Institutes of Health, Bethesda, Maryland 20892

SUMMARY AND CONCLUSIONS

1. Saccades are the rapid eye movements used to change visual fixation. Normal saccades end abruptly with very little postsaccadic ocular drift, but acute ocular motor deficits can cause the eyes to drift appreciably after a saccade. Previous studies in both patients and monkeys with peripheral ocular motor deficits have demonstrated that the brain can suppress such postsaccadic drifts. Ocular drift might be suppressed in response to visual and/or proprioceptive feedback of position and/or velocity errors. This study attempts to characterize the adaptive mechanism for suppression of postsaccadic drift.

2. The responses of seven rhesus monkeys were studied to postsaccadic retinal slip induced by horizontal exponential movements of a full-field stimulus. After several hours of saccade-related retinal image slip, the eye movements of the monkeys developed a zero-latency, compensatory postsaccadic ocular drift. This ocular drift was still evident in the dark, although smaller (typically 15% of the amplitude of the antecedent saccade, up to a maximum drift of 8°). Retinal slip alone, without a net displacement of the image, was sufficient to elicit these adaptive changes, and compensation for leftward and rightward saccades was independent.

3. It took several days to complete adaptation, but recovery (in the light) was much quicker. The decay of this adaptation in darkness was very slow; after 3 days the ocular drift was reduced by <50%. The time constants of single exponential curve fits to adaptation time courses of data from five animals were 35 h for acquisition, 4 h for recovery, and at least 40 h for decay in darkness.

4. Descriptions of the central innervation for a saccade are usually simplified to only two components: a pulse and a step. It has been hypothesized that suppression of pathological postsaccadic drift is achieved by adjusting the ratio of the pulse to the step of innervation (19, 26). However, we show that the time constant of the ocular drift is influenced by the time constant of the adapting stimulus, which cannot be explained by the simple pulse-step model of saccadic innervation.

5. A more realistic representation of the saccadic innervation has three components: a pulse, an exponential slide, and a step. Normal saccades were accurately simulated by a fourth-order, linear model of the ocular motor plant driven by such a pulse-slide-step combination. Saccades made after prolonged exposure to optically induced retinal image slip could also be simulated by properly adjusting the slide and step components. Thus we hypothesize that adaptive control of the gain of the step, and of both the gain and the time constant of the slide, is required to suppress postsaccadic ocular drift.

INTRODUCTION

Visual acuity begins to decline as images slip across the retina at more than a few degrees per second. It is therefore desirable that the eyes be reasonably stable during fixation of the stationary world. Fixation is changed with very rapid eye movements, called saccades, minimizing the period of poor visual acuity. However, the nervous system is not always successful in reestablishing fixation immediately after a saccade; occasionally there is an accompanying exponential drift of small amplitude, either onward or backward (3, 40). In normal subjects these postsaccadic drifts are *usually too small to compromise* acuity, but

they can be quite pronounced in patients with ocular motor nerve palsies (1, 19) and in some patients with cerebellar disease (20).

Kommerell et al. (19) demonstrated the existence of a long-term adaptive mechanism that operates to reduce this postsaccadic drift. Using human patients with abducens nerve palsies that result in hypometria and postsaccadic drift in one eye, they showed that the amount of saccadic dysmetria and postsaccadic drift could be altered by monocular patching. When the normal eye was patched for several days its saccades became hypermetric (went beyond the target) and were followed by drift. Switching the patch for 3 days, so that the normal eye was viewing, resulted in recovery of that eye, i.e., the saccades made by the normal eye were of normal amplitude and had no postsaccadic drift. Abel et al. (1) found similar adaptive changes in a patient with an ocular motor nerve palsy. In addition, they followed the time course of the saccadic gains in their patient after patching one eye. When the affected eye alone was viewing, the saccadic gain increased with a time constant of 0.85 days, and when the unaffected eye was viewing the gain recovered with a time constant of 1.54 days.

The rapid part of a saccade is due largely to a brief, high-frequency burst of innervation, or pulse, and the final eye position is determined by a tonic level of innervation, or step (31). Kommerell et al. (19) hypothesized that saccadic adaptation was achieved by altering the pulse and step of innervation. Drift suppression would then depend upon adjusting the ratio of the pulse to the step. Optican and Robinson (26) were able to show, with ablation studies, that the pulse and step gains were independent and that their control depended on different parts of the cerebellum. These workers tenectomized the horizontal recti muscles (excised their distal ends) in one eye of monkeys and allowed the stumps to reattach to the globe. This made saccades in the operated eye hypometric (too small) and induced an exponential drift back (in the direction opposite to that of the antecedent saccade). By patching one eye or the other they were able to study adaptive changes in saccadic gains. The amplitude of the saccade was measured at the end of the initial rapid phase to provide an estimate of the pulse gain and after the achievement of a steady-state position to provide an estimate of the step gain. Both gains were found to change with the same time course, increasing with a time constant of about 1 day, and decreasing with a time constant of about ½ day. Total cerebellectomy resulted in saccadic hypermetria and postsaccadic ocular drift and abolished control of both pulse and step gains. Ablations of the midline cerebellar vermis resulted in saccadic hypermetria and destroyed the animals' ability to adjust their pulse gain, but left intact their ability to adjust their step gain. The gain of the step was not adjusted to match the target displacement, but was always matched to the antecedent pulse of innervation, so that postsaccadic ocular drift was always suppressed despite steady-state position errors. Bilateral flocculectomies in monkeys have been shown to abolish the ability to suppress postsaccadic ocular drift, presumably by destroying the control of the step gain (27).

While the existence of the drift-suppression mechanism is now well established, the mechanism by which the system senses errors and implements corrective adjustments is not known. Two different afferent systems could be used to report the presence of ocular drift. Since the world is stationary, any postsaccadic ocular drift would result in full-field retinal slip, which could therefore be used to indicate the presence of such ocular drift. The assessment of ocular drift might also be made from muscle proprioceptive afference. The extraocular muscles contain many proprioceptors, and these are known to project into the paravermal cerebellum (on which the pulse gain is dependent) over pathways with a short latency in cats (5, 10, 37). Extraocular afferents have also been shown to project to the flocculus (on which the step gain is dependent) in rabbits (22). Since the previously mentioned studies of saccadic adaptation were done on patients with ocular motor nerve palsies or in animals with tenectomized muscles, it is difficult to determine the extent to which proprioception plays a role in drift suppression. It is also not known how the adaptive control of saccade amplitude, presumably effected by changing the gain of the brain's estimate of the target's position (23), interacts with the adaptive mechanism for drift suppression. Both mechanisms appear to have similar time courses of many hours in abnormal subjects (1, 26). However, another, faster adaptive mechanism that makes a parametric adjustment in saccadic size within a few minutes has also been

demonstrated in normal human subjects (8, 14, 41).

The present study was undertaken to characterize the contribution of retinal slip to the adaptive mechanism responsible for minimizing postsaccadic ocular drift. The visual experience of patients with extraocular muscle palsies (1, 19) and monkeys after tenectomies (26), i.e., exponential slips after saccades, was reproduced as closely as possible in these experiments in an attempt to stimulate the same gradual adaptive mechanism for drift suppression. Monkeys with intact extraocular muscles experienced optically imposed, full-field, exponential postsaccadic retinal slip. The monkeys responded to this retinal slip just as if it had been caused by pathological ocular drift: changes in saccadic innervation led to the development of a postsaccadic ocular drift that reduced the optically imposed postsaccadic retinal slip. Unexpectedly, the time constant of this ocular drift was dependent on the time constant of the adapting image's drift. Hence these studies show that, in addition to the amplitude of the drift, the time constant of the drift is also under adaptive control. These data lead to the proposal of a new model of the final common path, the brain stem network and ocular motor plant, which is common to all ocular motor systems. The new hypothesis accurately models both normal and adapted saccades, allowing for the suppression of postsaccadic ocular drift. A preliminary report of some of these results has been presented (25).

METHODS

Eye movements were recorded from seven adult rhesus monkeys (*Macaca mulatta*) before, during, and after they experienced optically imposed postsaccadic retinal image slip. All animals had previously been trained to fixate small lights for a liquid reward. Each animal was implanted with a head holder and a scleral search coil (15), using aseptic surgical procedures, while under pentobarbital sodium anesthesia. During the experiments animals were seated in a plastic chair, with their heads fixed, facing a translucent screen subtending 100° in both the horizontal and vertical direction at a distance of 29 cm. Highly textured, colored images were projected onto the back of the screen and were moved by a mirror galvanometer system under computer control. This arrangement was used to drift the scene with an exponential time course after every spontaneous saccade, thereby simulating the visual events associated with postsaccadic ocular drift.

Motion of the projected image was controlled by a PDP-11/34 computer driving a servo-controlled mirror galvanometer (General Scanning Corp. CCX-101 servo and G300-PD motor). The bandwidth of the scanner was ~100 Hz, and the control signal had a range of 100° of image motion with a resolution of 1 part in 4,096. Three signals, horizontal and vertical eye position and the transducer output of the mirror galvanometer, were low-pass filtered (−3 dB at 240 Hz) and digitized with a 12-bit analog-to-digital converter sampling 1,000 times per second.

Eye movements were recorded monocularly with the magnetic-field/search-coil technique (24, 30). A relative calibration was routinely made by moving the image with a saw-tooth waveform (constant-velocity slow phases at 10 deg/s, interrupted by 10-ms resets) and assuming that the maximum optokinetically induced eye velocity matched the velocity of the projected scene. Absolute calibrations for testing saccadic accuracy were made by having the monkey make saccades to targets at 20° eccentricity left, right, up, and down.

Adaptation paradigm

The adaptation paradigm was designed to elicit a change in the pulse-step ratio of saccadic innervation. While the animal faced the textured image and made saccadic eye movements spontaneously, the computer detected the saccades on the basis of velocity and duration criteria (2). At the end of each saccade (which could be determined with an accuracy of a few milliseconds by waiting for the eye velocity to fall below 12% of its peak value) the computer made the projected image move horizontally across the screen. There was a 5-ms latency between the computer command and the mirror movement. Since the computer detected a low eye velocity, and not the true end of the saccade, the movement of the image usually began within a few milliseconds of the actual end of the saccade. Generally, an exponential waveform with a 50-ms time constant was used. This value was chosen to be near that of the ocular drift found in a previous study of lesioned animals where adaptation was observed (26). Some experiments were done with exponential drifts having other time constants (25 and 100 ms), and in one experiment the scene was displaced abruptly. The amplitude of the image slip was always 50% of the amplitude of the horizontal component of the antecedent saccade. In some experiments the slip was onward, in the direction of the antecedent eye movement, and in others it was backward. Animals remained in the apparatus for the several days needed to complete a single experiment. They were given food and water by hand, at regular intervals, until satiated, regardless of their behavior. Animals were kept awake during recording sessions by loud noises. At other times six animals were not artificially aroused. The seventh animal received a liquid reward for making brisk sac-

cades. There was little difference in this animal's adaptive performance.

Latency of the ocular following response to the full-field, exponential slip stimuli was measured with the techniques of Kawano and Miles (16). The eye velocity was digitally differentiated to obtain an acceleration trace. We computed the mean and variance of this acceleration over the period before the stimulus. Onset of ocular drift was defined to be when the eye acceleration exceeded 2 SD from the mean. This was typically at $\sim 100°/s^2$.

Saccadic performance

Sample recordings of saccadic and postsaccadic waveforms were made while the animal was viewing the adapting stimulus and while it was in temporary darkness. For testing saccadic accuracy the eye without the coil was patched, and the animal tracked a spot of light that shifted abruptly among fixed positions at 0, ±5, ±10, ±15 and ±20° along the horizontal meridian. The sequence of the target movements was unpredictable and included various combinations of starting positions and amplitudes.

Data from the first two monkeys were measured by hand from chart paper records. Data from later monkeys were analyzed off-line on a PDP-11/44 computer. Velocities were obtained by digital differentiation, using a Chebyshev optimal nonrecursive linear filter acting as a low-pass filter (−3 dB at 30 Hz) (29). Each saccade was displayed on a video screen, and measurements were made of the beginning and ending positions of the saccades, their peak velocity, and the amplitude and duration of any postsaccadic drift. Time constants of image and ocular drift were estimated by a nonlinear regression technique with linear constraints on the parameters that determined the best fit, in the least-square-error sense, of a single exponential curve to the data (21, 38).

RESULTS

When the full-field image first begins moving after every saccade, the animal responds by tracking it with a delay of ~50–60 ms (cf. Ref. 16). If the lights are turned off after only a few minutes of such experience, the animal's spontaneous saccades in the dark appear normal. After several hours of such experience, however, the monkey begins to show a zero-latency ocular drift after each saccade in the light, and some of this drift persists when the lights are turned off. Our initial concern is entirely with the postsaccadic ocular drifts that persist in the dark (though a later section will consider some of the complex events recorded in the presence of the adapting stimulus in the light).

Optically induced postsaccadic ocular drift in the dark

Figure 1 shows the effect of prolonged exposure to the adaptation paradigm on spontaneous saccades made in the dark. In the normal state of the animal (Fig. 1*A*) the saccadic eye movement ended fairly abruptly and was followed by only a small amplitude drift back. Such small drifts are often present in the light as well as in the dark in the normal state. After several days of experiencing optically imposed retinal slip after every saccade, the eyes developed a drift in the direction of the adapting motion that followed almost immediately after the rapid part of the saccade was over (Fig. 1, *B* and *C*).

Comparing the panels in Fig. 1, we see that the adapted movement looks like a rapid saccade followed by a slow drift. To quantify this adaptive response, eye movements were divided into two parts: an initial rapid component of amplitude P, presumed to reflect a phasic change of innervation, or pulse, and a component of amplitude S that brings the eye to its final position, presumed to reflect a tonic level of innervation, or step. The size of component P is measured from the initial eye position to the inflection point during the deceleration phase of the rapid part of the saccade. The size of component S is measured from the initial eye position to the point where the eye velocity returns to zero.

The amplitude of the postsaccadic ocular drift (S − P) varied with the amplitude of the antecedent saccade. Figure 2 shows data from two monkeys, in which each point indicates the ocular drift following a spontaneous saccade in the dark, after 5 days of adaptation. In both cases the adapting stimulus was an exponential image drift with a time constant of 50 ms and an amplitude that was 50% of the antecedent saccade's. Circles show drifts from monkey OV, after adapting to a stimulus that drifted backward; plus symbols show drifts from monkey UL, after adapting to a stimulus that drifted onward; the straight lines are least-squares regressions of ocular drift on saccadic amplitude for amplitudes less than about 25° (for OV: slope = −0.17, intercept = −0.54°, $r = -0.97$; for UL: slope = 0.12, intercept = 0.10°, $r = 0.95$). For larger saccades the points tend to fall off the regression line, indicating the presence of an amplitude saturation for ocular drift. Indeed, ocular drifts in the dark

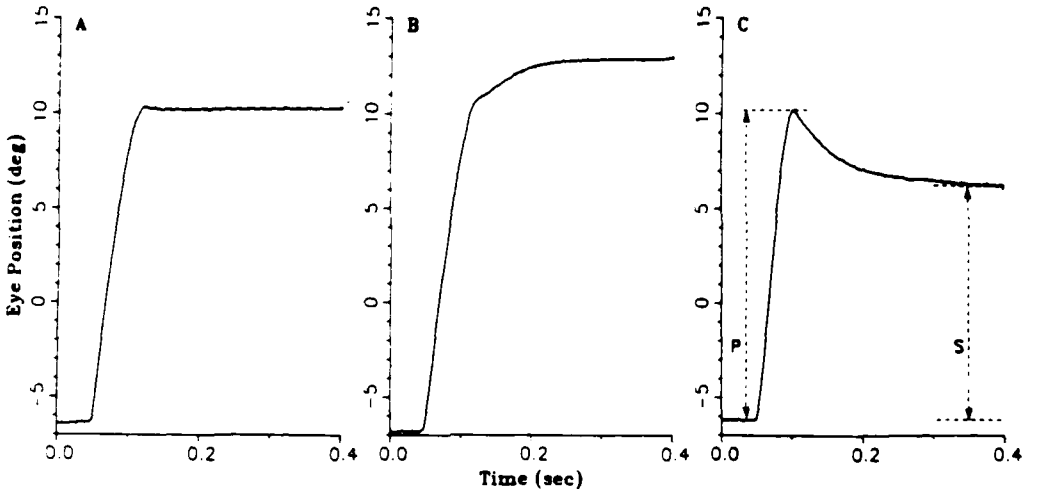

FIG. 1. Optically induced postsaccadic ocular drift persists in the dark. *A*: normal spontaneous saccade in the dark. Note small amount of drift back at the end of the rapid portion of the saccade. Spontaneous saccade in the dark after several days of exposure to an onward (*B*) and backward (*C*) exponential drift that followed every saccade. The saccade in the adapted state is followed by a zero-latency drift. To quantify the amount of ocular drift, the amplitude of the rapid part of the saccade (P) and the final position of the movement (S) are measured from the saccade's starting point. The portion P is called the saccade, and the portion (S − P) is called the postsaccadic ocular drift.

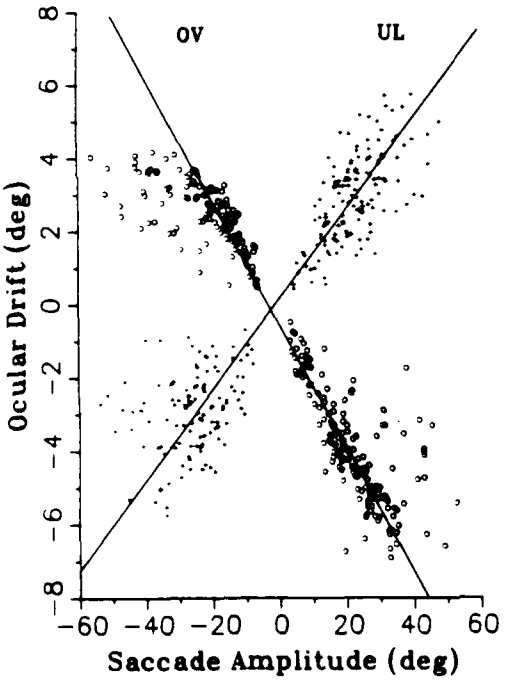

FIG. 2. The amplitude of ocular drift in the dark is proportional to the amplitude of the antecedent saccade. Ocular drift amplitudes were measured in monkey OV (with backward drifts, *circles*) and in monkey UL (with onward drifts, *plus symbols*). The *solid lines* are the regressions of ocular drift amplitude on saccade amplitude for saccades <25°.

with amplitudes >8° were not seen in any monkey.

The amount of drift was also expressed as a fraction of the pulse amplitude, (P − S)/P, and will be referred to as the pulse-step mismatch (psm). The relationship between the pulse and step components was also expressed by the fraction (P/S), called the pulse-step ratio (psr). The almost linear relationship between the amplitude of the ocular drift and its antecedent saccade suggests the presence of a parametric adjustment (with saturation), and supports the use of a single number, such as the psm or psr, to characterize the saccadic waveform in the presence of ocular drift. Table 1 shows the psm (in %) for four monkeys. The visual scene was made to slip either backward or onward 50% of the amplitude of the antecedent saccade. In each case the monkey, in response to the retinal slip, developed a postsaccadic ocular drift that was in the adaptive direction.

The amount of the postsaccadic drift in the dark was always less than that in the light. As a typical example, in monkey UL, the psm after 6 days of adaptation (to an exponential drift with 50% the amplitude of the antecedent saccade and a time constant of 50 ms) was 24.3 ± 1.2% (SE) in the presence of the adapting stimulus, but only 13.6 ± 0.3% in the dark.

TABLE 1. *Pulse-step mismatch of spontaneous saccades made in the dark*

Monkey	Normal, %	Adapted, %	
		Backward slip	Onward slip
OV	1.6 ± 0.2 (57)	17.5 ± 0.5 (107)	−17.3 ± 0.6 (84)
UL	2.5 ± 0.2 (108)	7.7 ± 0.5 (52)	−13.6 ± 0.3 (329)
RO	1.1 ± 0.2 (38)		−11.0 ± 0.8 (71)
QU	1.5 ± 0.2 (75)		−20.6 ± 0.6 (73)

Adapted state was induced by several days of exposure to an image slip whose amplitude was 50% of the amplitude of the antecedent saccade and which drifted exponentially with a time constant of 50 ms. Values are means ± 1 SE (*n*).

Time constant of ocular drift

The time constant of the ocular drift associated with an adapting stimulus of a given time constant was fairly consistent in the same animal on different days, although there were small differences between animals. The average time constant of ocular drift in four animals measured in nine separate experiments was 68.8 ms (SD = 10.8) when the adapting stimulus had a time constant of 50 ms. The time constants within this group ranged from 51.0 ± 1.4 (SE) (n = 84) to 87.1 ± 3.5 ms (n = 61); analysis of variance showed that the group was not homogeneous (F-test, $P < 0.01$), and hence the time constants among monkeys were significantly different.

These significant differences suggested that the time constant of the ocular drift might be an idiosyncrasy of the animal and independent of the time constant of the adapting stimulus. To test this hypothesis, the effect of varying the time constant of the exponential image drift used for adaptation was examined in two monkeys. In three separate experiments the time constant of image motion was either 25, 50, or 100 ms. Figure 3 shows that there was a strong correlation between the time constant of the ocular drift and that of the image drift used to adapt the animals. After adaptation the psm was about 15% in all experiments, and there was no marked difference in the acquisition time at the different adapting time constants. Nor was there any correlation between saccade amplitude and the time constant of the ocular drift; for two monkeys (OV and LF), with the three adapting image-drift time constants, the average of the absolute values of the correlation coefficients was 0.20 ± 0.22 (SD) (ranging from 0.003 to 0.500). Regression of the ocular-drift time constant on the image-drift time constant gives a line with slope 0.70 and intercept 19.61 ms (correlation coefficient 0.99) for the data of both monkeys. Hence the time constant of the ocular drift in the dark was dependent on the time constant of the stimulus used in the adaptation paradigm.

Time course of acquisition and recovery

The postsaccadic ocular drifts recorded in the dark develop gradually over time when an

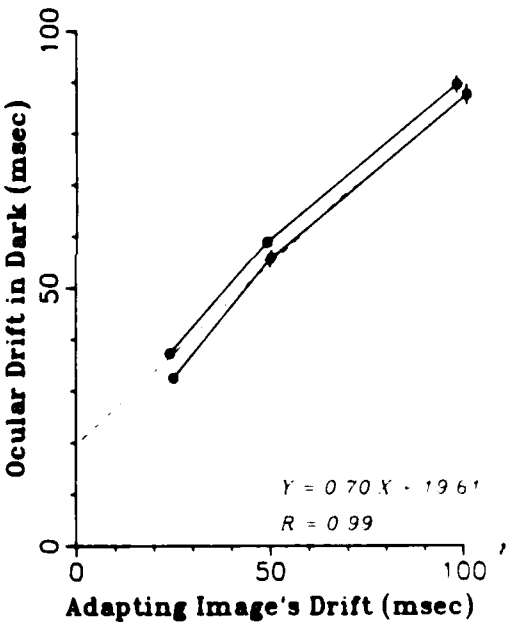

FIG. 3. Time constant of ocular drift measured from spontaneous saccades, made by monkey OV (*open circles*) and LF (*filled circles*) in the dark, depends on the time constant of the adapting stimulus. *Vertical* and *horizontal bars* are ±1 SE. *Dotted line* is from linear regression. Time constants of image drift are an average of 15, and time constants of ocular drift are averages of at least 60 nonlinear regression estimates (see METHODS). The correlation between ocular and image time constants is statistically significant ($P < 0.001$). [Actual time constants of image drift for monkey OV were 25.0 ± 0.1 (SE), 50.1 ± 0.1, and 101.0 ± 0.2; for monkey LF they were 24.1 ± 0.1, 49.1 ± 0.3, and 98.5 ± 0.5.]

animal is continually exposed to optically imposed postsaccadic slip. Figure 4 shows a typical time course for the adaptive change in the psm in monkey UL. The animal was adapted for 6 days to an exponential image drift (with a 50-ms time constant) that slipped onward in one experiment (open circles) and backward in another (filled circles). At the end of the 6th day the image motion was stopped, and the animal was allowed to recover while viewing the (now stationary) image. The recovery phase was much shorter than the acquisition phase, regardless of the direction of the gain change, even though the visual stimulus was the same in the two cases, and the monkey generated saccades at a similar rate. An effort was made to fit a single exponential function to the acquisition and recovery time courses. This was not possible in the acquisition phase when the step gain was increasing (where a dashed line connects the points); the gain appeared to increase in two stages for this monkey. When the step gain was decreasing, the acquisition phase had a time constant of 30.4 ± 6.4 h (SE). Both recovery phases were well fit by exponential functions. The time constant for recovery from a gain decrease was 5.4 ± 1.0 h, and that for a recovery from a gain increase was 4.7 ± 1.2 h. Time course data were also plotted using the number of saccades, instead of the elapsed time, as the independent variable. Essentially no difference in the smoothness or form of the curves resulted from expressing the data in this way.

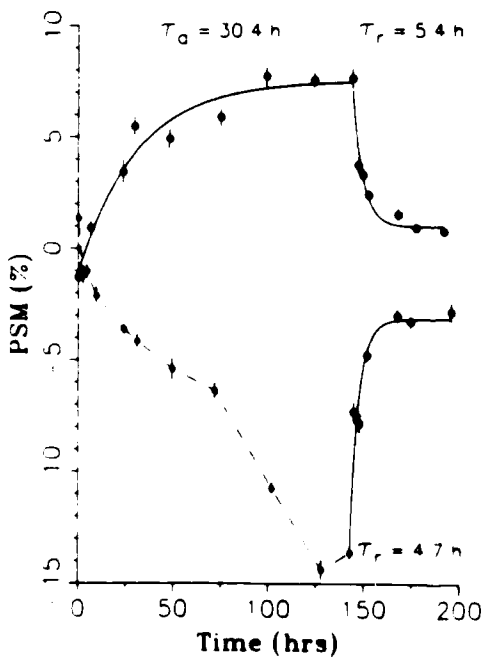

FIG. 4. Time course of adaptation in monkey UL. At time zero the animal was presented with exponential image slip that was 50% of the amplitude of the antecedent saccade. In one experiment the image drifted in the same direction as the antecedent saccade (*open circles*), and in the other the image drifted backward (*filled circles*). *Vertical bars* are ±1 SE.

The time course of the acquisition of an adapted gain was studied in five experiments on four monkeys. The time course of the recovery from the adapted state was studied in four experiments in three monkeys. In all the animals the change over time of the psm was usually smooth, although, as in Fig. 4, often one change was not well fit by a single exponential (but this could be the acquisition of either an increased or a decreased psm). There were no systematic differences across monkeys whether the gains were increasing or decreasing, or between gains for leftward or rightward movements. While there were differences in the time constants for leftward and rightward adaptation, this varied from monkey to monkey. In only two cases (out of 8) were the time constants of acquisition shorter than the time constants of recovery, and then only for one direction; combining leftward and rightward data to give a single time constant always gave an acquisition time constant that was larger than the recovery time constant. A characterization of the overall performance in all the monkeys was obtained by normalizing the psm so that the maximum value during each phase (acquisition or recovery) in each monkey was +1.0. All the normalized psm values from each monkey were divided into acquisition and recovery groups. The recovery values were time shifted so that all the recovery phases started at 167 h. Single exponential functions were fitted to all the points in both groups. In Fig. 5 the letters correspond to psm values from each monkey for leftward and rightward saccades. The solid lines are the least-squares best fit to the data of a single exponential function. The time constant of acquisition was 35.1 ± 6.5 h (SE), and that of recovery was 4.1 ± 0.7 h.

Decay of adaptation in darkness

If the postsaccadic ocular drift is to be ascribed to changes in some plastic neural gain elements, one would expect those changes to

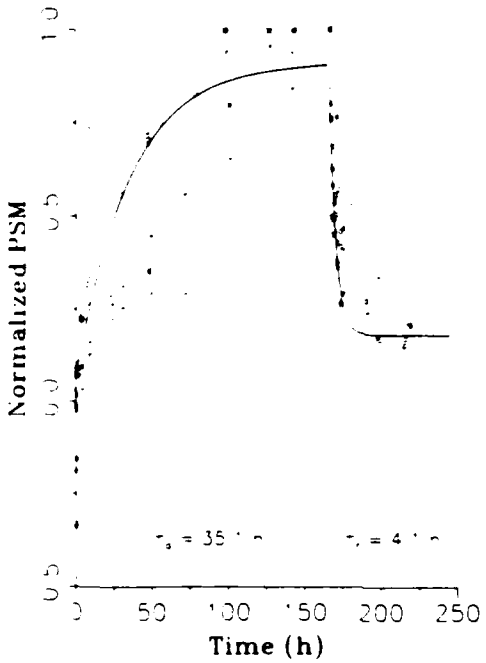

FIG. 5. Time course of adaptation averaged over 5 experiments in 4 monkeys. *Letters* represent individual monkeys. The *curves* represent the best-fit single exponential function to the pooled data.

persist in the dark when there can be no postsaccadic retinal slip. The long-term persistence of the psm was examined by adapting two monkeys (for 4 and 5 days, respectively) and then placing them in complete darkness. The amount of postsaccadic ocular drift associated with spontaneous saccades in the dark was measured by pooling the psm values for rightward and leftward data for each monkey (normalized to the value at time zero).

Figure 6 shows the pooled values (open circles are monkey OV, filled circles are monkey UL). Despite the variability of the data, reflected in the large standard errors, it is clear that the decay of the psm in darkness is less rapid than either the acquisition or recovery phases. For comparison with the time constants in Fig. 5, exponentials were fitted to the data in Fig. 6 as well. Fitting a single exponential gives a very long time constant for decay to zero [180 ± 31 h (SE), solid line]. As expected, fitting a single exponential that decays to a nonzero asymptote gives a shorter time constant (42 ± 32 h, with an asymptote of 0.53, dashed line), but one that is still longer than that for either acquisition or recovery. While the decay in the dark is not a simple process that can be well fit by a single exponential, the psm clearly does not go away rapidly in the dark, and there is considerable residual psm: even after three days in darkness both animals still retain >50% of their adaptation.

Directional selectivity

In all of these experiments the image drifted only in the horizontal plane, and ocular drift developed only in that plane. One experiment was performed (with monkey OV) to further demonstrate the directional specificity of the visually induced adaptive response. In this experiment the image was made to move onward after rightward saccades, and backward after leftward saccades. Thus, the optical drift was always in the same direction, so that the size of the step of neural innervation relative to

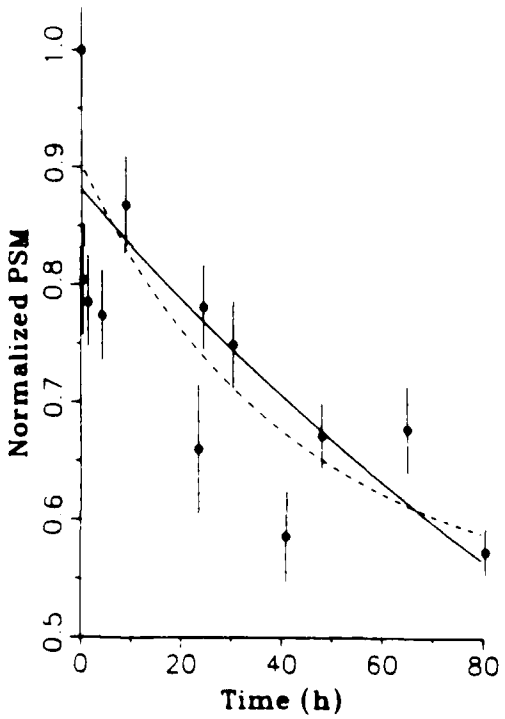

FIG. 6. Decay of adaptation in darkness. After adapting to exponential image slip, 2 monkeys were kept in complete darkness for several days. The values are pooled for each of 2 monkeys for leftward and rightward movements (*open circles* from monkey OV, *filled circles* from UL). *Vertical bars* are ±1 SE. The *solid curve* is the best-fit exponential (time constant = 180 ± 31 h) decaying to zero. The *dashed line* is the best-fit exponential with an asymptote of 0.53 (time constant of 42 ± 32 h).

the pulse was required to increase for rightward movements and decrease for leftward movements. This is exactly what happened, the psr being appropriate for the direction of the antecedent saccade and the direction of adapting image motion: The rightward psm was −9.1% (SE = 0.3, n = 116), while the leftward psm was +9.0% (SE = 0.2, n = 130).

Displacement vs. drift

An exponential pattern of image motion induces both slip and displacement of the retinal image. Several other patterns of image motion were used to study the adaptive mechanism. Prolonged exposure to step displacements (duration of 5–8 ms) in the same direction as the antecedent saccade did not elicit postsaccadic ocular drift; after several days of viewing step displacements that were 50% of the amplitude of the antecedent saccade, eye movements still ended abruptly. Hence displacement alone of the image on the retina is not sufficient to elicit postsaccadic ocular drift. Step displacements and exponential drifts were combined to give an image slip without net image displacement; at the end of a saccade the image stepped away by 50% of the amplitude of the antecedent saccade, then drifted back exponentially to its original position with a time constant of 50 ms. The response of the monkey to this step-back exponential was qualitatively identical to the response to the simple exponential image motion; the psm in the dark, after 3 days of adaptation, was −12% (SE = 0.4, n = 113), while after 3 days of adaptation to the simple exponential it was −17% (SE = 0.6, n = 84) in the same monkey. Thus, optically imposed postsaccadic retinal slip alone, without net retinal image displacement, is sufficient to elicit postsaccadic adaptation.

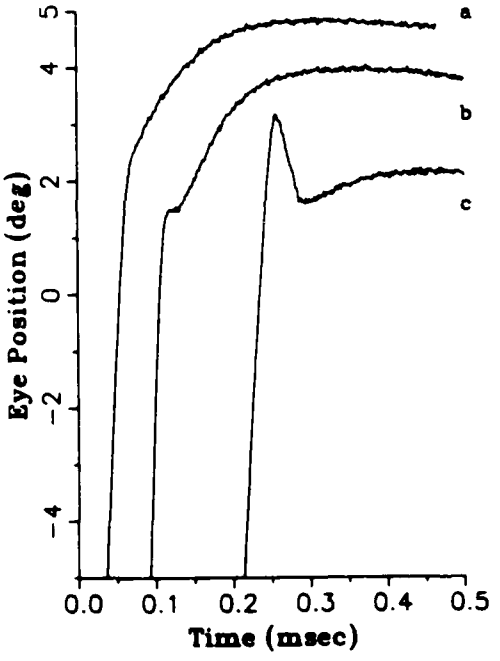

FIG. 7. Representative transition waveforms from saccade to ocular drift in spontaneous saccades in the dark. Eye movements were shifted and their beginnings removed. *a*: the drift begins immediately after the pulse-driven part of the saccade is over. *b*: there is a short period (~10 ms) of zero or low velocity before the drift. *c*: a small backward saccade, or dynamic overshoot, precedes the drift. All monkeys show this spectrum of response waveforms. Which form predominates varies with the monkey and the direction of the saccade.

TABLE 2. *Latency of ocular drift following spontaneous saccades in the dark*

Monkey	Normal	Adapted
OV	3.6 ± 0.4 (51)	3.4 ± 0.2 (107)
UL	6.2 ± 0.4 (108)	5.4 ± 0.2 (329)
RO	4.8 ± 0.8 (38)	4.6 ± 0.5 (71)
QU	3.3 ± 0.3 (75)	2.4 ± 0.1 (73)

Even normal saccades often have small ocular drifts. There is very little difference in the latency from the end of the saccade to the onset of drift between the normal and adapted states. Values are mean times in milliseconds ± 1 SE (n).

Time of onset of postsaccadic ocular drift

In the normal state, before adaptation, the exponential image drift gave rise to an ocular following response. The latency of this response, averaged over two experiments in each of two monkeys, was 56.7 ± 6.6 ms (SD). After several days of adaptation, the animals showed postsaccadic ocular drifts that had much shorter latencies and persisted in the dark. Figure 7 shows examples of the endings of eye movements made in the dark that resulted from adaptation to exponential image slip for several days, selected for their range of postsaccadic ocular drift onset times.

Zero-latency drifts, such as in Fig. 7*a*, represent only one end of a spectrum of latencies. Sometimes there is a short period between the end of the saccade and the beginning of the drift (Fig. 7*b*). In other cases the initial saccade will be followed by a dynamic overshoot (a small, backward saccade) before the drift begins (Fig. 7*c*). Which pattern predominates

varies from one monkey to the next and also depends on the direction of the antecedent saccade. The pattern in Fig. 7*c* was the most rare, occurring ~1% of the time in the dark. Table 2 shows the average latency in the dark to the onset of ocular drift in different monkeys. Ideally, in the normal state in the dark there should be no postsaccadic drift, and hence the latency measurement would be zero. The values for the latency in the animal's normal state in Table 2, however, reflect the fact that even many normal saccades are accompanied by small drifts. Also, there is a systematic error introduced by the method for determining the end of the pulse-driven part of the saccade and the beginning of the ocular drift, which limits the minimum measurable latency to ~2 ms. Clearly there is no significant change in drift latencies, measured in the dark, caused by adaptation.

Effect of adaptation on rapid component dynamics

The amplitude-peak velocity relationships of the initial rapid component of saccadic eye movements were not affected by the adaptation paradigm. Figure 8 shows examples of the amplitude-peak velocity relationship, often

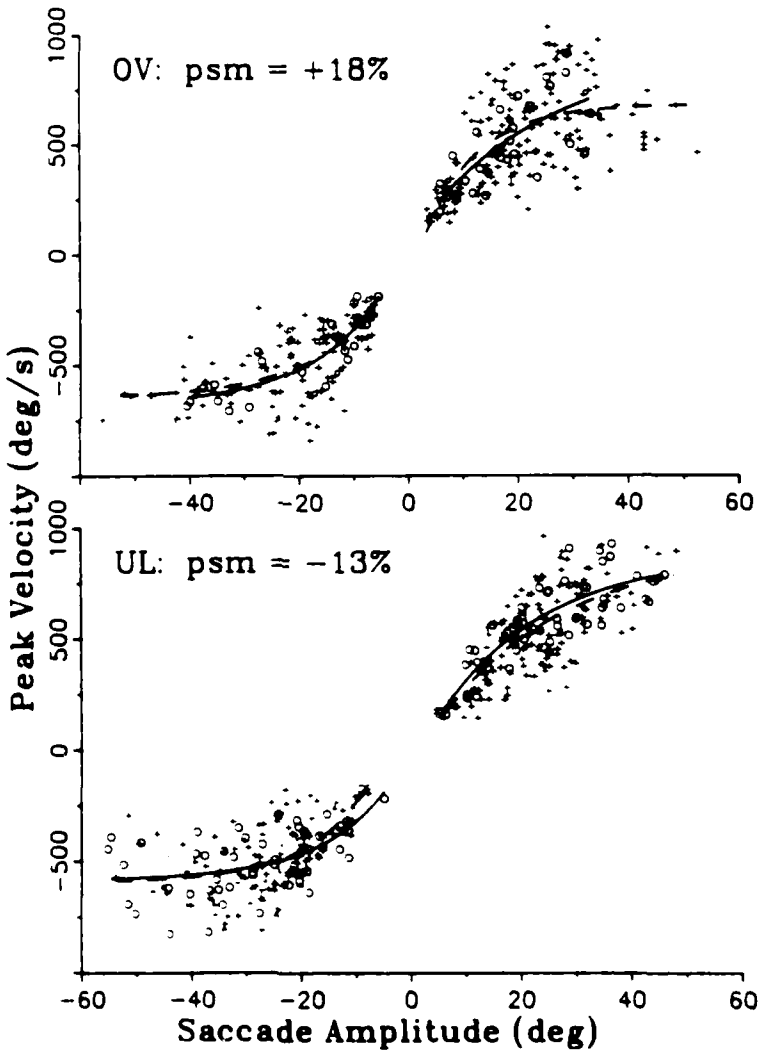

FIG. 8. Main sequence (amplitude-peak velocity relationship of the horizontal component of saccades) was the same for spontaneous saccades in the dark made in the normal (*circles*) and adapted (*plus symbols*) states.

referred to as the *main sequence* (2), obtained in the dark from two monkeys. Abscissa and ordinate values refer to the horizontal component of spontaneous saccades. Since the vertical component of saccades was not altered by this adaptation paradigm, we assume that any effect of oblique saccades on this main sequence would be the same in both the adapted and unadapted states. The circles are the values before adaptation, and the plus symbols are the values after 5 days of adaptation to a 50-ms time constant, exponential image motion that drifted 50% of the amplitude of the antecedent saccade. In Fig. 8, top, the data for monkey OV are shown before and after adaptation to backward image slip. In the adapted state the monkey's psm was +17.5% (SE = 0.5, n = 107). In the bottom part of Fig. 8, the data for monkey UL are shown before and after adaptation to onward image slip. In the adapted state the monkey's psm was −12.8% (SE = 0.3, n = 250). These mismatches were typical of those seen in our experiments.

Even the largest saccades, up to 50° in amplitude, still fell on the same main sequence. The amplitude-peak velocity main sequence can be characterized by a single exponential. The curves are the best-fit exponentials to the data values from the normal (solid) and adapted (dashed) states. The parameters of this exponential fit were compared for leftward and rightward movements by each monkey in both the adapted and normal states. There was no significant difference between the values in these two states (large sample test for difference of means could not reject the hypothesis of equal values even at the 70% confidence level). Parameters of these exponential fits are given in Table 3.

While the mean amplitude-peak velocity relationship did not change, there is clearly a wider range of velocities for a given amplitude in the adapted state when the ocular drift is backward (Fig. 8*A*). From looking at the least-upper-bound of this relationship, instead of the mean, it appears that the saccades in the adapted state can be faster than those in the normal state for amplitudes up to ~25°. (This characterization is not affected by the vertical component of oblique saccades, since slowing of the horizontal component will affect the mean, but not the least-upper-bound, of the data.) This increase in the upper limit of peak velocities for a given amplitude is presumed to be due to the fact that decreasing the step of innervation (to cause a drift back) subtracts a small amount from the portion of the saccade we call pulse-driven (the pulse is actually made up of a burst from the pulse generator and the ramp part of the ramp-step from the neural integrator, see below). Hence the pulse-driven saccadic amplitude is actually a little less than the amplitude programmed by the pulse-generator. The effect of this underestimate of saccade amplitude is to shift the amplitude-peak velocity relationship so that saccades in the adapted state (with backward drift) have larger velocities than normal saccades. Hence the asymptote for large amplitudes will remain the same, but the least-upper-bound will increase for small saccades.

TABLE 3. *Peak-velocity vs. amplitude relationship for monkeys OV and UL in the normal and adapted states (cf. Fig. 8)*

	K, deg/s	A, deg	V_m, deg/s
OV			
Normal			
R	−670 ± 406	23.5 ± 24.8	912 ± 434
L	487 ± 74	13.4 ± 7.5	−682 ± 88
Adapted			
R	−575 ± 57	9.5 ± 2.3	679 ± 36
L	398 ± 43	13.3 ± 3.9	−649 ± 43
Combined			
R	−579 ± 49	10.3 ± 2.3	688 ± 37
L	434 ± 38	13.3 ± 3.4	−654 ± 39
UL			
Normal			
R	−716 ± 92	19.8 ± 7.2	881 ± 112
L	401 ± 88	12.6 ± 5.4	−588 ± 45
Adapted			
R	−794 ± 111	23.0 ± 8.0	906 ± 136
L	440 ± 53	11.1 ± 3.4	−596 ± 41
Combined			
R	−794 ± 83	22.9 ± 6.1	914 ± 102
L	508 ± 60	11.9 ± 2.9	−596 ± 31

The curves are the least-squares best fit (21, 38) of a single exponential: $K \exp(-a/A) + V_m$ where a is the amplitude of the saccade, K is the slope constant, A is the angle constant, and V_m is the peak velocity asymptote. Curves were fit for saccades in both the rightward (R) and leftward (L) directions. The curves in the normal and adapted states were so similar that a single curve was also fit to the combination of the normal and adapted data sets for each monkey (see text). Each parameter is given ± 1 SE.

Effect of adaptation on pulse gain

To determine whether prolonged viewing of the exponential-drift stimulus would cause any change in the amplitude of the rapid com-

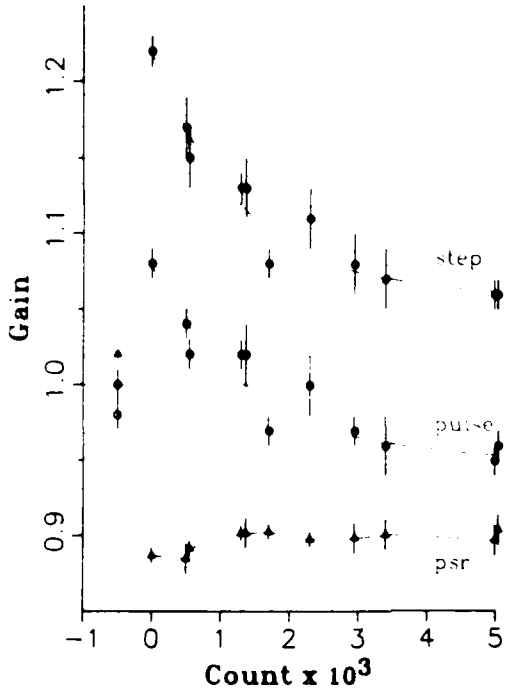

FIG. 9. Adaptation to amplitude dysmetria. Monkey UL was adapted for 3 days to a stimulus that drifted onward. The normal values of the pulse (*filled circles*) and step (*open circles*) gains, and their ratio (*triangles*) is shown at −0.5 on the *abscissa*. After adaptation, the pulse and step gains are raised (and the pulse-step ratio, psr, is lowered). In a spot-tracking task, where the monkey is rewarded for rapidly acquiring the target, the gain of the pulse and step are decreased until a slight hypometria of the pulse is restored. This happens with an exponential time course with a time constant of ~2 h. Since the gain change is in response to the saccades, however, the data is plotted versus total number of saccades since the beginning of the behavioral task.

ponents of saccadic eye movements, an animal that had been adapted for 3 days was examined on the saccadic tracking test. Figure 9 shows the pulse and step gains measured in monkey UL from responses to the movement of a spot target. (The pulse gain is the ratio of the amplitude of the pulse-driven part of the saccade to the initial distance to the target. The step gain is the ratio of the final amplitude of the eye movement to the initial distance to the target.) The step gain is indicated by open circles, the pulse gain by filled circles, and the pulse-step ratio (psr) by triangles. The values for these variables in the preadapted state are indicated by symbols at −0.5 on the abscissa. Note that the abscissa has units of thousands of saccades to facilitate easy comparison with the rapid saccadic amplitude changes seen in human subjects in psychophysical tests (8, 14).

The adaptation paradigm was designed to induce the monkey to adjust the size of the step of saccadic innervation to reduce image slip; however, as the saccade tracking test began it was evident that both the pulse and the step gains were larger than normal. In this test the projected image consisted only of a small spot of light, and the animal was rewarded only for acquiring this (stationary) target rapidly. For the first few movements of the saccade test, the high pulse and step gains drove the eye beyond the target, and the animal had to make corrective saccades. During testing, however, the animal began to decrease the amplitude of the rapid part of the saccade, so that large corrective saccades were no longer necessary; yet the ratio of the rapid component to the step component (psr) did not change. The pulse and step gains were both lowered with a roughly exponential course [step-gain decay constant: 1,308 ± 272 saccades (SE); pulse-gain decay constant: 1,438 ± 436 saccades]. This monkey made ~770 saccades per hour, so the equivalent time constant for the change of both the rapid and step components was ~2 h. This short course is longer than the rapid parametric adjustment of saccadic gain seen in psychophysical experiments on human subjects, which require only a few hundred saccades (8, 14), but is shorter than the several hours or days needed to adapt to pathological retinal slip (1, 19, 26, and Fig. 5 in this study).

DISCUSSION

Persistent postsaccadic retinal slip, induced optically, is sufficient to elicit a postsaccadic ocular drift that is evident even in the dark. When the animal first experiences the full-field exponential retinal slip there is an ocular following response with a latency of only 50–60 ms. This is shorter than the normal smooth-pursuit latency of 130–150 ms (32), and accords with the ultrashort latency ocular following response to full-field ramp movements described by Kawano and Miles (16). After a few hours of exposure to the postsaccadic retinal slip, the animal begins to develop a compensatory, often zero-latency, postsaccadic ocular drift.

This adaptation occurs in animals with intact extraocular muscles, so the ocular drift develops despite the normal proprioceptive signals coming from the extraocular afferents.

We assume that this is an adaptive response from a neural mechanism that normally operates to suppress postsaccadic ocular drift. This adaptive response is not just the uncovering of some intrinsic ocular drift, since it is only in the plane of the stimulus (horizontal), and since the direction of the drift is linked to the antecedent saccade and can be either onward or backward, independently, after rightward or leftward saccades according to the direction of the adapting stimulus. The data obtained with the step, drift, and step-drift adapting waveforms are consistent with the suggestion of Optican and Robinson (26) that the adaptive mechanism regulating postsaccadic ocular drift is sensitive to retinal slip but not retinal displacement. These workers showed that the step gain is adjusted to minimize postsaccadic ocular drift, rather than to match the desired final eye position. The matching of the step to the pulse occurred even when the pulse gain was incorrect, resulting in saccades of normal appearance but inappropriate amplitude.

The gain of the pulse component also increased slightly in response to the exponential slip stimulus (Fig. 9) and would have had the effect of reducing the final position error. The adapted animal in Fig. 9 had a pulse gain of $\sim$1.1 and a step gain of $\sim$1.3. The gain of the step (G_s) seems to be adjusted to match the pulse gain (G_p), as indicated by the almost constant value of the pulse-step ratio (psr) in Fig. 9 and by lesion studies in monkeys (26). Thus we assume we can write the step gain as G_p/psr. To acquire an initial eccentricity of amplitude K, the pulse drives the eye to G_pK, and the step carries the eye to G_pK/psr. The computer would detect the saccade, and move the image another $0.5G_pK$. So, the final image position is at $(1 + 0.5G_p)K$, which gives a position error, e, between intended and final eccentricities of $[1 + (0.5 - 1/\text{psr})G_p]K$. For this example, $e/K = [1 + (0.5 - 1.3/1.1)1.1] = 0.25$. Hence the position error when both the gain of the pulse and step are increased is 25% of the intended eccentricity. If only the step had adapted, (i.e., $G_p = 1$, $G_s = 1/\text{psr} = 1.18$), then the error would have been 32%. The change in pulse gain reduces the error by (32 − 25%) = 7%, hence it contributes an additional 7/32 = 22% to the reduction of the error.

Other studies have shown that changes in pulse gain can occur in man after only a few hundred saccades (8, 14, 41). Such rapid acquisition may be related to conscious strategies, or short time constant, plastic mechanisms. In contrast, the prolonged time course of the changes in ocular drift and their relatively slow decay in the dark are consistent with long-term, plastic alterations in neural components, rather than the short-term deployment of alternative strategies.

Figure 1 demonstrates for the first time that the saccadic system can reduce the amplitude of the step of saccadic innervation below normal. In previous studies (1, 19, 26) saccadic adaptation was always a response to a reduction of the effective strength of the extraocular muscles. Patching one eye or the other could only be used to increase the amplitude of the step, or return it to its normal value. Abel et al. (1) noted that the time constant for increasing the gain in their patient was 0.85 days, whereas the time constant for recovery was 1.54 days. Optican and Robinson (26) gave the time constant for increasing the step gain over three monkeys as $\sim$1 day, with a recovery time constant of $\sim$0.5 days. Since in these experiments the gains could only be made to increase above normal, or decrease to normal during adaptation, it was not clear whether the difference in the time constants between the acquisition and recovery phases was due to the direction of the change or somehow related to the phase (acquisition or recovery) of the adaptive process. In the present set of experiments it was clear that there was an order of magnitude difference in the time constants of the acquisition and recovery phases, regardless of the direction of the actual gain change.

Why the recovery phase, which always returns the step gain to $\sim$1.0, should be faster than the acquisition phase is not known. One hypothesis is that the ocular drift is a pattern of eye movement that the animal learns to emit after every saccade. Then learning the pattern would be slow, but recovery would only require that the pattern no longer be emitted. This explanation is not completely consistent, though, with the continued presence of the drift after prolonged periods in darkness or with the animal's inability to suppress the drift in the saccade test, apparently finding it easier to adapt the pulse gain instead (Fig. 9). Another potentially important factor is that during acquisition, proprioception and vision are in conflict, whereas in recovery they

are in accord. Another hypothesis is that the brain has a very stable set point for the pulse-step ratio that corresponds with minimal postsaccadic ocular drift. To change the pulse-step ratio away from the set point may require the long-term integration of persistent postsaccadic retinal slip. It may be possible to return the ratio to the value specified by the set point by quickly dumping the integrated error. The logical extension of this idea is that the set point itself must be either genetically determined, or under a very slow-acting form of adaptive control. If the latter is the case, patients with chronic disorders (e.g., a 6th nerve palsy) might have a set point that calls for a very high gain. In such a case, it might take longer for the gain to change to the value needed when only the normal eye is viewing and less time for the gain to go back to the raised value when only the paretic eye is viewing (1).

The amplitude of the induced ocular drift is not constant but is roughly proportional to the amplitude of the antecedent saccade. This ratio was typically ~15% for spontaneous saccades in the dark, but the drift amplitude was never >8°. Thus, while the ocular drift would tend to reduce the retinal slip seen just after a saccade, it could not completely cancel it. The adaptive mechanism was unable to fully compensate for the optically induced slip. In animals with peripheral muscle lesions, however, Optican and Robinson (26) found that postsaccadic drift suppression in the light was nearly complete after the operated eye had been viewing for several days. In this study the amplitude of the ocular drift was 15–20%, with a time constant of 40 ms. The imperfect compensation seen in the present study may have been because the optically induced retinal slip (50% of the antecedent saccade in amplitude) exceeded the physiological range in amplitude, or because of a difference in the proprioceptive afference in these two experiments (the animals of Optican and Robinson had surgically altered muscles). The amplitude of the ocular drift is larger in the light in the presence of the adapting stimulus than in the dark, presumably reflecting a contribution from some predictive tracking mechanism. One assumes that such mechanisms are disabled in the dark.

Kommerell et al. (19) hypothesized that the ocular-drift adaptation was simply a readjustment of the ratio of the pulse to the step of saccadic innervation, and thus the ocular drift was a passive consequence of an imbalance between the extraocular muscle forces and the orbital restoring forces at the end of a saccade (19). The time constant of the ocular drift would then reflect the dynamics of the ocular plant after a step input. The plant is not a simple linear system, however, and predicting the time constant of ocular drift is difficult. The dominant time constant of the orbital mechanics in the rhesus monkey is ~200 ms (34, 39). However, perturbations of the neuromuscular system can result in smaller time constants: 11 and 33 ms after oculomotor nerve stimulation (33), 95 ms after monocular forced ductions (18, 36), and 68 ms after stimulation of the medial longitudinal fasciculus (28). Thus it is not a simple matter to predict a priori what the time constant of postsaccadic ocular drift would be if it were determined passively by the mechanics of the orbit.

In our experiments, however, it has been shown for the first time that the time constant of postsaccadic ocular drift is not passively determined but is under adaptive control. The ocular-drift time constant is thus adjusted actively to minimize retinal slip throughout the period of ocular drift. This new result motivates the incorporation of a third adaptable component into the representation of saccadic innervation, and has important consequences for our understanding of how the brain controls eye movements.

A model of the final common path

Experiments on human eye movements led Robinson (31) to represent the plant mechanics as a fourth-order, linear model with one factor in the numerator (called a zero) and four factors (called poles) in the denominator (2 real poles and a complex-pole pair) of its transfer function. A similar transfer function can be used to get a good approximation of our monkeys' eye movements. As pointed out in the original study, the active state tension (and hence the innervation) needed to make a saccade with this fourth-order plant consists of a brief pulse, a small exponential slide, and a final step (31). There is also physiological support for this pulse-slide-step representation of saccadic innervation. Fuchs and Luschei (11) reported and Goldstein (13) quantified the exponential decay of the postsaccadic neural firing rate in abducens nucleus single units of monkeys. Collins et al. (7) recorded with implanted strain gauges during human

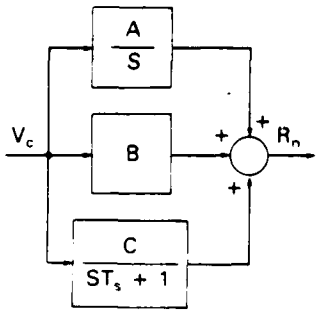

FIG. 10. Block diagram of brain stem network of the final common path for all ocular motor systems. V_c is the velocity command signal coming from the brain stem pulse generator. R_n is the saccadic innervation being sent to the extraocular muscles. The upper block represents the neural integrator, which provides a step with weight A. The middle block provides a pulse with weight B. The first 2 blocks are identical with the final common path previously proposed by Skavenski and Robinson (39). The bottom block is new, and provides an exponentially decaying innervation, or slide, with time constant T_s and weight C.

strabismus surgery and demonstrated exponential decays in the muscle tension after saccades.

The time constant of the neural slide and the time constant of the plant's lead factor (the numerator factor, or zero) have not been measured in the same species. Indeed, in Robinson's original study the value of this plant time constant depended upon certain assumptions about the distribution of stiffness in the model, and was not measured directly. Following Goldstein's approach (13), we propose that the purpose of the neural slide is to compensate for the lead element of the plant dynamics, and thus in our model they are made to have similar time constants. The importance of the slide of innervation to the present study lies in its potential for determining the time constant of postsaccadic ocular drift. We assume that the dynamics of the plant are almost completely compensated for by the dynamics of the brain stem neural network, and that eye velocity is determined solely by the firing rate of the medium lead burst neurons in the pontine reticular formation (6, 12, 17). If the firing rate of the bursters is proportional to eye velocity [neglecting an amplitude nonlinearity (12)], then the overall effect of the final common path must be to mathematically integrate a burst of neuronal discharge encoding eye velocity, thereby producing the eye position (39). Figure 10 shows a simplified block diagram (in Laplace transform notation) of the proposed brain stem neural network. The velocity command (V_c) is passed through three blocks, the sum of whose outputs constitutes the ocular motor control signal (R_n). The velocity command is essentially a brief pulse. The top block represents the neural integrator, with gain A, the output of which is a ramp-step obtained by integrating the input pulse. The middle block represents the direct velocity contribution of the pulse (with gain B), acting as a preemphasis for the sluggish plant. The bottom block represents a low-pass filter with time constant T_s and DC gain C. The output of this block is a low-pass filtered version of the pulse. Combining the output of these three branches gives a motor neuron command (R_n) consisting of a pulse, a slide, and a step.

The transfer function for the network shown in Fig. 10 is second order, having two factors in the numerator (zeros) and two in the denominator (poles). The overall transfer function of the final common path, obtained by cascading this neural network with a fourth-order plant, can give an approximation to the desired overall transfer function of $1/s$. Neglecting the high-frequency complex pole pair in the plant, the combined transfer function (E/V_c) is

$$\frac{s^2(BT_s) + s(AT_s + B + C) + A}{s(sT_s + 1)} \times \frac{(sT_z + 1)}{s^2(T_1T_2) + s(T_1 + T_2) + 1} \quad (1)$$

where T_z, T_1, T_2 represent the time constants in the plant's transfer function (factor on the right).

The zero in the plant dynamics can be compensated for by the pole in the neural network if $T_s = T_z$. In the model of normal saccades, the DC gain is one, which sets the value of A to one. The two zeros in the final common path can be used to compensate for two of the poles in the plant. Since T_s has already been fixed at T_z, we must choose the gain of the pulse as $B = T_1T_2/T_s$. The gain of the slide must then be $C = T_1 + T_2 - T_s - (T_1T_2/T_s)$. Hence, we can compensate for all the dynamics of the ocular motor plant (except the high-frequency, complex-pole pair, which, along with the dynamics of the pulse of innervation, will therefore determine the waveform of the saccade).

If the pulse, slide, and step components of innervation are not matched to the ocular plant, the eye will drift exponentially after the

rapid part of each saccade. An adaptive mechanism is presumed to exist that matches the parameters of the brain stem pathway postsaccadic retinal slip. Suppose that the gain of the step has been increased to suppress the postsaccadic retinal slip caused by our adaptation paradigm. If no other parameters were altered, the ocular drift that follows the end of the pulse-driven part of the saccade would have a very long time constant (due to the large plant time constant). Ocular drifts with longer time constants are produced by reductions in the amplitude of the slide, which shifts the time constant of the ocular drift toward the dominant time constant of the plant. To make ocular drifts with shorter time constants the amplitude of the slide must be increased. At some point (for ocular drifts with time constants of ~50 ms), however, further increases of the amplitude of the slide do not decrease the time constant of the ocular drift; instead they cause the eye to overshoot the final position (determined by the step) and drift back to it. To shorten the time constant of the ocular drift further therefore requires another mechanism. The simplest approach is to decrease the time constant of the neural slide component. By changing both the amplitude and the time constant of the slide it is possible to match time constants over the range of ocular drifts that we observed (~30–80 ms).

Simulation of spontaneous eye movements made in the dark

The above linear systems analysis suggests that the neural slide may be contributing to postsaccadic ocular drift. Individual eye-movement records from a monkey in both the normal and adapted states were simulated to evaluate the ability of the new model of the final common path to adequately reproduce actual eye movements. Simulation of course, requires specification of more than just the final common path. The complete model of the saccadic system we used was very similar to one published earlier (42), with the exponen-

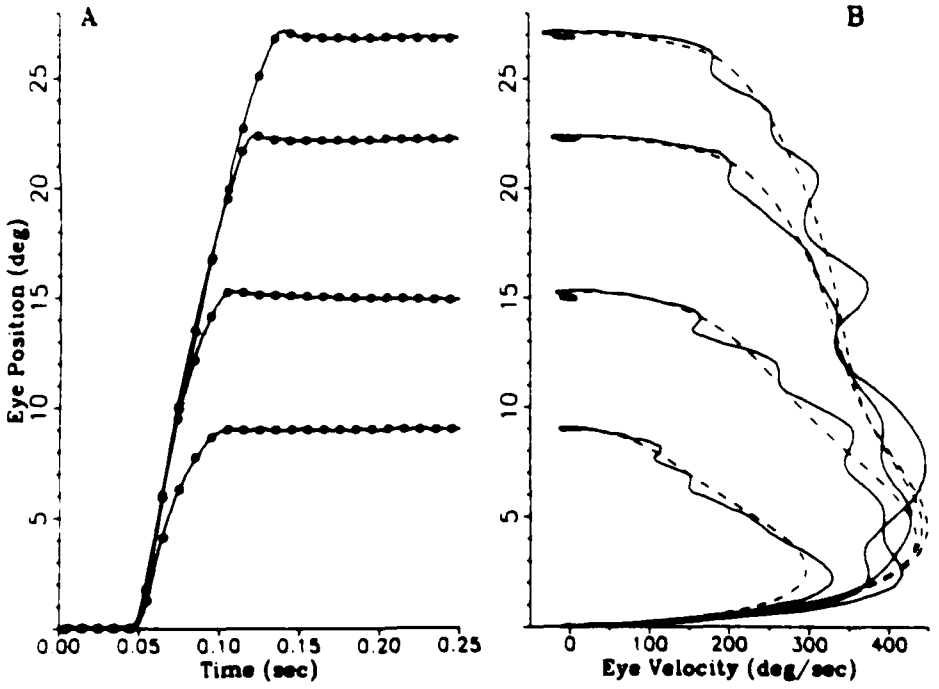

FIG. 11. Recordings and simulations of normal spontaneous saccades made in the dark. *A*: four individual eye movements from monkey OV were offset so that their initial positions were at zero. Superimposed on each data trace is a *dotted curve* obtained by simulating the eye movement with a model based on the brain stem network shown in Fig. 10 *B*. *B*: eye position versus eye velocity phase plane. The eye-position values from the actual and simulated eye movement were differentiated with the same digital filter to obtain an eye-velocity signal. The phase-plane trajectories of the simulations (*dashed curves*) are superimposed on their corresponding data trajectories (*solid curves*). The fit is excellent for the beginning and ending (i.e., low-velocity portions) of the saccades.

tial burst-cell nonlinearity replaced by a power function, the brain stem network replaced by the one shown in Fig. 10, and with a fourth-order, lumped linear plant.

Figure 11 shows a family of spontaneous saccades made by monkey OV in the dark and simulated with the new model. Figure 11*A* shows four individual saccades of various amplitudes (offset to start at zero), and superimposed upon them, their four simulations (circles). (Model parameters were adjusted by hand to obtain a reasonable fit to the normal saccades.) The simulations and the eye movements are virtually identical. The fit of the model to the rapid part of the movement can be better appreciated in Fig. 11*B*, which plots each eye movement (solid curve) as a trajectory in the phase plane of eye position versus eye velocity. The simulations are shown as dashed curves. Comparison of the phase plane trajectories reveals that the model matches the eye movements closely, except for the oscillations in the eye velocity >100°/s. Since both the data and the simulated eye movements were processed with the same digital filter, the oscillations on the eye-velocity data indicate a true physiological phenomenon. This would be consistent with more detailed models of the ocular motor plant, which are of at least sixth order (4, 9, 35). Consideration of the higher-order terms in the plant will not be necessary for our study of the adaptive behavior of the saccadic system.

Two examples of spontaneous saccades in the dark from the range of ocular drift time constants are shown in Fig. 12 (τ_m is the time constant of the adapting image motion). Superimposed on the eye-movement traces are the corresponding simulated movements (circles). The fits are fairly good, except that in the simulation, after the pulse-driven part of the saccade is over, the overshoot of the plant (caused by the underdamped complex pole pair) always brings the eye to an almost complete stop before the ocular drift begins. Figure 12*A* shows that a saccade with a long time

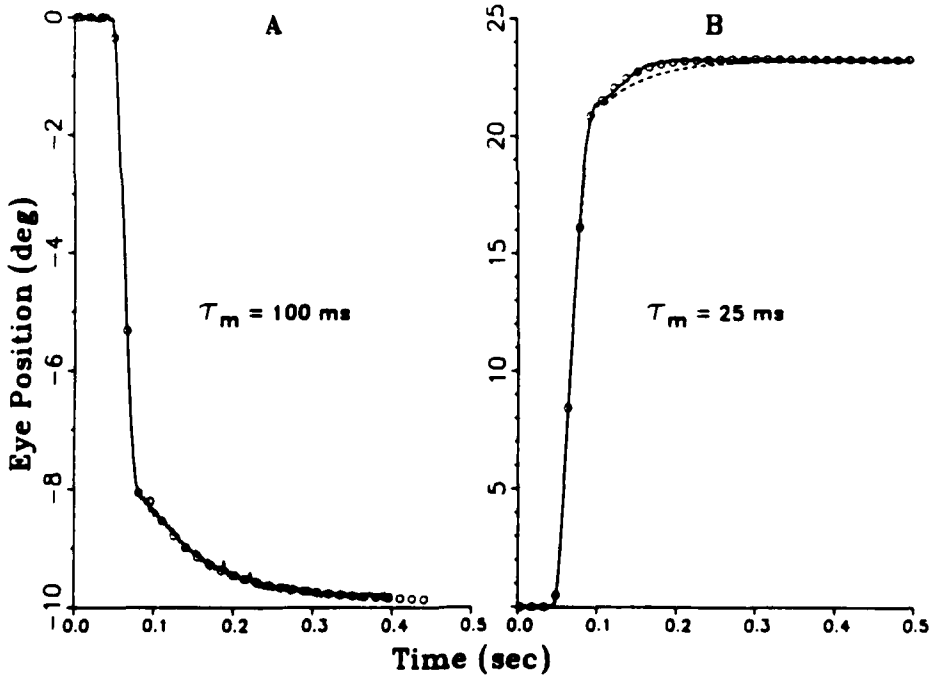

FIG. 12. Recordings and simulations of adapted spontaneous saccades made in the dark. Individual responses were chosen from monkey OV and offset to start from zero. *A*: eye movement (*solid curve*) and simulation (*circles*) after adaptation to exponential image slip with a time constant of 100 ms. The ocular drift has a time constant of ~80 ms. *B*: eye movement after adaptation to exponential image slip with a time constant of 25 ms. The ocular drift has a time constant of ~34 ms. The *dashed curve* is the best-fit simulation that can be obtained by changing only 2 elements: the gain of the step and the gain of the slide. The *circles* are the best fit that can be obtained by changing 3 elements: the gain of the step and both the gain and the time constant of the slide.

constant ocular drift (~80 ms) can be simulated by changing just the gain of the step and the slide components. Figure 12*B* shows that a saccade with a short time constant ocular drift (~34 ms) can not be simulated very well by changing just the step and slide gains (dashed curve). The model makes a good simulation of this eye movement, though, if the gain of the step and both the gain and the time constant of the slide can be adjusted (circles).

Adaptive control

The analytical discussion above, and the results of the simulation, demonstrate that both the step and slide components of ocular motor innervation are needed to describe the characteristics of postsaccadic ocular drift. The amplitude of the step of innervation and both the amplitude and the time constant of the neural slide need to be under adaptive control to compensate for changes in ocular motor strength and to exactly cancel the equivalent zero in the plant dynamics. Since the effect of the newly proposed pole in the brain stem network is to hide the zero of the plant neither the pole nor the zero have been taken into account in previous studies of the saccadic system. However, we now suggest that the suppression of postsaccadic ocular drift is achieved by adaptively changing three elements: the gain of the step of innervation and both the gain and the time constant of the slide of innervation. This detailed understanding of the nature of the adaptive changes in the brain stem pathways makes it possible to study the interaction between this part of the saccadic system and other ocular motor systems. Since the new branch (bottom of Fig. 10) is needed to compensate for the zero in the plant dynamics, it should be shared by all ocular motor systems, thereby justifying its inclusion in the final common path, rather than relegating it to the saccadic system alone. This shared role may be tested experimentally by measuring the performance of other ocular motor systems before and after adaptation of the saccadic system to persistent postsaccadic retinal slip.

ACKNOWLEDGMENTS

We are grateful for the assistance of Dr. Kenji Kawano in measuring the latencies of the ocular following responses. We thank Dr. Herschel Goldstein for many helpful discussions about the pulse-slide-step firing patterns of abducens neurons. We are grateful to Dr. Lawrence Stark for suggesting the use of the least-upper-bound to characterize the main sequence data.

Partial support for L. M. Optican was provided by National Eye Institute Fellowship EY-05291.

Received 4 October 1984; accepted in final form 10 May 1985.

REFERENCES

1. ABEL, L. A., SCHMIDT, D., DELL'OSSO, L. F., AND DAROFF, R. B. Saccadic system plasticity in humans. *Ann. Neurol.* 4: 313–318, 1978.
2. BAHILL, A. T., CLARK, M. R., AND STARK, L. The main sequence, a tool for studying human eye movements. *Math. Biosci.* 24: 191–204, 1975.
3. BAHILL, A. T., CLARK, M. R., AND STARK, L. Glissades—eye movements generated by mismatched components of the saccadic motoneuronal control signal. *Math. Biosci.* 26: 303–318, 1975.
4. BAHILL, A. T., LATIMER, J. R., AND TROOST, B. T. Linear homeomorphic model for human eye movement. *IEEE Trans. Biomed. Eng.* 27: 631–639, 1980.
5. BAKER, R., PRECHT, W., AND LLINÁS, R. Mossy and climbing fiber projections of extraocular muscle afferents to the cerebellum. *Brain Res.* 38: 440–445, 1972.
6. COHEN, B. AND HENN, V. Unit activity in the pontine reticular formation associated with eye movements. *Brain Res.* 46: 403–410, 1972.
7. COLLINS, C. C., O'MEARA, D., AND SCOTT, A. B. Muscle tension during unrestrained human eye movements. *J. Physiol. London* 245: 351–369, 1975.
8. DEUBEL, H., WOLF, W., AND HAUSKE, G. Corrective saccades: effect of shifting the saccade goal. *Vision Res.* 22: 353–364, 1982.
9. ENDERLE, J. D., WOLFE, J. W., AND YATES, J. T. The linear homeomorphic saccadic eye movement model—a modification. *IEEE Trans. Biomed. Eng.* 31: 717–720, 1984.
10. FUCHS, A. F. AND KORNHUBER, H. H. Extraocular muscle afferents to the cerebellum of the cat. *J. Physiol. London* 200: 713–722, 1969.
11. FUCHS, A. F. AND LUSCHEI, E. S. Firing patterns of abducens neurons of alert monkeys in relationship to horizontal eye movement. *J. Neurophysiol.* 33: 382–392, 1970.
12. GISBERGEN, J. A. M. VAN, ROBINSON, D. A., AND GIELEN, S. A quantitative analysis of generation of saccadic eye movements by burst neurons. *J. Neurophysiol.* 45: 417–442, 1981.
13. GOLDSTEIN, H. P. *The Neural Encoding of Saccades in the Rhesus Monkey* (PhD thesis). Baltimore, MD: Johns Hopkins Univ., 1983.
14. HENSON, D. B. Corrective saccades: effect of altering visual feedback. *Vision Res.* 18: 63–67, 1979.
15. JUDGE, S. J., RICHMOND, B. J., AND CHU, F. C. Implantation of magnetic search coils for measurement of eye position: an improved method. *Vision Res.* 20: 535–538, 1980.
16. KAWANO, K. AND MILES, F. A. Adaptive plasticity in short-latency ocular following responses of monkey. *Soc. Neurosci. Abstr.* 9: 868, 1983.
17. KELLER, E. L. Participation of medial pontine reticular

formation in eye movement generation in monkey. *J. Neurophysiol.* 37: 316–332, 1974.

18. KELLER, E. L. AND ROBINSON, D. A. Absence of a stretch reflex in extraocular muscles of the monkey. *J. Neurophysiol.* 34: 908–919, 1971.
19. KOMMERELL, G., OLIVIER, D., AND THEOPOLD, H. Adaptive programming of phasic and tonic components in saccadic eye movements. Investigations in patients with abducens palsy. *Invest. Ophthalmol.* 15: 657–660, 1976.
20. LEIGH, R. J. AND ZEE, D. S. *The Neurology of Eye Movements.* Philadelphia, PA: Davis, 1983, p. 215–216.
21. MARQUARDT, D. W. An algorithm for least-squares estimation of nonlinear parameters. *J. SIAM* 11: 431–441, 1963.
22. MIYASHITA, Y. Eye velocity responsiveness and its proprioceptive component in the floccular Purkinje cells of the alert pigmented rabbit. *Exp. Brain Res.* 55: 81–90, 1984.
23. OPTICAN, L. M. Saccadic dysmetria. In: *Functional Basis of Ocular Motility Disorders,* edited by G. Lennerstrand, D. S. Zee, and E. L. Keller. Oxford, UK: Pergamon, 1982, p. 441–451.
24. OPTICAN, L. M., FRANK, D. E., SMITH, B. M., AND COLBURN, T. R. An amplitude and phase regulating magnetic field generator for an eye movement monitor. *IEEE Trans. Biomed. Eng.* 29: 206–209, 1982.
25. OPTICAN, L. M. AND MILES, F. A. Visually induced adaptive changes in oculomotor control signals. *Soc. Neurosci. Abstr.* 5: 380, 1979.
26. OPTICAN, L. M. AND ROBINSON, D. A. Cerebellar-dependent adaptive control of primate saccadic system. *J. Neurophysiol.* 44: 1058–1076, 1980.
27. OPTICAN, L. M., ZEE, D. S., MILES, F. A., AND LISBERGER, S. G. Oculomotor deficits in monkeys with floccular lesions. *Soc. Neurosci. Abstr.* 6: 474, 1980.
28. POLA, J. AND ROBINSON, D. A. Oculomotor signals in medial longitudinal fasciculus of the monkey. *J. Neurophysiol.* 41: 245–259, 1978.
29. RABINER, L. R. AND GOLD, B. *Theory and Application of Digital Signal Processing.* Englewood Cliffs, NJ: Prentice-Hall, 1975, chapt. 3.
30. ROBINSON, D. A. A method of measuring eye movement using a scleral search coil in a magnetic field. *IEEE Trans. Biomed. Eng.* 26: 137–145, 1963.
31. ROBINSON, D. A. The mechanics of human saccadic eye movement. *J. Physiol. London* 174: 245–264, 1964.
32. ROBINSON, D. A. The mechanics of human smooth pursuit eye movement. *J. Physiol. London* 180: 569–591, 1965.
33. ROBINSON, D. A. A note on the oculomotor pathway. *Exp. Neurol.* 22: 130–132, 1968.
34. ROBINSON, D. A. Oculomotor unit behavior in the monkey. *J. Neurophysiol.* 33: 393–404, 1970.
35. ROBINSON, D. A. Models of mechanics of eye movements. In: *Models of Oculomotor Behavior and Control,* edited by B. L. Zuber. Boca Raton, FL: CRC Press, 1981, p. 21–41.
36. ROBINSON, D. A. AND KELLER, E. L. The behavior of eye movement motoneurons in the alert monkey. *Bibl. Ophthalmol.* 82: 7–16, 1972.
37. SCHWARZ, D. W. F. AND TOMLINSON, R. D. Neuronal responses to eye muscle stretch in cerebellar lobule VI of the cat. *Exp. Brain Res.* 27: 101–111, 1977.
38. SHRAGER, R. I. Nonlinear regression with linear constraints: an extension of the magnified diagonal method. *JACM* 17: 446–452, 1970.
39. SKAVENSKI, A. A. AND ROBINSON, D. A. Role of abducens neurons in vestibuloocular reflex. *J. Neurophysiol.* 36: 724–738, 1973.
40. WEBER, R. B. AND DAROFF, R. B. Corrective movements following refixation saccades: type and control system analysis. *Vision Res.* 12: 467, 1972.
41. WOLF, W., DEUBEL, H., AND HAUSKE, G. Properties of parametric adjustment in the saccadic system. In: *Theoretical and Applied Aspects of Eye Movement Research,* edited by A. G. Gale and F. Johnsons. Amsterdam: Elsevier/North-Holland, 1984, p. 79–86.
42. ZEE, D. S., OPTICAN, L. M., COOK, J. D., ROBINSON, D. A., AND ENGEL, W. K. Slow saccades in spinocerebellar degeneration. *Arch. Neurol.* 33: 243–251, 1976.

END

5-81

DTIC